Understanding the Rheology of Liquid Protein Formulations

Andrea Domingues Gonçalves

Thesis submitted to the University of Nottingham for the degree of Doctor of Philosophy

December, 2013

Abstract

The work described in this thesis had the main aim of understanding protein solution rheology. This was from a biopharmaceutical perspective, with account of the biophysical properties of proteins and in particular their level of aggregation. Molecular interactions influencing the rheology of a range of protein solutions were studied. Proteins were selected to relate directly to the diversity of protein types used in biopharmaceuticals. In addition, the roles of a surfactant formulation additive and synthetic amphiphilic polymers in the flow behaviour of protein solutions were studied.

The effect of protein concentration on solution viscosity in a commercially available biopharmaceutical formulation of a recombinant albumin (rAlbumin) was studied. The effect of the level of protein aggregation, variation in protein concentration and its impact on solution viscosity was revealed. Theoretical models predicting the increase of viscosity with concentration were applied to these data. A recent model that accounts for multiple protein species in solution, predicted the experimental data best. The rAlbumin study, although a relatively simple system, represented a 'real-life' formulation with results highlighting the need to account for heterogeneity in the level of aggregation when addressing the increase of viscosity observed at high concentration of protein solutions.

β-lactoglobulin (β-LG) excipient-free solutions were characterised by bulk and interfacial shear rheology. Solutions at various concentrations, characterised using conven-

tional rheology instrumentation, evidenced an apparent yield stress behaviour at a low shear rate range (0.01 - 10 s^{-1}), whilst showing constant viscosities throughout higher shear rates. Comparing interfacial shear rheology, air-water interface-free bulk rheology measurements, and tensiometry results, it was demonstrated that the complexity of this protein's solution rheology was due to the formation of a protein viscoelastic film at the air-water interface, as present in conventional rheometry. This is in agreement with literature. Further studies considered the effect of insoluble β-LG aggregates on the solutions' rheology, linking with their characterisation in size and quantification. The presence of insoluble proteinaceous particles was suggested to have an impact on the solution's flow behaviour, particularly at the lower shear rates.

Excipient-free monoclonal antibody (mAb) solutions were studied with the aim of generating protein aggregates (soluble and insoluble) to explore their impact on solution rheology. mAb samples were subjected to thermal stress and were characterised for their purity, aggregate content and size. The change in species content did not alter the original protein's yield-stress behaviour at low shear rates. An increase in aggregate content was related to the increase of viscosities observed at high shear rates. Establishing a relationship between species content (in volume fraction) and viscosities, as for the rAlbumin study, was not possible due to this mAbs specific aggregation behaviour. However, from the β-LG and mAb case studies, our results highlight the importance of detailed characterisation of protein solutions with orthogonal biophysical techniques so as to better understand protein solution rheology.

An additional study looking at the effect of polysorbate-80 upon protein rheology was made. In agreement with literature, this commonly used excipient in biopharmaceuticals was demonstrated to affect the rheological measurements of globular protein solutions. Amphiphilic brush-like poly(ethylene glycol) methacrylate polymers were also synthesised and tested as novel additives with β-LG and mAb solutions, for their potential effects

on protein solution rheology, similar to those observed with polysorbate-80. Preliminary results showed that the effects of these polymers are likely related to competition for the air-water interface, between these and the proteins involved. This competition leads to changes in the yield-like behaviour at low shear rates.

Acknowledgements

I would like to thank my supervisors Dr Stephanie Allen, Prof Cameron Alexander and Prof Clive Roberts for their guidance, support, patience and encouragement throughout these years.

I would like to thank my industrial supervisors, Dr Jai A. Pathak and Shahid Uddin, for their support, valuable input and suggestions throughout this work. I am grateful to Dr Jai A. Pathak for providing the opportunity of developing part of this dissertation's work at MedImmune, Gaithersburg, MD, USA. I am equally grateful to Shahid Uddin for allowing me to work at MedImmune, Cambridge, UK, for all the time needed to complete part of work presented here.

I would like to acknowledge the EPSRC and AstraZeneca, PLC, in partnership with the Centre for Doctoral Training (CDT), for the financial support of this project.

I am grateful to both MedImmune, LLC and Novozymes Biopharma, Ltd. for kindly donating material for this project.

At MedImmune I would like to thank: Dr Steven Bishop and Dr Andrew Donnelly, for allowing my visit to MedImmune, Gaithersburg, to happen; all those at the Formulation Sciences group, both at Gaithersburg and Cambridge, with whom I shared the labs, for providing training and for the welcoming work environment; Leanne Amery, for all the support during to my visits at MedImmune, Cambridge; Natalie DeJesus for assistance and advice on HPSEC while I was at MedImmune, Gaithersburg; Tom

Leach, for valuable input regarding the provided protein; Hardeep Samra, for training on CG-MALS experiments; Jared Bee, for training with tensiometry; Chris Van der Walle, Prasad Sarangapani, Malgorzata Tracka for useful discussions; Christel Veyssier (Analytical Characterisation, at Cambridge), for her guidance with SEC-MALS experiments; Marcia Carlson and Valeria Riguero (Purifications team at Gaithersburg) for assistance and guidance with monoclonal antibody purification; Arun Parupudi and Kathy Yu (Analytical Biochemistry group at Gaithersburg) for their assistance in CG-MALS training and surfactant quantification, respectively.

At the University of Nottingham, I would like to thank Dr Giuseppe Mantovani and Dr Johannes Magnusson for their input and support regarding the polymer synthesis stage of this project. Thank you to Dr Sebastian Spain for his assistance with chromatography characterisation and his valuable input and discussions.

I would like to thank Mr Paul Cooling and Mrs Christine Grainger-Boultby for their technical support at the University's laboratories. Thank you to Dr Claudia Matz and Dr Christina Grindon for their administrative support regarding CDT issues.

Special thanks to Mr Steve Goodyer at Anton-Paar, UK, as well as to the engineers, for their assistance in solving problems regarding the Anton-Paar instrumentation. Thank you to Dr Daniel Some, Dr Sophia Kenrick and Dr Julia Ferullo at Wyatt Technologies for their help regarding the CG-MALS experiments.

Thank you to all my colleagues, past and present, at the CDT, the LBSA group, Prof Cameron Alexander's laboratory, and to fellow graduate students working at MedImmune's labs, who made each lab such an enjoyable place to work. A warm thank you to those colleagues that became dear friends, for being supportive and sharing both the highs and lows of this journey: Abdennour, Valeria, Paulina, Andrea, Gökçen, and Aalae. My acknowledgements also go to my dear friends in Portugal - Sofia, Alexandra, Ana Sofia and Ângela - that always encouraged me, despite the distance.

I am extremely grateful to my family for their kind support, encouragement and their individual examples of preseverance that inspired me throughout these years.

I am forever indebted to Pedro Varela Saraiva for his loving friendship, encouragement and support, his infinite patience and understanding at all times, but especially when it was most required.

Contents

List of Figures

List of Tables

Abbreviation	Explanation
β-LG	β-lactoglobulin
$[\eta]$	intrinsic viscosity
A_2	self (or second) virial coefficient
ATRP	Atom transfer radical polymerisation
CD	circular dichroism
CG-MALS	composition gradient multi-angle light scattering
cIEF	capillary isoelectric focusing
CP	cone-and-plate
CSR	controlled shear rate
CSS	controlled shear stress
Cu	Copper
DG	double-gap
DI	Deionised
DLS	Dynamic Light Scattering
DSC	Differential scanning calorimetry/ calorimeter
DWR	Double wall-ring

Abbreviation	Explanation
ECD	equivalent circular diameter
HMWS	High molecular weight species
HPSEC	high performance size exclusion chromatography
HSA	Human Serum Albumin
H_D	Hydrodynamic diameter
kDa	kilo Dalton = 10^3 g/mol
LMWS	Low molecular weight species
LRP	Living radical polymerisation
LVE	linear viscoelastic
mAb	monoclonal antibody
MALS	multi-angle light scattering
MCR	Modular compact rheometer
MFI	micro-flow imaging
M_n	Number average molecular weight
Mw	Weight average molecular weight
Mp	peak molecular weight
MW	molecular weight
mVROC	microviscometer/rheometer-on-a-chip

Abbreviation	Explanation
NTU	nephelometric turbidity units
PEG	Poly(ethylene glycol)
pI	isoelectric point
PS-80	polysorbate-80
rAlbumin	recombinant human albumin
RI	refractive index
SDS-PAGE	Sodium dodecyl sulfate polyacrylamide gel electrophoresis
SEC	Size exclusion chromatography
SLS	static light scattering
TEA	triethylamine
TFF	tangential flow filtration
UV	Ultraviolet

Chapter 1

Introduction

1.1 Introduction

For the past two decades, advances in recombinant DNA technology have allowed a progressive change in therapeutics from small molecule therapies to biological macromolecular formulations, including medicines where the active ingredients are peptides, proteins and nucleic acids. The target specificity of protein drugs, reaching the potential for low side effects in comparison to small molecule drugs, along with advances in protein production at large scales with lower costs, lead to a significant role of protein therapies in the pharmaceutical industry [1, 2].

Currently there are various protein formulation strategies, spanning from the traditional parental administration route of a protein solution with stabilizing additives, to new strategies that explore new administration routes (e.g. non-invasive mucosal route) or others which are more adequate to the macromolecule's specific properties or pharmaceutical needs (e.g. sustained protein formulations) [3].

In protein therapeutics, monoclonal antibodies (mAb) have been essential in medicine targeting many diseases such as rheumatoid arthritis, inflammation, cancer and infectious diseases [1]. Monoclonal antibodies constituted 20 % of biopharmaceutical

products in 2008, where projections were that this value would increase in coming years [1, 2]. With advances in biotechnology, in particular of methods to clone murine and human antibody sequences, the generation of monoclonal antibodies has moved from fully murine to fully humanised constructs. Also contributing to the success of monoclonal antibody therapeutics are the technological developments related to mAb expression and purification [4]. However, to formulate such complex molecules in stable formulations, it is necessary to understand the protein's physicochemical properties and thermodynamic stability [1, 2].

The administration route normally chosen for protein formulations has largely been intravenous, since it is a faster and easier way to formulate; allowing better bioavailability than most other routes and good control in administration [5]. The subcutaneous route presents a good alternative for products that require a higher frequency of administration. This route also has the advantage of allowing a better quality of life for the patient, providing the potential of using devices such as auto-injectors or pre-filled syringes permitting home use [6]. However, therapeutic proteins such as monoclonal antibodies often need to be delivered in high concentration for increased bioavailability even if administered frequently, due to its low potency. At high concentrations, e.g. 100 mg per dose or higher, special care is required in formulating these medicines so that a convenient use of an aqueous low volume (1 - 1.5 mL) solution can be administered through the subcutaneous route [7, 8].

Many challenges arise when formulating a suitable aqueous highly concentrated protein formulation. Not only there are difficulties in stability, but there can be challenges in manufacturing processes and delivery [5]. Considering stability challenges, these are present in general protein formulations and are divided between chemical and physical instabilities [1]. Aggregation and denaturation are the major pathways to physical instabilities in protein formulation. In medicines where protein is in high concentration,

the presence of water is reduced and chemical instabilities that are hydrolytically driven are less expected to induce degradation. However, aggregation is highly dependent on concentration, and therefore is the primary expected pathway to instability of high concentration protein formulations [1, 5]. With reduced volume and the increased possibility of occurring aggregation, high viscosity is frequently observed in these formulations. Highly viscous solutions can impair the manufacturing process, and are impractical for patient use because using a larger needle gauge can lead to pain at administration as well as more force required to inject [2, 9].

Characterising and studying the properties of a high concentration protein formulation often involves dilution for sample analysis since commonly used techniques require this (e.g. such as dynamic light scattering, size-exclusion chromatography, analytical ultracentrifugation) [10]. By diluting the sample, one may possibly create artifacts (e.g. dissociating soluble aggregates), thus disallowing a proper investigation of high concentration formulation [11]. Due to such analysis challenges, the effect of high concentrations within protein formulations is still poorly understood at a molecular level, and in particular how molecular interactions within these formulations can lead to aggregation and high viscosity [6, 9]. In addition, understanding the effect of excipients on such processes/properties is crucial, so that we are able to understand and manage the challenges.

1.2 Main Aims

The work described in this thesis had the main aim of understanding protein solution rheology from a biopharmaceutical perspective, with account of the biophysical properties of proteins and in particular their level of aggregation. Therefore, one of this thesis aims was focused on understanding the molecular basis of rheological properties of high protein concentration solutions using a commercially available biopharmaceut-

ical formulation as a model. The other aim of this thesis was to understand how the level of aggregation of protein solutions and their underpinning molecular interactions can influence their rheological measurements. Finally, another aim of this thesis was to explore the impact of surface active organic molecules on protein solution rheology.

1.3 Protein formulations - monoclonal antibody formulations

As mentioned earlier, monoclonal antibody formulations constitute an important section within protein formulations. However, it is assumed that achieving commercially viable antibody products is not straight-forward [1]. Consequently, this has translated into a thriving development of technology involved in formulating such therapeutic biomacromolecules.

The following sections describe briefly the antibody structure and function, their common instabilities, and a general background on formulation development and characterisation, focusing on high antibody concentration formulations and its relationship with viscosity, fitting the remit of this thesis.

1.3.1 Antibody structure and function

Antibodies, immunoglobulins, are a family of multidomain glycoproteins in a Y-shape or can be a combination of such molecules. These soluble proteins are present in the serum, tissue fluids or on the cell membranes. Their purpose is to help eliminate their specific antigens or microorganisms bearing these antigens [12]. The structure of an immunoglobulin is divided into two regions: the variable (V) region, which is on the top part of the Y-shape; and the constant (C) region, which is the stem of the Y. Immunoglobulins comprise five classes - IgA, IgD, IgE, IgM and IgG. This division is based on

the C region, denominated as α, δ, ϵ, μ, and γ, respectively.

IgGs are the most abundant immunoglobulin, accounting for 70-75% of total serum immunoglobulin pool, occurring as monomers. Also, IgGs are widely used for therapeutic purposes as a therapeutic agent (monoclonal IgGs) [1,12]. The primary structure of IgGs is defined by a four-chain structure with two identical heavy chains - H, 50 kDa - and two identical light chains (L, 25 kDa) (Figure 1.1). The typical molecular weight of IgG is between 146-170 kDa [1,12]. IgGs are divided into subclasses: IgG1, IgG2, IgG3 and IgG4, which is in order of typical quantity present in human plasma. This division is due to different heavy chains, named γ1, γ2, γ3, and γ4, respectively. The difference among the isotypes (subclasses) are the interchain disulfide bonds (number and location) and the length of the hinge region [1,12]. Regarding the light chains, which can be of two types: lambda (λ) and kappa (κ). Either light chain type may combine with any of the heavy chain types, but within any individual immunoglobulin molecule both light and heavy chains are of the same type [12].

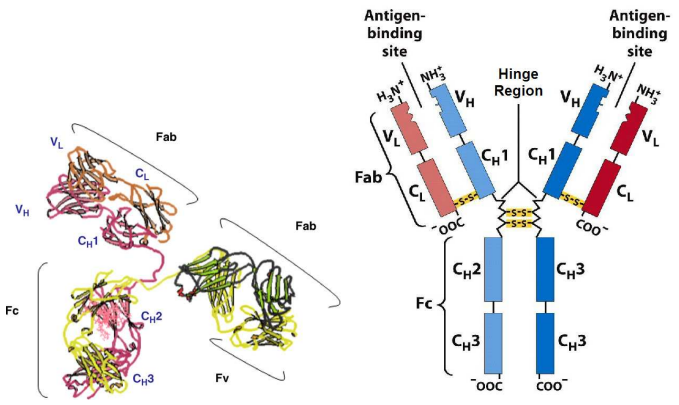

(a) (b)

Figure 1.1: Molecular architecture of an IgG: a) ribbon model (adapted from [4]); b) schematic model (adapted from [13]).

The variable regions of both light and heavy chains consist approximately of 110

amino acids, forming the antigen-binding regions (Fab fragment). The remaining sequence of amino acids are part of the constant region, forming the Fc region (fragment crystallisable) [1]. The constant domains of the heavy chains are generally designated as C_H1, C_H2, C_H3 and C_H4. The V regions are divided into hypervariable sequences - HV1, HV2 and HV3 - on both heavy and light chains. The HV sequences are referred to as complementarity determining regions - CDR1, CDR2 and CDR3, which form three loops at the edge of the β barrel. The three CDRs from the light chain are called L1, L2 and L3, in order of appearance in the sequence. Correspondingly, the three CDRs from the heavy chain are called H1, H2 and H3. Other sequences are the framework regions - FR1, FR2, FR3 and FR4. These form β-sheets and determine the fold that help the CDRs to be close to each other, maintaining the folded structure [1, 12, 14].

The secondary structure of IgGs comprises the polypeptide chains assembled in anti-parallel β-sheets which represent roughly 70% of total structure. Two domains form the light chains while four domains form the heavy chains, each of these domains are approximately 110 amino acid long ($\sim$12 kDa in size). All of these domains form a β barrel, called the immunoglobulin fold [12]. This structure is stabilised by a disulfide bond and hydrophobic interactions. Each of these domains interact amongst themselves, are linked by the hinge region and form three spherical shapes of similar size. These spheres give the Y-shape configuration to the antibody. Its less globular shape is stabilised by interactions via disulfide bonds and strong non-covalent between the heavy chains and each of the heavy/light chain pairs [1, 12].

In general, IgGs have four interchain disulfide bonds: two connecting the two heavy chains at the hinge region; and two connecting the two light chains to the heavy chains. Four intrachain disulfide bonds are also present within each domain of the heavy and light chains which help stabilise the domains. The intrachain dissulfide bonds between the V_H and V_L are required for functional antigen binding [1].

As mentioned above, IgGs have two functional areas - the V and C regions. The CDR regions with the framework regions are specifically the antigen-binding sites at the end of the Fab arms, shown to have a unique surface topography that seems to be complementary to structures on the antigen [4,12]. Regarding the constant region of antibodies, these have three main effector functions: (1) initiating antibody-dependent cell cytotoxicities (ADCC), being recognised by receptors on immune cells; (2) by binding to complement; and (3) being transported throughout the organism to many places, such as tears and milk [1]. The IgG subclasses interact with cellular Fc receptors (FcγRI, FcγRII and FcγRIII) expressed on various cell types (e.g. monocytes, neutrophils, eosinophils, lymphocytes). These receptors are characterised by a glycoprotein α chain that binds to the antibody and has extracellular domains homologous with the IgG domains, i.e. they belong to the immunoglobulin super family. These receptors may be upregulated or induced by environmental factors (e.g. cytokines) [12].

An oligosaccharide chain is found in IgGs, typically N-linked to the conserved asparagine Asn 297 residue present between the C_H2 domains. This oligosaccharide is normally fucosylated in antibodies produced in CHO or myeloma cell lines and may differ in other cell lines [1]. There are many factors that determine the nature of the glycan micro-heterogeneity on IgGs, including cell line, the bioreactor conditions and downstream processing. It has been shown that the sugar composition also influences functionality. For example, other oligosaccharides can be found in IgGs due to process, and the presence of oligosaccharides in other regions rather than in C_H2 domain, can influence the antibody's activity. It is essential that correct glycosylation of the antibody occurs, since it is critical for the binding and activation of Fc receptor. Also, it has been shown that glycosylation can affect antibody conformation, since it can form multiple non-covalent interactions with the polypeptide [1, 12].

All purified monoclonal antibodies (mAbs) are heterogeneous in structure due to

differences in glycosylation patterns, instability throughout production and terminal processing. Examples of this are occurring deamidation forms in both heavy and light chains or, more rarely, formation of abnormal heavy chains with less amino acid residues than normal heavy chain. [1] Undesirable post-translational chemical modifications, such as asparagine deamidation, or degradation products are also sources of molecular variability in antibody engineering. However, these problems can be solved by prediction of problematic residues and omitting these from the sequence of the coding gene [4].

1.3.2 Instability in protein formulations

Like other proteins, antibodies are subject to a number of degradation pathways. These pathways are divided into chemical and physical instabilities.

1.3.2.1 Chemical Instability

Numerous chemical degradation pathways have been reported. Proteins may lose biological activity depending on the site where the chemical changes occurred [1]. The major chemical degradation pathways occurring in an antibdoy are dissulfide formation/ exchange, cross-linking, deamidation, isomerisation, oxidation and fragmentation.

Disulfide Formation or Exchange

In native proteins / peptides, cystein is rarely in the reduced form, being present typically linked with another cysteine residue as a cystine disulfide (R-S-S-R). In the presence of other thiols (H-S-R'), a disulfide can interchange to give a mixed disulfide (H-S-S-R') [15]. This type of chemical instability a common pathway for cross-linking, influencing increased protein aggregation [11]. A participating thiolate ion can come

from a free cysteine in a reduced peptide or protein, or it can come from species added or occurring during numerous processing steps, such as lyophilisation [1, 15]. This type of degradation reaction is base catalysed, which means that peptides or proteins cystine-rich should not be stored in alkaline pH buffers [1, 15].

Non-reducible Cross-Linking

Non-reducible cross-linking between proteins has also been observed as a possible degradation pathway. Nonreducible cross-linking can lead to high molecular weight aggregates that cross-link due to other chemical pathways than disulfide formation, such as oxidative steps. It can occur during storage in either liquid or solid protein products [1].

Deamidation

Deamidation has been extensively reported in literature [1, 16–19]. It is the most common chemical degradation pathway that occurs in proteins which is a nonenzymatic covalent modification. Deamidation can occur in both liquid and solid state and during storage [1]. In proteins corresponds to conversion of asparagine aminoacid residue (Asn) to aspartate or iso-aspartate, by loss of an amide functional group, release of ammonia and transformation to acidic groups. The pathway goes through the intermediate of succinimide at Asn and Gln (glutamine), occurring more readily in the former [1, 20]. This reaction occurs in water-accessible regions of proteins at basic or neutral conditions. The key step is the formation of a deprotonated amide nitrogen which attacks a side-chain carbonyl, resulting in a tetrahedral intermediate and formation of the succinimide ring. The ring is then subject to hydrolysis, resulting in either aspartic acid or the iso-aspartic acid [20]. Although depending on the protein, deamidation can result

in thermal instability or further chemical susceptibility, influencing in many cases the protein's secondary structure by affecting its folding pattern [20, 21].

Many factors, such as sequence, steric effect and pH can affect the deamidation rate via succinimidation in proteins. Buffers, ionic strength, solvents and polymers and sugars have been studied to allow stabilisation of proteins and peptides in order to minimise deamidation [20].

Isomerisation

Isomerisation in proteins commonly occurs with formation of iso-aspartic acid, which results from direct isomerisation of aspartic acid (Asp) and from hydrolysis of succinimide intermediate. This intermediate's production can be pH dependent occurring either due to asparagine deamidation or aspartate dehydration. It has been shown that pH and steric effects can influence the rate of this degradation [22, 23]. In general, modifications of amino acid side chains by both deamidation and isomerisation may lead to a different conformation of the protein which can potentially lead to aggregation or self-association [11].

Oxidation

Amino acid residues in proteins that can be oxidisable are methionine (Met), tyrosine (Tyr), tryptophan (Trp), histidine (His), cysteine (Cys), phenylalanine (Phe) and proline (Pro). Although not as prevalent as deamidation or isomerisation, oxidation can easily occur during storage of antibodies. A variety of oxidation initiators have been reported, such as photochemical, metal ion catalysed, high energy γ-radiation and sonication by generation of reactive oxygen species [1, 20]. This degradation pathway

can lead to a change in biological activity of the therapeutic protein if a critical residue for that particular activity is oxidised, or by leading to conformational change due to oxidation [20].

Fragmentation

This kind of chemical degradation may occur in antibodies during production processes: acidic and basic treatments, thermal stress, freeze-thaw and storage [1,24]. Fragments can be masses of antibodies without a light-chain or a Fab arm, or separation of heavy-chain and light-chain. The hinge region is very susceptible to enzymatic and nonenzymatic cleavage, leading to fragmentation of the antibody. As examples of enzymatic fragmentation, papain and pepsin are the most common enzymes to generate antibody fragments, cleaving the antibody in the hinge region or in its proximity (C_H2 domain) [24]. Hydrolysis is the mechanism that can explain nonenzymatic fragmentation in the hinge region, being pH and temperature two accelerating conditions for this degradation pathway [24]. Other less common species, resulting in both peptide and/or disulfide bond cleavage can occur as fragments [1].

Other chemical degradation pathways

Additional degradation pathways include the formation of acidic and basic species and terminal clipping.

Acidic and basic species formation is influenced by deamidation, making the formation of acidic or basic species of an antibody an easy indication of deamidation. pH-dependency is most likely to be the source of this chemical instability. Another pathway that can lead to acidic or basic forms of antibodies is the Maillard reaction, where re-

ducing sugars can react with amino acid residues leading to glycosylation [20, 25]. This reaction results in more acidic antibody species (negatively charged). The formation of basic species can also result from succinimide formation or removal of sialic acids [1].

Terminal clipping can occur during antibody production and processing, possibly due to the action of basic carboxypeptidases during product processing [1, 15, 26].

1.3.2.2 Physical Instabilities

Two major physical instabilities are protein denaturation and aggregation [1, 27].

Denaturation

When proteins cannot remain stable indefinitely in the folded native state, they undergo processes of denaturation, i.e. changes of its conformation, thus changing from its native state (unfolding) [27]. A protein unfolding process can include an intermediate step, usually unstable, between the completely folded and the unfolded protein monomer [27, 28]. At an extreme state, these unfolded monomers can eventually lead to protein aggregation (see below for more detailed explanation). However, not only the unfolding state can be reversible but this process can involve partially the native state, i.e. unfolding can be localised within the protein monomer [28].

There are many conditions that can lead to antibody denaturation, including temperature change, and processing steps.

In terms of protein unfolding due to temperature, it occurs only when above a certain temperature, denoted as 'melting temperature', where the higher this temperature is, the more thermally-resistant the protein is. Proteins can exhibit more than one melting temperature, depending on the experimental and analytical settings used [27]. In the case of monoclonal antibody formulations, it is often to evaluate conformational stabil-

ity in the presence of various formulation (solution) conditions via determination of the protein's melting temperature [7].

As mentioned above, proteins can suffer denaturation (and eventually aggregation) during production, transportation, storage and delivery steps, during which shaking and stirring may occur. It has been recently demonstrated that denaturation due to shear/ shaking is more likely to occur when air-liquid or solid-liquid interfaces are present [29–32]. As an example, a study evidenced that directly inserting a needle through an air-liquid interface of a protein solution yielded to observation of protein aggregates that are suggested to only occur at the interface [33].

Indeed, protein adsorption to surfaces is a well documented circumstance that can lead to protein unfolding [34–37]. This can occur since proteins present surface activity, where in the case of fluid interfaces, this translates in a decrease of interfacial surface tension [35]. It is the molecular structure of proteins the main factor which controls adsorption to interfaces, with its charge distribution and hydrophobicity determinant to this phenomenon, depending on the interface, e.g. if it is highly charged or highly hydrophobic [34]. In its native folded state, a protein monomer tends to have its amino acids with h hydrophobic residues buried in its core, hidden from contact with solvent to allow the protein to remain molecularly soluble. However, proteins can still have some amino acids with hydrophobic side chains in towards the surface of the molecule, which can readily absorb at the interface. After adsorption, the protein can suffer conformational rearrangements that lead to partial or further unfolding [28, 34]. Once unfolding occurs, inter-protein associations can occur and lead to aggregation [38].

Aggregation

Aggregation in antibody formulation is the most common manifestation of physical

instability. Protein aggregates can be present and produced in liquid and solid formulations depending on various conditions. Protein aggregation can be due to protein-protein interactions, depending on the diffusion rate and geometric constraints of the interaction sites. Factors such as concentration, pH, ionic strength, viscosity, and temperature can influence the aggregation rate. Other factors such as shearing/shaking, long-term storage or freeze-thawing may also affect antibody aggregation [1].

For therapeutic antibodies, a consequence of aggregation is that aggregates can lead to reduced activity and increased immunogenicity potential due to conformational changes and/or higher recognition by the immune system [10]. Therefore, it is important to control the aggregate level in antibody formulations assuring that therapeutic protein formulations remain at their highest purity levels possible complying with U.S. and European Pharmacopoeias [39].

Protein aggregation is comprised of multiple pathways. Figure 1.2 shows a scheme that demonstrates the various steps involved, focusing on bulk solution conditions. In the figure, starting with a folded protein ($\mathbf{F}$) in its native state, it can form strongly associated multimers between two or more folded monomers ($\mathbf{N}_y$) [40]. Another type of folded self-association is when self-association oligomers ($\mathbf{F}_2$, $\mathbf{F}_3$) form from folded monomers. These monomers are formed via colloidal forces, i.e. "weak" inter-particle interactions. Due to the nature of these interactions, formation and dissociation of these protein oligomers can be described as an equilibrium [41].

The other steps represented in this figure refer to aggregation starting from a non-native (partially unfolded) protein monomer ($\mathbf{R}$). In this case, $\mathbf{R}$ is representative of a 'reactive' monomer that will form oligomers of irreversible nature ($\mathbf{A}_x$), at the conditions the aggregation occurred (e.g. due to thermal stress) [28]. The 'reactive' partially unfolded monomer can generate further oligomers ($\mathbf{R}_2$, $\mathbf{R}_x$), denoted pronuclei that can

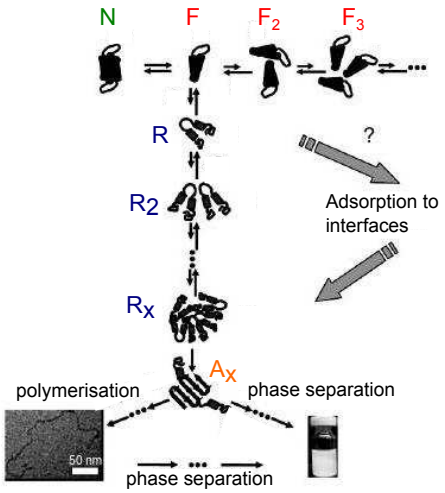

Figure 1.2: Scheme illustrating multiple stages and pathways to protein aggregation (adapted from [28]).

be of reversible nature. It is from these pronuclei that a further step leads to irreversible aggregates ($\mathbf{A}_x$). These can be termed nucleus, and can include several monomer chains (x), constituting dimers ($x = 2$), oligomers ($x = 3$ - 10) or multimers [28, 42]. The mechanisms described here are related to non-native aggregation occurring in bulk solutions, however the presence of interfaces (e.g. air-liquid, or solid-liquid) can integrate this scheme as precursor of those species [28]. Finally, Figure 1.2 refers to behaviour that aggregates can follow: 1) remaining soluble in solution while not suffering substantial addition of 'reactive' monomers; 2) remaining soluble but continue to increase the monomer chains associated, creating higher molecular weight species (in relation to the monomer's molecular weight); 3) are soluble but can self-assemble to create protein precipitates (visible particles) or even lead to a change in phase (e.g. gel) [43].

As discussed earlier, in bulk solution, thermal stress can induce chemical degradations to proteins, also leading to non-native forms [11, 38]. A chemical modification of native form of the protein can lead to aggregation, since it often induces change to non-native form. [11, 38]. Another possible mechanism can imply the generation of critical nucleation due to a possible formulation contaminant. In this case, continuous addition

of native protein to the nucleus will eventually lead to visible particulates or even precipitation [38]. Freeze-thawing is an example where such aggregation mechanism could occur, not only due to ice-solution interface present, but also due to pH changes when crystallisation of buffer occurs as well as saturation of protein and solutes when cryo-concentration occurs [11].

1.4 Types of formulations

According to Wang (1999), protein stability can be defined by the result of balancing between the stabilising forces, provided by protein-protein interactions, and destabilizing forces, mainly due to the protein's tendency to unfold [27]. The balance can be disrupted to by one or several of the degradation pathways which were described in the previous section. Therefore, formulating monoclonal antibodies as therapeutic agents has the purpose of controlling degradation and instability in order to allow for an adequate shelf life for commercialisation. The most adequate formulation is done by choosing formulation excipients (also denoted as additives) and conditions. However, it is known that conditions and excipients chosen for a specific antibody to be formulated might not be appropriate for another molecule due to small structural differences in each protein. A successful formulation is defined as providing stability of the antibody as well as keeping its activity and reducing potentiality of immunogenicity. Ideally excipients should remain inert, be well tolerated and should not interfere with antibody's structure and activity, but contribute to protein stability [1, 2, 44].

In recent years, several reviews have been published regarding therapeutic protein formulations (generally applied to antibodies) [1, 2, 27], types available [1, 3], and regarding excipients commonly used and their effect in protein stabilisation [44].

Liquid formulations are easily administrated and typically less expensive to produce

compared to lyophilised drug products. However, A successful liquid formulation needs to consider several aspects: protein concentration; effect of pH; buffering agents; effect of formulation excipients including preservatives; effect of shearing / shaking; process equipment used and product containers [1, 2].

Some antibodies cannot be formulated in liquid state, hence the necessity of turning to lyophilised formulations. Critical issues of formulating in this solid state are to be considered, such as the state that the protein is more stable at, the effect of formulation excipients, effect of pH and buffering agents, protein concentration and moisture content [1, 27]. Lyophilising a protein formulation not only focuses on maintaining stability, it also means focusing in appropriate tonicity. However, during lyophilisation, isotonicity can be difficult to achieve since both the protein and the formulation excipients can be highly concentrated [5].

A widely applied method of increasing plasma half-life of proteins is to increase its size by conjugating a poly(ethylene glycol) (PEG) molecule to the protein. This technique has been applied to antibody fragments that showed less half-life than when the molecule contained its Fc portion. Conjugation of PEG is usually performed by attaching site-specifically a PEG to an engineered antibody showing a PEG-reactive residue. Site-specificity is important to reduce interference on losses in binding activity when PEGylation occurs [1, 27].

Controlled release systems have been applied for proteins. The use of biodegradable polymers, such as poly (lactic-glycolic) acid (PLGA), can offer controlled release of antibodies [1, 3].

1.5 Formulating Solutions of High Protein Concentration

Typically, the amount of therapeutic protein tends to become relatively large per dose ($>$ 1 mg/kg), to attain the therapeutic effect [1]. A higher dose can mean that a large

volume has to be infused, but due to out patient administration requirements, other routes of administration are needed, such as subcutaneous route. Hence, it is necessary to formulate therapeutic antibodies in high concentrations (> 50 mg/mL) with reduced volume (< 1.5 mL) [8].

Formulating at high protein concentration has shown to present many challenges. Not only it can affect protein stability, but it poses challenges to manufacture as well as the administration of the protein drug by injection. Subcutaneous syringes are equipped with 26 or 27 gauge needles (or of even higher gauges) which, if the preparation is too viscous, may restrict administration. This represents the most challenging factor for formulation at high protein concentration. Not only viscosity is related to painful delivery but also means that it takes longer to deliver the requested amount, even if in a pre-filled syringe. Therefore, it is very important to adjust and carefully study how to formulate in order to prevent or control the product's viscosity towards a good performance, not only keeping in mind stability, but also manufacturing and delivery issues [1, 5, 8].

Achieving high concentration largely depends on the solubility of each therapeutical potein. For practical purposes, protein solubility can be described as the maximum amount of protein in co-solution with excipients, where the solution does not precipitate nor generate a sediment [5]. Therefore, low protein solubility refers to *in vitro* situations, which involves proteins that are expressed, purified and folded at room temperature, but cannot be concentrated sufficiently for pharmaceutical or industrial applications [45]. Knowing what is the highest protein concentration achievable is still an empirical task due to the protein's conformational change, adsorption to surfaces and specific excipients, and more importantly, its capability to self-associate [5].

Factors such as ionic strength, salt form, pH, temperature and excipients, can condition protein solubility [5, 45]. Protein solubility can also depend on how hydrated proteins are by certain salts, amino acids or sugars, depending on these excipients' in-

teraction with the macromolecule [46, 47]

1.5.1 Factors leading to high viscosity at high protein concentration

From the study of flow and hydrodynamics in colloidal suspension rheology, it is known that a material's viscosity is a physical property which is sensitive to the material's characteristics and to the properties from its surrounding environment [48, 49]. Therefore, in protein solutions, it is assumed that its specific properties such as shape, size and charge, are important to consider when studying its flow behaviour [50].

Aggregation is expected to be the primary degradation pathway in highly concentrated protein formulations, since it depends in protein solubility and is influenced by various interactions including protein-protein, protein-water, protein-ion and ion-water interactions [5, 9, 45]. As previously described, aggregate formation depends on the size of aggregates as well as the numerous mechanisms of association, which can occur simultaneously within the same product [38].

As described earlier, one form of protein aggregation is reversible self-association, of either native monomer or non-native (partially unfolded) monomers. Reversible self-association has been poorly studied, since the reversible aggregates may not be present after a dilution is performed, thus being a limitation of analytical methodologies commonly used for aggregate detection. Moreover, when the rate of self-dissociation is low, this condition may impact formulation and possibly affect the protein's activity and pharmacokinetics [51]. At high protein concentration, the equilibrium could be shifted towards a greater amount of aggregates due to macromolecular crowding effects [5].

Whilst aggregation is due to formation of intermediate states leading to reversible association or aggregation, protein-protein interactions are predicted to be the major precursors of high viscosity at high concentrations [9, 52].

Macromolecular crowding, as defined by Zhou *et al.*, are the effects attributed to excluded volume on the energetics and transport properties of macromolecules within a solution of high concentration of macromolecules [53]. The author also refers macromolecular confinement to be related to the effects attributed to excluded volume on the free energy and reactivity of a macromolecule with fixed boundary, i.e. small compartments such as cytoskeletal structures, with an interior dimension only slightly larger than the dimension of the largest macromolecule. Both macromolecular crowding and confinement influence the equilibria and kinetics of macromolecule association [5,53]. As the protein concentration increases, the fraction of total volume occupied by the protein increases resulting in the effective volume available to the protein decreasing. This leads to an apparent higher protein concentration that favours self-association. This association is thought to be one of the common macromolecular reactions to crowding and confinement to increase the available volume, as well as formation of irreversible aggregates. These solutions represent a non-ideal solution behaviour of increasing thermodynamic association which may be shelf-life limiting, particularly when the aggregates become irreversible [5, 53–55].

Apart from these thermodynamically driven reactions, non specific protein-protein interactions occurring in solution also play a part in highly concentrated macromolecular solutions. The effects of protein-protein interactions have been explained by a model in which macromolecules in solution, such as proteins, are comparable to effective hard spheres, whose apparent size reflects not only steric effect but also short-ranged attractions or repulsions [53, 56]. However, this theory does not explain fully what occurs in solutions containing high concentration of multiple solute species [56].

Non specific protein-protein interactions are mainly contributed by hydrogen bonding, steric (excluded volume - i.e. volume of solution unavailable for another incoming molecule), electrostatic, van der Waals and hydrophobic interactions. Of these, elec-

trostatic and hydrophobic interactions are the major forces conducting protein-protein interactions in a dilute solution. When a protein solution is highly concentrated, this is changed [9]. The strength of the overall forces present between protein interactions is expressed as a potential (W). This potential measures the force between two protein molecules averaged over all possible orientations and configurations of the solute and solvent molecules. The intermolecular centre-centre distance is represented by (r). The following equation represents the potential between two interacting proteins (W_{22}):

$$W22(r) = W_{hs}(r) + W_{charge}(r) + W_{disp}(r) + W_{osm}(r) + W_{assoc}(r) + W_{dip}(r) \qquad (1.1)$$

In this equation, W_{hs} is the hard sphere (excluded volume) potential, W_{charge} refers to charge-charge interactions, W_{disp} is the attractive potential referred to van der Waals forces, W_{osm} accounts for osmotic effect of added salt, W_{assoc} is related to the self-association interaction of proteins, and W_{dip} represents the interactions due to permanent and induced dipole moment of interacting molecules [9, 57].

Forces that are inherently repulsive are charge-charge interactions and excluded volume, resulting in a positive second virial coefficient. Excluded volume interactions arise due to the inability of the centre of the molecule to penetrate the surface of another molecule, hence becoming a repulsive force [50]. In high protein concentration, due to smaller centre-centre distance, attractive and excluded volume forces are largely responsible by protein-protein interactions. Although all the interactions mentioned above have their role in a protein solution, it is still difficult to predict solution behaviour in all highly concentrated protein solutions, since it depends strongly on the involved protein [9].

It has been discussed in literature that strong protein-protein interactions may explain deviations from ideal behaviour of protein solutions, detected in different properties, such as osmotic pressure, density, rheology, sedimentation, among others [9]. Thus,

studying and identifying non specific protein-protein interactions is important to protein stability when the solution is modified under different conditions.

Factors influencing viscosity in protein solutions also include the molecule's intrinsic viscosity and hydrodynamics [9]. Intrinsic viscosity is dependent of the protein's hydrodynamic behaviour in solution and represents the effective molecular volume when at (i.e. close to) infinite dilution [48]. The electroviscous effect is discussed to be a overall sum of three effects that influence a protein's intrinsic viscosity: (i) a diffuse double layer of the macromolecule; (ii) repulsion caused by double layers of two macromolecules; and (iii) intermolecular repulsions that affect the shape of the molecule. Thus, this effect is dependent on pH and ionic strength [50, 58].

1.5.2 Brief review of revelant studies concerning therapeutic protein solution rheology

Rheology is the study of the flow or deformation of materials [48, 59]. It has been applied to the study of globular protein solutions, mainly due to the interest of food science [60–62] and biologically relevant fluids (e.g. blood and synovial fluid) [63, 64]. In this section we summarise recent developments in the study of the flow properties of therapeutic protein solutions.

Reversible self-association in therapeutic monoclonal antibodies and its relationship with solution viscosity has been studied [6, 51, 65]. The work of Liu *et al.*, demonstrated that the viscosity of one of the study's mAbs was highly dependent on its concentration, pH and ionic strength of the buffer used. This study found that reversible self-association was the cause behind the solution's high viscosity, where at high ionic strengths a decrease of solution viscosity was observed, thus related to a disruption of electrostatic charge interactions [6]. This study also demonstrated the effects of arginine to reduce

the viscosity of a highly concentrated mAb solution [6]. Arginine is an amino acid commonly used in protein formulations due to its studied interactions with protein, which have also been reported to generally improve a mAb's solubility and stability. The mechanisms involved in arginine-protein interactions appear to be of various nature, that include preferential hydration of the protein molecule [44].

The work by Kanai *et al.* studied the effect of different ions of the Hofmeister series (from kosmotropes to chaotropes: SO_4^{2-}, Cl^-, Br^-, I^-, and SCN^-) with solution rheology of the same monoclonal antibodies used in the previously described study [51, 66]. It has been shown that the Hofmeister phenomenon has implications in direct interactions between the ions and macromolecules, which cannot be fully explained by changes in bulk water structure caused by these ions [66]. Kanai *et al.* showed that chaotropic agents (which destroy bulk water structure), such as urea and guanidine HCl, reduced solution viscosity more than kosmotropic agents (which contribute to bulk water structure). The authors also compared between full length mAb with its fragments, to understand which domain would be implicated in reversible self-association [51].

Studies have also attempted at relating opalescence at high protein concentration with high viscosity and degree of aggregation [67, 68]. The degree of opalescence in a solution is related to the light absorbed or scattered on account of submicroscopic optical density inhomogeneities of opalescent / turbid suspensions or solutions [69]. These authors were able to demonstrate the relationship between ionic strength on the effective charge of mAbs and its effects on viscosity and opalescence [50, 67].

It has been demonstrated how the non-ideality of rheological behaviour of high protein concentration is influenced by protein-protein interactions as well as fundamental properties of the therapeutic molecules, such as their charge [50, 52, 70–73]. With high surface charge and low ionic strength, this overall effect is expected to govern protein solution behaviour [50]. Specific highly attractive interactions present in therapeutic

proteins have been evidenced to influence the studied proteins' charge-dependent interactions, suggesting that it can explain the pH dependency of the measured high viscosities, relating this to electroviscous effects [70, 71].

Regarding rheometry and viscometry in most literature studying rheology of therapeutic protein solutions, the type of instrumentation typically chosen is cone-and-plate[1] rheometers [6, 9, 50, 51, 74]. Glass capillary or falling ball viscometers have also been used [74, 75].

However, as antibody products are still relatively expensive to produce, contributing to the difficulty of accessing large quantities of material, there has been development of instrumentation and techniques capable of measuring viscosities from materials at sample volumes in the order of μL, constrasting to the volume of up to 1 mL when using a cone-and-plate rheometer.

The system devised by Kalonia and colleagues, is based in a piezoelectric quartz crystal, which is sensitive to the mechanical properties of the liquid placed on top of it. By monitoring the quartz crystal's electrical properties, it is possible to take measurements at high frequencies (10 000 Hz), imparting such high stresses to the sample and extracting its viscosity. An announced advantage of this system is the possibility of using microlitre volumes (10-20 μL) [50,76,77]. Another example of an instrument using relatively low quantities of sample is the microfluidics microviscometer/rheometer-on-a-chip which has also been proven to be useful for protein solution rheology measurements [78]. Due to its construction and the operating principle[2], this instrument typically allows only measurements at high flow rates (that translate into shear stresses) [79]. This can be an advantage, since it can allow exploring the viscosities of antibody formulations at high flow rates similar to those achieved during syringe injection [8].

[1]The theoretical background to rheology and relevant instrumentation is described in Chapter 2.

[2]Detailed information regarding the microviscometer/rheometer-on-a-chip can be found in Chapter 2.

An indirect measurement of protein solution viscosity using dynamic light scattering has been reported [80–82]. In this case, polystyrene particles of known diameter are mixed with protein solutions and the particles' apparent hydrodynamic size is measured. Based on this instrument's operating principle, this apparent size can then be converted to viscosity. It has been regarded as a technique with potential advantages due to small sample volume used and fast measurements. However, in this context, protein solutions are assumed to have the same flow properties throughout the concentrations studied, and problems may arise in terms of protein-particle interactions [82].

More details regarding recent developments in protein solution rheology studies are addressed in the introduction to Chapter 4.

1.6 Characterisation of protein formulations

There are several techniques used in current research laboratories to characterise protein formulations. There are many reviews in literature regarding this matter, referring to advantages and disadvantages of each technique, its operating principle and [1,44,83]. A key concept from the literature concerning the techniques used for protein formulation characterisation, is that it is important to combine information from several techniques with different measuring principles, known as orthogonal characterisation [10].

Several of these techniques were used throughout the work presented in this thesis and their theoretical background is described in Chapter 2 (Materials and Methods).

Differential scanning calorimetry (DSC) is useful for determination of glass transition temperatures and phase transitions of the solid-state lyophile or dried matrix at high protein concentration. Its use in liquid protein formulation (micro-DSC) has been related to the determination of melting temperature of a protein when under different formulation settings, thus determining which excipients contribute best to an increase

of the protein's melting temperature.

The use of vibrational spectroscopy is also important and practical to use in this type of formulation since it is possible to analyse directly the sample without the need for diluting or pre-analysis preparation. Fourier-Transform Infrared (FTIR) and Raman are vibrational spectroscopy techniques that can give information on the protein's secondary, which gives information on denaturation of the protein. Applications of FTIR have been also on helping determining the protein's melting temperature, for the same purposes as those used with DSC [84].

Other techniques useful for determination of protein conformation are ultraviolet absorption (UV), fluorescence, and near-UV (tertiary structure) and far-UV (secondary structure) circular dichroism [5, 84].

As previously mentioned, protein aggregation is important to monitor, several techniques can be used for this monitorisation [10]. Separation techniques for the characterisation of protein monomers and their aggregates include size exclusion chromatography and protein electrophoresis using sodium dodecyl sulfate polyacrylamide gels. Techniques such as dynamic and static light scattering, optical microscopy, light obscuration and micro-flow imaging and visual inspection, are typically used for the detection and size characterisation of protein aggregates or particulates.

Since protein aggregation can generate multiple oligomeric species of different size range or due to different aggregation behaviour (reversibility), there have been recent discussions in the terminology of such categories [85]. In attempt of harmonising such terminology within the field, Nahri *et al.* have proposed classification of protein aggregates by five different categories: size, reversibility, secondary or tertiary structure, covalent modification and morphology (Table 1.1). Throughout this thesis, aggregate denomination was related to its size characterisation, thus following the 'size category'

proposed. In addition, aggregate terminology can also be addressed as soluble and insoluble. This has to do with the mechanism of aggregate growth, where a soluble oligomer is molecularly soluble and grows with addition of one monomer at a time; whilst insoluble aggregates refer to rapidly growing oligomers that eventually precipitate or lead to phase separation [28].

Table 1.1: Protein aggregate terminology proposed categories (adapted from [85]).

Proposed Category	Proposed Classification
Size	<100 nm (nanometer), 100-1000 nm (submicrometer), 1-100 µm (sub-visible), >100 µm (visible)
Reversibility	Reversible, irreversible, dissociable, dissociable under physiological conditions, dissociable under defined conditions
Secondary/ tertiary structure	Native, partially unfolded, unfolded, inherently disordered, Amyloid
Covalent modification	Cross-linked, reducible cross-link, nonreducible cross-link, intramolecular modification, oxidation, deamidation, no modification
Morphology	Number of monomeric subunits, aspect ratio, surface roughness, internal morphology, optical properties, translucent, heterogeneous

A major problem with analysis and characterisation of highly concentrated protein formulations is that most of the analytical techniques require dilution prior analysis [5]. Diluting to lower concentration may have an impact on the result of the assay since there will be a change in solvent concentration and content, possibly affecting the protein's state that may differ from the original conditions [5]. To address the issues of reduced sample volume availability and to shorten analysis and measurement times, it has become increasingly important to develop techniques in a high throughput methodology. An example of this is the conversion of conventional protein characterisation techniques in a high throughput setting that allows faster formulation screening [83].

Chapter 2

Materials and Methods

In this chapter a description of materials and methods will be made. Information on the proteins studied throughout the work can be found in the Materials section. A general explanation of protocols used for buffer exchange using desalting columns and dialysis cassettes, as well as sample concentration are also described. An account is made for the purification, dialysis and concentration of the monoclonal antibody studied. Specific sample preparation details will be addressed in its respective experimental chapter.

A summary of the theory related to rheology and its instrumentation is made, since this was the principal technique used between all experimental chapters. Specific rheological protocol details will be addressed in each of the experimental chapters.

Other techniques such as UV-visible spectroscopy, light scattering, size exclusion chromatography, tensiometry, density, micro-differential scanning calorimetry, protein electrophoretic methods, circular dichroism, flow imaging microscopy for sub-visible particle counting and visual inspection, are also described here since these will be referred to in more than one experimental chapter. Each experimental chapter will include specific method details. Polymer synthesis and related characterisation methods, the protein solubility assay and determination of critical micellar concentration via fluorescence spectroscopy, were left to be described only in Chapter 6.

2.1 Materials

2.1.1 Proteins used

2.1.1.1 Recombinant human albumin

Recombinant Human Albumin was kindly donated by Novozymes Biopharma UK, Ltd. (Nottingham, UK) in the form of Recombumin® Prime (batches used: 1104 and 1101). The protein comes as a liquid formulation of concentration 200 mg/mL, stored at 2-8 °C. The formulation buffer is composed of NaCl 145 mM, sodium octanoate 32 mM and polysorbate-80 15 mg/L, at pH 7.0 ± 0.3.

2.1.1.2 Beta-lactoglobulin

The protein beta-lactoglobulin was obtained from Sigma-Aldrich (product L3908, batches 097K7012 and 080M7312V) as the mixture of bovine variants A and B, in a lyophilised powder containing sodium chloride.

2.1.1.3 Monoclonal antibody, Immunoglobulin

The humanised monoclonal antibody studied was provided by MedImmune, LLC. (Gaithersburg, Maryland, USA). It is an IgG_1 of 145.461 kDa. The protein was supplied in a lyophilised formulated format containing other additives, including a surfactant. The formulation additives were removed by purifying the reconstituted material, as per description in section 2.2.3 of this chapter.

2.1.2 Sample and buffer preparation details

2.1.2.1 Preparation of Buffers

All prepared buffers had a 2-month expiry date and were kept at 5 °. Ultrapure water was obtained from a water cleaning resin system from NANOpure Diamond (Barnstead, USA) with water quality of >18.0 mΩ-cm, and 0.22 μm filtered (PVDF membrane, EMD Millipore, USA). All buffers were filtered using 0.22 μm vacuum-driven filter units (Nalgene, USA), unless when 0.1 μm pore-size filtering was necessary (using syringe-filters PDVF Millex-VV from EMD Millipore, USA).

(a) rAlbumin

For rAlbumin samples, the formulation buffer was composed of NaCl (145 mM), Polysorbate-80 (145 mM) and sodium octanoate (32 mM) in ultrapure water (pH = 7.0 ± 0.3 at room temperature). Polysorbate-80 was obtained from Fluka and of grade meeting the standards from the European Pharmacopoeia. All other reagents were obtained from Sigma-Aldrich, UK and were of analytical grade. Another buffer was prepared containing only NaCl (145 mM) in ultrapure water, maintaining the pH at 7.0.

(b) β-Lactoglobulin and mAb

All reagents were purchased from J.T. Baker Chemicals (Pennsylvania, USA) and were of analytical grade. A histidine buffer was prepared containing L-Histidine and L-Histidine monohydrochloride at 10 mM in ultrapure water (pH = 6.0 ± 0.2 at room temperature). For circular dichroism analysis of mAb samples, a 10 mM sodium phosphate buffer pH 6.5 was prepared using monosodium phosphate monohydrate and dibasic sodium phosphate heptahydrate in ultrapure water.

Buffer characterisation

The pH of buffers and samples was measured using a pH meter (model PHM220, Radiometer Analytical, SAS, France) with combined Ag/ AgCl pH electrode, calibrated with appropriate pH buffers traceable to NIST (all pH related components, including pH calibrating buffers obtained from Radiometer Analytical SAS, France.

The buffers' osmotic strength was measured for comparison when different samples were dialysed into their respective buffers. A freezing-point osmometer Osmomat O30-D (Gonotec GmbH, Germany) was used, zeroed with ultrapure water and calibrated with a 300 mOsmol/kg NaCl aqueous solution (Gonotec GmBH, Germany). In this method, the osmolality of a sample is measured by comparing the freezing point of pure water with the freezing point of a sample which, if containing osmotically active compounds, will depress water's freezing point. For example, water has a freezing point of 0 °C whereas an aqueous solution of NaCl at 1 Osmol/kg has a freezing point of -1.858 °C [13].

2.2 Methods

2.2.1 Buffer exchange desalting columns and sample concentration

For buffer exchange of mAb samples, disposable buffer exchange/ desalting columns were used (PD-10 GE Healthcare, USA). These Sephadex G-25 matrix packed columns were used via the centrifugation method, as per the manufacturer's instructions, to avoid sample dilution as much as possible. The columns were equilibrated with equilibration buffer (that the samples would be exchanged to) prior to sample elution. Sample loading was typically 2.5 mL. To guarantee an effective buffer exchange the same procedure was repeated on freshly-equilibrated PD-10 columns.

Centrifugal concentrators were used since it was needed to concentrate protein samples

to achieve a higher concentration than the starting material. The centrifugal concentrators were chosen accordingly to the protein's size, as the membrane cut-off size should always be at least 10 times smaller than the size of protein monomer. For rAlbumin samples, the concentrators used were Vivaspin 20 5 kDa molecular weight cut-off size of PES (polyethersulfone) membrane (Sartorius Stedim, Ltd., UK). For mAb samples the centrifugal concentrators used were Amicon Ultra 30 kDa molecular weight cut-off size of regenerated cellulose membrane (EMD Millipore, USA). For sample concentration the procedure was followed by the manufacturer's recommendations and adapting to the laboratory centrifuges available at the time: either a swing-bucket rotor (Heraeus Mega Fuge 11R, Thermo Fisher Scientific, USA); or a fixed 45-angle rotor (Hermle Z400, Labortechnik GmbH, Germany). On all occasions, the centrifugal concentrators were rinsed before used. After centrifugation, all samples were collected, mixed and checked for their concentration.

2.2.2 β-Lactoglobulin sample dialysis

For β-lactoglobulin samples, as the protein was obtained as a lyophilised powder, sample preparation consisted of dissolving in a 10 mM His-His.HCl buffer (pH 6.0) with aid of a oscillatory shaker at mild shaking conditions ($\sim$ 70 rpm) until all sample was dissolved. After complete dissolution, sample dialysis was done using a 3.5 kDa membrane cut-off dialysis cassette (Slide-a-lyzer, Pierce Lab, Thermo Fisher Scientific, USA). Dialysis in the appropriate buffer, in a volumetric ratio of 200 times more than sample volume, was performed and repeated at least 3 times. After the dialysis, the sample was either kept as an unfiltered stock or it was filtered using specific syringe-filters according to the experiment requirements. After this procedure, the β-lactoglobulin samples were checked for protein concentration, pH and osmolality.

2.2.3 Purification, dialysis and concentration of the IgG_1 mAb

For complete removal of additives present in the original lyophilised formulation of the mAb purification of the reconstituted material was performed with affinity chromatography. This technique separates proteins based on a reversible interaction between a protein and a ligand attached to the chromatographic matrix when the elution conditions are set up to enhance this interaction. In the case of immunoglobulins G, purification can be made with high affinity of protein A and protein G for the Fc region of the IgG-type of antibodies. Protein A and protein G are bacterial proteins (from *Staphylococcus aureus* and *Streptococcus sp.* bacteria, respectively) which can be covalently attached to the inert matrix and have relative binding strengths according to the different immunoglobulins, making these ligands a useful media for antibody purification [86, 87]. In the case of the IgG_1 studied in this work, the media used was an agarose matrix with an alkali-stabilised recombinant protein A.

A typical affinity chromatography method for protein purification involves the following steps (Figure 2.1) :

1. column equilibration with buffer that provides conditions for protein-ligand binding;

2. injection of the sample, where target protein(s) will bind reversibly and specifically to the ligand while the unbound material will be eluted out of the column;

3. a recovery step where by changing the conditions to allow elution of the bound protein(s) (e.g. change in pH, change in ionic strength or competitive binding);

4. column re-equilibration with binding buffer.

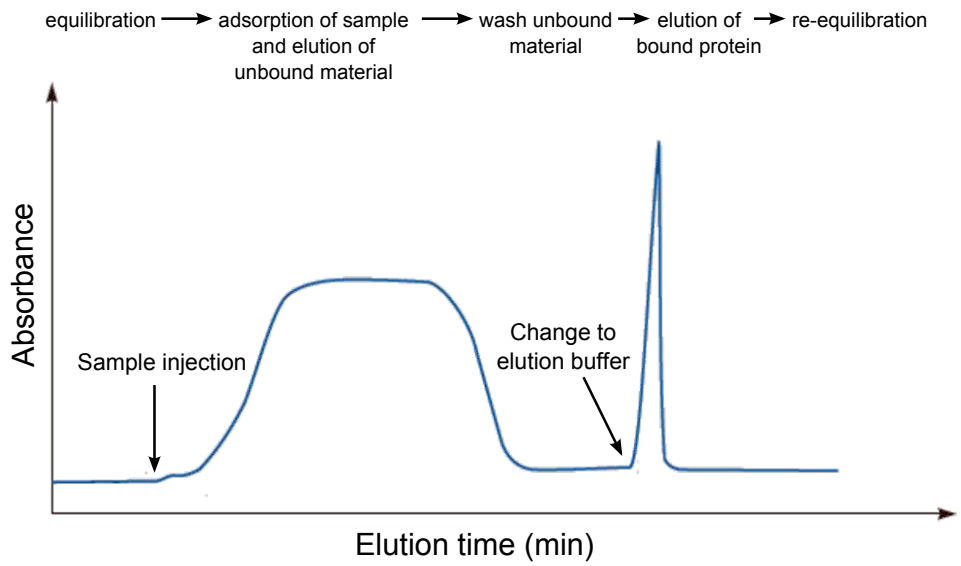

Figure 2.1: Scheme showing the general steps for affinity chromatography. Affinity chromatography was used to recover the mAb from a formulated product containing a surfactant. The ligand that specifically bound to the IgG_1 was a recombinant protein A, which is effectively and widely used for purification of IgGs. (Image adapted from reference [87].)

mAb Purification protocol details

The chromatographic system used was an *Ä*KTA purifier 10, with a pH detector and UV spectrophotometer detector (measuring absorbance at 280 nm). The column used was a HiScale column (ID 2.6 mm x 40 cm) with MabSelect SuRe resin (with a capacity of $\sim$ 30 mg of mAb/ 1 mL of resin). All components were obtained from GE Healthcare, USA.

The following buffers were prepared/ used:

1. Dulbecco's PBS 1x at pH 7.2 (from Sigma-Aldrich, USA) - equilibrating and elution buffer for non-bound components;

2. 50 mM sodium hydroxide (NaOH) + 1 M sodium chloride (NaCl) - sanitising buffer;

3. 50 mM glycine + 30 mM NaCl pH 3.5 - elution buffer for bound material;

4. 1 M Tris pH 9.0 - titration buffer;

5. 10 mM His-His.HCl pH 6.0 - sample's target buffer;

6. Water/ ethanol 80/20 %v/v - column storage buffer.

After loading the column with the resin, the run began with a sanitising elution with buffer 2. Column equilibration with PBS followed this sanitising step until the pH of the column eluant reached pH 7.2. After this was achieved, the reconstituted mAb sample was loaded and the elution with PBS continued until at least 10 column volumes. To elute the mAb, 50 mM glycine and 30 mM NaCl pH 3.5 buffer was used. Collection of the material was monitored with the change in pH and absorption at 280 nm. After all the product was eluted and collected, it was immediately titrated with 1 M Tris pH 9.0 buffer to pH 6.0. After titration, the material was filtered using a 0.22 μm pore size membrane vacuum-driven filter unit (Nalgene, USA). Meanwhile, the column was sanitised again with buffer 2 and re-equilibrated with PBS. These steps were repeated until all mAb material was purified. If the column was not to be used again, it was stored in water/ethanol 80/20 %v/v after running at least 5 column volumes and kept in this buffer at 2-8 °C.. Flow rate in all steps was 10 ml/min.

For this study the mAb was purified using the protocol above on two different occasions. It was the subsequent concentration step that differed between batches. The concentration methods were chosen differently depending on the amount of protein material that needed to be concentrated. Therefore, from this point forward, the material that was concentrated using the stirred cell method is referred to as mAb batch 1 (mAb b1), and the material that was concentrated using tangential flow filtration is referred to as mAb batch 2 (mAb b2).

Diafiltration and concentration steps

(a) Stirred ultrafiltration cell (mAb batch 1)

An Amicon Stirred cell system (EMD Millipore, USA) was used for batch 1 of the purified mAb as the total volume collected was $\sim$ 400 mL. This method provides diafiltration and concentration of the material by use of a magnetic stirring bar which keeps the fluid movement during operation thereby reducing the build-up of concentrated material on the membrane. An auxiliary reservoir containing the desired sample buffer is coupled to the stirred cell system which will keep the stirred fluid volume and concentration constant as the filtrate volume is replaced by the new buffer. This is a substitution for membrane dialysis (such as that described in section 2.2.2). After dialysis, the material was then concentrated on the same device by direct application of gas pressure. The solutes above the membrane molecular weight cut-off (Ultracel PL regenerated cellulose membrane, 30 kDa molecular weight cut-off, EMD Millipore, USA) are retained in the cell, while water and solutes below the cut-off flow into the filtrate. This batch was concentrated to $\sim$88 mg/mL.

(b) Tangential flow filtration (mAb batch 2)

Tangential flow filtration (TFF) is a pressure-driven ultrafiltration/concentration method that uses membranes to separate proteins in a liquid solution on the basis of size/ molecular weight. TFF differs from the method described above (stirred cell) in the way that the fluid flows while it is being filtered. In the stirred cell, the fluid containing its solutes is pushed against the membrane by applying gas pressure. In TFF, the solute-containing fluid is flowing tangentially along the surface of the membrane. Hence, TFF is designed so that the retained molecules do not build up at the surface of the membrane [88]. This process also allows combination with diafiltration, where the concentration of protein is maintained but a buffer exchange occurs while the filtrate is

removed.

A Pellicon 2 mini cassette was used for diafiltration and TFF of this batch, the polyethersulfone void free membrane was of 30 kDa molecular weight cut-off, surface area 0.1 m^2 with coarse screened feed channels (EMD Millipore, USA). The system was composed of membrane, membrane holder, peristaltic pump, reservoirs, tubes and manometers to measure the pressure applied to the membrane.

After concentrating most of the material to ∼100 mg/mL, another batch of material was collected (∼17 mg/mL) by flushing out the remaining mAb left in the TFF system with sample buffer (10 mM His-His.HCl, pH 6.0). Thus, mAb batch 2 was divided in two sub-batches 2a and 2b, corresponding to the concentrated and dilute materials.

Independent of the diafiltration/ concentration method used, all mAb batches were checked for concentration, pH, osmometry, aggregation level by HPSEC. Additionally, all batches were checked for presence of the non-ionic surfactant that was an additive in the original mAb lyophilised formulation (this procedure was performed at and by MedImmune staff, in Gaithersburg, MD, USA). The three batches were collected in Nalgene (ThermoScientific, USA) PET (polyethylene terephthalate) bottles of appropriate volume, filtered with 0.2 μm pore-size membrane filters before storage and kept at 2-5 °C conditions until used for experiments.

2.2.4 Rheology

2.2.4.1 Basic definitions

Rheology is the study of deformation of solids and the flow of fluids. This branch of physics allows the study and characterisation of materials when under shear. Thus, materials can be characterised between extremes between being ideal viscous fluids, e.g.

a low-viscosity mineral oil, or purely elastic solids, e.g. a piece of steel. In between there are materials that combine both viscous and elastic components, being therefore denominated viscoelastic materials (e.g. toothpaste or shower gel). However, to determine these characteristics, it is important to understand that the rheological behaviour of materials is dependent on the shear applied (e.g. low-shear or high-shear), the way the sample is loaded (e.g. force applied), temperature and time, as well as many other parameters (e.g. pH, concentration, presence and size of particles, etc.) [48, 49]

For easy understanding of the fundamental rheological parameters, a two-plates model is used. In this case, the sample is between two plates and it is sheared in the gap (h). The upper plate is set in motion by a shearing force (F) on the shearing area (A), while the lower plate remains fixed, with a resulting velocity (v) (Figure 2.2). In this simple case, two assumptions are made: the sample does not slip nor slide out of its shearing gap; the conditions are for laminar flow (i.e. flow in layers) [59, 89, 90].

From this model it is possible to define shear stress:

$$\tau = \frac{F}{A} \tag{2.1}$$

with the force (F, in [N]) and the shearing area (A, in [m^2]), the S.I. unit for shear stress is [Pa]). The shear rate will be defined by:

$$\dot{\gamma} = \frac{v}{h} \tag{2.2}$$

with velocity (v, in [m/s]) and the distance (h, in [m]), the S.I. unit for shear rate is [1/s or s^{-1}]. For many processes, a shear rate can be calculated or estimated to have an idea of relevant shear rate range where a sample should be studied at.

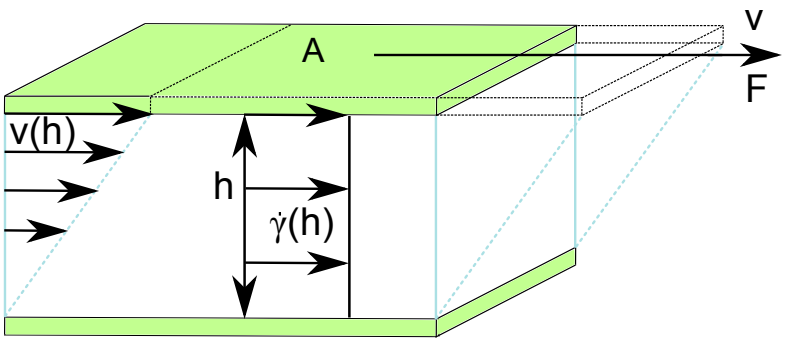

Figure 2.2: Schematic of the velocity of a fluid using the two-plates model for shear rheology. The top plate (boundary) moves due to an applied force (F), causing the fluid to shear, while the bottom plate remains stationary.

Shear viscosity can be defined from the previous equations,

$$\eta = \frac{\tau}{\dot{\gamma}} \tag{2.3}$$

where viscosity (η) has S.I. units of [Pa.s]. Physically, viscosity represents the resistence to flow that all materials will inherently show, since upon shear the molecules constituting the material will move in relation to each other, thus contributing to an internal friction forces [49, 89]. Although not a S.I. unit, the [P] (Poise) is still sometimes a unit used for viscosity; 1 P converts to 0.1 Pa.s. Kinematic viscosity (ν) is defined by,

$$\nu = \frac{\eta}{\rho} \tag{2.4}$$

with the density ρ [kg/m^3], where the S.I. unit for ν is [mm^2/s] [49, 89, 90].

2.2.4.2 Flow curves and viscosity functions

Newton's Law describes the flow behaviour of a purely viscous material:

$$\tau = \eta\dot{\gamma} \tag{2.5}$$

The flow behaviour can be represented using flow curves and viscosity curves. A flow curve represents the dependence of shear stress τ on shear rate $\dot{\gamma}$, while a viscosity curve

represents the dependence of shear viscosity η on shear rate.

Typically, in order to characterise the test material, if possible, flow and viscosity curves are perfomed since the results can give an idea whether the material is ideal-viscous or if appears to have signs of elasticity. In figure 2.3(a) (and corresponding flow curve in figure 2.3(b)), the most common possible sample profiles are represented for different flow behaviours: ideal-viscous, with constant viscosity along the applied shear rates; shear-thinning, when there is a decrease of viscosity with shear rate; and shear-thickening, when the viscosity increases with shear rate. The practical tests that can yield these type of curves are denominated rotational tests. Rotational tests can be performed with presets controlling the rotational speed (n, in [min^{-1}]), thus collecting torque (M, in [mN.m]) as response of the sample; or by controlling the shear stress, where the opposite occurs. These parameters (speed and torque) are the raw parameters measured by a rheometer, and via the instrumental software are converted automatically into shear rate, shear stress and shear viscosity. Examples of materials with shear-thinning properties are polymer dispersions and polymer melts [49, 90]. The case of shear-thinning materials represents the circumstance where the internal friction forces are shear-load dependent. The ratio at which this happens can vary, thus it is often to refer to "apparent shear viscosity" where the viscosity at each shear rate represents that point only. Shear-thinning is often related to the structure of molecules and the way these are originally entangled and disentangle as shear is applied, as an explanation of how the intermolecular forces yield less flow resistance with the increase of shear load. This is commonly interpreted with samples such as polymer solutions [49, 89]. In the case of colloidal dispersions, for example, the explanation is given in relation to the intermolecular forces that can become weaker and weaker as the shear-load increases [48, 49, 90].

Examples of shear-thickening materials are those dispersions with very high concen-

tration of solids or gel-like particles, such as ceramic suspensions or starch dispersions. The term "apparent shear viscosity" is also applied in this case. For shear-thickening materials, which are less common in industry, the rationale to account for the increase of viscosity with the increase of shear load is related to increased interaction between molecules or particles present in the dispersions [89, 90].

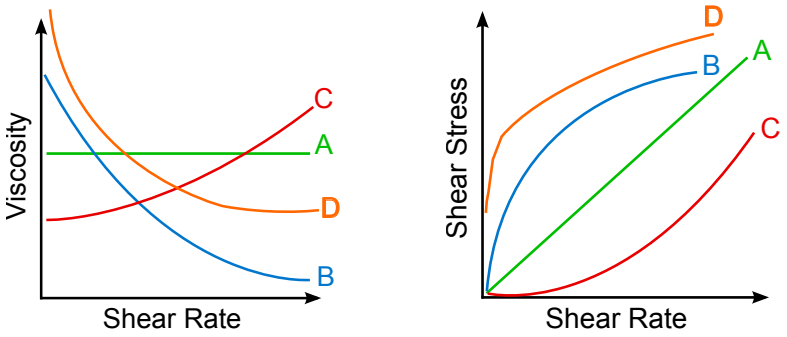

(a) (b)

Figure 2.3: Examples of general of viscosity curves (a) and flow curves (b) for materials showing: A - idealviscous (Newtonian flow), B - shear-thinning, and C - shear-thickening behaviour, and D - yield behaviour with a yield point. Note that the axes are represented in linear scales.

However, it should be noted that shear-thickening effects can also appear during experimental conditions due to flow instabilities and turbulance. These have to do with hydrodynamic flow and the appearance of centrifugal or inertial forces due to the mass of the fluid [49]. These can be particularly important for low-viscosity liquids. Therefore there is one important dimensionless number that is critical to determine if the experimental conditions are due to create hydrodynamic flow instabilities. The Reynolds number (Re) represents the ratio between the force due to mass inertia of the fluid and the force due to its flow resistence:

$$Re = \frac{v_m L \rho}{\eta} = \frac{v_m L}{\nu} \tag{2.6}$$

with v_m as the mean velocity of the fluid, and L as the characteristic length of the geometry used in the measurement [48]. Re numbers are thus used to characterise

flow conditions. In the case of a couette (cup-and-bob) geometry, if Re $<$ 1000, the conditions are of laminar flow; 1000 $<$ Re $<$ 2000, correspond to a transition range; and if Re $>$ 2000, the conditions are of turbulent flow [48, 49]. This turbulence can occur in low-viscosity fluids particularly when using couette geometries where the cup is rotating and the bob stationary, and is related to the dimension of the annular shearing gap in this type of geometry [49, 59].

There are materials can show yield type of behaviour (see general curve D, in Figure 2.3). Materials that yield only start flowing when the external applied force is larger than the internal forces that are resistant to flow. Typically, below the material's yield point, it shows an elastic behaviour, a solid-like behaviour where the material flows to a small degree. Yield stress (also called yield point) can be determined by controlled shear rate experiments, where shear stress is measured in function of the shear rate. Curve-fitting can be performed choosing one of the different models that account for yield behaviour (e.g. Bingham, Casson or Herschel/Bulkley), where the yield point is extrapolated to when $\dot{\gamma} = 0$ [48, 49]

Time dependency of a material's response is important to its rheological characterisation. To monitor the shear behaviour of a sample in function of time, all the other applied parameters (shear stress or shear rate, temperature) should remain constant. Different behaviours can occur with time, such as thixotropy and rheopectic behaviours. A material that shows thixotropy typically has its shear viscosity reduced when shearing occurs. After this, and if left at rest, the same material can increase its viscosity, showing a degree of 'memory', regenerating the possible interactions that were present before it was sheared. A thixotropic material thus undergoes a reversible deformation process. When the opposite occurs, irreversibility of deformation, of the test sample is considered 'non-thixotropic'. Another time-dependent behaviour is rheopexy. In rheopetic fluids, when there is an increase of shear viscosity, structural

strengthening can occur as result, which when followed by complete rest shows complete decomposition of the structure [49, 89].

2.2.4.3 Oscillatory shear rheology

Oscillatory rheology concerns the detailed measurement of the material's relative contributions of its viscous and elastic properties. If a test material is again imagined in between two-plates (Figure 2.4(a)), during an oscillatory test the moving top plate will oscillate back and forth with a specific frequency and amplitude. The bottom plate remains stationary and it is where the resulting force is measured. It is assumed that homogeneous deformation occurs in the sample across the shear gap. When a strain (or stress) is applied on the top plate at different frequency and amplitude, these will be the parameters that define the timescales to which the material will respond to. Thus, when a sinusoidal strain is applied to a material, the deformation function can be expressed as:

$$\gamma(t) = \gamma_o \sin \omega t \tag{2.7}$$

where γ is strain, γ_o is the shear strain amplitude (in [%]) and ω is the angular frequency (in [rad/s]).

The linear response of the material can be given by:

$$\tau(t) = \tau_o \sin(\omega t + \delta) \tag{2.8}$$

where τ is the stress, and δ is the phase shift (in [°] between applied strain and measured stress (see figure 2.4(b)). Typically, linear responses are obtained if small amplitudes are used of the applied strain. If larger stresses and/or amplitudes are used, the measurement will tend to yield non-linear responses of the materials [48, 90]. In this thesis, viscoelasticity of samples was investigated using small amplitude oscillatory

shear (SAOS).

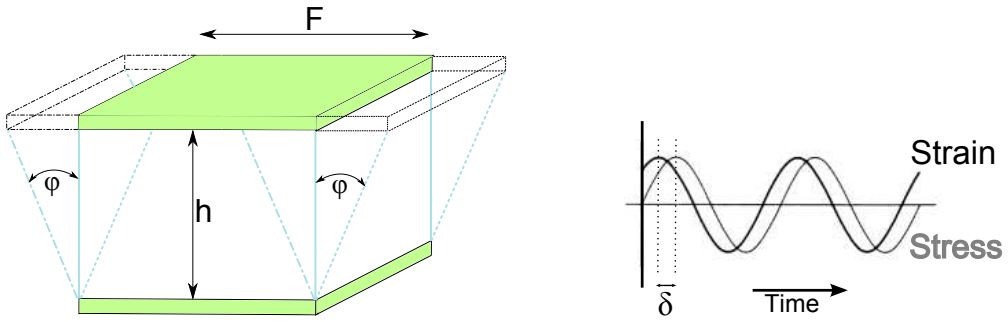

(a) (b)

Figure 2.4: (a) Two-plates model to represent oscillatory shear with the top plate oscillating sideways due to the applied force (F). The bottom plate remains stationary and the deflection angle (φ) in the shear gap (h) is shown to represent the shearing of the material. (b) Shear strain function ($\gamma(t)$) is represented with the resulting shear stress function ($\tau(t)$). In this case, both functions have the same frequency, but between the applied strain and the resulting stress there is a phase shift angle (δ).

For an idealviscous fluid, Newton's law applies:

$$\tau(t) = \eta^* \dot{\gamma}(t) \tag{2.9}$$

where η^* is complex viscosity, τ and $\dot{\gamma}$ are sine functions in order of time. For these type of samples the phase shift angle between strain and stress is $\delta = 90°$ [49, 89, 90].

For idealelastic materials, Hooke's law applies:

$$\tau(t) = G^* \dot{\gamma}(t) \tag{2.10}$$

where G^* is the complex shear modulus, with τ and $\dot{\gamma}$ being time-dependent in sine functions. The phase shift angle for purely elastic samples will be $\delta = 0\circ$.

For viscoelastic samples, the phase shift will have an angle value between $0° < \delta < 90°$. The rheological behaviour of these samples comprises both viscous and elastic deformations, which can be characterised and quantified with the use of complex math-

ematics by calculating the loss modulus (relative to the viscous portion) and the storage modulus (relative to the elastic portion) [49, 89, 90]. The loss modulus, G'', measures the deformation energy used by the sample during and after shear. The energy loss occurs while there is loss of the material's structure, i.e. when the sample flows while its molecules or particle components are moving in relation to each other, thus showing an irreversible deformation behaviour. G'' (the imaginary component) is defined by:

$$G'' = \frac{\tau_o}{\gamma_o} \sin \delta \tag{2.11}$$

The storage modulus, G', measures the deformation energy stored by the sample during shear. After shearing, the sample can recover partially or completely to compensate the previous structure deformation, thus showing a reversible deformation behaviour. Therefore, G' represents the sample's elasticity (the real component), which can be defined by:

$$G' = \frac{\tau_o}{\gamma o} \cos \delta \tag{2.12}$$

From equation 2.8, and based on the material properties G' and G'', this function can be written as:

$$\tau = G'(\omega) \sin \omega t + G''(\omega) \cos \omega t \tag{2.13}$$

The relation between G', G'' and G^* is that $|G^*| = \sqrt{(G')^2 + (G'')^2}$. The damping factor, $\tan \delta = G''/G'$, is the ratio between the viscous and elastic portion of a sample, and for viscoelastic samples, it will have a value between $0 < \tan \delta < \infty$.

A simple model that describes the behaviour of viscoelastic materials is the Maxwell model that relates the response of the material based on its characteristic relaxation time (λ), i.e. time that the material takes to respond to the applied strain.

$$\tau + \lambda \frac{\partial \tau}{\partial t} = \eta_0 \dot{\gamma} \tag{2.14}$$

Large values of λ in practice mean that the material has elastic behaviour, while lower values of λ represent a viscous behaviour. In this equation, η_0 represents zero-shear

viscosity, which is the viscosity at the limiting value of complex viscosity (η^*) at infinitely low angular frequencies ($\lim_{\omega \to 0} \eta^*(\omega)$) [49, 89, 90].

Therefore, in the case of the Maxwell model for viscoelastic fluids, G' and G'' can be represented as follows [89]:

$$G' = \frac{\eta \omega^2 \lambda}{1 + \omega^2 \lambda^2} \qquad (2.15) \qquad\qquad G'' = \frac{\eta \omega}{1 + \omega^2 \lambda^2} \qquad (2.16)$$

In oscillatory shear rheology it is common to perform an amplitude test to determine the linear viscoelastic range (LVE) of a material. In this type of test the angular frequency (ω) is kept constant while the amplitude of the applied strain is varied. Monitorisation of G' and G'', as well as δ and η^* (or $\tan \delta$), in function of the strain. Typically, if the applied strain is too large the sample's structure or network (held by either chemical or physical interactions) can be irreversibly affected. From that point onwards, it is common to observe decrease of both loss and elastic moduli. The strain values before this occurs are due to a stable structure where reversible deformation occurs nondestructively, hence denominating this range of linear viscoelastic range (usually performed at small amplitudes) [90].

The linear viscoelastic range is defined by the proportionality of the applied strain and measured parameters. If analysing the material's behaviour well within its LVE range, it is common to relate the resulting G' and G'' to characterise the sample. Therefore, if $G' > G''$, the elastic behaviour dominates over the viscous portion, indicating a solid-like behaviour; if $G'' > G'$, the viscous behaviour is dominating the elastic characteristics of the sample, indicating a liquid-like character. Another situation could be if $G' = G''$, in which case the material has balanced characteristics of both elasticity and viscosity [89].

From the discussion above, it is clear that for an unknown sample it is desirable to determine the LVE range and critical strain, and it is important to keep in mind that these parameters are valid only for the angular frequency tested. Following the amplitude sweep, is usual to test sample's rheological behaviour at variable frequencies, keeping the amplitude at a constant value. In a oscillatory frequency sweep the information collected on the sample's rheological behaviour (G' and G''), studied in the LVE, is time-dependent. The sample's behaviour can be interpreted in terms of its response to the applied strain at long times (low frequencies) compared to its response to the same strain at short times (high frequencies).

Knowing the amplitude and angular frequency that can relate to practical use of the specific test sample, varying the temperature, pressure or analysing its behaviour along time, are common experiments that can yield further information on the sample's rheology [49].

2.2.5 Rheometry and instrumentation

The rheological characterisation can be challenging due to the importance of choosing the most suitable hardware to correctly characterise the sample. In this section, the focus is on explaining how a conventional (rotational/ oscillation) rheometer works, what were the different geometries used for all rheology experiments and an explanation of how these measure the viscosity, as well as describing other instrumentation, such as viscometers, used to acquire viscosity values at different conditions than those measured with the rheometer. The equipment and techniques described in this section were those proven to be the more convenient and available at the time to use for an appropriate rheological measurement of protein solutions. It is worth noting that there are more measurement equipment and for a complete revision of the different equipment and techniques available, particularly for traditional techniques and instrumentation,

references such as [91] and [59] are compreehensive sources for this information.

2.2.5.1 Rheometer

The rheometer is an advanced instrument that allows the user to characterise the rheological properties of samples through various rheological tests, such as stress or shear rate controlled tests, creep and relaxation tests, including various types oscillatory tests.

Conventional rheometers have a single-head where the motor and transducer are in the same system on the side which connects to the measuring geometry. This single-head can be controlled in two modes: 1) controlled shear rate (CSR) , where the deflection angles and rotational speeds are controlled by the motor, with the resulting torques being detected; or 2) controlled shear rate (CSS) , where the torques are set by the motor and the deflection angles or rotational speeds are detected by the position sensor.

A bearing is needed in a rheometer to allow that its movable part can rotate around a fixed axis. Bearings can be of different types (e.g. air, mechanical, or magnetic) and their use in rheometer instrumentation are to reduce the internal friction effects and inertia effects to the minimum, so that the total torque (M_{total}) measured is due to the rheological response of the test sample only. In an air bearing, the rotating parts float on an air 'bed' created by the continuous supply of compressed air into a gap between the rotor and the stationary component. This is to reduce direct mechanical contact between moving and fixed parts, and to reduce potential increase of internal frictions [49].

The rheometers used throughout this work were an Anton-Paar (Graz, Austria) Modular Compact Rheometer (MCR) 301, MCR 302 and MCR 501; as well as a TA Instruments (New Castle, Delaware, United States of America) AR-G2 model.

2.2.5.2 Bulk measurements

Bulk rheology measurements can be performed with different type of geometries. In this case, since protein solutions are generally considered low viscosity samples, the choice of geometries is largely due to this fact. Besides low viscosity, the other limiting factor can be availability of sample volume. For these reasons, this section will only focus on the measuring geometries that were used specifically for the studies presented in this thesis.

1. **Cone-and-plate**

   A cone-and-plate geometry is composed by a lower fixed flat circular plate and a top moving shallow cone which has a truncation (Figure 2.5)The dimensions of the geometry are given by its radius (R) and its angle (α). Truncation of the cone avoids any friction between cone and the bottom plate, and allows a fixed gap setting for analysis (as opposed with plate-plate geometry, where different gap settings may be chosen). With a cone-and-plate, the measurement of shear stress depends of torque (M) and its radius (R), where C_{ss} is the measuring system's constant depending on the radius:

   $$\tau = \frac{3M}{2\pi R^3} = C_{ss}M \tag{2.17}$$

   Therefore an increased sensitivity can be achieved if the cone's radius is larger [48, 49].

   To calculate the shear rate in a cone-and-plate gap,

   $$\dot{\gamma} = \frac{v_{max}}{h_{max}} = \frac{\omega R}{R\tan\alpha} = \frac{\omega}{\tan\alpha} \approx \frac{\omega}{\alpha} \tag{2.18}$$

   where the maximum velocity and gap are reached at the edge of the cone, and for cones with small angle (e.g. $< 3°$) $\tan\alpha$ is approximately equal to α. In these

cases, and from this equation, the shear rate will be independent of cone angle and radius, therefore, it will remain constant throughout the sample [48].

The advantages of the cone-and-plate geometry are: it shows constant shear rate throughout the conical gap (in contrast to the varying shear rates conditions in a parallel plate geometry); the sample volume can be very small; cleaning and filling the gap is relatively easy. Disadvantages are: the limitation of particle size regarding the fixed measurement gap; as the sample contains an air/water interface at the cone's edge, evaporation can be a problem [49].

Cone-and-plate geometries used throughout this study were stainless steel CP50-1 (R = 50 mm and cone angle = 1°) and CP40-0.3 (R = 40 mm and cone angle = 0.3°), both from Anton-Paar. Sample volume for CP50-1 was 675 μL and for CP40-0.3 was 150 μL. This geometry was always used with an evaporation blocking system/ peltier hood.

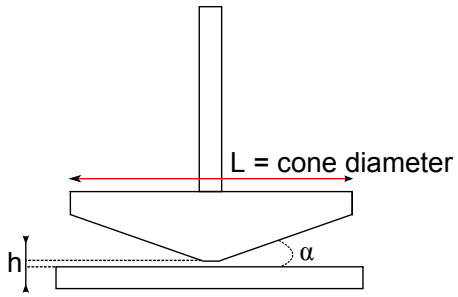

Figure 2.5: Schematics of the cone-and-plate measuring system. L represents the geometry's diameter, α is the cone angle and h is the cone's fixed gap related to its truncation.

2. **Double-gap concentric cylinder**

The double-gap concentric cylinder geometry is a modified concentric cylinder that allows measurement of low viscosity samples due to its increased shear area which is in contact with the sample. An inner cylinder is in the centre of the cup which

results in an annular gap (see figure 2.6). To achieve uniform shearing (rate) conditions in the inner and outer gap, the length of the immersed part of the rotating bob is $L \geq 3R_3$ and the ratio between radii is $\delta_{cc} = R_4/R_3 = R_2/R_1 \leq 1.15$ [49]. The major advantage of this geometry is the capability of achieving lower torques. However, sample volume is much larger than that used for cone-and-plate and it can be more difficult to clean [49].

The double-gap geometry used in this work was a stainless steel DG26.7 (Anton-Paar, Graz, Austria). Sample volume when using this measuring system was 3.8 mL. The relevant dimensions of the DG26.7 were: $L = 40$ mm; $R_1 = 11.914$ mm; $R_2 = 12.333$ mm; $R_3 = 13.334$ mm; and $R_4 = 13.795$ mm (Figure 2.6).

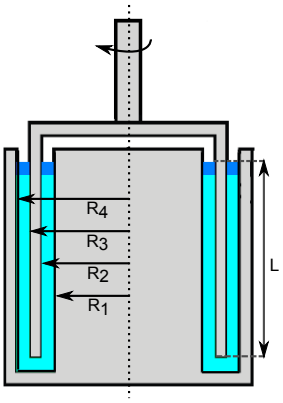

Figure 2.6: Schematics of the double-gap concentric cylinder measuring system. L represents the length of the geometry immersed in the sample, R_1 to R_4 are the different radii that define the annular gap where the sample is loaded.

2.2.5.3 Interfacial shear rheology with the double wall-ring geometry

Interfacial rheology studies the fluid dynamics of films or layers that are formed on the interfaces of liquids by measuring their response to a dilatational deformation or a shear deformation. Interfacial rheology describes the relationship between the deformation of the surface, the stresses applied on and in it, and the resulting flows in the sub-phases. There are many techniques that can be used to describe the rheology of an interface,

some being indirect by measuring via imaging and other being direct methods, measuring directly the surface [92]. Examples of direct interfacial rheology measurement techniques are with the double wall-ring, a bicone geometry, oscillating needles and torsion pendulum technique [92, 93].

In interfacial shear rheology, where the measurements are typically performed with a constant surface area, the flows are generated by moving solid geometries within the interface or by applying varying surface pressures [93]. It is therefore important that the resulting flow can be decoupled only for the interfacial layer rather than having contributions due to the sub-phases. For this, the design of the geometry is very important where the measurement of interfacial viscosity can be maximised. A dimensionless parameter, the Boussinesq number, can describe the ratio of the interfacial stresses to bulk stresses,

$$B_o = \frac{(\eta_s V/L)P_s}{(\eta V/L_B)A_B} = \frac{\eta_s}{\eta l_G} \tag{2.19}$$

where η_s is the interfacial shear viscosity, η is the bulk shear viscosity and L and L_B are characteristic length scales for the shear flow in the interface and bulk, respectively. P_s is the contact perimeter between the interface and the geometry, A_B is the contact area between the geometry and the bulk, V is velocity, and l_G is the characteristic length scale of the geometry. If $B_o \gg 1$, the surface shear viscosity dominates over bulk. This can be increased with use of a geometry that has a larger contact area or that minimises the characteristic length scale [93, 94]. This is the case of the double wall-ring, since the dimensions of the ring yield a $l_G = 0.7$ mm, leading to higher Boussinesq numbers when compared to the bicone [94].

The double wall-ring (DWR) (Figure 2.7) is a geometry composed by a trough and a ring that is positioned at the gas/liquid or liquid/liquid interface and which is connected to the rheometer (in this case, a AR-G2, TA Instruments, USA). The sample holder, made of Teflon material, was placed on the bottom peltier plate of the rheometer. The ring was square-shaped (cross-section), made of platinum/iridium so that it could be

flamed to remove organic contaminants. The walls of the ring had a step to prevent meniscus effects at the inner and outer sides of the trough. According to the developers of this fairly recent geometry, the DWR presents a ration A_s to P_s, respectively, interfacial contact area and perimeter, is about 48 times smaller when compared to a bi-cone geometry with a similar radius that of the ring, which results in a high Boussinesq number for a given surface viscosity [94]. Sample volume for these experiments was of ∼18 mL of fresh sample. After sample loading, the ring was lowered and positioned on the freshly formed air/water interface.

According to Vandebril *et al.*, it is sometimes necessary to correct the experimental data for the case that deviations between this data and theoretical values occurs. Correction of data is performed by computing corrected values via an algorithm developed by the authors [94]. However, the authors also demonstrated that corrections are only necessary when surface viscosities reach values below 10^{-5} Pa.s.m. In all the cases of our measurements, our data points were above this limit.

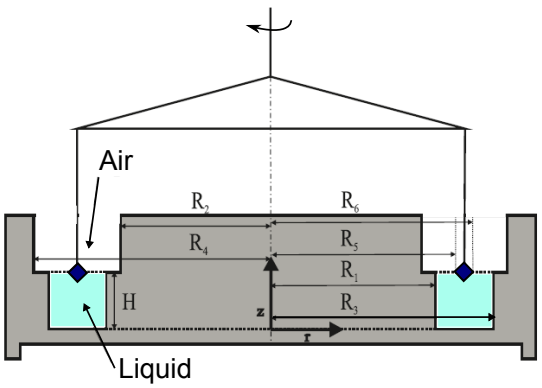

Figure 2.7: Schematic of double wall-ring (DWR) measuring system for interfacial shear rheometry (adapted from reference [94]). The ring has a square-shaped cross-section, with width of 1 mm and is made out of Pt/Ir. The radii R_1 to R_6 are represented to show the different dimensions of the fixture, the height H from the interface to the bottom of the channel measures 10 mm.

2.2.5.4 Rheometer calibration check

Calibration tests with ideal viscous (Newtonian) fluids such as deionised water or other solvents of similar viscosity (at 20 or 25 °C) were run to test if the instruments showed the minimal torque according to expected (typically 0.1 μmN.m or better, depending on the instrument).

The calibration checks, which were run for all geometries used, also served as diagnostic that thel instruments were measuring the correct viscosities for the standard oils. An error of 2 % was allowed for each of the standard oils being measured. The measurements were done both at 20 and 25 °C. The standard oils were bought from Paragon Scientific Ltd. (Wirral, UK) and Cannon Instruments (State College, Pennsylvania, USA) in a range of viscosity that would cover the low viscosities of the test samples. These general purpose viscosity reference oils were blends of hydrocarbonate oils. Viscosities for all these general purpose standard oils were based on the value for the viscosity of water (1.0016 mPa.s at 20 °C; defined by NIST).

2.2.5.5 Sample preparation for rheological analysis and other measurement details

For all rheological experiments performed, the experimental settings had to comprise of devices that would allow a constant temperature during analysis. For this reason, the lower fixed plate or cup were connected to a peltier unit. As the moving fixtures (cone or cylinder) were not connected to a peltier device, if possible, the measurement temperature was maintained by use of a peltier hood.

An evaporation blocking system was used with the cone-and-plate to prevent evaporation of sample. This system is comprised of a inner metal ring inside the peltier hood that would sit in a solvent trap around the lower plate. Plastic vapour locks were used to sit on top of the solvent trap present on top of the peltier hood.

It was important to reduce the appearance of air bubbles in the samples and during loading to avoid artifacts in the measurements. Regarding loading, this would be resolved by fine tuning the speed used to lower the upper fixture. Generally, depending on how concentrated the samples were, a low vacuum was used to induce bursting of air bubbles. It was important to do this procedure for short times (<10 s) to prevent sample evaporation.

Further protocol details for the rheological tests can be found in the methods section of each of the experimental chapters.

2.2.6 Viscometers

The terms viscometer and rheometer are not well defined, however it is suggested that a viscometer can be a simple device that can only measure flow and viscosity of fluids, with some devices built to allow controlled shear rate rotational tests [49].

2.2.6.1 Falling ball viscometer

An example of a viscometer is the falling ball viscometer where a steel ball is sinking due to gravity through the liquid which is filled in the glass capillary of define inner diameter [49,59]. These viscometers track the time that a ball takes to move downwards through the test fluid over a defined distance between two level marks. The viscosity is then determined from this, based on the calibration of the system using viscosity standards of known viscosity. By using different angles at which the glass capillary is set, different velocities can be achieved by the falling ball, and thus different shear rates can be experienced by the fluid. Testing with a falling (or rolling) ball viscometer is a single-point viscosity test. During a test period, where the ball rolls at a particular angle,

the shear rates are changing within a certain range depending on the uncontrolled motion of the ball, on the distance of the ball to the capillary's wall, and on its velocity. Only ideal-viscous samples should be measured without error with this instrumentation as the shear rate conditions are not constant [49,59]. From these measurements, the kinematic viscosity is usually reported. As mentioned in section 2.2.4.1, by knowing the density of the analysed samples, the kinematic viscosity can be converted to shear viscosity. Throughout this work, viscosity values obtained from the falling ball viscometer are reported in [Pa.s], since density measurements of the samples were performed (see section 2.2.11).

Some advantages of this instrumentation are its ease of use and that the measurement is free of evaporation or any air/water interface. Micro falling-ball viscometers allow the use of low sample volumes ($\sim$ 1 mL) and in the case of protein solution analyses, the inner interface can be silanised to prevent protein deposition and interaction with the solid glass interface [49].

An automated micro falling-ball viscometer (AMVn) from Anton-Paar (Graz, Austria) was used. The capillary used had an inner diameter of 1.6 mm and a steel ball of diameter 1.5 mm. With this instrument the motion of the ball was detected via induction using magnetic sensors. For a simple measurement, the inclination angle was set at 70° (and -70°). This instrument allowed temperature control via an attached peltier unit.

Calibration of the capillary to be used with the test samples was performed by running DI water and a viscosity standard oil at measurement angle matching that for the sample measurement.

2.2.6.2 mVROC - microviscometer/rheometer-on-a-chip

Another type of viscometer used was the microviscometer/ rheometer-on-a-chip (mVROC), by Rheosense, Inc. (San Ramon, California, USA). The mVROC is a microfluidics

slit rheometer where the microfluidics chip is composed of a microchannel (rectangular slit) made of borosilicate glass mounted on a gold-coated silicon base. Viscosity is measured as a function of pressure drop as the fluid flows in the microchannel (width = 3.02 mm; depth depends on the chip used). As the fluid flows through the slit, pressure is measured through three sensors located at increasing distances from the inlet [79] (Figure 2.8). The pressure drop (ΔP) which drives the flow (Q) streamwise through a distance (L), is related to the wall shear stress (τ_w) by the following expression [79]:

$$wd.\Delta P = 2L(w+d)\tau_w \tag{2.20}$$

The nominal wall shear rate ($\dot{\gamma}_w$) associated to laminar flow of a Newtonian fluid is a linear function of flow rate (Q), by the equation:

$$\dot{\gamma}_w = \frac{6Q}{wd^2} \tag{2.21}$$

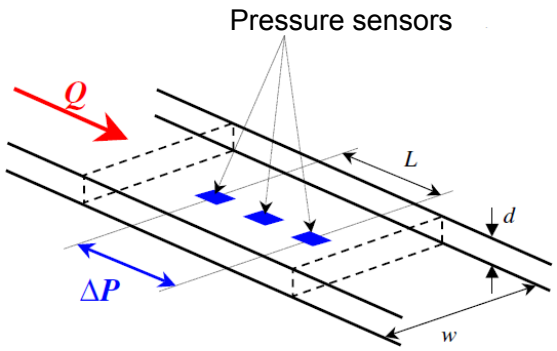

Figure 2.8: Schematics of the Rheosense slit microviscometer/rheometer-on-a-chip (mVROC). L is a length of 6.5 mm representing the distance where all pressure measurements are done streamwise. ΔP represents the measured differential pressure; Q represents the flow and the arrow is pointing in its direction; w and d represent the width and the depth of the channel, respectively.

In a typical experiment, the flow rate, Q is varied using a syringe pump and Hamilton gastight glass syringes (Reno, Nevada, USA). The mVROC device outputs the pressure

drop as a function of flow rate, which is used to calculate the nominal or apparent viscosity via $\eta(\dot{\gamma}) = \tau_w/\dot{\gamma}_w$ [79]. For incompressible 2-D ows of liquids with a rate-dependent viscosity, the calculation of $\dot{\gamma}_w$ is more complex since the velocity prole is no longer parabolic. The true shear rate ($\dot{\gamma}_{w,true}$) and true shear viscosities ($\eta(\dot{\gamma}_{w,true})$) can therefore be calculated, respectively, using the Weissenberg-Rabinowitsch-Mooney equation [59, 79]:

$$\dot{\gamma}_{w,true} = \frac{\dot{\gamma}_a}{3}[2 + \frac{d(ln\dot{\gamma}_a)}{d(ln\tau_w)}] \tag{2.22}$$

$$\eta(\dot{\gamma}_{w,true}) \equiv \frac{wd\Delta P}{2L(w+d)}\frac{1}{\dot{\gamma}_{w,true}} \tag{2.23}$$

The chips used in this work were A05 and D05, with a channel depth of 50 μm each, with different maximum pressure capability of 10 kPa and 1000 kPa, respectively [95].

2.2.7 Quantification of protein concentration by UV-visible spectroscopy

Ultra-violet (UV) spectroscopy is a method to analyse quantitatively the concentration of a protein solution. The peptide bond has an absorption maximum at λ=205 nm, but it is the absorbance of the aromatic rings of the amino acids tryptophan and tyrosine that show its maxima between 275 nm $< \lambda <$ 280 nm, also contributed by the disulfide bonds although in less quantity [86, 96].

According to Lambert-Beer's Law, that states that molar absorptivity (also known as molar extinction coefficient)(ε) is constant and absorbance (A) is proportional to concentration (c) for a given substance dissolved in a solute and measured at a specific wavelength (λ):

$$A_\lambda = \varepsilon cl = \varepsilon c \tag{2.24}$$

with absorbance having arbitrary units, concentration in molar (M), when l is the pathway in cm (usually 1 cm), and ε in L.mol^{-1}cm^{-1} [86]. The molar extinction coefficient (ε_{molar}) converts into percent extinction coefficient ($A^{1\%}_{1cm}$) by $\varepsilon_{molar} \times 10 = \varepsilon_{\%} \times MW_{prot}$. The proportions of the aminoacids tryptophan and tyrosine vary between different proteins, thus for individual proteins its extinction coefficient will vary. Extinction coefficients can be calculated theoretically by knowing the numbers of Trp, Tyr and disulfide bonds and then calculating by linearly combining the individual contributions of these amino acid residues, knowing their respective extinction coefficients [97]. The extinction coefficients for these residues depends on their microenvironment. In most globular proteins, most of these cromophores are buried in hydrophobic patches in the interior of these proteins. [97, 98].

For rHA solutions, the percent extinction coefficient, $A^{1\%}_{1cm}$, of 5.8 was used [99]. For β-lactoglobulin solutions,$A^{1\%}_{1cm} = 9.6$ [100]. For the mAb solutions, $A^{1\%}_{1cm}$ was 1.45, calculated theoretically and provided by MedImmune.

2.2.7.1 UV-Vis spectrophotometer

An Agilent 8453 UV-Vis spectrophotometer was used (model G1103, Agilent Technologies, Germany). A quartz cuvette with 1 cm path length (Hellma, Germany) was used for measurements. Cleaning of the cuvette was done with an aqueous solution of 2% v/v Hellmanex (Hellma, Germany), and thoroughly rinsed with acetone and deionised water.

The spectrophotometer had a range of 190 to 1100 nm, collecting spectra with a resolution of 2 nm or better. This spectrophotometer had a UV light source, deuterium lamp, as well as a visible light source from a tungsten-halogen lamp. It used on single

beam mode, where the buffer solution was used as blank before measuring the absorbance of diluted protein solutions.

For all protein solutions at higher concentration than 50 mg/mL, a double dilution scheme was followed to allow a measurement of sample diluted to 0.5 mg/mL. Protein samples diluted to this concentration would typically guarantee an absorbance value at the mid-range of linearity for the Lambert-Beer function. Each second dilution was produced in triplicate so that the absorbance measurement (and posterior concentration calculation) was reported as an average of 3 measurements. Dilution factors were calculated and used for determination of concentration. Dilutions were chosen so that the dilution factors would not exceed 1000. An error of up to 10 % was accepted for these measuremets.

Besides the absorbance measurement at 280 nm, absorbances at 310 and 340 nm were also monitored. Protein concentrations were reported with its concentration corrected for absorbance at 310 nm, related to possible interference of aggregates absorption. Thus, the following equation was applied to calculate the protein sample concentration:

$$c = \frac{A_{280m} - A_{310nm}}{A^{1\%}_{1cm} \times 0.10 \times DF} \tag{2.25}$$

where DF is the dilution factor.

2.2.7.2 NanoDrop - microquantitation spectrophotometer

When samples were not in sufficient volume to use for conventional UV-spectrophotometry measurements, the NanoDrop 2000 spectrophotometer was used (Thermo Scientific, UK). This microquantitation spectrophotometer uses samples of 2.5 μL to measure UV-Vis absorbance. The sample was held in place by its surface tension between two optical fibers on a pedestal that could optimise the pathlength according to the sample concentration, thus allowing measurement of UV -Vis absorbance for highly concentrated protein samples. The instrument used a Xenon pulse lamp, with

a wavelength range between 190-840 nm, and a linear CCD array detector analysed the light with a spectral resolution below 2 nm. The pathlength could be fixed to 1 mm, as well as it could automatically vary for high concentration samples [101].

2.2.8 Light Scattering techniques

When a solution with molecules is illuminated by light, depending on the optical parameters of the instrumentation, part of this light will be scattered by the molecules. This scattered light can be analysed regarding its intensity or its fluctuations. Scattered light measured in terms of its time-averaged intensity is called static light scattering. Whereas when it is measured in terms of the fluctuation of intensity with time, it is called dynamic light scattering. With the former, the parameters that can be derived are the weight-average molecular weight of the molecules present in solution, as well as their radius of gyration and self virial coefficient. DLS allows to characterise the molecule's translation diffusion coefficient and obtain a hydrodynamic radius (or diameter) [102, 103].

2.2.8.1 Particle sizing using dynamic light scattering

Dynamic light scattering (DLS) is a technique for measuring the size of particles within the sub micron region. DLS measurements are based on Brownian motion, the random movement of particles in solution due to displacement of solvent molecules, and relates to the size of the particles. An estimated measure of the hydrodynamic diameter (H_D) of the analysed particles is based on the measurement of the translational diffusion coefficient (D) of particles in a solution using the Stokes-Einstein-Sutherland equation:

$$H_D = \frac{k_B T}{3\pi\eta D} \tag{2.26}$$

where k_B is Boltzmann's constant, T is temperature and η is the solvent viscosity. H_D measured by DLS refers to the diameter of a sphere that has the same diffusion coefficient as the sample particle. Besides temperature and viscosity, the diffusion speed can also

be influenced by ionic strength of the medium [104]. From equation 2.26, the larger the diameter of the particle, the lower its diffusion speed will be. The DLS instrument thus measures the diffusion and relates to the size of the particles by illuminating these with a laser and analysing the intensity fluctuations of the scattered light. The diffusion coefficient is measured from the time correlation function:

$$g(\tau) = 1 + B\exp[-2Dq^2\tau] \tag{2.27}$$

where τ is the time (in μs), B is the signal amplitude of the correlation function. q , the scattering vector, is defined from the equation:

$$q = \left(\frac{4\pi n}{\lambda_0}\right)\sin(\frac{\theta}{2}) \tag{2.28}$$

where n is the refractive index of the solvent, λ_0 is the wavelength of the laser, and θ is the scattering angle. The instrument uses a digital correlator to produce correlation functions which relate to the particle size in the suspension tested by the rate of decay of the correlation function - smaller particles show a rate of decay faster than larger particles. The software then calculates statistically (through algorithms) the size distribution of the test sample. The typical size distribution graph is a distribution of size classes on the x-axis, while the y-axis shows the relative intensity of scattered light (intensity distribution). This distribution can then be converted to volume distribution and number distribution [105, 106].

Sizing measurements were performed using the Zetasizer NanoZs dynamic light scattering instrument by Malvern Instruments (Malvern, UK). Samples were illuminated by a 633 nm laser and light scattering was detected at 173° by an avalanche photodiode. DLS results were managed and analysed using Malvern's Zetasizer software version 7.01. The quartz cuvette was for low sample volume (12 μL), and it was extensively cleaned with detergent (2% v/v Hellmanex), thoroughly rinsed with DI water and acetone of HPLC grade (Fisher, UK). An air duster was used to prevent any dust contamination

that could originate artifacts during readings. Protein samples were measured at 1 mg/mL diluted in sample buffer, to reduce non-linearity effects on measurements by increased viscosity of solvent with higher concentrations. Detailed protocols for these measurements will be referred in each of the experimental chapters methods subsection on DLS.

2.2.8.2 Static light scattering theory

The equation that relates the intensity of scattered light with the properties of the macromolecules in solution is:

$$\frac{R_\theta}{K^* c} = MP(\theta) - 2A_2 cM^2 P^2(\theta) + ... \tag{2.29}$$

where R_θ is the excess Rayleigh ratio, c is the concentration of the macromolecule in solution (g/mL), M is the molecular weight, A_{22} is the self (or second) virial coefficient, K^* is the optical constant, and $P(\theta)$ is the particle scattering function. The excess Rayleigh ratio (R_θ) is the normalised scattering intensity for a specific scattering angle, relating the intensity of light, measured as voltage by photodiodes, to the scattering intensity (I_T), refractive index (n_T and Rayleigh ratio (R_T) of a known reference compound, e.g. toluene (equation 2.30).

$$R_\theta = \frac{I_A n_0^2 R_T}{I_T n_T^2} \tag{2.30}$$

The optical constant K^* is defined for a vertically polarised incident light by the following equation:

$$K^* = \frac{4\pi^2 n_0^2}{\lambda_0^4 N_A}(dn/dc)^2 \tag{2.31}$$

This constant is therefore a function of n_0 the refractive index of the solution, λ_0 the incident light wavelength, N_A Avogadro's number, and of dn/dc the refractive index increment specific for the scattering macromolecules.

With infinitesimal dilutions ($c \to 0$) and scattering angle tending to zero ($\theta \to 0°$), the equation 2.29 can be simplified to

$$\frac{R_\theta}{K^* c} = M_w \tag{2.32}$$

which determines the value of molecular weight for the macromolecule in solution. Since in practice, static light scattering measurements are made of finite dilutions and scattering angles, an extrapolation to zero needs to be made with one or both limiting conditions in order to calculate the molecular weight. Therefore, for polydisperse solutions this molecular weight will be apparent, since higher concentrations may yield non-ideality in solution, where non-specific interactions may occur between protein species causing the molecular weight to differ from the actual molecular weight. It will also be a weight-averaged molecular weight, since it accounts for the presence of more than one species in solution [102, 103].

The particle scattering function $P(\theta)$ refers to the change of scattered light intensity with the angle of detection. It is typically a decline of scattered light with increasing angle and it is due to intramolecular interference of light scattered by different points of the same particle [102]. For protein species with a maximum dimension $< \lambda_0/20$ there is small angular dependence, thus behaving as isotropic light scatterers. In contrast, for much larger sizes, protein species will scatter light differently from different points of its structure, thus creating an angular dependence. It is from the particle scattering function (2.33) that the radius of a particle (e.g. higher order protein species) can be calculated [102, 103].

$$\lim_{\theta \to 0} \frac{1}{P(\theta)} = 1 + \frac{16\pi^2}{3\lambda^2} R^2 \sin^2(\theta/2) = 1 + \frac{q^2}{3} R^2 \tag{2.33}$$

where λ is the wavelength of incident light in a given solven, R^2 is the mean square radius of the macromolecule, and q is the scattering vector. According to equation 2.33, for small angles, plotting $P(\theta)$ against $\sin^2(\theta/2)$ will yield straight lines with slopes pro-

portional to R^2. This means that the slope of the angular variation of scattered light intensity, when extrapolated to angle zero, gives the root mean square radius of the macromolecule (R). The radius can thus be determined without knowing the concentration and dn/dc of the scattering particles. For the case of proteins, R can be used to model protein conformation and understand better its triaxial structure [103].

Equation 2.29 can be represented in the following form:

$$\frac{K^*c}{R_\theta} = \frac{1}{MP(\theta)} + 2A_2c + 3A_3c^2 + ... \tag{2.34}$$

Equations 2.29 and 2.34 represent formalisms, i.e. different ways of processing the experimental data and are denominated Debye and Zimm formalisms, respectively.

Performing measurements at multiple angles allows extrapolation of the ratio K^*c/R_θ to zero angle ($sin^2(\theta/2)$, which with an extrapolation to zero concentration forms the basis of the Zimm plot (Figure 2.9(a)). In this case, both concentration and scattering angle dependence is taken in account. A Zimm plot is an analysis method to extrapolate weight-average molecular weight, the second virial coefficient and the radius of the macromolecule, based on the Zimm formalism.

A simpler way of processing the data is by plotting K^*c/R_θ versus concentration (c) neglecting the scattering angle dependency, thus generating a Debye plot (figure 2.9(b)). This can be the case for protein monomers when dimensions can be $< \lambda_0/20$. From this, by extrapolating to zero concentration, the (apparent) weight-averaged molecular weight can be estimated from the interception at y-axis, and the self virial coefficient can be estimated from the slope of the linear regression [102]. Note that processing experimental data via a Debye plot can be performed by either using the Zimm or the Debye formalisms and the same applies when processing data via a Zimm plot.

The parameter from equation 2.29, A_2 the self virial coefficient, is related to the thermodynamic aspect of the solution. The equation 2.29 has further terms for cross (third) and higher virial coefficients that can be ignored for dilute concentrations. When

plotting R_θ/K^*c against concentration (c), the function becomes linear at the low concentration region, with its slope directly proportional to the self virial coefficient. The deviation from linearity occurs at higher concentrations, hence when working at these conditions non-linearity terms need to be considered [102, 103, 107].

A_2 can be useful in protein formulation since it helps characterise non-specific intermolecular interactions. The buffer conditions (e.g. ionic strength, pH) can change the virial coefficients, thus giving information on the effect of the buffer constituents on the interactions. The virial coefficients do not give a specific form of interaction, only the net average interaction. A positive value indicates a net repulsion, while a negative value indicates a net attraction. It is also possible to calculate cross virial coefficients which represent the non-specific interactions between different species in solution [107, 108].

Experimental details

1. **Self virial coefficients**

   To determine the self virial coefficient for both the β-lactoglobulin (12.7 mg/mL) and the mAb (5 mg/mL) in their buffers (10 mM His-His.HCl, pH 6.0), a composition gradient multi-angle light scattering (CG-MALS) Calypso I instrument from Wyatt Technology Corp. was used. This system allowed samples to mix through a series of feed syringe pumps that were controlled by the software. Therefore, a protein stock solution would be continuously diluted with buffer in the number of step dilutions required, in a continuous process. The mix was then fed into a multi-angle light scattering system (DAWN-HELEOS II, λ_0=658 nm, 18 angles, fused-silica flow cell) and an OptilabREX differential refractometer (light source 660 nm) (both detectors from Wyatt Technology Corp., Santa Barbara, Califor-

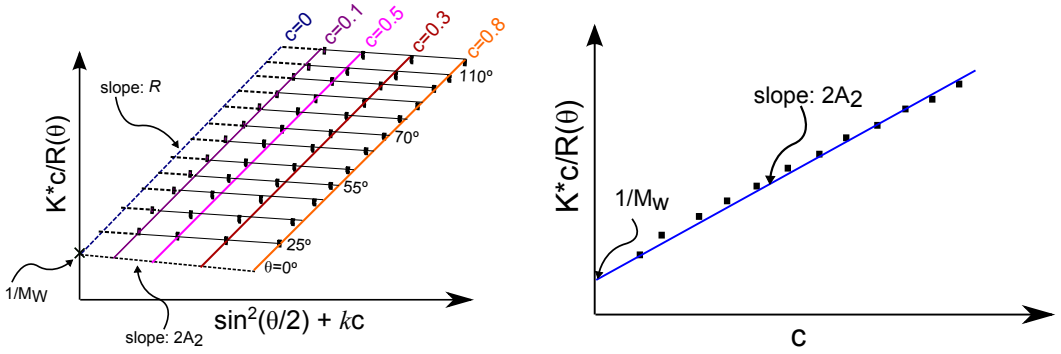

(a) (b)

Figure 2.9: (a) Example of a Zimm plot, where K^*c/R_θ is plotted for four different concentrations (c in mg/mL) and for various scattering angles (θ) (Zimm formalism; k is an arbitrary offset factor). The molecular weight is calculated by common intercept of the extrapolation of each concentration curve to zero angle (θ=0°) and the extrapolation to c=0 mg/mL intercept. The slopes can give the radius of the molecule (R) and the self virial coefficient values (A_2). (Image based on reference [103].) (b) Example of a Debye plot, where K^*c/R_θ is plotted in function of concentration, using scattering data from only one angle (θ) (Zimm formalism). In this case, molecular weight can be calculated from the intercept at y-axis and the slope can give the self virial coefficient value.

nia, USA). All protein samples and buffers were filtered prior to analysis, using 0.1 μm pore-size Millex-VV PVDF syringe filters. Measurements were taken at 25 °C. The system was extensively cleaned with a detergent aqueous solution of 5% v/v Contrad 70, followed by a thorough flush with ultrapure water. Cleaning solutions were filtered with 0.22 μm pore size Millex-GV PVDF membrane syringe filters (EMD Millipore, USA). All buffers and solutions were previously degassed to avoid presence of air bubbles.

2. **Size-exclusion chromatography with static light scattering**

   Multi-angle light scattering was used for the determination of molecular weight and radius of mAb monomer and aggregated species. The MALS detector was a DAWN HELEOS II (λ_0=658 nm, 18 angles, fused-silica flow cell), connected to an

Agilent Technologies 1200 series liquid chromatography system (Agilent Technologies, Germany). Details of this experiment are described in section 2.2.9.3.

2.2.9 High performance size exclusion chromatography

Size exclusion chromatography (SEC) is a liquid chromatography technique, also known as gel permeation chromatography (GPC) or known as gel filtration chromatography. SEC will be referred to in this work as the general term that describes the method of separation of molecules by molecular weight distribution via a chromatographic method. This method was used in its high performance liquid chromatography format, for quantitative analysis purposes only and not for fractionation of materials. The use of high performance size exclusion chromatography (HPSEC) allowed the analysis of synthetic polymers and/or biomacromolecules in an appropriate mobile phase in less than 30 minutes.

SEC separates on the basis of molecular hydrodynamic volume or size, and not by an enthalpic interaction with stationary phase, such as ionic exchange or adsorption partition chromatography. The sample is dissolved in its solvent and injected into a column packed with porous particles of an average pore size and particle size. The mobile phase can be the same as the sample's solvent. After injection, the molecules elute through the column and those which are too large to penetrate the pores of the stationary phase will elute out first, in the column's void volume. If smaller sized molecules are present, these will penetrate the pores respectively to its pore size. The smallest material will freely diffuse into and out of the pores, thus taking longer to elute from the column. In summary, the high molecular weight material will elute first from a SEC column, followed by low molecular weight species (Figure 2.10) [102, 109].

This basic principle of separation is generally accepted as the major separation mechanism and is termed steric exclusion. However, there are other mechanisms that can play

an important role, such as restricted diffusion and separation by flow. Restricted diffusion refers to the depth of permeation of each molecule being governed by its diffusion coefficient, which is indirectly related to the molecule's size. In this case, the elution volume (time that each molecule takes to elute out of the column) should depend on the method's flow rate. The concept of separation by flow is related to narrow capillary flow that can be considered to be the case of the exclusion volume around the particles contained in a SEC column. The larger molecules occur closer to the centre of capillary flow and thus flow faster than the smaller molecules, which are statistically situated close to the wall (stationary particles) where the flow is slower. Therefore, there is separation due to hydrodynamic size and exclusion volume [102].

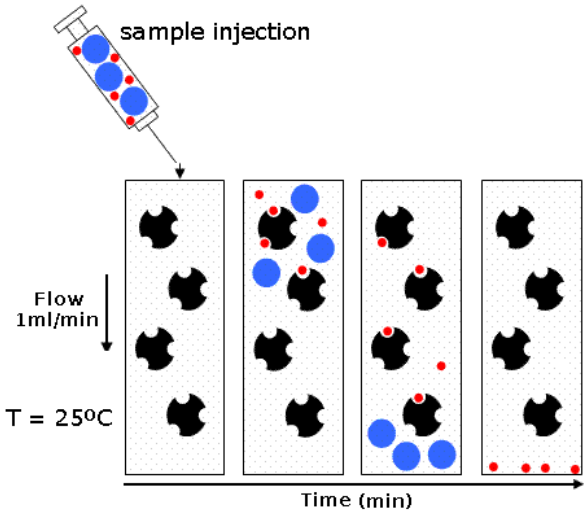

Figure 2.10: Basic schematics of how a size exclusion chromatography method works. After sample is injected, the separation is based on the molecular size of the solution's components. The larger molecular weight species will flow out first and the smaller molecular weight species will be eluted later.

In pratical SEC experiments, one can often encounter evidence of sample - stationary

phase interaction by the appearance of peak tailling or changes in elution times. This is related to various types of interactions between sample and column packing and/ or long-term use of the column. It is possible to minimise this by selecting suitable column packing, as well as suitable mobile phase, temperature, possible use of additives to the mobile phase or sample solvent. Peak broadening can also be another problem in SEC experiments affecting the determination of molar mass distribution. Therefore, it is necessary to tightly control the column's efficiency throughout its lifetime. SEC results, as with all other liquid chromatography techniques, will be highly sensitive to variables such as temperature, flow rate, and sample concentration. The latter is the most dependable of the user and therefore it is crucial to keep this parameter in mind for sample comparability [102, 109].

2.2.9.1 Calibration and detectors for HPSEC

As HPSEC is a relative and not an absolute molecular weight determining technique, the column needs to be calibrated appropriately with standards of known molecular weight. The most simple way of running a SEC system is the conventional SEC method where only a concentration detector is connected on-line with the column. The concentration detector can be a UV detector or refractive index, RI, detector. Calibration is then performed and established, allowing the analysis of samples and determination of their molecular weight in relation to the elution volume. To achieve the most accurate calibration it is necessary to use a series of well-characterised narrow standards as chemically similar as possible in composition to that of the sample to be analysed. However, it is often the case that this is unavailable, therefore the alternative is to use broad standards or a universal calibration [102].

Another method for HPSEC calibration can be the universal calibration method,

where chemically different standards can be compared to the samples' chemistry. The use of universal calibration is related to the assumption that the hydrodynamic volumes of all species eluting at the same elution volume are identical and that the product $[\eta]M$ represents a universal calibration parameter [102]. In this type of calibration, the intrinsic viscosity can be measured by use of a viscometer on-line with the SEC column and the concentration detector (e.g. RI).

Another alternative is triple detection and its calibration. The detectors used for this type of calibration are: a concentration detector (UV or RI), a viscometer (for measurement of intrinsic viscosity) and a light scattering detector. This type of detection has the advantage of providing with weight-average molecular weight, molecular size (within the system's resolution), and intrinsic viscosity, along with information on the molecular structure and aggregation - in the case of polymer samples.

In triple detection, the system can be calibrated by running only a single narrow standard to verify the instrument constants of the detectors and allow to correct for inter-detector shifts and inter-detector preak broadening effects [110].

Column calibration should occur at identical conditions as those chosen for sample characterisation (same solvent, temperature, and flow rate). A good calibration usually comprises that the standard selection covers the entire molar mass range of the samples to be analysed.

2.2.9.2 HPSEC for the determination of level of protein aggregation

To relatively quantify the level of protein aggregation, the HPLC system used was from Agilent Technologies 1200 series (Germany) with the following components: degasser, binary pump with a 100 μL injection loop, an autosampler, thermostatted sample tray (usually at 5 °C, unless noted otherwise), a thermostatted (at room temperature) column

holder and a UV detector. The software used for this system was Chemstation for LC systems, by Agilent Technologies.

A Tosoh Biosciences, LLC (USA), model TSK gel G3000SWxl column was used (7.8 mm (ID) x 30 cm (L)), composed of silica gel particles with mean particle size of 5 μm and pore size of 250$\dot{A}$. A guard column (silica particles of 7 μm, 6 mm (ID) x 4 cm (L)) was also used with the analytical column.

Throughout this work for all protein sample HPSEC analysis, the mobile phase was an aqueous buffer of 0.1 M sodium sulfate ($NaSO_4$) and 0.1 M dibasic sodium phosphate anhydrous (Na_2HPO_4), titrated to pH 6.8 with 6N HCl. This buffer was filtered with 0.22 μm pore size vacuum-driven filter units (PES membrane, EMD Millipore, USA).

All protein samples were diluted to 10 mg/mL, injection volume was of 25 μL. Run time was 20 minutes at a flow rate of 1 ml/min. Each sample was injected at least three times, unless stated otherwise. Formulation buffers respective to the protein samples were also injected.

As this chromatography system allowed variable injection volumes, it was possible to change both protein sample concentration and injection volume, keeping constant the sample loading, to check for changes in aggregation level of protein species.

For this method the column was not calibrated for molecular weight analysis, the chosen standards were used for system suitability. Bio-Rad gel filtration protein standards (Bio-rad Laboratories, Inc., USA) were prepared according to the manufacturer's instructions and an aliquot was injected (25 μL) once after every 20 injections of unknown protein samples. Bio-Rad protein standards are composed of a mixture of five molecular weight markers ranging from 1.35 to 670 kDa. The mixture includes vitamin B_{12}, myoglobulin, ovalbumin, bovine gamma-globulin and thyroglobulin. An example for the Bio-Rad protein standards chromatogram is in Figure 2.11. The system suitability criteria were as follows:

- resolution of peak 4: ≥ 2.00;

- peak symmetry for peaks 4 and 5: > 0.65 and < 1.20.

All samples (including buffers and Bio-Rad protein standards) were filtered through 0.45 μm centrifugal filters (Ultrafree-MC PVDF, EMD Millipore, USA). The obtained chromatograms followed integration and peak symmetry and resolution were calculated via the method analysis used on the software.

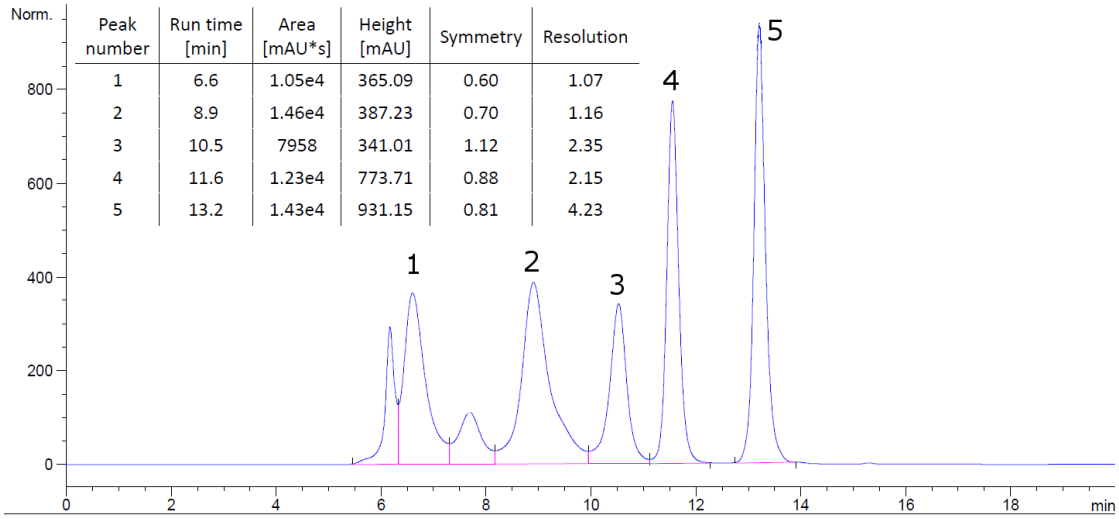

Peak number	Run time [min]	Area [mAU*s]	Height [mAU]	Symmetry	Resolution
1	6.6	1.05e4	365.09	0.60	1.07
2	8.9	1.46e4	387.23	0.70	1.16
3	10.5	7958	341.01	1.12	2.35
4	11.6	1.23e4	773.71	0.88	2.15
5	13.2	1.43e4	931.15	0.81	4.23

Figure 2.11: Typical chromatogram obtained with high performance size-exclusion chromatography systems described in section 2.2.9.2 for the Bio-rad gel filtration standards. Peaks correspond to the following proteins present in the standards mixture: 1) thyroglobulin (670 kDa); 2) bovine gamma-globulin (158 kDa); 3) ovalbumin (44 kDa); 4) myoglobulin (17 kDa); and 5) vitamin B (1.35 kDa). Inset table refers to chromatography data obtained to assess system suitability.

2.2.9.3 HPSEC protein analysis with multiple detectors

Two systems were used depending on the information needed: molecular weight, size and intrinsic viscosity; or only molecular weight and size of protein species.

1. **Calculation of molecular weight and intrinsic viscosity of protein monomer and its associative species for rAlbumin solutions**

   The system used for this experiment was a Polymer Labs GPC 50 (Agilent Technologies, USA) gel permeation chromatography unit that comprises an autosampler, a fixed volume injection loop (20 μL), thermostatted column holder, and the following detectors: a 90° light scattering detector, a refractive index detector, and a differential pressure viscometer.

   The column and guard column used in this experiment were the same as for the previous section. Protein samples were diluted to 15 mg/mL. For system suitability, Bio-Rad protein standards were injected after every 20 injections of unknown samples. Each sample was injected three times, with buffers injected at least once. Elution time was kept to 20 minutes, flow rate of 1 ml/min. The mobile phase was the same as for the conventional HPSEC set-up described previously.

   Calibration of this system was according the triple detection method described earlier, following the software's algorithm for calibration. The standard used were solutions of Polyethylene oxide in PBS. dn/dc used was 0.185 mL/g.

2. **Calculation of molecular weight of monomer and its associative species for mAb solutions**

   For this experiment the system used an Agilent Technologies system as described in section 2.2.9.2 with a change in the detectors used. For concentration, an Optilab REX RI detector was used and an on-line DAWN-HELEOS II multi-angle light scattering detector was added. Details on both these detectors can be found in section 2.2.8.2. The following method details were kept constant as stated in section

2.2.9.2: HPSEC analytical column and guard column (Tosoh Biosciences), mobile phase, run time, flow rate, number of injections per sample, injection volume (25 μL), column temperature and system suitability checks with Bio-Rad protein standards.

Calibration of this experimental setup was made using a BSA standard at 2 mg/mL in phosphate buffer and sodium azide 0.2 % (dn/dc of 0.185 mL/g), obtained from Pierce Labs (Thermo Scientific, UK). Analysis and integration of the chromatograms was performed using Astra 6 software (Wyatt, Santa Barbara, California, USA).

2.2.9.4 HPSEC for synthetic polymers

The system used was a Polymer Labs GPC 50 (Agilent Technologies, USA) gel permeation chromatography unit that was constituted by an autosampler, a degasser, a fixed volume injection loop, and thermostatted column holder. The following detectors were used: 90° light scattering detector, a refractive index detector, and a differential pressure viscometer.

Two Polymer Labs PLgel mixed-D columns were used (porous polystyrene and divinylbenzene matrix, 5 μm mean particle size, ID 7.8 mm x 30 cm) with a corresponding guard column (5 μm mean particle size, ID 7.8 mm x 50 mm) (Agilent Technologies, USA). For all the polymers analysed, the sample dissolving solvent and the mobile phase were chloroform / triethylamine ($CHCl_3$/TEA) 95/5 % v/v. Sample concentration was typically 3 mg/mL, except for intrinsic viscosity measurement where several dilutions were injected. Injection volume was of 100 μL. All samples were injected three times, with a runtime of 30 min, flow rate at 1 ml/min and column temperature at room temperature.

1. **Determination of molecular weight and intrinsic viscosity of polymers**

   Calibration of the system for this purpose was performed according to the triple detection method where a narrow standard was a polystyrene polymer (2-5 mg/mL). Linear polyethylglycols (PEGs) were also analysed for validation and for comparison purposes.

2. **Determination of molecular weight of polymers**

   The same system was calibrated using the conventional method where only the RI detector was used for concentration detection. A mixture of narrow polystyrene standards were used for calibration (EasiVials polysterene PS-M 2mL, Agilent Technologies, Germany).

2.2.10 Tensiometry

Tensiometry is a measurement of surface tension at an interface, e.g. liquid - vapour. Surface tension can be defined as a force resisting change and acting in right angles to a line of unit length in the surface of a liquid [111].

This technique was used to measure the surface tension of β-lactoglobulin samples (see Chapter 4), and polymer solutions (see Chapter 6). Tensiometry was measured using a Krüss K100 tensiometer using a curved Wilhelmy plate with 40.2 mm wetted length (dimensions: 19.9 mm width, 0.2 mm thickness, 10 mm height). Experiments were performed at room temperature ($\sim$ 25 °) for at least 2 hours, and were performed with freshly prepared samples. Sample volume was 1.2 mL and contained in a steel vessel during measurements. Ultrapure water fitered with 0.22 μm pore-size syringe filters (Millex-GV PVDF, EMD Millipore, USA) was measured to prior any sample measurement, and after the plate was thoroughly cleaned. Cleaning the plate was done with ultrapure water and then burning until incandescent to eliminate any contamin-

ants. Sample buffer's surface tension was also measured for comparison. Surface tension measurements were taken every second and values were reported when equilibrium was attained as an average with standard deviation.

The plate was made of roughened platinum and optimally wetted so that the contact angle is close to 0°, meaning that $\cos 0° = 1$. According to the equation below,

$$\gamma_{ST} = \frac{F}{L \cos \theta} \tag{2.35}$$

surface tension should only be dependent of the force measurement, since the wetted length is also fixed. Using a Wilhelmy plate had the advantages of not needing any correction nor knowing the densities of the analysed liquids.

2.2.11 Density measurement

Density measurements were performed in order to determine the density of all protein samples that were used throughout this work for later calculation of viscosity using the falling-ball viscometry data. In all cases, the measurement was kept the same. The densitometer DMA 35N was used (Anton-Paar, Graz, Austria). This instrument measures density via the oscillating U-tube principle, which is a U-shaped borosilicate glass tube that contains the sample and is electronically vibrated at a specific frequency. The characteristic frequency will change depending on the density of the sample. As density is temperature dependent, the temperature of the measurement needs to be determined with accuracy via a temperature sensor which is part of the instrument [112].

The densitometer was cleaned extensively with DI water and absolute ethanol before and in between all measurements. Before every measurement of sample, the instrument's calibration was checked by measuring the density of DI water at room temperature (typically 23 °C) and cross-checked with the reference table provided by the manufacturer. For each sample, the density measurement was made at the same temperature that was

chosen for the viscometry measurement (with the AmVn). For this purpose, the densitometer was kept in an incubator for the time needed until the adequate temperature was reached. Measurements were conducted in triplicate, recording also the temperature. All samples were at a concentration of 1 mg/mL.

2.2.12 micro-Differential scanning calorimetry

Calorimetry is a technique for measuring the thermal properties of materials to directly measure the enthalpy associated to physico-chemical processes related to thermal changes [113]. Generally, there are two types of differential scanning calorimeters: heat-flux and power-compensated. In a heat-flux calorimeter, the sample and a reference are enclosed within a furnace which is heated at a linear rate. The thermocouples measure the difference in heat capacity (C_p) and the heat flow is determined by the following equation:

$$q_h = \frac{\Delta T}{R} \tag{2.36}$$

where q_h is the heat flow, ΔT is the temperature difference between the sample and reference, and R is the resistence of the thermoelectric disk that transfers heat to the sample and the reference [113, 114]. A power-compensated calorimeter has the sample and reference in separate furnaces heated separately. This technique measures the difference in thermal power, in function of temperature or time, necessary to keep the sample and reference at the same temperature [114].

Micro differential scanning calorimetry (μDSC) is a commonly used technique used and applied to protein physical-chemical analysis. μDSC is typically used to determine the transition temperature (T_m - also called melting temperature) and obtain thermodynamic analysis of protein folding and unfolding. The μDSC measures the excess heat capacity of a sample relative to a reference, which in this case is the sample buffer, as a function of temperature. Several parameters can be measured,

such as the transition temperature at a peak maximum, the difference in enthalpy (ΔH_m) which is calculated via area under the heat capacity curve (C_p), and the change in heat capacity (ΔC_p) for the transition between folded and denatured state of the protein sample. These parameters are related to the free energy change, calculated by the Gibbs-Helmholtz equation 2.37, from disruptions of the stabilized native protein structure to an unfolded state (ΔG_{unf}) [84, 113, 115].

$$\Delta G_{unf} = \Delta H_{unf}\left(1 - \frac{T}{T_m}\right) - \Delta C_p\left[(T_m - T) + Tln\left(\frac{T}{T_m}\right)\right] \tag{2.37}$$

As the μDSC is sensitive enough, it can help identify the most stable protein mutant, describe the unfolding process and its kinetics (e.g. if it is reversible or irreversible), and determine the interaction of proteins with various molecules (e.g. DNA, ligands, ions). In addition, the DSC technique is increasingly used for biopharmaceutical formulation as it can help detect and quantify the potential stabilisation effects of additives, as the addition of excipients/additives can alter the transition temperature of the protein. Therefore, DSC is widely used as one of the techniques for formulation screening, as pH, ionic strength and the additives can influence the thermodynamics of protein unfolding [84, 113].

For this study, DSC was used for the determination of the monoclonal antibody's melting temperatures, as this molecule was the only without any literature reference for its transition temperatures. For an IgG_1 monoclonal antibody, a μDSC scan can show melting temperatures for the C_H2, Fab and C_H3 domains. Depending on the secondary structure for the IgG_1 and if the mAb is glycosylated or not, the melting temperature for each of these domains may or may not be resolved as individual transitions. An advantage of using μDSC to study antibodies is that the transitions corresponding to these domains can be identified and compared in most cases. Besides this, by comparing

mAb μDSC analysis with the use of different formulation buffers, one can detect changes in peak shape or peak area hence evaluating the possible influence of buffer excipients on the unfolding of the analysed domains. In the case of storage stability being influenced by conformational stability, the higher the thermal transition temperature is, often corresponds to higher stability (keeping the same buffer conditions as studied) [116,117].

2.2.12.1 μ-DSC experimental details

DSC measurements were carried out in the temperature range 25 - 100 °C by using a microcalorimeter VP Capillary DSC (MicroCal Inc., Northampton, MA, USA). A scan rate 95 °C/h was performed for the present study. DSC curves were analysed with MicroCal LLC Auto sample Origin software. The data were corrected for the calorimetric baseline (by subtracting water - water scan) and for the difference in heat capacity between the initial and the final state by choosing a sigmoidal baseline. System calibration was performed with injection and measurement of melting temperature for a lysozyme solution at a concentration of 3 mg/mL in ultrapure water (Lysozyme and ultrapure water obtained from Sigma-Aldrich, UK). All monoclonal antibody samples were measured at 5 mg/mL. Samples ran three times, each with volume of 500 μL. The standard lysozyme solution was injected before and at the end of the DSC run, with ultrapure water as reference. In this study all protein samples were dissolved in the same buffer (10 mM His-His.HCl, pH 6), therefore only one pair of reference buffer was needed.

2.2.13 Protein electrophoretic methods

Protein electrophoretic methods are techniques that allow separation and identification of proteins with basis on applying an electric field and therefore promoting migration

of the charged biomacromolecule. Separation can be made on basis of the protein's size (sodium dodecyl sulfate polyacrylamide gel electrophoresis - SDS-PAGE) or the protein's charge (isoelectric focusing) [86].

2.2.13.1 Microfluidic chip SDS-PAGE

SDS-PAGE protein electrophoresis is a technique widely used for separation of proteins according to their size under denaturing conditions by using the anionic detergent SDS (sodium dodecyl sulfate). It can also determine the relative molecular mass of the proteins analysed. This technique can allow the detection of dissulfide bonds in protein structure where samples are diluted in a reducing buffer containing a reducing agent, either β-mercaptothiol or dithiothreitol (DTT). These agents reduce the accessible reducible covalent dissulfide bonds responsible for associating species, or associating domains within the protein monomer (as in the case of an IgG_1 antibody). As a comparison, samples are also ran in a non reducing buffer, where these dissulfide bonds are not reduced. Therefore, in protein formulation, SDS-PAGE has the utility of separating aggregate, monomeric and fragmented protein forms in the 10 - 250 kDa range, identifying the covalent aggregates and fragments [86, 118].

A microfluidic chip protein electrophoresis system was used for rapid qualitative protein electrophoretic analysis. This recent 'lab-on-a-chip' technique follows the same principles as SDS-PAGE for proteins with the advantage of allowing to run samples at the microscale using a microfludics chip with microliter sample volumes, therefore providing much faster results [119, 120].

Microfluidic SDS-PAGE experimental details

An Agilent 2100 Bioanalyzer system and its corresponding Protein 230 kit were used (Agilent Technologies, Germany). All the kit components, including the microfluidics chip, were proprietary to Agilent Technologies. The kit reagents were: gel matrix solution, protein dye concentrate, a marker protein sample buffer solution (containing both a high and low molecular weight fluorescent marker, also present in the protein ladder, as well as SDS) and a protein molecular mass ladder solution.

The gel matrix and destain solutions were prepared following the manufacturer's protocol with only slight changes. To prepare a 1 M DTT solution (dithiothreitol; reducing agent), the contents of one tube of 'No-weigh' DTT (Pierce Labs, Thermo Fisher Scientific, UK) were added to 50 μL of ultrapure water. A reducing sample buffer was prepared by adding and vortexing 3.6 μL of 1 M DTT solution to a sample buffer 60 μL aliquot. 1 M Non-reducing NEM (N-ethylmaleidemide, Fluka Biochemika, UK) solution was prepared by weighing 12.5 mg of NEM into 100 μL of ultrapure water. This sample was vortexed and left for 2 min at 80 °C for full dissolution. The non-reducing sample buffer was prepared by adding 3.6 μL of 1 M NEM solution into 60 μL of sample buffer. Protein samples to be analysed were individually diluted to 4 mg/mL in phosphate buffered saline (PBS) (constituting individual protein sample stock solutions). From each of these sample stock solutions, 5 μL were taken and added to 5 μL of either non-reducing or reducing sample buffers in small tubes. The protein ladder was prepared by aliquoting (6 μL) separately into a new tube. The protein samples and protein ladder were heated at 80 °C for 5 minutes (reduced samples and protein ladder) and for 1 minute (non-reduced samples). After heating, all tubes were cooled down by centrifuging at 13 000 rpm for 1 minute (Haereus Pico, Thermo Fisher Scientific, UK). In new tubes, 84 μL of ultrapure water was added to 6 μL of each reduced and non-reduced samples, and to the protein ladder. All protein samples, protein ladder,

reducing and non-reducing sample buffers were freshly prepared, thoroughly mixed and used only within 24 hours.

After priming the chip with gel-dye mix, each of the 4 wells were filled with more gel-dye mix (12 μL each). The destain solution (12 μL), protein ladder (6 μL) and protein samples (6 μL each) were then aliquoted to their corresponding well (Figure 2.12). Detection of protein was made by laser-induced fluorescence. After reading the chip, the software used a method for automated integration for the peaks detected in each sample well.

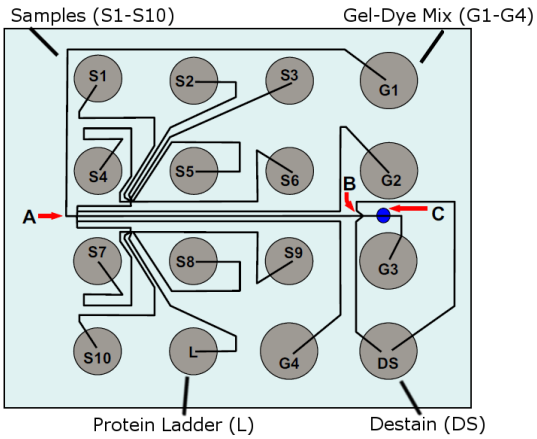

Figure 2.12: Microfluidics SDS-PAGE chip schematics. There are a total of 16 wells where four are for the gel-dye mix, one is for destain solution, another for the protein ladder and the remaining wells for samples (all assigned in the figure). Also highlighted are the separation channel (A), the position for destaining (B) and the position where fluorescence is detected (C) (figure is adapted from reference [121]).

In this technique, migration times are normalised since the sample buffer contains low and high molecular weight markers as internal standards. A calibration curve is created from all the molecular weight markers present in the protein ladder sample [121, 122]. System suitability criteria were followed, particularly concerning the protein ladder used, to check that the chip had run and samples were integrated correctly. The following

parameters were checked for system suitability [119]:

- six ladder peaks should be observed;
- the lower molecular weight marker (4.5 kDa) should fall between migration times of 15 - 22 seconds;
- the mid-molecular weight marker (63 kDa) should fall between migration times of 27.23 - 28.31 seconds;
- the upper marker (240 kDa) should fall between migration times of 37 - 46 seconds.

2.2.13.2 Isoelectric Focusing

Capillary isoelectric focusing (cIEF) is an protein electrophoretic technique that separates proteins based on the macromolecule's charge according to the protein's isoelectric point (pI) . In this method a pH gradient is formed by a mix of ampholytes, typically polyamino-polycarboxylic acids which can cover either a wide or a narrow range of pH, according to the expected pI of the proteins being analysed/ separated [86, 123]. Capillary electrophoresis uses very narrow bore tubes, allowing faster method preparation and run time. As IEF is sensitive to any molecular differences that can cause a change in the protein's net charge, ciEF can be used to check for batch-to-batch differences [124, 125]. Imaging capillary IEF was used to analyse each of the mAb batches available.

IEF experimental details

An iCE280 IEF analyser (ProteinSimple Ltd., California, USA) was used, with a microinjector autosampler and a cIEF cartridge fluorocarbon-coated filled with electrolyte solution. For imaging, the system has a CCD camera with a UV absorption detector.

A light source of 280 nm, from a deuterium lamp, was focused onto the capillary. All reagents and other system specific components were supplied by ProteinSimple, Ltd.. 4 mL glass vials were placed on the autosampler containing 0.5% methyl cellulose solution (in two vials, respectively, buffer and balance vials), a rinse vial with ultrapure water and an empty vial. After the instrument start-up procedure, to ensure that the capillary system was running correctly, it was checked that the anolyte (80 mM phosphoric acid) and catholyte solutions (19 M sodium hydroxide) were full in their respective tanks (no leakages were to be observed).

All samples (from the batches: mAb b1, b2a and b2b) were diluted in ultrapure water to stock concentrations that when added to sample buffers would yield a final concentration of 0.25 mg/mL. For each sample a buffer was prepared containing 8 μL of pH 8 - 10.5 Pharmalyte (GE Healthcare, USA), 70 μL of 1% w/w methylcellulose (ProteinSimple, Canada), and 1 μL of each of the pI markers (8.18 and 9.77) (ProteinSimple, Canada), and remaining volume of ultrapure water (Sigma-Aldrich, UK) to make up to 250 μL total sample volume. Samples were aliquoted (100 μL) to appropriate glass vials and were analysed in duplicate.

A hemoglobin control was ran for system suitability. This sample was freshly prepared using the ProteinSimple iCE280 suitability kit: 2.5 μL of a hemoglobin stock solution provided was added to a buffer solution already containing a 8% v/v pH 3-10 Pharmalyte, internal pI markers 4.22 and 9.46 in 0.35% v/v methyl cellulose. The control was always included in a cIEF run, typically running twice before and twice at the end of each group of samples to be analysed. An example of hemoglobin control is showed in 2.13. Acceptance criteria for the hemoglobin sample were the following:

- absorbance data for each of the pI markers needed to be within $\pm$ 3 times the standard deviation of the mean of absorbance;
- HbA1c shoulder should be observed;

- Four major peaks of hemoglobin control must be present (HbA, HbF, HbS and HbC);

- HbA peak pI should be between 6.85 - 7.45.

Focusing conditions for hemoglobin controls were as follows: pre-focusing period - 1 min and 1500 V; main focus period - 4.50 min and 3000 V. Focusing conditions for mAb samples were as follows: pre-focusing period - 1 min and 1500 V; main focus period - 7 min and 3000 V. Both hemoglobin and mAb samples were further analysed using the analysis software ChromPerfect iCE280. The pI was reported for the main peak observed.

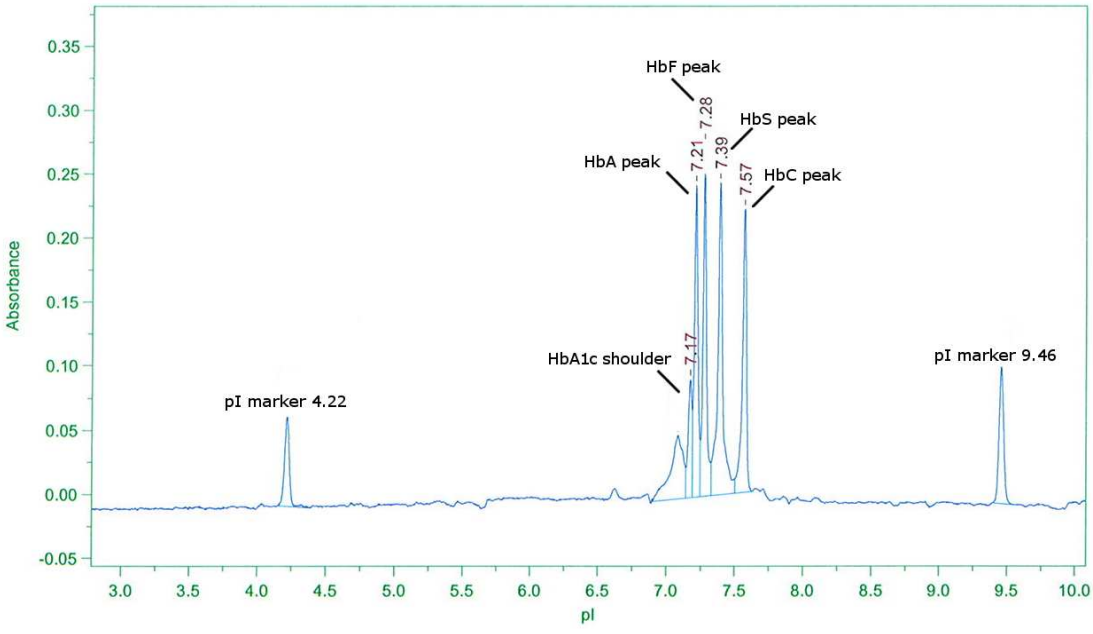

Figure 2.13: Typical chromatogram obtained with capillary isoelectric focusing electrophoresis for the hemoglobin standard. Peaks are assigned and identified according to manufacturer's details for the product, containing normal hemoglobins A (and its shoulder HbA1c) and F, and abnormal hemoglobins S and C. pI markers are also assigned.

2.2.14 Circular Dichroism

Circular dichroism (CD) was used to check the mAb's conformation after its purification and concentration. CD is a technique that refers to the difference in absorption of two circularly polarised components of polarised UV light, left and right. These components of polarised light (of the same amplitude and frequency) will be absorbed by the protein, an optically active - chiral - solute, in different ways according to its secondary and tertiary structures. The CD measurements are reported in ellipticity which is the angular difference in absorbance (in mdegs), between left and right circularly polarised light, in function of the wavelengths screened. The secondary structures existing in a protein (α-helices, β-sheets, turns and random coils) can be identified by screening in the far UV region (180 to 260 nm). The tertiary structures are identified when screening the near UV region (250 to 360 nm) [86].

As all batches of mAb were in a 10 mM His-His.HCl pH 6.0 buffer and L-histidine is an amino-acid commonly present in proteins, thereby showing chirality and absorbing UV light, aliquots of each batch were buffer exchanged to 10 mM sodium phosphate pH 6.5. Samples were diluted to 1 mg/mL and measured for both far UV and near UV using a Jasco J815 circular dichroism spectrometer (Jasco, UK). Near UV required a 10 mm pathlength quartz cuvette (sample volume $\sim$ 1 mL), while for far UV slides of 0.1 mm pathlength were used (all optical cuvettes from Starna, UK). Each sample was ran in triplicate and each final spectrum was an accumulation of 3 scans. For near UV the wavelength range was between 250 - 320 nm, whereas for far UV the wavelength range was 180 - 260 nm. All scans were performed with a 1 nm step and a scan rate of 20 nm/min. Scans were collected at 20 °C using of a peltier cell holder and a water cooling system. Blank scans with buffer only were also collected for posterior blank subtraction from sample scans. For both far UV and near UV data collections, data were converted using the Jasco Spectra Analysis software, from ellipticity degrees to

molar ellipticity by accounting for mAb molar concentration ($\sim 6.3\times10^{-6}$ M) and the optical pathlength. Data was further converted into molar residue ellipticity by dividing the molecular ellipticity by the total number of amino-acids present in the mAb. For far UV, final data analysis was performed using CDPro software package which provided secondary structure information in relative % for each type of structure.

2.2.15 Flow imaging microscopy for sub-visible particle counting

Flow imaging microscopy is a technique that is currently used in biopharmaceutical industry for the quantification and characterisation of sub-visible proteinaceous particles in protein formulation [126]. Various protein degradation pathways can generally lead to aggregation and the formation of sub-visible (1 - 100 μm) and visible ($>$ 100 μm) particulates, depending on their size. These proteinaceous particulates represent a loss of monomeric species, potentially containing numerous monomer units [127]. Flow microscopy, along with light obscuration particle counting and membrane microscopy methods, are used in the biopharmaceutical industry to characterise and quantify these proteinaceous particulates to monitor the potential link between protein aggregation and immunogenicity [128].

Flow microscopy operates by digital image analysis to count the suspended particles in the flowing liquid. The sample is pumped by a peristaltic pump through a flow cell (100 μm, 1.6 mm), while images are recorded. The images are analysed relative to the variations in transmitted light intensity, resulting from particles present in the fluid [39, 129].

A micro-flow imaging microscope DPA4200 (Brightwell Technologies Inc, Canada) was used to detect and count particles sized between 1 - 150 μm for mAb solutions and for β-lacroglobulin solutions, both at different concentrations and conditions. On the

sample inlet, a 10 mL glass syring was fixed with a luer lock and through it 20 mL of ultra pure water and 10 mL of Decon 90 10% v/v were flushed (6.65 mL/min) into the flow cell to ensure the system was clean. This cleaning procedure was repeated between samples and higher volume of water or detergent would be used until the system was acceptably clean. During this step, it was important to ensure no air bubbles were present in the flow cell.

The buffer (10 mM His-His.HCl pH 6.0) was run in triplicate as a sample for negative control. The buffer was filtered prior analysis (0.1 μm pore size syringe filters). Details on the protein samples' concentration will be described in the experimental chapter's methods section. The filtered buffer was typically sonicated for 20 minutes prior analysis. All protein samples were gently mixed for homogeneity, with care to not introduce air bubbles. All liquids were left to equilibrate at room temperature for at least 30 min to release air bubbles. 1 mL of sample buffer was ran before every sample for baseline purposes, followed by measurement of 1.1 mL protein sample at a flow rate of 0.22 mL/min. A purge volume of approximately 250 μL was done for all samples. Data analysis was made with MFI View application software package. A filter was applied to ignore all particles with an aspect ratio of $\geq$0.85. The results were reported as average cumulative particle numbers per mL or particle counts per size range from 1 - 150 μm. The particle size was reported as equivalent circular diameter (ECD). The cleaning procedure was resumed after measurements with aid of the glass syringe. Flow cell calibration was performed with polysterene beads of referenced size (10 μm diameter).

2.2.16 Visual inspection of protein solutions

Presence of visible translucent particles in the samples and determination of colour were determined against a black and white panel under white fluorescent light. The samples were visually analysed and compared against particle standards, opalescence standards, colour standards, and their respective blanks. Prior to analysis, standards and samples were left at room temperature for equilibration and the illumination lamp was left on for at least 30 minutes. Analysis consisted on gently shaking the vials (standards and samples) for 15 seconds and visually inspect immediately after shaking. To improve probability of detection of particles, if needed, this procedure was repeated multiple times. In any case of doubt, a (blinded) second opinion by another trained person was asked for confirmation of analysis.

The particle standards were aqueous dilutions from stock containing 1 mg/mL barium sulfate ($BaSO_4$) and 0.1% w/w sodium azide (NaN_3). Six dilutions were prepared (0.001 mg/mL to 0.2 mg/mL) as well as a blank (ultrapure water vial). Three degrees of classification for presence of particles were: free from particles, corresponding to the blank vial; practically free of particles, corresponding to standards 1 - 5; and containing particles, corresponding to standards 5 - 7.

The opalescence standards were formazin references standards and its dilutions described in the European Pharmacopeia [130]. Eight standards were prepared of increasing nephelometric turbidity units (NTU) ranging from 3 (standard 1) to 1000 (standard 1000) and related to a blank (ultrapure water vial). The classification of samples according to their opalescence were divided in four categories: clear, when comparable to standards 0 - 1 (0 - 3 NTU); slightly opalescent, when comparable to standards 1 - 3 (3 - 18 NTU); opalescent, when comparable to standards 3 - 6 (18 - 120 NTU); and opaque, when comparable to standards 6 - 8 (120 - 1000 NTU).

The colour references solutions (according to the European Pharmacopeia, Fluka,

Sigma-Aldrich, UK) were of three types: yellow, brown and brown-yellow. Classification of samples was made according to four categories, compared to the provided blank solution, as follows: colourless, if comparable to standards 7 - 8; slightly coloured, if comparable to standards 4 - 7; coloured (yellow, brown-yellow or brown) if comparable to standards 2 - 4; and intensively coloured, if comparable to standards 1 - 2.

Chapter 3

The effect of protein concentration on the viscosity of a recombinant albumin solution formulation

3.1 Introduction

The viscosity of protein formulations is an important issue for the biopharmaceutical industry due to its practical implications [5]. As discussed earlier in the main introduction, biopharmaceutical liquid formulations are frequently created with high protein concentration, due to the need for high mass delivery to overcome low potency, and low volumes to allow patient self-administration in cost effective devices [5,8]. However, when biomacromolecules reach high solution concentrations problems such as high viscosity and poor flow properties, as well as stability issues, can arise.

Several theories from colloidal science have been used to understand observed increases in solution viscosities with increases in macromolecular content. Some of these models are based on approximations to hard spherical repulsive particles, and have been applied to proteins with some success. However, it has been suggested that there are more factors, such as shape [131], charge distribution [67, 71] or kinetics of association [6, 51, 72] which need to be considered for successful prediction of protein solution viscosity.

The present theoretical models tend to assure that any change in composition of

protein species in solution is negligible. Parameters present in these models typically account for only one species of a specific shape and size. In the colloidal suspension literature, some authors have addressed the problem for binary mixtures of different sized particles, to predict the impact of this on the solution viscosity [132–135]. In the biopharmaceutical literature, recent reports have studied binary blends of proteins by controlling the content of each protein in solution and understanding the effect of this on the overall solution viscosity [136, 137]. Nevertheless, a real biopharmaceutical formulation will depend on various factors such as pH, temperature, ionic strength, different stabilising additives in solution, and it will most likely be a solution composed of the monomeric biomacromolecule coexisting with self-associative species that may or may not be of reversible nature.

From a practical point of view, while developing protein solution formulations, it is important to understand what the most important factors are in the prediction of protein solution viscosity. In the work presented here, a recombinant human albumin solution formulated in a buffer containing salt and a surfactant was studied. Samples were prepared ranging from 0.1 mg/mL to approximately 500 mg/mL, and were investigated for their rheological characteristics using steady shear rheology with a torsional rheometer and other viscometric measurements. A detailed biophysical characterisation of these samples was performed to account for its level of aggregation, size and shape of protein species. Using this information, a comprehensive analysis of the rheometric data was performed by applying the most commonly used models that predict protein solution viscosity. This included a most recent approach reported in the literature, which takes in account the variation in solution composition [136, 137]. Additional experiments were also done to understand the impact of the formulation buffer and its components.

The main aim of this work was to understand if at higher concentrations of rAlbumin, there is a relationship between the level of aggregation and the solution viscosity

observed. By investigating this possible relationship, we aim at better understanding why the highly concentrated globular protein solutions (> 200 mg/mL) are often found to deviate from theoretic models.

3.2 Materials and Methods

3.2.1 Materials

3.2.1.1 Protein sample

Recombinant human albumin (rAlbumin) was donated by Novozymes Biopharma UK, Ltd. (Nottingham, UK) in the form of Recombumin® Prime (batches used: 1104 and 1101). The product is a liquid formulation of concentration 200 mg/mL, stored at 2-8 °C. This rAlbumin is expressed in *Saccharomyces cerevisiae* and is identical to human serum albumin (HSA) [138]. HSA is the most abundant protein in the blood at a concentration of ∼40 mg/mL. It is the major transport protein for unsterified fatty acids, having the capacity of binding numerous metabolites, active pharmaceutical ingredients as well as other organic molecules [139].

Figure 3.1: Ribbon model of the x-ray chrystal structure of HSA marking the three domains I, II and II, labeled in red, green and blue, respectively. Generated using the UCSF Chimera package [140] using X-ray coordinates 1AO6 (Protein Data Bank, taken from reference [139]).

HSA has three repeating domains (I-III), each divided into two sub-domains [139] (Figure 3.1). The protein has an average molecular weight of 66.5 kDa, is comprised of 585 amino acids, and its secondary structure has approximately 67% α-helix content with the remainder is β-turns and extended polypeptide chains [141]. HSA has 17 disulfide bonds. In physiological conditions there is only one free cysteine residue (Cys 34) [131, 138, 139]. The protein's isoelectric point has been reported to be between 4.7-5.7 depending if the protein is lipid-bound and on the buffer used [106, 141]. In physiological pH (pH = 7.4), HSA has a negative net charge, calculated to be -19e [141]. HSA has been commonly used as stabiliser for biological materials and with the availability of recombinant human albumin, the latter has been approved as a substitute for HSA as a formulation excipient [138].

3.2.1.2 Sample preparation

All reagents were obtained from Sigma-Aldrich, UK and were of analytical grade.

The formulation buffer of Recombumin is composed of NaCl (145 mM), polysorbate-80 (15 mg/L) and sodium octanoate (32 mM) in ultrapure water (pH = 7.0 $\pm$ 0.3 at room temperature). Another buffer was prepared containing only NaCl (145 mM) in ultrapure water (pH = 7.0 $\pm$ 0.3).

Centrifugal concentrators (Vivaspin 20 - 5 kDa molecular weight cut-off - with PES (polyethersulfone) membrane (Sartorius Stedim, Ltd., UK) were used to concentrate rAlbumin samples to a higher concentration than the starting material (200 mg/mL). The procedure recommended by the manufacturer was followed, using a fixed 45° rotor centrifuge (Hermle Z400, Labortechnik GmbH, Germany). After centrifugation, samples were collected, mixed and checked for their concentration using UV-Vis spectroscopy. The stock solution of rAlbumin, as well as all samples in their respective buffers, were

kept stored at 2 - 8 °C.

3.2.2 Methods

3.2.2.1 Quantification of protein concentration by UV-Vis spectroscopy

For the determination of concentration of rAlbumin solutions, the percent extinction coefficient ($A_{1cm}^{1\%}$) used was 5.8 [99]. The concentrations reported were calculated as an average of measurements of 3 separate dilutions prepared from each sample or, in the case of the NanoDrop, 3 separate samples when no dilution was required. An error of up to 10 % was accepted for these measurements.

All details related to this method are described in section 2.2.7 in Chapter 2.

3.2.2.2 Rheology

The rheometers used were Anton-Paar (Graz, Austria) modular compact rheometers (MCR) , models 301 and 501. Cone-and-plate geometries used throughout this study were stainless steel CP50-1 (diameter = 50 mm and cone angle = 1°) and CP40-0.3 (diameter = 40 mm and cone angle = 0.3°). To prevent evaporation of sample and to maintain a constant temperature of 20 °C ± 0.1 °C throughout the measurements, an evaporation blocking system equipped with a peltier unit was used.

Reducing the presence of air bubbles in the samples and during loading was important to avoid artifacts during measurements. Depending on how highly concentrated the samples were, a low vacuum was used to induce bursting of air bubbles. This procedure was done for short periods of time (∼10 s) to prevent sample evaporation. Prior to measurements, all samples were allowed to equilibrate to room temperature (∼ 23 °C) for at least 40 minutes.

Rotational tests (flow curves and viscosity curves) were performed by controlling the

shear rate typically from 0.01 to 1000 s^{-1}, and measuring torque, shear viscosity and shear stress. To increase data validity and sensitivity of the method, each shear-rate step had a 60 second duration time during which the instrument was averaging over the collected data. Typically, two shear-rate sweeps (ramping down and up) were performed per sample, without waiting time between sweeps.

3.2.2.3 Falling-ball viscometer

For the calculation of intrinsic viscosity (in section 3.3.3) was determined using the bulk viscosity of lower concentrations of rAlbumin (0.1 - 2 mg/mL), an automated micro capillary viscometer (Anton-Paar, Graz, Austria). The capillary had an inner diameter of 1.6 mm and contained a steel ball of 1.5 mm diameter. For a standard measurement, the inclination angle was set at 70° (and -70°). Temperature control at 20 °C ±0.1 °C was ensured via a peltier unit attached to the instrument. The capillary was calibrated by running DI water and a viscosity standard oil at the same angle used for the sample measurement. Viscosity values were calculated from measured kinematic viscosities, accounting with the density values obtained for the studied samples, as described in section 2.2.11.

3.2.2.4 Micro-viscometer/rheometer on-a-chip (mVROC)

The microviscometer/ rheometer on-a-chip (mVROC), by Rheosense, Inc. (San Ramon, California, USA) was used for measurement of bulk viscosity at high shear rates. Samples analysed were rAlbumin solutions at 200 and 500 mg/mL. For these measurements, the A05 and D05 chips were used and temperature was kept constant at 20°C ± 0.1°C using a water circulation system (ThermoCube, SS cooling systems, USA) (for additional information, see section 2.2.6.2 in Chapter 2).

3.2.2.5 High performance size exclusion chromatography (HPSEC)

(a) Determination of level of protein aggregation

rAlbumin samples were analysed for their level of aggregation on HPSEC. Details related to method and equipment are described in section 2.2.9.2 in Chapter 2.

(b) Analysis with multiple detectors for determination of molecular weight and intrinsic viscosity of rAlbumin solutions

For the calculation of bulk molecular weight and intrinsic viscosity, the chromatography system used was a Polymer Labs GPC 50 Plus (Agilent Technologies, USA) gel permeation unit. Calibration of the system was made with polyethylene oxide solutions in PBS.

The method details chosen for these experiments were almost the same as in section the previous section with minor differences; samples were diluted to 15 mg/mL thus injecting 300 μg of total protein. System suitability was still performed with Bio-rad protein standards and the same buffer was used as mobile phase. Each rAlbumin sample was injected three times, with buffers injected at least once. dn/dc used for protein analysis was 0.185 mL/g [142].

3.2.2.6 Dynamic light scattering (DLS)

Details related to this method are described in section 2.2.8.1 in Chapter 2.

Measurement settings for rAlbumin size readings were at a constant temperature of 20 °C, performing 15 runs of 10 seconds each. An equilibration time of at least 5 minutes was set before the measurement started. For all protein samples, size measurements were made in triplicate with fresh aliquots for each reading.

3.2.2.7 Microfluidic chip sodium-dodecylsulfate polyacrylamide gel electrophoresis (SDS-PAGE)

All details related to this method are described in section 2.2.13.1 in Chapter 2.

The samples that were analysed were rAlbumin at ∼200, 250, 300, 350, 400, 450 and 500 mg/mL.

3.3 Results and Discussion

3.3.1 The rheological analysis of formulated recombinant human albumin solutions

The rheological analysis of rAlbumin solutions in its original formulation buffer (containing polysorbate-80 as a surfactant and salt) was done using a conventional rheometer equipped with cone-and-plate geometries (CP50-1 and CP40-0.3). As the commercially available solution is provided at 200 mg/mL of rAlbumin, it was the only sample studied directly from the manufacturer's vial. All other samples were prepared by either diluting in formulation buffer or concentrating using centrifugal concentrators.

Figures 3.2(a) and 3.2(b) showed that rAlbumin solutions showed constant shear viscosities for the increasing shear rates applied (0.01 to 1000 s^{-1}). Figure 3.3 showed a linear increase of shear stress with the increasing applied shear rates. For the higher concentration materials (400 - 500 mg/mL) the shear viscosities were from ∼1 s^{-1} onwards, while showing slight non-linear increase of viscosities when < 1 s^{-1}. However, in general, throughout the range of concentrations of rAlbumin presented and the applied shear rates, it was considered that these solutions exhibited a Newtonian-like behaviour. This is a clear contrast to what has been observed in previous studies of the rheology of globular proteins [60–62, 78] where an apparent yield-behaviour has been reported, particularly at lower shear rates. The reason for this purely viscous Newtonian-like

behaviour is likely due to the presence of polysorbate-80, a well known surfactant used in biopharmaceutical formulations. Similar rheological behaviour has been reported for globular protein solutions in a buffer also containing a polysorbate [74, 143].

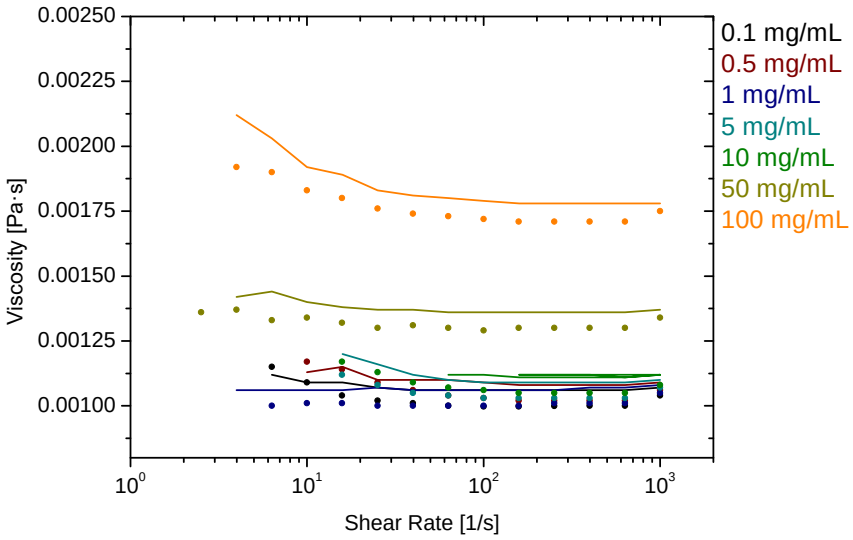

(a)

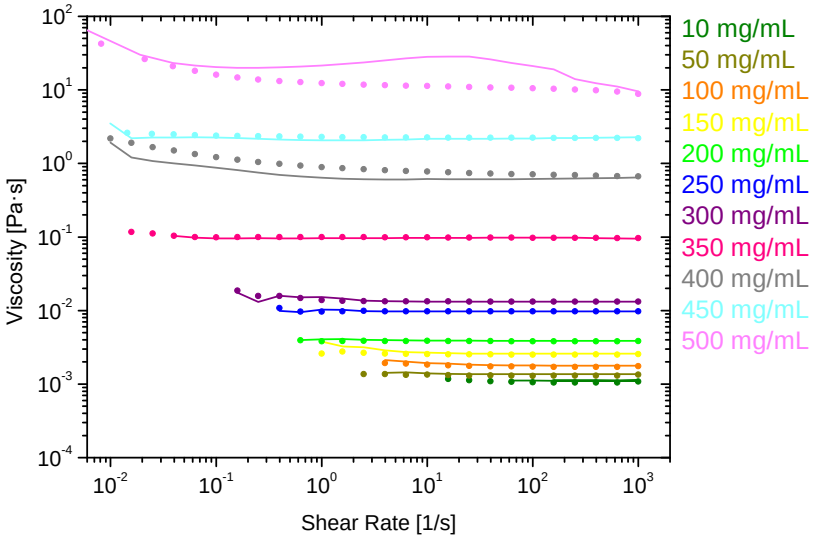

(b)

Figure 3.2: Experimental steady shear rheology of rAlbumin solutions. Viscosity values are shown for ramping down (closed circles) and ramping up (lines) shear rates. (**a**) Samples from 0.1 to 100 mg/mL. (**b**) Samples from 10 to 500 mg/mL. All data collected with cone-plate 50 mm, 1°, and cone-plate 40 mm, 0.3°, at 20 °C.

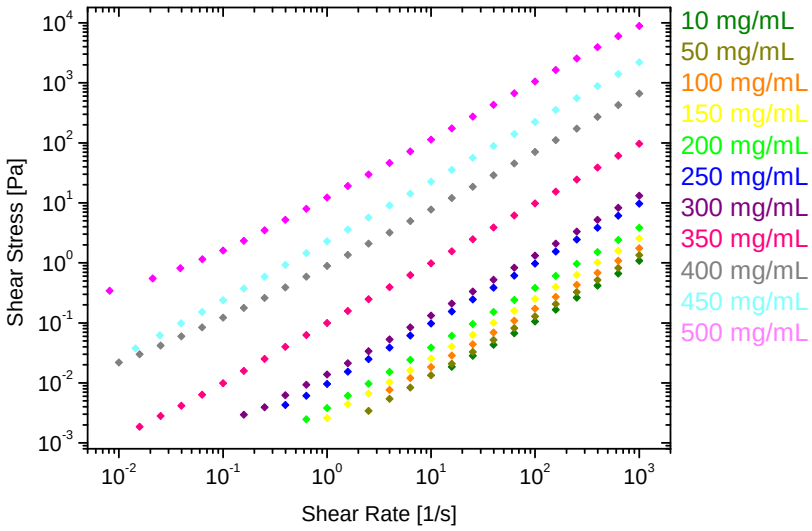

Figure 3.3: Flow curves for experimental steady shear rheology of rAlbumin solutions from 10 to 500 mg/mL. Shear stress values are shown only for ramping down shear rates. Data collected with cone-plate 50 mm, 1°, and cone-plate 40 mm, 0.3°, at 20 °C.

Each sample was measured using two consecutive shear rate sweeps, ramping down and up, after a 10 minute waiting time (Figures 3.2(a) and 3.2(b)). Hysteresis effects were not observed, in agreement with the literature [60, 61, 78]. However, the sample identified as ∼500 mg/mL seemed to show a different behaviour when sweeping up the shear rates, compared to the result seen with ramping down (Figure 3.2(b)). This was possibly due to an artifact caused by the presence of air bubbles. As this sample presented the highest concentration and was the most viscous, loading it on the lower plate of the rheometer was difficult and small air bubbles could have been introduced. After the slight increase in viscosity at mid range of shear rates, this sample showed a gradual decrease of viscosity to values similar to those seen before, particularly at the higher shear rates. This is an artificial shear-thinning-like behaviour, most likely to do with presence of air bubbles being squeezed out of the sample as it was sheared at higher shear rates ($> 100\ s^{-1}$) [144].

The instrument's lower detection limit for valid torque measured, according to the manufacturer, is 0.1 μN.m for steady shear experiments. Therefore, rAlbumin samples of concentrations from 0.1 up to 50 mg/mL, with viscosities very close to 1×10^{-3} Pa.s, showed valid data only up to $\sim$6 s^{-1}. Below this shear rate, torque values were not considered as valid. To demonstrate this in a clear way, a comparison was made with calibrant standard hydrocarbonate oils N1.0 and N14 (Cannon Instruments), with reported viscosities at 20 °C of 0.93 mPa.s and 24 mPa.s, respectively (Figure 3.4). As the rAlbumin samples increased in protein concentration, with a corresponding increase in viscosity, the measured torque was increasingly higher than the lower detection limit, therefore increasing the data validity towards lower shear rates (0.01 s^{-1}).

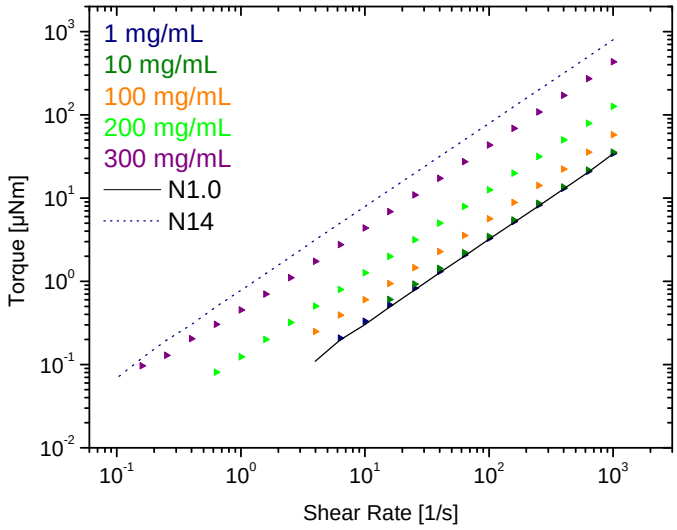

Figure 3.4: Torque values from experimental steady shear rheology of rHA solutions. Triangles - torque values for rAlbumin samples. Lines are representative of torque values for calibration standard oils, N1.0 (solid line, η = 0.93 mPa.s) and N14 (dashed line, η = 24 mPa.s). Data collected with cone-plate 50 mm, 1° at 20 °C.

For comparison between the concentration of samples and the obtained shear viscosities, the viscosity values at 1000 s^{-1} were taken from three separate readings per sample

and are reported in Figure 3.5 as an average with the respective standard deviation. The viscosity values reported here are those at high shear viscosity, η_∞, and it is assumed that it is correct to extrapolate a similar viscosity per sample at zero shear (η_0), since the viscosities of these samples were overall shear-rate independent [78].

Table 3.1 shows the measured concentrations of samples in comparison to the target concentrations. It was difficult to achieve targeted concentration values with higher concentrations ($\geq$ 300 mg/mL), due to the difficulty of accurately achieving such values using centrifugal concentrators. This was mostly relevant with the sample targeted at 500 mg/mL, where its higher viscosity yielded difficulties in further concentrating the sample.

From Figure 3.5, it can be clearly seen that for lower protein concentrations the viscosity values were similar. An increase of viscosity with increasing of concentration was clearly seen, in agreement to what has been reported throughout the literature with regards to serum albumin solutions [71,78,145]. Most importantly, the exponential trend observed from the data in Figure 3.5 is also reported for other globular proteins, such as immunoglobulins [6, 51, 70, 72].

From correlation of the data in Figure 3.5 and Table 3.1, it is clear that the larger increase in viscosity occurred between concentrations ~250 and ~500 mg/mL. The ~500 mg/mL sample reached a high shear rate viscosity of ~10000 times larger than that of water (1.0016 mPa.s at 20 °C, as defined by NIST). Although biopharmaceutical formulations are not formulated at such high concentrations (> 400 mg/mL), particularly for monoclonal antibodies formulations, the literature has discussed similar increases of viscosity [70, 136, 137]. Therefore, analysing the viscosity increase with concentration of rAlbumin solutions as a biopharmaceutical formulation model will help understand what factors govern this exponential function.

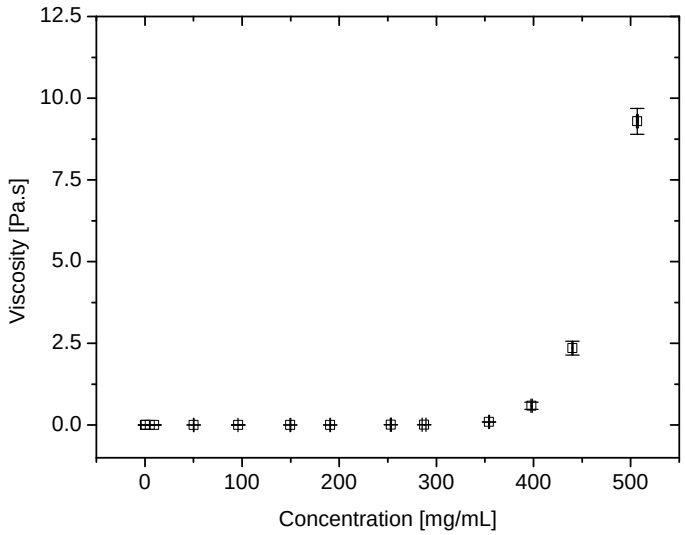

Figure 3.5: Viscosity of rAlbumin solutions ranging from 0.1 mg/mL to 500 mg/mL (target concentrations). Viscosites are taken at high shear ($\dot{\gamma} = 1000\ s^{-1}$) and at 20 °C. Viscosity values are represented as an average and standard deviation (error bars) of 3 separate measurements for each sample. Concentrations are represented as average of 3 measurements and error bars are standard deviation.

Table 3.1: Measured concentrations and respective viscosities corresponding to target concentrations of rAlbumin samples. All values reported are an average of 3 measurements, with corresponding standard deviations.

Target Concentration (mg/mL)	Measured Concentration (mg/mL ± st dev)	Viscosity (Pa.s ± st dev)
0.1	0.10 ± 0.001	$1.06 \times 10^{-3} \pm 1.2 \times 10^{-5}$
0.5	0.36 ± 0.01	$1.09 \times 10^{-3} \pm 6 \times 10^{-6}$
1	0.96 ± 0.01	$1.08 \times 10^{-3} \pm 6 \times 10^{-6}$
5	5.01 ± 0.02	$1.09 \times 10^{-3} \pm 1.7 \times 10^{-5}$
10	9.84 ± 0.18	$1.11 \times 10^{-3} \pm 6 \times 10^{-6}$
50	50.2 ± 0.27	$1.37 \times 10^{-3} \pm 6 \times 10^{-6}$
100	96.0 ± 0.08	$1.78 \times 10^{-3} \pm 0.0$
150	149.6 ± 0.41	$2.59 \times 10^{-3} \pm 6 \times 10^{-6}$
200	190.8 ± 0.26	$3.89 \times 10^{-3} \pm 1.2 \times 10^{-5}$
250	253.1 ± 0.49	$9.74 \times 10^{-3} \pm 2.2 \times 10^{-4}$
300	287.4 ± 2.03	$1.36 \times 10^{-2} \pm 3.5 \times 10^{-4}$
350	354.2 ± 0.40	$9.35 \times 10^{-2} \pm 4.3 \times 10^{-3}$
400	398.0 ± 0.71	0.59 ± 0.11
450	440.2 ± 0.51	2.35 ± 0.21
500	506.8 ± 0.95	9.29 ± 0.39

3.3.2 Characterisation of protein species present in recombinant human albumin solutions

Our aim was to correlate the observed increase in viscosities with the level of aggregation present in the increasing concentrations of rAlbumin samples. Therefore, an identification, relative quantification and size characterisation of the monomeric and oligomeric species present in solution was done using HPSEC, DLS and microfluidics SDS-PAGE.

3.3.2.1 High-performance size exclusion chromatography (HPSEC)

High performance size exclusion chromatography (HPSEC) was used to determine the level of protein aggregation as a function of concentration. Retention times for

the protein species typically present were $\sim$ 7.9, 8.7 and 9.8 minutes, corresponding to trimer, dimer and monomers, respectively (Figure 3.6). This method of analysis produced good resolution between the different identified species and it was comparable to literature values using a similar setup [146]. No higher molecular weight species other than dimers and trimers were found in any of the solutions analysed. This reflects the high purity of the recombinant albumin material due to its manufacturing process generating only a small percentage of trimers and dimers [138]. In this case all samples analysed were not thermally stressed. Therefore, the monomer showed the highest relative percentage with a peak area of >90%. Comparing peak areas between the samples (50 - 500 mg/mL), showed that the samples from 50 to 200 mg/mL have similar peak areas for all protein species. Only when concentrations reached approximately 250 mg/mL and over, a trend could be detected on the increase of dimers and trimers with a corresponding decrease of monomer. This trend was clearer for samples $\sim$ 350, 400, 450 and 500 mg/mL (Figure 3.7).

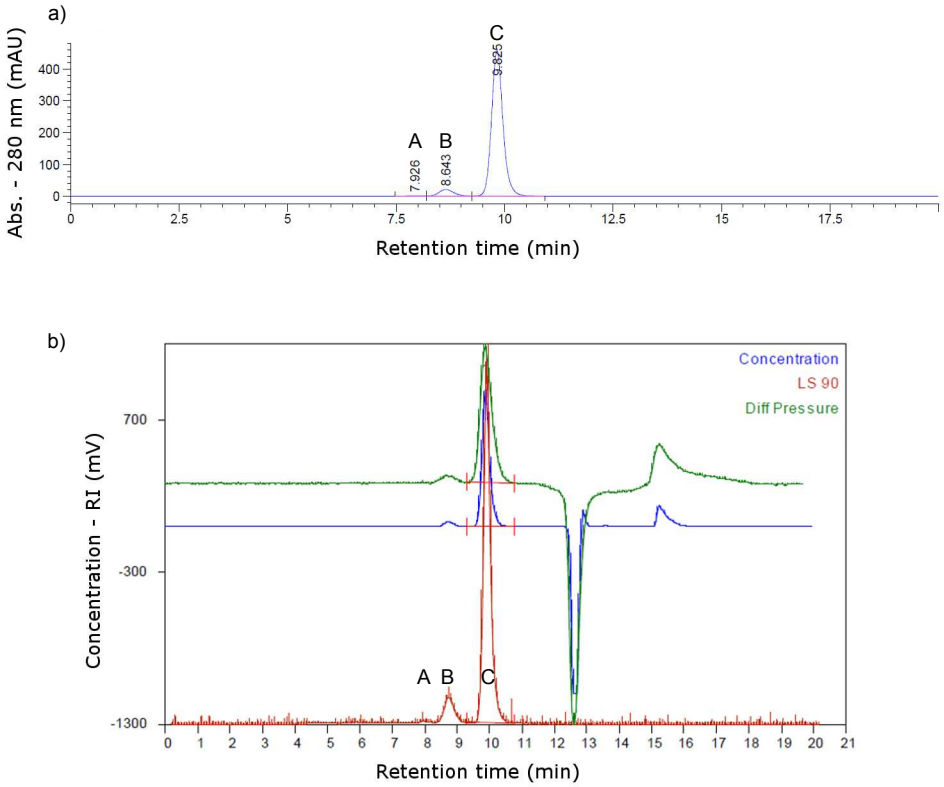

Figure 3.6: Size exclusion chromatograms for a 200 mg/mL rAlbumin solution, diluted to 10 mg/mL and analysed on a) HPSEC for level of aggregation and b) HPSEC with triple detection to determine bulk intrinsic viscosity and bulk molecular weight. In the chromatograms, the letters correspond to: A - trimer; B - dimer and C - monomer.

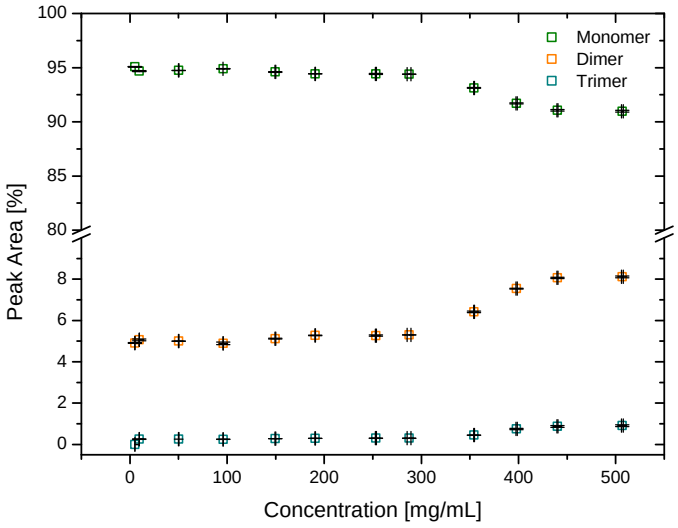

Figure 3.7: HPSEC conventional method for determining level of aggregation of rAlbumin solutions showing relative peak areas in %. Data in squares and represents an average of 3 readings. Error bars are standard deviation per sample for peak area % (y-axis) and for concentration (x-axis). All samples were diluted to 10 mg/mL prior to analysis.

Size exclusion chromatography required sample dilution for analysis when concentrations were >10 mg/mL. Dilution can be a limitation of the method since it can influence the material's content in relative percentage of each species, as it can be a factor for some aggregates to disassociate, and therefore be considered reversible [147, 148]. It was important to understand if this was the case with rAlbumin solutions. By comparing neat injections of 50 mg/mL and 10 mg/mL, it was observed that their respective peak areas were different in less than 1 % (Figure 3.8). Such low difference suggested that reversibility of trimers and dimers could be negligible. Moreover, this complies to the irreversibility of associative species that has been reported in literature [149].

In addition, a stability study of four weeks was done for fresh dilutions of rAlbumin (10 and 50 mg/mL) stored at 5 °C. The aim was to confirm that rAlbumin solutions would not aggregate when stored at 2-8 °C. It was found that within four weeks, a decrease of approximately 1 % of dimer occurred, corresponding to a similar increase

of monomer. This change attained a plateau after the first two weeks (Figure 3.8). It has been found that it is possible that dimerisation of albumin can also be due to self-association, not involving the free cysteine [150]. Therefore, in the case here, it could be possible that the low relative percentage of dimers may have formed by self-association during manufacture, remaining constant while the stock kept at 200 mg/mL and only dissociating after dilution along the time. When comparing injections of neat rAlbumin solutions, varying the sample concentration and injection volumes would possibly force faster dissociation, which would explain why there was not a difference in the relative peak areas between low and high concentrations of rAlbumin.

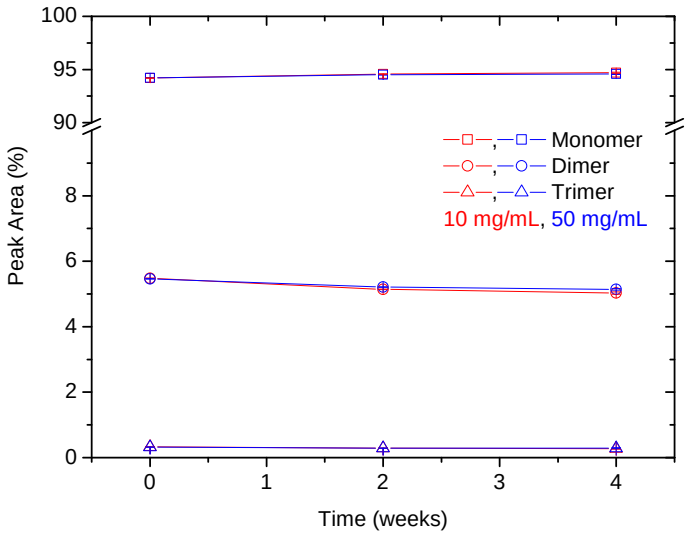

Figure 3.8: HPSEC conventional method comparing neat injections of 10 and 50 mg/mL rAlbumin solutions along 4 weeks with storage at 5 °C. Average and standard deviation (error bars represented) were reported from 3 separate readings. Line is for eye guidance only.

Triple-detection HPSEC was used to experimentally determine the intrinsic viscosity for each of the protein species present in rAlbumin samples: monomer, dimer and trimer. The information provided by triple detection HPSEC is advantageous as it typically allows the measurement of molecular weight, radius of gyration and intrisic viscosity for the individual species present in the samples and separated by the analytical column

[102]. Here, the determination of intrinsic viscosity and MW of rAlbumin species was relevant for subsequent analysis discussed in the following section (section 3.3.3).

The results presented are relative to the two peaks detected which were the monomer and dimer, since the differential pressure viscometer could not detect the low percentage of trimers present in solution (Figure 3.6). Analysis of peak areas per sample showed the same trend of increasing rAlbumin dimers, similar to what was observed previously for conventional HPSEC (Table 3.2).

Bulk intrinsic viscosity and bulk molecular weight values match well with the values reported in literature for human serum and bovine serum albumin [146]. No variation within these parameters with concentration was observed, which is a good indication of validity for both the samples and the experimental set-up.

Table 3.2: HPSEC triple detection values of peak area, bulk MW and bulk intrinsic viscosity (IV) for monomers and dimers detected in rAlbumin solutions. Average and standard deviations are reported for 3 separate measurements per sample.

Sample (mg/mL)	Monomer			Dimer		
	Peak Area (%)	Bulk MW (kDa)	Bulk IV (dL/g)	Peak Area (%)	Bulk MW (kDa)	Bulk IV (dL/g)
50	96.1 ± 0.03	65.0 ± 0.3	0.0408 ± 0.0004	3.9 ± 0.02	121.2 ±1.2	0.0482 ± 0.0014
100	96.0 ± 0.10	65.4 ± 0.9	0.0402 ± 0.0017	4.0 ± 0.10	143.0 ± 12.5	0.0446 ± 0.0089
200	95.7 ± 0.01	64.6 ± 0.6	0.0408 ± 0.0006	4.3 ± 0.01	130.4 ± 1.6	0.0477 ± 0.0044
250	95.7 ± 0.01	64.8 ± 0.7	0.0409 ± 0.0006	4.3 ± 0.01	132.5 ± 5.4	0.0505 ± 0.0072
350	94.7 ± 0.24	66.1 ± 1.8	0.0412 ± 0.0005	5.3 ± 0.24	138.3 ± 8.1	0.0441 ± 0.0101
400	94.5 ± 0.02	65.3 ± 0.2	0.0410 ± 0.0003	5.5 ± 0.02	132.7 ± 3.7	0.0489 ± 0.0050
450	94.3 ± 0.01	65.4 ± 0.2	0.0408 ± 0.0004	5.7 ± 0.01	131.7 ± 3.9	0.0462 ± 0.0046
500	93.9 ± 0.01	65.1 ± 0.2	0.0412 ± 0.0006	6.1 ± 0.01	132.1 ± 4.7	0.0467 ± 0.0056

3.3.2.2 Dynamic light scattering

The hydrodynamic size analysis of rAlbumin solutions by DLS was performed for the entire range of solutions 1 - 500 mg/mL after dilution to 1 mg/mL, when applicable. All solutions were analysed without prior filtration to assess if there were aggregates

present within the instrument's detection limit (up to 1 μm hydrodynamic diameter). In all cases, the samples did not show presence of other aggregates and only one broad peak was observed for size distribution by intensity (Figure 3.9). The hydrodynamic size distribution by volume also resulted in a broad peak, with its mean peak value skewed towards lower sizes, similar to that of the monomer. This reflects the higher relative contribution of monomer in comparison to the low contribution of dimers and trimers present in solution. For all the analysed samples, the measured hydrodynamic radii from the size distributions by intensity ranged between 3.8 - 4.5 nm corresponding to values commonly reported in literature [106] for a unstressed pure albumin solution.

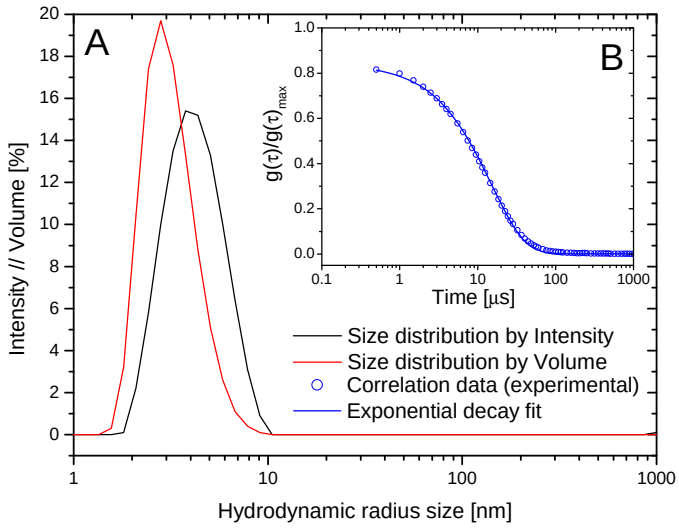

Figure 3.9: Dynamic light scattering plots for 200 mg/mL rAlbumin solution diluted to 1 mg/mL. A) Size distributions by intensity (black line), and by volume (red line). B) Correlation data versus the decay time (in [μs]) via the correlation function of measured intensity. Measurements taken at 20 °C.

3.3.2.3 Microfluidics SDS PAGE

Analysis with microfluidics SDS PAGE system allowed for further characterisation of rAlbumin solutions of higher concentrations. The samples chosen for comparison

were from 200 mg/mL to 500 mg/mL, since all prepared rAlbumin samples with concentration below 200 mg/mL would have been diluted from the same stock solution. For all analysed samples and in both reducing and non-reducing conditions, the major peak/ band detected at approximately 63 kDa was attributed to rAlbumin's monomer, in agreement to literature [138]. The purity of rAlbumin solutions via SDS PAGE showed consistency with the level of aggregation measured via HPSEC as it did not detect any protein fragments nor other protein species besides the expected dimerisation of monomers (peak/band present in reducing and non-reducing conditions, between 95 and 150 kDa markers). The absent detection of trimers, which are expected to have a molecular weight of approximately 200 kDa [138], could be due to their low quantity also observed in the HPSEC results (Figure 3.7).

Dimerisation of human serum albumin or bovine serum albumin is mostly due to formation of a covalent disulfide bridge between the free cysteine present in the monomer [151]. It was expected that dimers in rAlbumin solutions would be reduced by dithriothreitol (DTT) at reducing conditions, although it has been reported that HSA's oligomeric species can remain present even at similar reducing conditions [138]. It was seen that the peak percentage correspondent for dimer, although present in both gels (Table 3.3), exhibited lower values at reducing conditions compared to non-reducing conditions. To further reduce remaining dimers present in reducing conditions, it would be the case of further method optimisation by adding higher concentration of reducing agent (DTT) or allowing for longer heating time.

The protocol followed for this method was originally optimised for monoclonal antibody analysis. To allow for system suitability evalution, a stable and high purity (> 98 % by HPSEC) mAb (IgG_1) sample was added as a control to each of the microchips (reducing and non-reducing). The peak/band detected on the non-reducing gel could be attributed to a mAb monomer of approximately 150 kDa. Upon reducing conditions the

mAb sample yielded two peaks/bands at approximately 50 and 25 kDa, corresponding respectively to the heavy and light chains present in a IgG_1 [1, 12] (Figures 3.10(b) and 3.10(a)).

Table 3.3: Microfluidics protein electrophoresis results for non-reducing and reducing conditions of rAlbumin samples, showing peaks for relative quantity of monomer and dimer and corresponding molecular weight.

Sample	Non Reduced gel				Reduced gel			
	Peak 1		Peak 2		Peak 1		Peak 2	
	MW (kDa)	Relative quantity %	MW (kDa)	Relative quantity %	MW kDa	Relative quantity %	MW kDa	Relative quantity %
200	54.8	96.0	110.1	4.0	60.4	95.2	124.5	2.8
250	53.1	96.2	108.7	3.8	59.2	96.3	123.8	3.2
300	53.2	90.4	108.5	9.6	59.3	93.0	124.0	5.9
350	52.8	91.7	108.6	8.3	58.9	94.9	123.6	5.1
400	54.5	94.0	109.8	1.2	61.0	96.3	124.9	3.0
450	53.7	94.2	110.0	5.8	60.5	95.0	124.4	4.4
500	54.6	94.4	110.9	5.6	60.8	94.4	124.5	3.3

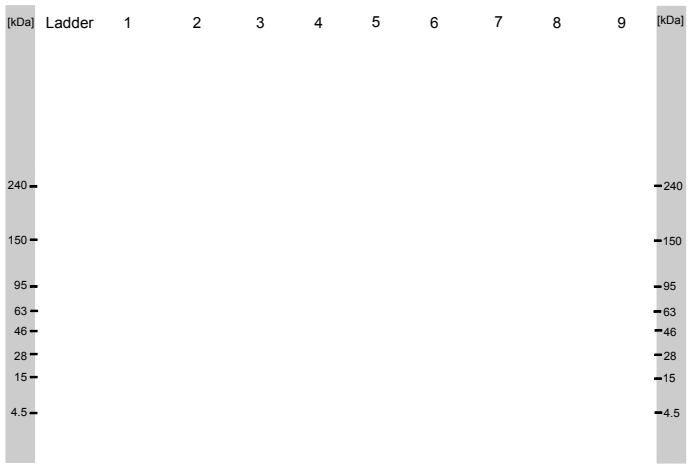

(a)

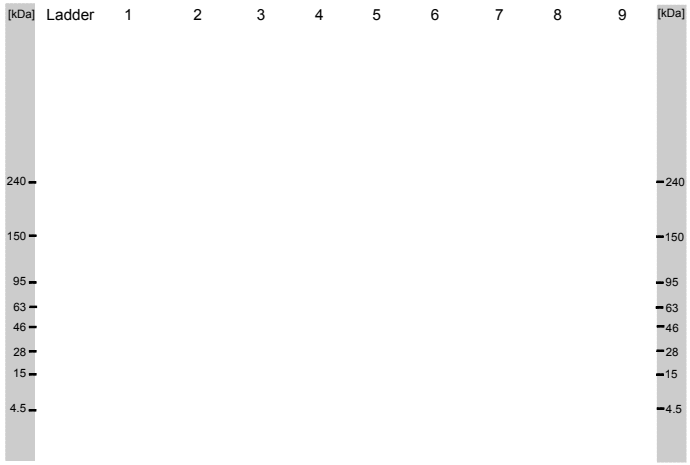

(b)

Figure 3.10: Microfluidics protein electrophoresis gel image for rAlbumin solutions originally at high concentration. (**a**) Gel in reducing conditions and (**b**) gel in non-reducing conditions. For both gels : [rAlbumin] = 200 (lane 1), 250 (lane 2), 300 (lane 3), 350 (lane 4), 400 (lane 5), 450 (lane 6) and 500 mg/mL (lane 7); formulation buffer (lane 8) and monoclonal antibody control (lane 9).

3.3.3 Effect of high protein concentration on solution viscosity

The effect of protein concentration on solution viscosity has been discussed by several authors [71, 137, 145, 152–155]. At dilute concentrations, protein solution viscosity has been studied and accounted for by predictions that account for the hydrodynamic

behaviour of proteins in a fluid [145]. Other theories that account for inter-protein interaction potential and excluded volume have been applied with relative success in predicting the increase of viscosity with protein concentration [78, 156]. In general, all these models assume that (globular) proteins are hard spherical or quasispherical macromolecules, and to some extent, this has been shown to explain the increase of viscosity with concentration and allow a comparison with the behaviour of colloidal dispersions. So far, there has not been a theoretical model that is capable of predicting the viscosity of protein solutions in a range from dilute to highly concentrated ($\gg$200 mg/mL). The following section provides an account for the analysis according to the most used theories in literature.

(a) Analysis using Hard (quasi) spherical models: Ross-Minton and Krieger-Dougherty equations

From polymer and protein rheology, the intrinsic viscosity is defined in terms of concentration (c, in mg/mL) by the following equation:

$$[\eta] = \lim_{c \to 0} \frac{(\eta - \eta_0)}{c\eta_0} \tag{3.1}$$

where η is the solution's viscosity and η_0 is the viscosity of the solvent. Intrinsic viscosity is a hydrodynamic parameter that can pinpoint the overall aspect ratio of a molecule in dilute solution and represents the effective molecular volume at these conditions [75]. By preparing various dilute solutions (0.1 - 2 mg/mL) and measuring its bulk viscosity in a capillary viscometer, the reduced (η_{red}) (eq. 3.2) or inherent (η_{inh}) (eq. 3.3) viscosities of these solutions can be plotted versus its concentrations and the intrinsic viscosity can be found by extrapolation to zero concentration.

$$[\eta] = lim_{c \to 0}(\eta_{red}) = lim_{c \to 0}\left(\frac{\eta_{sp}}{c}\right) \tag{3.2}$$

$$[\eta] = lim_{c\to 0}(\eta_{inh}) = lim_{c\to 0}\left(\frac{ln(\eta_{rel})}{c}\right) \tag{3.3}$$

where relative viscosity (η_{rel}) is defined by the following $\eta_{rel} = \frac{\eta}{\eta_0}$ and specific viscosity (η_{sp}) is defined by $\eta_{sp} = 1 - \eta_{rel}$ [75, 145].

The first approach to the data was to experimentally determine the intrinsic viscosity of this protein from viscometric data obtained via a falling ball capillary. The results (Figure 3.11) demonstrated that by extrapolating to zero concentration via both η_{red} and η_{inh}, the intrinsic viscosity had a similar value between the two methods, $[\eta]_{inh} =$ 0.00678 mL/mg and $[\eta]_{red} = 0.00677$ mL/mg. The intrisinc viscosity of human serum albumin has been reported to be of 0.00473 $\pm$ 1.2$\times 10^{-3}$ mL/mg, for similar solution conditions (temperature at 20 °C, pH $\sim$ 7.0) [131]. Values of intrinsic viscosity for bovine serum albumin, have been reported to be 0.0037 mL/mg [145] or similar values [75, 157]. Our intrinsic viscosity values, although agreeable between both methods, were slightly increased to the expected value (between 0.003 - 0.004 mL/mg). Also, it did not correspond to values measured via triple detection HPSEC (Table 3.2).

These experiments are sensitive to errors in sample preparation, where pippetting errors can affect both sample preparation and an accurate concentration calculation, compromising the viscosity measurements. Although various dilutions were prepared, only four data points were selected to fit the data, thus reducing the accuracy in computing the intrinsic viscosity of rAlbumin.

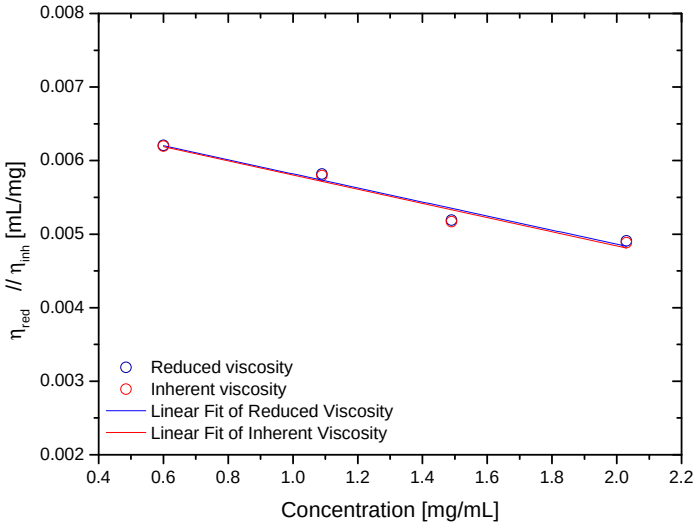

Figure 3.11: Inherent and reduced viscosities of dilute samples of rAlbumin. The bulk viscosities (circles) of these samples were measured with a capillary viscometer (AMVn, Anton Paar) at 20 °C. Bulk viscosity of the formulation buffer was 1.0487 ± 0.0013 mPa.s. Samples were measured in triplicate. Linear fit for reduced viscosity (blue line): r^2=0.9461, $[\eta]_{red} = 0.00678 \pm 1.83\times10^{-3}$; linear fit for inherent viscosity (red line): r^2=0.9473, $[\eta]_{red} = 0.00677 \pm 1.83\times10^{-3}$.

The obtained intrinsic viscosity value, as well as values from literature [131, 145], were used to fit the rheometry data (Figure 3.12) using the one of the hard (quasi)-spherical models relating protein viscosity and concentration. This model was the modified Mooney equation [158] as per Ross-Minton's approach [153] defined by:

$$\eta_{rel} = \frac{\eta}{\eta_0} = \exp\left[\frac{[\eta]c}{1 - \frac{\kappa}{\nu}[\eta]c}\right] \tag{3.4}$$

where relative viscosity is an exponential function of concentration (c in [mg/mL]), intrinsic viscosity ($[\eta]$, in [mg/mL]), a crowding effect factor (κ, dimensionless) and Simha's shape factor [145] (ν, dimensionless). As the crowding effect is a consequence of the excluded volume when the protein concentration increases, the model predicts solution viscosity not only accounting for the protein's shape but also its excluded volume.

Data was fitted with constraint to intrinsic viscosity but not the κ/ν factor (Figure 3.12). The computed values for κ/ν respective to the fixed intrinsic viscosities chosen from literature were: $\kappa/\nu = 0.42$, using $[\eta]_{Tanford}$; and $\kappa/\nu = 0.31$, using $[\eta]_{Monkos}$. These values were in agreement with the literature values reported for other globular proteins, such as IgG ($\kappa/\nu = 0.37$ to 0.49) and hemoglobin ($\kappa/\nu = 0.40$) [51, 70, 153]. The calculated κ/ν value (0.18) obtained using the experimentally determined intrinsic viscosity is far from the reported values in literature, thus suggesting no significance.

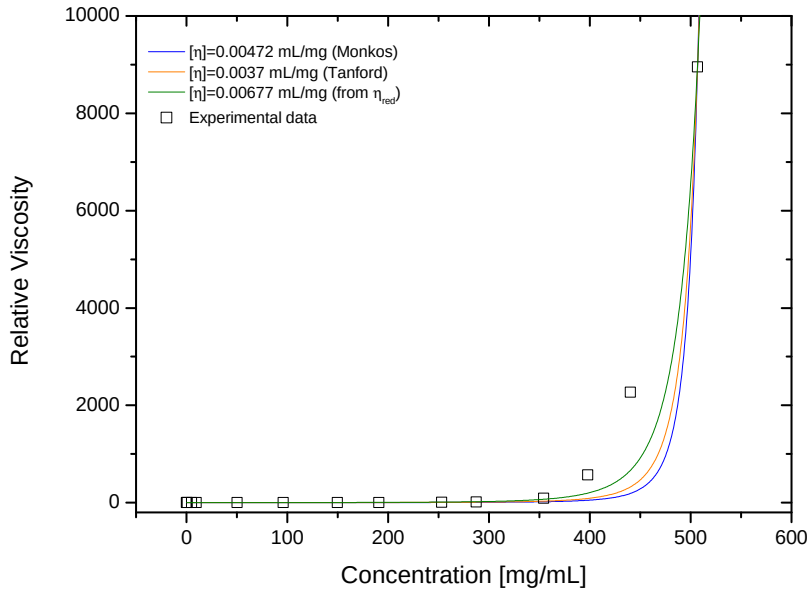

Figure 3.12: Experimental cone-and-plate rheometry data (squares) fitted to Ross-Minton's equation (eq. 3.4). Relative viscosity was obtained by dividing each of the samples high shear viscosity ($\eta_{1000s^{-1}}$) by the averaged buffer viscosity 1.038 ± 0.013 mPa.s. Fits were calculated by fixing $[\eta]$ and leaving the parameter κ/ν free and are as follows: Blue line, $[\eta] = 0.00472$ mL/mg (from [131]), $\kappa/\nu = 0.31 \pm 6.6\times10^{-4}$, $r^2 = 0.95$; red line, $[\eta] = 0.0037$ mL/mg (from [145]), $\kappa/\nu = 0.42 \pm 6.9\times10^{-4}$, $r^2 = 0.94$; green line, $[\eta] = 0.00677$ mL/mg (from η_{red}), $\kappa/\nu = 0.18 \pm 5.6\times10^{-4}$, $r^2 = 0.96$.

The Ross Minton model was also fitted to the data allowing free parameters. The

best fit computed was using experimental data up to $\sim$ 350 mg/mL (Figure 3.13). Both the $[\eta]$ (0.0042 mL/mg) and κ/ν (0.45) values were in agreement to the values reported in literature [75, 131, 145]. Also, this fitted intrinsic viscosity was similar to the intrinsic viscosity value calculated with triple detection HPSEC for the monomer peak of rAlbumin (Table 3.2). However, the Ross-Minton model did not predict solution viscosity for the highest concentrations ($\geq$ 350 mg/mL) which indicates that there are other factors to consider to predict all of our experimental data.

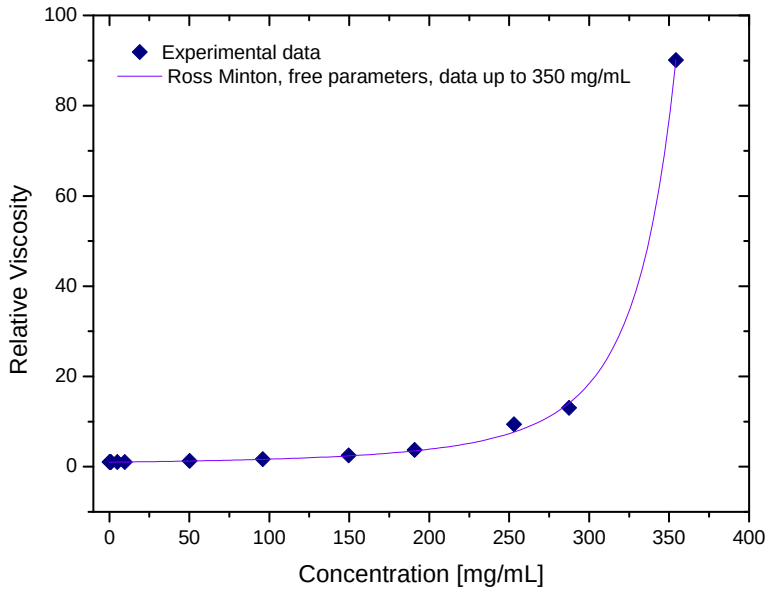

Figure 3.13: Experimental cone-and-plate rheometry data (squares) fitted to Ross-Minton's equation (eq. 3.4), using free parameters. Relative viscosity was obtained by dividing each of the samples high shear viscosity ($\eta_{(1000s^{-1})}$) by the buffer's viscosity 1.038 $\pm$ 0.013 mPa.s. Fit was calculated leaving both $[\eta]$ and κ/ν free: $[\eta]$ = 0.00421 $\pm$ 1.5$\times 10^{-4}$ mL/mg; κ/ν = 0.45 $\pm$ 0.024; r^2 = 0.999 and χ^2 = 0.40. Experimental data used for this fit was only up to 350 mg/mL.

From colloidal rheology, the Krieger-Dougherty model (eq. 3.5) was also applied to our experimental data [159].

$$\eta_{rel} = \frac{\eta}{\eta_0} = \left(1 - \frac{\phi}{\phi_{max}}\right)^{-\phi_{max}[\eta]} \tag{3.5}$$

As the Krieger-Dougherty equation is originally applied to infinite dilutions of hard spherical particles, the intrinsic viscosity ($[\eta]$) in eq. 3.5) was fixed to 2.5, and is dimensionless since it is defined in function of volume fraction (ϕ), with a maximum packing fraction (ϕ_{max}) of 0.64 in the case of random close packing of spheres at low deformations [48, 156]. Still assuming the spherical shape, this maximum packing fraction has been discussed to be around 0.71 [156] when the particles are exposed to higher shear rates. In both cases, fixing intrinsic viscosity to 2.5 and ϕ_{max} could only predict the data up to 100 mg/mL, which is in agreement with the literature [78] (Figure 3.14).

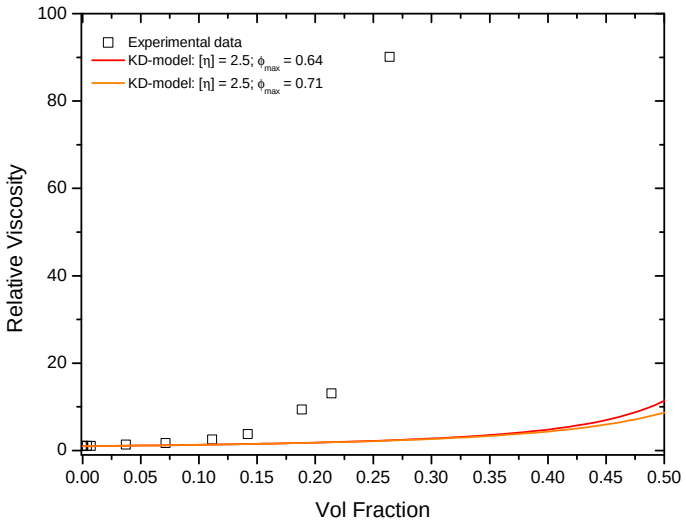

Figure 3.14: Experimental cone-and-plate rheometry data (squares) plotted against expected data (lines) from Krieger-Dougherty's equation (eq. 3.5) with fixed parameters. Relative viscosity was calculated by dividing each sample's $\eta_{(1000s^{-1})}$ by the buffer's viscosity (η_0= 1.038 ± 0.013 mPa.s). For both lines, $[\eta]$ was fixed to 2.5, but different ϕ_{max} were used: 0.64 (red line); 0.71 (orange line).

Conversion of weight/volume concentration to volume fraction was calculated via the polymer chemistry equation for volume fraction ($\phi = \frac{N_A V c}{MW}$), taking into account

the hydrated molecular weight of the protein - MW_h (eq. 3.6). The hydrated protein molecular weight was calculated from $MW_h = MW_p(1+\delta)$, where MW_p is the molecular weight of the protein and δ is the amount of water associated to the macromolecule in g/g [131, 145].

$$\phi = \frac{c}{MW_h} \cdot \left(N_A V + \frac{MW_p \delta}{\rho} \right) \tag{3.6}$$

where c is the concentration in mg/mL, N_A is Avogadro's number, V is the protein's hydrodynamic volume (113.4 nm^3), and ρ is the density of water at 20 °C (998.2×10^3 mg/mL) and $\delta = 0.379$ [131].

The data was also fitted to equation 3.5 with free parameters, allowing a prediction of viscosity applied to non-spherical particles (Figure 3.15). The parameters which were best fits using data up to 350 mg/mL, where $[\eta] = 6.94 \pm 0.14$ and $\phi_{max} = 0.298 \pm 0.002$ (with $r^2 = 0.9996$ and $\chi^2 = 0.26$). In this case, the fitted intrinsic viscosity showed a higher value than that corresponding to spheres, indicating that particle aspect ratio had increased and the ϕ_{max} decreased respectively. These values suggest good physical significance since their product is still within their usual range $1.4 < [\eta]\phi_{max} < 4$ [90]. The fitted intrinsic viscosity value of ∼6.9 also agreed with the reported aspect ratio of albumin, known to be a prolate ellipsoid [106, 131, 145]. These parameters, along with the observations previously made from the Ross-Minton model, point to a difficulty in prediction towards concentrations > 350 mg/mL (see Figures 3.13 and 3.15).

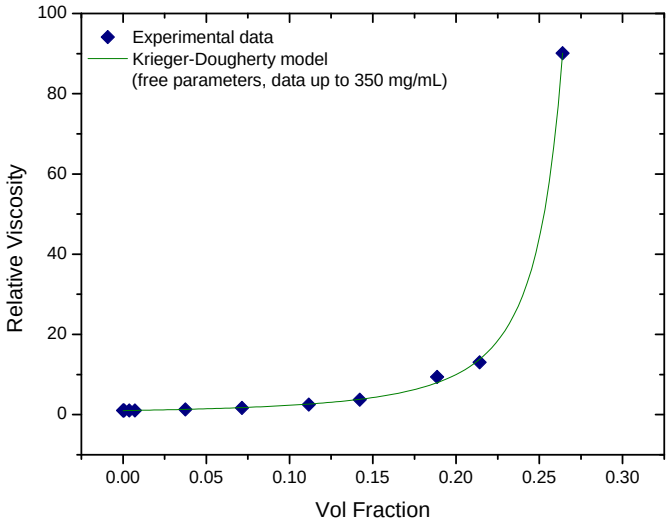

Figure 3.15: Experimental cone-and-plate rheometry data (blue diamonds) fitted to Krieger-Dougherty's equation using free parameters (eq. 3.5). Relative viscosity was calculated by dividing each of the sample's viscosity ($\eta_{(1000s^{-1})}$) by the buffer's viscosity (1.038 ± 0.013 mPa.s). Fitting parameters were $[\eta] = 6.9 \pm 0.14$, $\phi_{max} = 0.30 \pm 0.0025$, with $r^2 = 0.999$ and $\chi^2 = 0.26$. Experimental data used for this fit was up to 350 mg/mL.

(b) Analysis using Hard-spherical model considering interparticle interaction: Batchelor's equation

A more complex model, Russel's revision of Batchelor's equation [156], was also applied to the experimental data (Equation 3.7). This model predicts the increase of viscosity of hard spherical particles while taking into account the interparticle interaction based on the effective distance between particles.

$$\eta_{rel} = \frac{\eta}{\eta_0} = 1 + 2.5\phi + s\phi^2 + O(\phi^3) \tag{3.7}$$

In equation 3.7, the coefficient s of the quadratic term is defined by,

$$s = 2.5 + \frac{3}{40}\left(\frac{d_{eff}}{a}\right)^5 \tag{3.8}$$

being dependent of the effective interparticle distance, d_{eff}, and the radius of particle, a. In its turn, d_{eff} is dependent on both the hydrodynamic contributions of the particle as well as the interaction potential, relevant to the dispersion conditions. Batchelor showed that for a concentrated dispersion of hard spherical repulsive particles, the value of s is equal to 6.2, where $d_{eff} = 2a$ [156]. Sharma *et al.* showed that the data of BSA concentrated solutions up to 250 mg/mL could be fit with this model (with data up to $\approx$ 250 mg/mL) using a value $s = 10$. The authors suggested that this value would correspond to an interaction potential corresponding to a $d_{eff} = 2.5a$, reflecting BSA's repulsive net negative charge in a saline buffer.

Applying this model to the data could not anticipate the viscosity at concentrations higher than $\sim$ 150 mg/mL ($\phi = 0.11$), even when fixing $s = 10$ (Figure 3.16). The discrepancies between our data and that of Sharma *et al.* could be due to the source of raw viscosity data, since the authors used a mVROC. Our data, although collected using a torsional rheometer with cone-and-plate, were of rAlbumin solutions in a buffer containing a surfactant. There is no likely relation to measurement artifacts influencing our results (see discussion further ahead in this chapter for more details). The solutions studied by Sharma *et al.* were of the bovine version of albumin, a slightly different protein. Moreover, this model fixes the intrinsic viscosity at 2.5 for hard spheres, while it has been previously discussed that rAlbumin (and BSA) are not spherical but prolates. Thus, the model may well not be the most appropriate to fit this data albeit being the only model presented so far that includes surface charge as determinant to the viscosity of globular protein solutions. It was not possible to fit this model to the data when leaving the parameter s free.

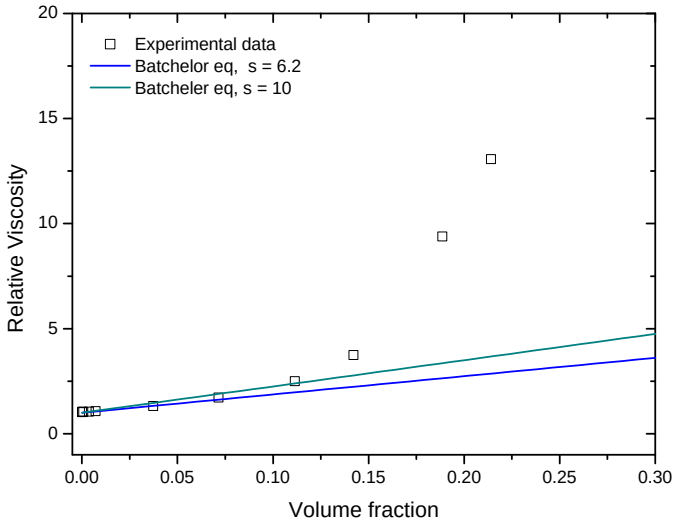

Figure 3.16: Experimental cone-and-plate rheometry data (squares) plotted against expected data (lines) from Russel's equation (eq. 3.7) using fixed parameters. Relative viscosity was calculated by dividing each of the sample's viscosity ($\eta_{(1000s^{-1})}$) by the buffer's viscosity (1.038 ± 0.013 mPa.s). For both lines, $[\eta]$ was fixed to 2.5, but s was: 6.2 (blue line); 10 (green line).

(c) Analysis using the generalised Ross-Minton and generalised Krieger-Dougherty equations

Recently, Galush *et al.*(2012) presented a study on the viscosity of mixed protein solutions, using mixtures of different monoclonal antibodies (mAbs) and of one mAb with BSA. Their conclusions derived from measuring the viscosity of both the individual protein solutions and blends. They proposed that the viscosity of protein blends could be predicted by an additive function of the viscosity of each individual protein multiplied by its respective known weight fraction (eq. 3.9).

$$ln\,\eta(w_{tot}, f_2) = (1 - f_2)\,ln\,\eta_1(w_{tot}) + f_2\,ln\,\eta_2(w_{tot}) \tag{3.9}$$

where η_1 and η_2 are the viscosities of pure protein 1 and 2, respectively, f_1 and f_2 are the weight fractions corresponding to the protein 1 and 2 present in the blend and

w_{tot} is the total weight/volume concentration of the protein mixture.

Minton [137] has recently contributed with the generalisation of equation 3.4 and equation 3.5 and application to predicting the viscosity of globular protein solutions containing only one protein, but with relatively well-known fractions of its monomeric and higher order associative species. The generalised models of Ross-Minton (eq. 3.10) and Krieger-Dougherty (eq. 3.11) models, as proposed by Minton, are as follows:

$$\frac{\eta}{\eta_0} = \exp\left[\frac{[\eta]_w w_{tot}}{1 - \frac{w_{tot}}{w^*}}\right] \tag{3.10}$$

$$\frac{\eta}{\eta_0} = \left(1 - \frac{w_{tot}}{w^*}\right)^{-[\eta]_w w^*} \tag{3.11}$$

Note that the Krieger-Dougherty equation has been modified to allow the use of weight/volume concentrations (w_{tot}, in [mg/mL]), rather than volume fractions. Both equations 3.10 and 3.11 are now represented as functions of w_{tot}, $[\eta]_w$ and w^*. The parameter $[\eta]_w$ is weight-averaged intrinsic viscosity (in [mg/mL]), described in equation 3.12. The parameter w^* represents an estimated protein concentration above which the solution cannot flow, referred to as jamming concentration [48, 137].

$$[\eta]_w = \sum \frac{w_i [\eta]_i}{w_{tot}} \tag{3.12}$$

By fitting these two generalised models to the experimental rheology data, it was found that the best fits would be achieved if the concentration range would not include either the last three (generalised Krieger-Dougherty eq.) or two data points (generalised Ross-Minton eq.) (Figures 3.17(a) and 3.17(b) respectively). The fitted weight-averaged intrinsic viscosity and w^* values suggest conformity between both generalised models. Again, it is noted that using these generalised models it is still not possible to predict the higher concentrations above $\sim$ 350 mg/mL. When fitting the

experimental data, using all the data points available, the fitted parameters usually presented poor statistical correlations ($r^2 < 0.9$, $\chi^2 >> 1$) as well as higher values for $[\eta]_w$ with no physical significance.

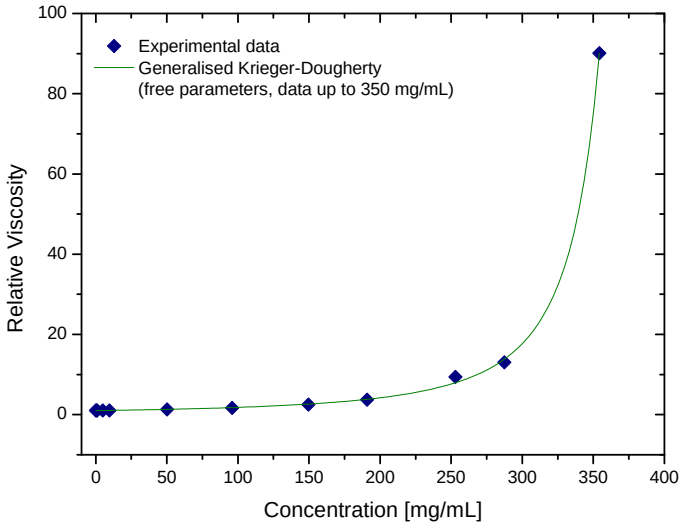

(a)

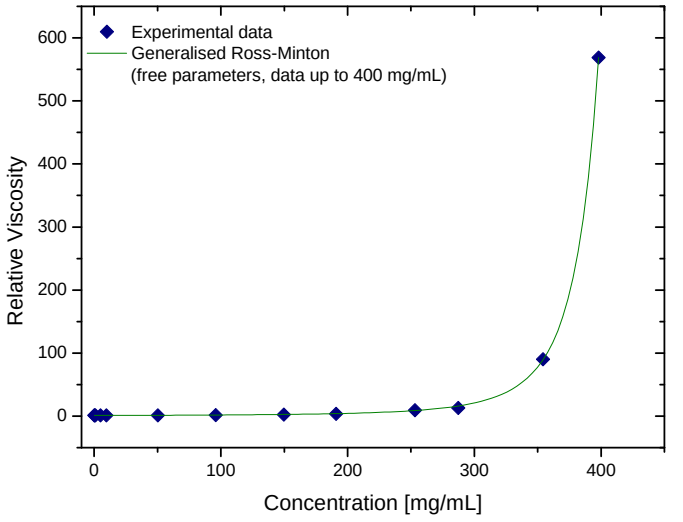

(b)

Figure 3.17: (**a**) Experimental data fitted to the generalised Krieger-Dougherty equation (eq. 3.11). Fitting parameters were $[\eta]_w = 0.00517 \pm 1.1{\times}10^{-4}$ mL/mg, $w^* = 399 \pm 3.4$ mg/mL, with $r^2 = 0.999$ and $\chi^2 = 0.26$. Data used for this fit was up to 350 mg/mL. (**b**) Experimental data fitted to the generalised Ross-Minton equation (eq. 3.10). Fitting parameters were $[\eta]_w = 0.00479 \pm 4.0{\times}10^{-5}$ mL/mg, $w^* = 569 \pm 2.2$ mg/mL, with $r^2 = 1.0$ and $\chi^2 = 0.91$. Data used for this fit was up to 400 mg/mL. For both plots, relative viscosity was calculated by dividing the sample's $\eta_{(1000s^{-1})}$ by the buffer's viscosity (1.038 ± 0.013 mPa.s).

In the study by Galush *et al.*(2012), the protein mixtures were always prepared to a known total weight/volume concentration and known weight fractions of each of the proteins in the mixture. In our case, the presented HPSEC results (Figure 3.7) showed that the monomer, dimer and trimer composition was changing with sample concentration. Therefore, a weight-averaged intrinsic viscosity was calculated per sample, instead of being assumed to remain constant (Table 3.4), using the data obtained by triple detection HPSEC (Table 3.2). The weight-averaged intrinsic viscosity values were only slightly affected.

Table 3.4: Table with calculated $[\eta]_w$ for rAlbumin solutions based on the experimental HPSEC triple detection data. $[\eta]_1$ and $[\eta]_2$ correspond to the average experimental intrinsic viscosity for monomer and dimer, respectively. f_1 and f_2 correspond to the fraction of relative peak area for monomer and dimer, respectively.

Sample Concentration (mg/mL)	**Monomer**			**Dimer**			$[\eta]_w$
	f_1 , peak area fraction	w_1 , mass fraction	$[\eta]_1 * w_1$ ($[\eta]_1$ = 0.00409 mL/mg)	f_2 , peak area fraction	w_2 , mass fraction	$[\eta]_2 * w_2$ ($[\eta]_2$ = 0.00471 mL/mg}	
50.2	0.961	48.24	0.197	0.039	1.96	0.009	0.00411
96.0	0.960	92.16	0.377	0.040	3.84	0.018	0.00411
190.8	0.957	182.60	0.747	0.043	8.20	0.039	0.00412
253.1	0.957	242.22	0.991	0.043	10.88	0.051	0.00412
354.2	0.947	335.43	1.372	0.053	18.77	0.088	0.00412
398.0	0.945	376.11	1.538	0.055	21.89	0.103	0.00412
440.2	0.943	415.11	1.698	0.057	25.09	0.118	0.00413
506.8	0.939	475.89	1.946	0.061	30.91	0.146	0.00413

Using the calculated weight-averaged intrinsic viscosity, and assuming different w^* values based on the fitted parameters obtained above, the viscosities were computed for the studied concentrations (Figures 3.18(a) and 3.18(b)) for both generalised models. When choosing w^* of higher values (derived from fits using all data points), the viscosities were typically underestimated. On the other hand, using w^* values that

were derived from the best fits, 568 mg/mL for the generalised Ross-Minton model, or 399 mg/mL for the generalised Krieger-Doughery model, the viscosities could not be correctly predicted for the higher concentrations: >400 mg/mL and > 350 mg/mL, respectively.

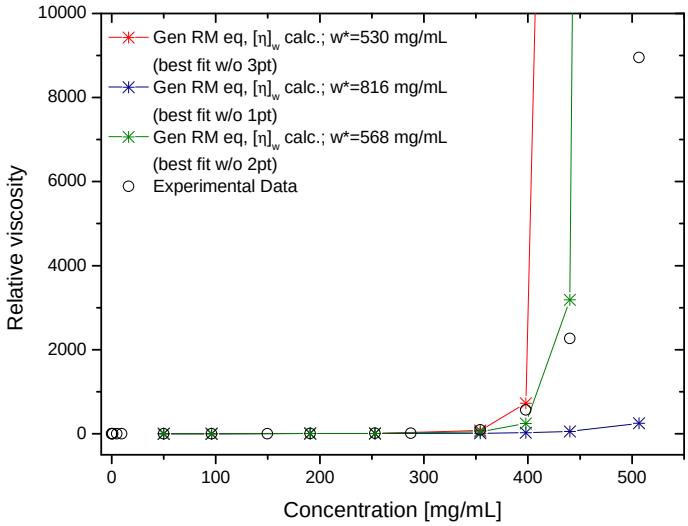

(a)

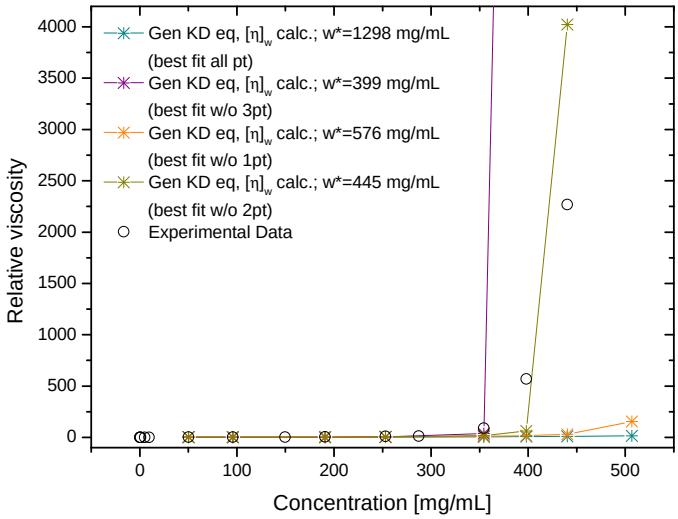

(b)

Figure 3.18: (**a**) Experimental data (circles) plotted against the calculated viscosities (stars) based on the generalised Ross Minton equation (eq. 3.10). Data in stars calculated when fixing the w^* to 530 mg/mL (red), 816 mg/mL (blue) and 568 mg/mL (green). Fitted w^* values used were from best fits to eq. 3.10. (**b**) Experimental data (circles) plotted against the calculated viscosities (stars) based on the generalised Krieger-Dougherty equation (eq. 3.11). Data in stars calculated when fixing the w^* to 1298 mg/mL (dark cyan), 399 mg/mL (purple), 576 mg/mL (orange), and 445 mg/mL (light green). Fitted w^* values used are from best fits to eq. 3.11. For both plots, expected viscosities were calculating using $[\eta]_w$ calculated in Table 3.4. Lines are represented for guidance to the eye.

In summary, the analysis suggested that concentrations above $\sim$ 350 mg/mL have a solution viscosity that depends on factors other than those taken into account by the models explored here. Most likely, at this concentration range, the protein solution can be behaving in a different way to that observed in the less concentrated solutions. As these models have been developed based on their application to low concentrations of particle suspensions, where each particle would be far apart from another enough to not influence each particle's flow [145]. Therefore, it is not surprising that the equations so far always apply well to lower concentrations of albumin.

Although the models presented here are based on hard quasi-spherical repulsive particles and their excluded volume, the predicted data typically suggest that a maximum packing fraction of rAlbumin (based on the best fits) will always be lower than the highest concentrations achieved experimentally ($\sim$ 450 and 500 mg/mL). In addition, viscosity prediction according to pure hard-sphere particle models clearly underestimates the viscosity values for concentrations higher than $\sim$ 100 - 150 mg/mL.

One possible suggestion to explain such deviation from predictions at high concentrations, is that the maximum packing concentration could be dependent on solution composition (e.g. the relative quantity of monomers, and oligomeric species such as dimers and trimers). It is known that suspensions composed of binary sized spherical particles yield a maximum packing fraction approximately larger than the random close packing for a homogenous suspension [132–135]. However, the protein has a different shape which has been shown to also influence the maximum packing fraction. It has been predicted that for globular protein solutions up to approximately 250 mg/mL with the protein having a 5:1 aspect ratio, the increase of jamming limit would not be significant [137]. Analysis so far has always assumed that associative species remain with the same globular quasispherical shape, which is clearly not the case.

Apart from shape, it is possible that rAlbumin would likely resemble a nearly hard

sphere, as its homologous HSA has been reported to exhibit a drop in intrinsic viscosity with temperature increase, thus a sign of less rigidity [131]. Moreover, as the protein is further concentrated, less rigidity could be an added factor to account for the slow increase of viscosity compared to hard sphere model predictions. This could be due to repulsive nature of inter-particle interactions, which is a phenomenon that has been observed for sterically stabilised colloids [48].

The deviation to models seen at higher concentrations ($\geq$ 350 mg/mL) could be related to a glass transition similar to what occurs with colloidal hard spheres. In this case, accounting for repulsive excluded volume, suspensions are expected to approach a glass transition at volume fractions $\phi \approx 0.58$ before approaching the random close packing fraction ($\phi = 0.64$) [48]. When the concentration approaches a glassy state, the particle is caged by the presence of neighbouring particles thus slowing down its flow and leading to increased viscosities. In the case of rAlbumin, an analogous glass transition behaviour could be taking place at the concentrations between $\sim$ 400 to $\sim$ 500 mg/mL based on similar results seen with highly concentrated solutions of BSA [160]. This would suggest that these concentrations are approaching the jamming limit but does not explain why viscosities cannot be predicted in conventional models. Finally, it is precisely the range between 350 mg/mL and 500 mg/mL samples that showed an increase in relative quantity of dimers (with a respective decrease of monomers). So it does suggest that the change of composition and the increase of viscosity with increase of concentration are somehow connected.

3.3.4 Surface tension effects on rheology measurements and other control experiments

To ensure that the rheological measurements were taken as accurately as possible and were free of artifacts related to both the method or preparation of samples and the

rheometer's characteristics, a series of additional experiments were carried out.

The influence of surface tension at the air/water interface of protein solutions in surfactant-free buffers has been shown to present apparent high-viscosities at low shear rates. The use of conventional rheometer with cone-and-plate was suggested as not being the most appropriate instrumentation for this type of samples precisely as it isn't an air/water interface-free technique [78].

The microfluidics slit rheometer (mVROC) was used to compare to the rheometry results. rAlbumin solutions at 200 mg/mL (from the original formulation) and 500 mg/mL were analysed with the mVROC in separate microchips adequate to the sample's viscosities (A05 chip for 200 mg/mL and D05 chip for 500 mg/mL). Both samples showed Newtonian-like behaviour, with the calculated shear viscosities remaining constant as the the true shear rates were applied (Figure 3.19).

When superimposing the cone-and-plate (CP) rheometer data with mVROC data, the sample at 200 mg/mL showed no difference in its viscosity values. As an example, at shear rate $\dot{\gamma} \approx 1000$ s^{-1}, the average viscosities measured with each instrument were $\eta_{CP} \approx 3.5$ mPa.s and $\eta_{mVROC} \approx 3.4$ mPa.s (Figure 3.19). This clearly showed that the CP rheometer data were most likely free of air/water interfacial artifacts.

The sample at 500 mg/mL showed a difference of approximately one decade between CP and mVROC data (Figure 3.19). Although subsequent repeats had similar values and rheological characteristics, it was not possible to further explain the sharp difference. An explanation based on surface tension effects on CP rheometer data might be ruled out since this data showed constant viscosities along the shear rates applied up to relatively low shear rates ($\dot{\gamma} \approx 0.01$ s^{-1}), whereas a surface tension induced apparent yield-behaviour would be expected. To our knowledge, there are no other reports in literature analysing globular protein solutions at this level of concentration using a mVROC. It could be possible that such high concentrations of protein solutions

are problematic samples for this system due to, for example, a higher propensity of adhesion to the construction materials.

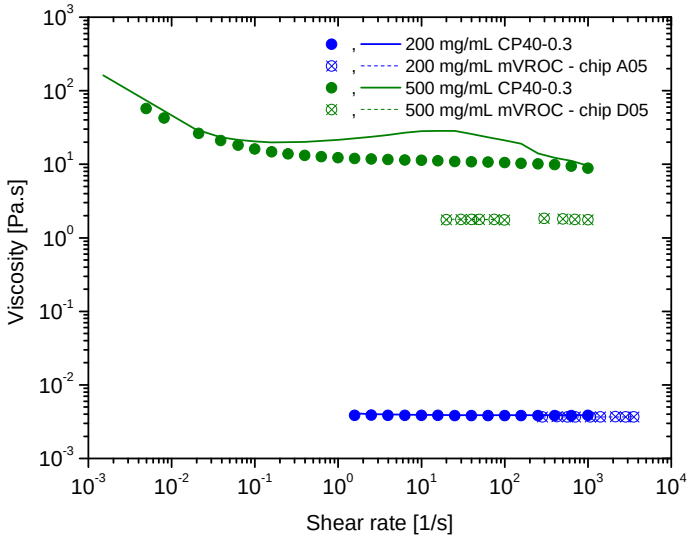

Figure 3.19: mVROC data for 200 (blue) and 500 (green) mg/mL of rAlbumin in comparison to the cone-and-plate rheology data. mVROC data: crossed circles - ramping up shear rates, dashed lines - ramping down shear rates; CP rheology data: closed circles - ramping up shear rates; lines - ramping down shear rates.

In another experiment samples were prepared by diluting in a aqueous NaCl 145 mM surfactant-free solution. Dilutions at 5, 10, 50 and 100 mg/mL were analysed on the CP rheometer as well as their level of aggregation was assessed by HPSEC and DLS. Results from HPSEC and DLS analyses were similar to those of formulated rAlbumin. A few differences were identified with the CP rheometer data. Samples at 5, 10 and 50 mg/mL in NaCl 145 mM showed an increase of viscosities towards low shear rates; only the sample at 100 mg/mL of rAlbumin in NaCl 145 mM presented constant viscosities throughout a similar shear rate range (Figure 3.20). Samples at 5 and 10 mg/mL showed a slightly increased high shear viscosity (η_∞ at $\dot{\gamma} = 1000$ s^{-1}), when compared to the data collected from formulated samples.

These two differences are possibly related to the lower concentration of polysorbate-80 present in samples 5 and 10 mg/mL, and to some extent, 50 mg/mL. Polysorbate-80 is present in the formulation to prevent the macromolecule reaching the air/water and solid/water interface [138]. As polysorbate was also diluted during sample preparation below a critical concentration, it allowed the protein to form films at the air/water interface present with the CP geometry. Such surface tension effects are proposed to influence torque measurements at low shear rates, creating an apparent yield-behaviour translated in a pronounced increase of the viscosity function's slope [78, 143]. Other authors also observed similar differences when adding surfactants to globular protein solutions [8, 74]. By measuring the viscosity of protein samples prepared in surfactant-containing buffer, true values of viscosity and shear stress are being measured and is similar to a measurement performed with an air/water interface-free instrumentation, such as the mVROC.

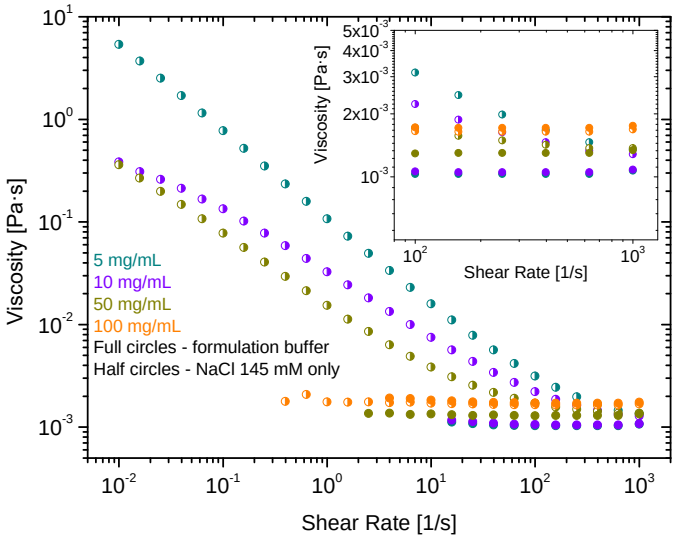

Figure 3.20: Viscosity curves for rAlbumin solutions diluted in 145 mM NaCl buffer, in comparison to the formulated material at the same concentrations: 5, 10, 50 and 100 mg/mL. Half circles - rAlbumin in 145 mM NaCl only; full circles - rAlbumin in formulation buffer.

To demonstrate that using centrifugal concentrators would not affect the rheological behaviour nor increase the level of aggregation, an aliquot of the original rAlbumin solution at 200 mg/mL was diluted in formulation buffer to 50 mg/mL and then concentrated back to 200 mg/mL. The centrifugal concentrators used would allow smaller molecules to pass through, such as water, salts and polysorbate-80. The comparison of the rheological behaviour between this control sample and the original formulation showed that both had superimposable profiles (Figure 3.21). This sample at $\sim$ 200 mg/mL showed similar results to the original 200 mg/mL sample via HPSEC and DLS.

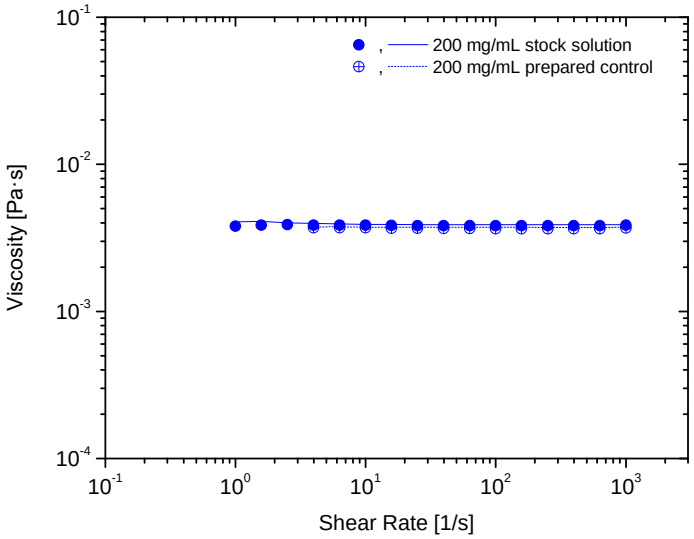

Figure 3.21: Comparison of the viscosity curve between 200 mg/mL control sample prepared via centrifugal concentration (crossed circles) and the originally formulated 200 mg/mL sample (full circles). Respective lines correspond to ramping up shear rates, while the circles correspond to ramping down data.

The possibility remains that polysorbate-80 was concentrated along with rAlbumin for those samples between 250 and 500 mg/mL. In order to fully address this issue, it would be necessary to directly quantify the presence of this surfactant in the protein

solutions, which could not be done at the time of this study. To address the analysis made here, the simplest case was considered, where the polysorbate would have diffused through the concentrator's membrane during centrifugation.

3.4 Conclusions

In this work a range of rAlbumin solutions, in a formulated buffer containing salt and a surfactant, were analysed for their rheological behaviour with the aim to understand the effects of high concentration on the solution viscosity. Rheological measurements showed that the solutions (0.1 - ∼500 mg/mL) behaved as purely viscous fluids in the range of the applied shear rates. It was observed that as the protein concentration increased in solution, the samples presented an increase of viscosity.

Characterisation regarding the level of aggregation and species size was also made. By HPSEC, all samples showed the same species were present in solution; monomers, dimers and trimers of rAlbumin. The relative quantity of each species was fairly similar between 0.1 - 200 mg/mL but as concentration increased to ∼500 mg/mL, the relative quantity of dimers and trimers increased along with a corresponding decrease of monomer. By DLS and SDS-PAGE (microfluidics) analysis, the solutions showed no other signs of impurities such as other higher order aggregates or protein fragments. Throughout this study several experiments proved that concentrating the rAlbumin ≥200 mg/mL did not seem to have any other effect besides the increase of solution viscosity and the change in relative composition of protein species. HPSEC was also used with aid of triple detectors for the determination of the intrinsic viscosity and bulk molecular weight. These results showed consistency throughout the concentrations studied, which was a sign of method and sample validity. Rheological analysis of rAlbumin diluted in a surfactant-free buffer suggested that presence of polysorbate-80 in the formulation buffer contributed for artifact-free measurements in rheometry, in light of what

has been discussed in recent literature.

A comprehensive theoretical analysis of the rheological experimental data was performed using different models that are currently assumed to be the most appropriate to predict protein solution viscosity. These models are considered for hard spherical or quasispherical particle suspensions and when plotted against the experimental data, fixing the fitting parameters to the known shape and crowding conditions of spherical particles, they could only predict the viscosity of rAlbumin up to ∼100 mg/mL. By leaving these parameters free, the Ross-Minton and Krieger-Dougherty equations were demonstrated to predict the solution viscosity well, up to 350 mg/mL, when excluding concentrations >350 mg/mL. When applying an equation that accounted for the protein interdistance and thus, the effect of interaction potential upon viscosity (the Russel equation), it couldn't be applied to concentrations $\geq$ 150 mg/mL.

Generalised versions of the Ross-Minton and Krieger-Dougherty equations were also studied and our best results showed that the former could successfully fit when using experimental data up to ∼400 mg/mL of rAlbumin. These generalised models, although still based on just two factors (shape or aspect/ratio and particle packing), introduce the concept of a weight-averaged intrinsic viscosity. Our study showed that this approach was the best to address the variation of protein species composition in solution. The fact that our analysis produced better fits using these altered equations, further highlights the importance of considering this variation in composition within a protein solution, thus justifying its complete characterisation of oligomeric species. It is important to note here that, so far no other analysis typically accounts for this variation within a sample of one protein only - Galush *et al.*(2012) analysed binary mixtures of different mAbs and a mAb and BSA. Moreover, while assuming there is no variation in protein species composition, the same theoretical models assume that the jamming limit remains unaltered with changing composition. We still suggest that other factors related to highly con-

centrated solutions may need to be considered, particularly since those concentrations not fitted were the most concentrated (>400 mg/mL), where crowding effects should be more accentuated.

In conclusion, our rAlbumin example explored here may well be a situation close to what happens to reality in biopharmaceutical formulation science. Although a rather complicated system, it highlights that the variation of protein species composition between samples is a key factor for predicting the solution viscosity of protein solutions.

Chapter 4

The effect of insoluble protein aggregates on the rheology of beta-lactoglobulin solutions

4.1 Introduction

The rheology of protein solutions have frequently been addressed in the literature with regards to the flow properties of biological fluids, such as blood [64] and synovial fluid [63], as well as food materials, including milk [161]. In recent years, due to the rapid development of biopharmaceutical industry, attention has also turned to therapeutically proteins such as monoclonal antibodies.

Although many of these studies have focused on different aims, it is easily noticed that measurements performed with a conventional torsional rheometer show a flow behaviour often addressed as being 'solid-like' or 'shear thinning' [61, 62]. The observations constantly point to this flow regime, commonly seen at lower shear stresses, where viscosity seems to decrease as stress increases. This has been observed for BSA, β-LG, ovalbumin and other globular proteins at concentrations ranging from 0.03 - 10 % (w/w) [60]. It has been discussed that this solid-like behaviour is due to strong long-range repulsive interactions between globular protein monomers in solution [60–62, 162].

Recently, the work of Sharma *et al.*(2011) has suggested that the observed solid-

like characteristics are typical of a material showing yield-behaviour. In colloidal suspensions, viscosity is known to depend on the solids content of the suspension, as well as interparticle interactions. These interactions confer specific behaviours to the fluids depending on the force that must be overcome to create a deformation, i.e. to flow. Following this logic, authors have suggested the existence of long-range interactions that could generate a colloidal crystalline-like structure within a globular protein solution [60–62, 162]. However, no evidence of such structures has yet been demonstrated [63]. Sharma *et al.*(2011), proposed that protein-protein interactions are responsible for this yield-behaviour. This suggestion was based on the fact that most conventional bulk rheology measurements are performed with measuring systems where a small air-water interface is present. Since macromolecules such as proteins are known to be surface active [35, 163], it is proposed that inter-protein interactions are responsible for a protein film that forms at the air-water interface which leads to the observed yield-stress behaviour [78].

Yield-behaviour is commonly characterised in materials that only flow once a critical stress is overcome [48, 49]. In colloids, yield stress is explained by the interactions between the suspended material, which contribute to a strengthened network, and can thus be related to interaction potential [90]. The work by Sharma *et al.*(2011) is important since it was the first attempt at deriving a quantitative model of bulk rheology including the influence of the air-water interface. However, other authors have reported this viscoelastic behaviour to air-water interfacial effects when studying biological solutions [164] and food materials [165]. Moreover, the rheology of globular proteins in the presence of surfactant molecules (polysorbates) is Newtonian-like, with no signs of yield-stress [74, 143]. This suggests that the presence of a surfactant competes with the protein at the air-water interface enough to diminish the solid-like behaviour observed in surfactant-free protein solutions [74, 166].

The study presented here focuses on the rheology of β-lactoglobulin (β-LG) solutions in surfactant-free aqueous buffer at pH 6.0. β-LG is a globular protein present in milk whey and has been studied for its surface activity, flexible structure and ability to foam and form stiff films at the air-water interface [163, 167, 168]. A conventional torsional rheometer was used to characterise these solutions with cone-and-plate (CP) and double-gap (DG) couette measuring systems, both of which exhibit a surface area exposed to air. Interfacial shear rheology, using the double-wall ring (DWR) was also performed. In addition, air-water interface-free measurements were obtained with a microfluidics rheometer and the falling ball viscometer. Tensiometry data was collected to compare with time-dependent bulk shear rheology measurements in an attempt to understand the influence of the interfacial protein film and its effects on the solution rheology. Further analysis was subsequently performed to quantify the bulk and interfacial contributions on the observed solution rheology.

One of the aims of our work was to use β-LG as a model protein to identify the origins of yield-behaviour often observed in protein solution rheology. Therefore we hoped to contribute to a better understanding of excipient-free protein solution rheology by demonstrating that this behaviour, and its causes, are inherent to such materials in similar conditions. Our work also included a characterisation of protein species present in the β-LG solutions, in terms of insoluble and soluble protein aggregates [85]. Generally, in protein solution rheology it is common to notice a lack of this type of biophyiscal characterisation. However, as already outlined, the viscosities of protein solutions are expected to depend not only on inter-particle interactions but the physical characteristics of the components present in the fluid. Therefore, our other aim in this work was to understand if by including an extendend particle characterisation, it would be possible to relate the presence of insoluble particles to the observed yield-like behaviour.

4.2 Materials and Methods

4.2.1 Materials

4.2.1.1 Protein sample

β-LG was obtained from Sigma-Aldrich (product L3908, batches 097K7012 and 080M7312V) as a mixture of bovine variants A and B, in a lyophilised powder containing approximately 10% w/w of sodium chloride.

This protein is found in large quantity in the whey fraction of the milk of ruminants (1.8 - 5 g/L) but not in human milk. It is a globular protein with molecular weight 18.4 kDa, with 162 amino acids and one free cystein (Cys121). There are more variants of β-LG but variants A and B are the most common, of which differ by two amino acids. The structure of β-LG is an eight-stranded, flattened β-barrel and flanking three-turn α-helix with a ninth β-strand flanking the first strand (Figure 4.1). This protein has been reported for having a pI at 5.2 [169]. It has a tendency to self-associate depending on the pH and ionic strength of the buffer. Below pH 3 and above pH 9, β-LG is usually present mainly as a monomer. Whereas between pH 5.2 and 9, monomers and dimers coexist in equilibrium, with the dimers being more predominant. The dimer is stabilised by hydrogen bonds between the surface of the AB loop and the ninth β-strand present in each monomer, and by tight packing of the residues in the interface [169–172].

β-lactoglobulin undergoes changes of physical, chemical and spectroscopic properties over the neutral pH range (6 - 8), which is related to the opening of the β-barrel (also denominated *calyx*). At basic pH, the calyx has an "open" conformation providing access of ligands to the hydrophobic cavity at its center. At acidic pH, there is structural rearrangement to "close" the calyx. This might help explain the physiologic relevance

of this protein as having a possible role as a transporter of small hydrophobic ligands protecting these from acidic pH present in the stomach [171, 173].

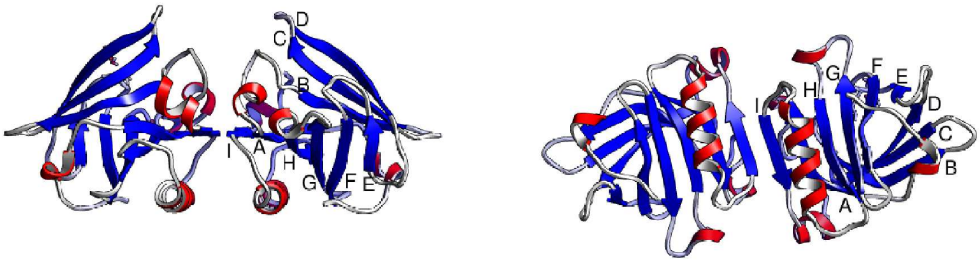

(a) (b)

Figure 4.1: Structure of the β-lactoglobulin dimer from the X-ray coordinates, 1BEB (from the RCSB Protein Data Bank, cited in [170]), showing a side view (a) and a top view (b). Letters A-I are labels to the nine β-strands, coloured in blue. Figures were generated using the UCSF Chimera package [140].

4.2.1.2 Sample preparation

Sample preparation for β-LG is described in section 2.2.2 in Chapter 2. For the work presented in this chapter, a fresh batch of dialysed β-LG solution in 10 mM His-His.HCl pH 6.0 was prepared at a stock concentration of ~86 mg/mL. β-LG samples were checked for protein concentration, pH and osmolality. Osmotic strength was measured using a freezing-point osmometer (Osmomat O30-D, Gonotec GmbH, Germany), zeroed with ultrapure water and calibrated with a 300 mOsmol/kg NaCl aqueous solution (Gonotec GmBH, Germany). Samples were also checked for osmolality before and after dialysis.

4.2.2 Methods

4.2.2.1 Quantification of protein concentration by UV spectroscopy

All details related to this method are described in section 2.2.7 in Chapter 2.

The percent extinction coefficient ($A^{1\%}_{1cm}$) used was 9.6 [100]. The concentrations reported were calculated as an average of 3 measurements of separate dilutions prepared from each sample or, in the case of the NanoDrop, 3 separate aliquots when no dilution was required. An error of up to 10 % was accepted for these measurements.

4.2.2.2 Bulk Rheology

The rheometers used were Anton-Paar (Graz, Austria) modular compact rheometers (MCR) 301 and MCR 501 models. A CP geometry stainless steel CP50-1 (diameter = 50 mm and cone angle = 1°) was used, purchased from Anton-Paar. To prevent evaporation of sample and to keep constant temperature of 25°C ± 0.1°C throughout the measurements, an evaporation blocking system equipped with a peltier unit was used with the CP50-1. A double gap concentric cylinder (DG26.7) stainless steel geometry with an inner diameter of 26.7 mm was also used. In this case, the lower outer cylinder was embedded in the peltier unit that kept the temperature at 25°C ± 0.1°C. Sample volume for this geometry was of 3.8 mL sample, while for the CP50-1 it was of 650 μL. Both measuring systems and rheometers were calibrated with hydrocarbonate standard oils (N1.0 and N14) from Cannon Instruments (USA) using the same method for data collection. Prior to measurements, all samples were allowed to equilibrate to room temperature ($\sim$ 23°C) for at least 40 minutes. Samples that were analysed after filtration were filtered immediately before the start of a measurement.

Rotational tests (flow curves and viscosity curves), on the MCR 301 and 501 rheometers using both geometries, were performed by controlling the shear rate from 0.01

to 1000 s^{-1}. Each shear rate step had a 60 second duration time during which the instrument was averaging over the collected data. For standard flow behaviour sample characterisation, two shear rate sweeps (ramping down and up) were performed per sample, without waiting time between sweeps. This set of two sweeps was measured at least twice, per sample concentration. When testing for hysterisis, the same sample would be repeatedly sheared after a first set of sweeps, testing the effect of waiting time (0 minutes or 5 minutes) between ramping.

Steady shear time sweeps were performed with the CP. The method consisted of loading a freshly prepared sample and as soon as the measuring gap position was reached, the sample was sheared at constant shear rate of $\dot{\gamma} = 1000\ s^{-1}$ for 10 minutes. The shear rate was then reduced to $\dot{\gamma} = 0.01\ s^{-1}$ for 60 minutes, followed by a period of rest ($\dot{\gamma} = 0\ s^{-1}$) for 10 minutes, and finally subjected to a $\dot{\gamma} = 0.01\ s^{-1}$ for 20 minutes.

4.2.2.3 Interfacial shear rheology with the double wall-ring geometry

For interfacial shear rheology measurements a double wall-ring (DWR) geometry was used. The DWR is composed of a trough and a ring that is positioned at the air/liquid and connected to the rheometer - in this case, an AR-G2 rheometer (TA Instruments, USA). The sample holder was placed on the bottom peltier plate of the rheometer. The ring had a square-shaped cross-section and was made of platinum/iridium. The sample volume for these experiments was ∼18 mL. After loading, the ring was lowered and positioned on the freshly formed air-water interface. Measurements were conducted at 25°C. Samples were filtered prior the measurement, and analysed immediately, unless otherwise stated.

With the DWR, flow and viscosity curves were obtained by controlling the shear rate from 0.01 - 100 s^{-1}, ramping down and up, collecting data every 45 seconds. Oscillatory tests started with amplitude sweeps in order to determine the linear viscoelastic range of

the studied sample. These sweeps were run separately at different but constant angular frequencies: 0.1, 0.5, 1, 5, 10, 50 and 100 rad/s. Frequency sweeps were then performed with a new sample where the range of studied angular frequencies was between 0.1 to 100 rad/s. Throughout the angular frequency sweep, constant strains used were of 2, 1.7 and 1.5 % for the frequency steps of 0.01 - 0.5 rad/s, 0.5 - 5 rad/s, and 5 - 50 rad/s, respectively.

Time sweeps with the DWR were performed for oscillatory shear at a constant strain of $\gamma = 1\%$ and constant angular frequency of $\omega = 5$ rad/s, for 90 minutes. All interfacial shear rheology tests were started immediately after a fresh sample was loaded and as soon as the ring was set at the air-liquid interface.

4.2.2.4 Falling-ball viscometer

An automated micro capillary viscometer (Anton-Paar, Graz, Austria) was used as a complimentary technique to determine bulk viscosity. The capillary had an inner diameter of 1.6 mm and contained a steel ball of 1.5 mm diameter. For a standard measurement, the inclination angle was set at 70° (and -70°). Temperature control at 25°C ± 0.1°C was ensured via a peltier unit attached to the instrument. The capillary was calibrated by running DI water and a viscosity standard oil at the same angle used for the sample measurement. β-LG samples analysed with this technique were filtered (0.1 μm pore size) prior to these measurements. Viscosity values presented were computed using the measured density of the analysed samples (for details of density measurement procedure, see section 2.2.11 in Chapter 2).

4.2.2.5 Micro-viscometer/rheometer on-a-chip

The microviscometer/ rheometer on-a-chip (mVROC), by Rheosense, Inc. (San Ramon, California, USA) was also used to measure the bulk viscosity of filtered (0.1 μm pore size)

β-LG solutions only. For these measurements, the A05 chip was used and temperature was kept constant at 25°C ± 0.1°C using a water circulation system (ThermoCube, SS cooling systems, USA) (for additional information, see section 2.2.6.2 in Chapter 2).

4.2.2.6 High performance size exclusion chromatography for the determination of level of protein aggregation

All the details related to this method are described in section 2.2.9.2 in Chapter 2.

4.2.2.7 Dynamic light scattering

All details related to this method are described in section 2.2.8.1 in Chapter 2.

β-LG samples were measured at 1 mg/mL diluted from samples that at their original concentration were either unfiltered or filtered (0.1 μm pore size). The measurement settings for size readings were at a constant temperature of 25°C ± 0.1°C, performing a total of 20 runs of 5 seconds duration each. Prior to the measurement, all samples had an equilibration time of 5 minutes at the same temperature. Size measurements were made in triplicate with fresh aliquots for each reading.

Time-dependence size measurements were performed using 1 mg/mL β-LG solution filtered (0.1 μm pore-size) directly into the clean quartz cuvette. The measurement duration was the same as for size characterisation, but repeated up to 40 consecutive times with no delay between each measurement.

4.2.2.8 Microfluidic chip sodium-dodecylsulfate polyacrylamide gel electrophoresis (SDS-PAGE)

All details related to this method are described in section 2.2.13.1 in Chapter 2.

A gel was run to compare dilutions of unfiltered and filtered β-LG solutions

(originally at ∼68 mg/mL) .

4.2.2.9 Composition-gradient multi-angle light scattering (CG-MALS) for the determination of protein self-virial coefficient

For the CGMALS experiment see details on section 2.2.8.2 of Chapter 2. The analysed β-LG solution was a 12.7 mg/mL, doubly filtered with 0.1 μm pore-size syringe filters. The sample was in 10 mM His-His.HCl pH 6.0 buffer and the successive dilutions were analysed with the filtered sample buffer (0.1 μm). Data analysis was performed using Calypso software (Wyatt Corporation Technologies, Santa Barbara, California, USA).

4.2.2.10 Tensiometry

All the details referring to this technique are described in section 2.2.10 in Chapter 2.

A freshly prepared filtered sample (0.1 μm pore size) of β-LG solution ∼68 mg/mL in buffer was analysed.

4.2.2.11 Flow imaging microscopy for sub-visible particle counting

All details related to this method are described in section 2.2.15 in Chapter 2.

β-LG samples were either filtered (0.1 μm) or measured without prior filtration. β-LG samples at 0.1, 10 and 35 mg/mL were measured without prior dilution. Since the β-LG ∼68 mg/mL unfiltered solution showed visible particles and opalescence, it was diluted to 10 mg/mL to prevent clogging of the flow cell. A dilution to 10 mg/mL of the filtered β-LG 68 mg/mL solution was also analysed. All samples were measured at least once, except for the diluted sample for β-LG 68 mg/mL which was measured three

times (unfiltered and filtered samples).

4.2.2.12 Visual inspection of protein solutions

All details related to this method are described in section 2.2.16 in Chapter 2.

β-LG samples analysed for visual inspection were ∼0.1, 10, 35 and 68 mg/mL, before and after filtration.

4.3 Results and Discussion

4.3.1 Bulk and interfacial shear rheology of β-LG solutions

β-LG solutions with concentrations of approximately 68, 35, 10 and 0.1 mg/mL were prepared after dialysis and its rheology was characterised using CP and DG geometries (Figures 4.2(a) and 4.2(b)). Samples exhibited a strong viscoelastic behaviour, showing decreased shear viscosity as the shear rates were increased. Analysis of the shear viscosity dependence on applied shear stresses, revealed a very sharp decrease of viscosity at the lower shear stresses (Figure 4.3). The same observations could be drawn for measurements from both type of geometry.

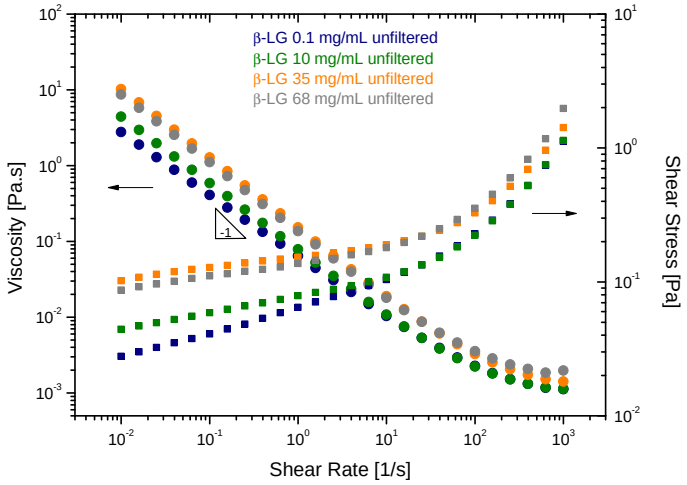

(a) CP data

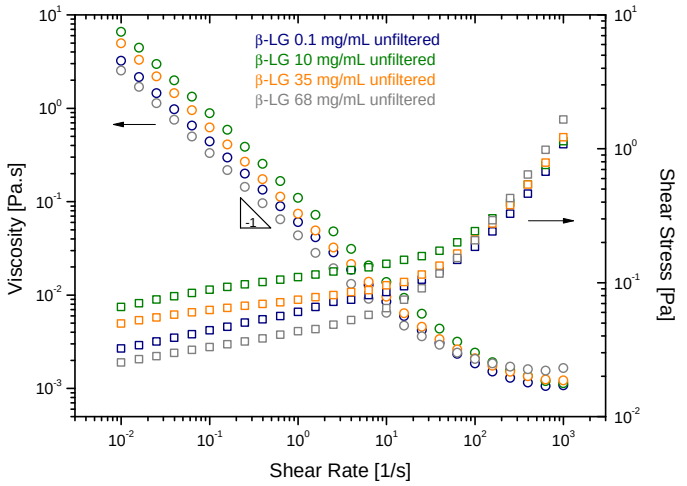

(b) DG data

Figure 4.2: Viscosity and flow curves of β-LG solutions using (a) CP and (b) DG geometries. Circles represent the viscosity values, while the squares represent the shear stress values. Samples were 0.1, 10, 35 and 68 mg/mL, all unfiltered solutions, measured at 25 °C.

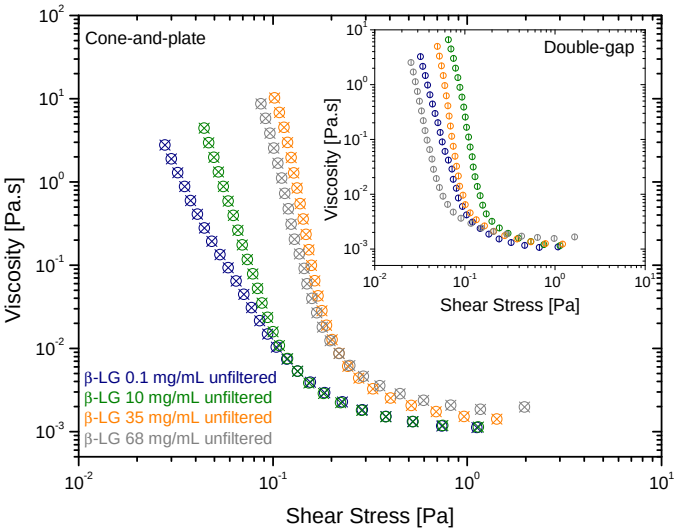

Figure 4.3: Viscosity curves versus shear stress for CP (larger graph) and DG rheology (inset graph) of β-LG. Samples were 0.1, 10, 35 and 68 mg/mL, all unfiltered solutions, measured at 25 °C.

At low shear rates all samples showed a common linear slope of -1 representing the decrease of viscosity. The results also pointed to a non-monotonic dependence of viscosity with concentration at the lower shear rates ($\dot{\gamma} < 10$ s^{-1}), whereas this dependence could be observed at higher shear rates (e.g. $\dot{\gamma} = 1000$ s^{-1}). Similar observations can be identified in the literature with regards to globular protein solution rheology, including that of β-LG solutions in similar excipient-free buffers [60–62]. The observed behaviour at low shear rates has been often classified as shear-thinning. However, it has been recently suggested that it is actually an apparent yield stress behaviour [78]. Analysis of Figures 4.2 and 4.3, with shear stress pointing towards a finite value at the lower shear rates, and the sharp drop of viscosity at these low deformations, are evidence of yield stress, i.e. where little flow is detected up to a point where external forces overcome internal forces from which the material will deform [49]. Many authors who referred to this behaviour as shear-thinning, suggested that it was related to the

possible existence of colloidal crystals at low deformations, a consequence of long-range electrostatic interactions [60–62]. Nevertheless, such globular proteins solutions did not reveal the existence of any crystalline-like network [63]. However, shear-thinning behaviour is typically characterised with stress increasing non proportionally to the shear rate, often resulting in a linear plot in a log-log representation, which is different to what was seen in our results at lower shear rates [48, 49] (Figure 4.3). Shear-thinning is a typical behaviour of a fluid, since by definition a shear-thinning fluid cannot be in equilibrium if at rest [48].

For the highest concentration used, β-LG $\sim$68 mg/mL, steady state as well as oscillatory interfacial shear rheology was studied. The use of the double wall ring as an interfacial shear rheology geometry is one of the most adequate methods to measure the surface viscosity due to its ratio of contact surface area to wetted perimeter [94].

A flow and viscosity curve characterisation of the air-water interface for β-LG at 68 mg/mL showed a linear decrease of viscosity with the applied shear rates (0.01 to 100 s^{-1}) and a slope of -1 (Figure 4.4).

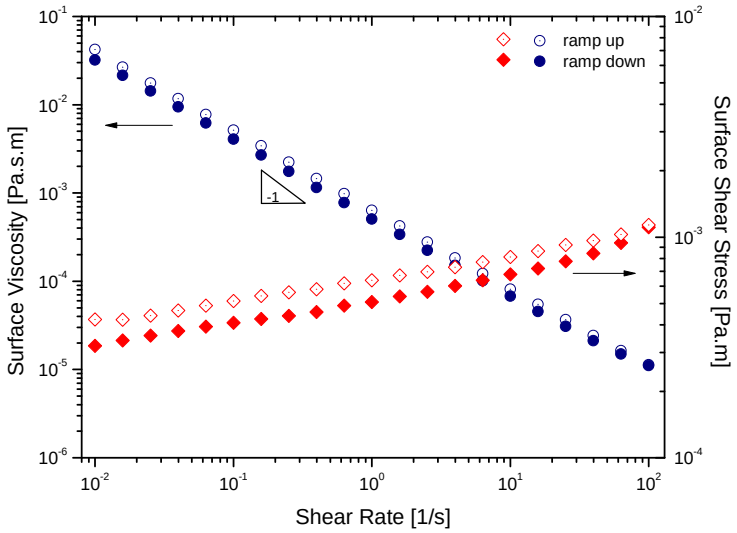

Figure 4.4: Interfacial shear rheology flow and viscosity curves for β-LG at 68 mg/mL (filtered 0.1 μm). The experiment was run immediately after the interface was formed. There was no waiting time between sweeps.

Further interfacial shear rheology characterisation included oscillatory studies, with strain and frequency sweeps (Figures 4.5(a) and 4.5(b)). For both strain and frequency sweeps the material always showed storage moduli (elastic portion) of higher values than the loss moduli (viscous portion), $G'_s >> G''_s$.

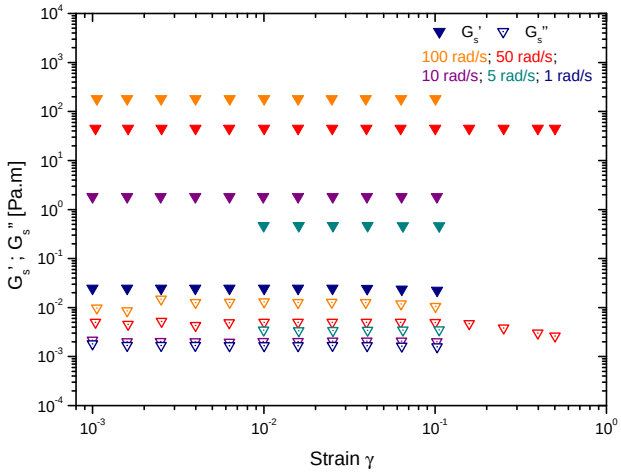

(a)

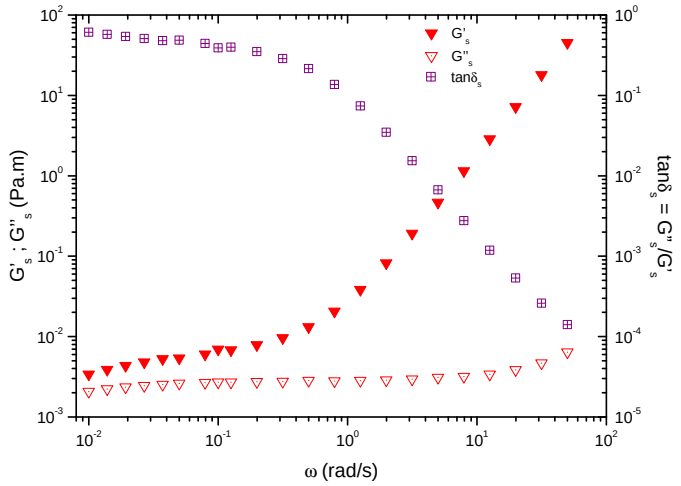

(b)

Figure 4.5: Interfacial shear oscillatory rheology for β-LG 68 mg/mL filtered (0.1 μm). (a) Strain sweeps at constant ω = 100; 50; 10; 50; 5; and 1 rad/s. (b) Frequency sweep was run from 0.01 to 50 rad/s, with constant strains at 2, 1.7 and 1.5 % from low to higher frequencies. For this test, the sample had an interface age of approximately 1.5 hour.

The strain sweeps with different constant angular frequencies of a range between 0.1 to 100 rad/s showed that the sample could still respond within the linear viscoelastic range throughout the chosen angular frequency range. It was only for a strain sweep

with $\omega = 50$ rad/s that a drop in G_s'' occurred at strain from 0.1 onwards, even though G_s' remained constant. This was a signature of how strongly elastic this protein solution's interface was, at the conditions studied.

For the interfacial shear frequency sweep (Figure 4.5(b)), G_s' was always larger than G_s'' at all applied ω, showing a narrow difference of values at $\omega = 0.01$ rad/s but increasing G_s' as ω increased, a sign of increased surface stiffness. This stiffness was accompanied with the damping factor $tan_s\,\delta$ <1, suggesting a solid-like state. This indicated that the phase angle δ, i.e. the shift between applied strain and the resulting deformation, was approaching 0°. All of these observations were signs characteristic of viscoelastic behaviour, which in this case reflected in a protein solution with a surface of increasingly stiff (elastic) characteristics. These observations were in agreement with literature for interfacial shear rheology of β-LG films in similar experimental conditions [167]. It was also noted that our frequency sweep did not show signs of cross-over between G_s' and G_s'' at lower frequencies, possibly indicating the fast transport of this protein to the air-water interface.

The linear increase observed for G_s' from $\omega = 0.3$ rad/s onwards was related to fluid inertial effects inherent to the DWR geometry [94, 174] and accounted for by evaluation of the Reynolds number (Re) and consideration of the DWR's characteristic geometry length (1 mm).

Drawing together the viscosity curves of interfacial and bulk shear rheology (Figure 4.6) it is clear that similar flow behaviour can be identified independent of the geometry used. Assuming that yield behaviour better explained these results, the simple Bingham model for yield-stress of viscoelastic fluids (Equation 4.1) was fitted to these data.

$$\tau = \tau_{BY} + \eta_{BY}\dot{\gamma} \tag{4.1}$$

This model is commonly used to find the yield point value (τ_{BY}) by extrapolating

the function $\tau(\dot{\gamma})$ to the zero shear rate value ($\dot{\gamma} = 0$ s^{-1}), where η_{BY} represents the function's coefficient. Plotting the calculated viscosities (Figure 4.6), based on the obtained fitting parameters (all with r^2 >0.97), these fitted data (lines in the graph) correlated well with the experimental data, highlighting that the underpinning factors leading to the yield behaviour seen on bulk rheology (CP and DG) could indeed relate to what causes the same behaviour at the interface of β-LG solutions. In addition, the observations so far noted for this protein have been similarly made for bovine serum albumin (BSA) solutions in PBS [78].

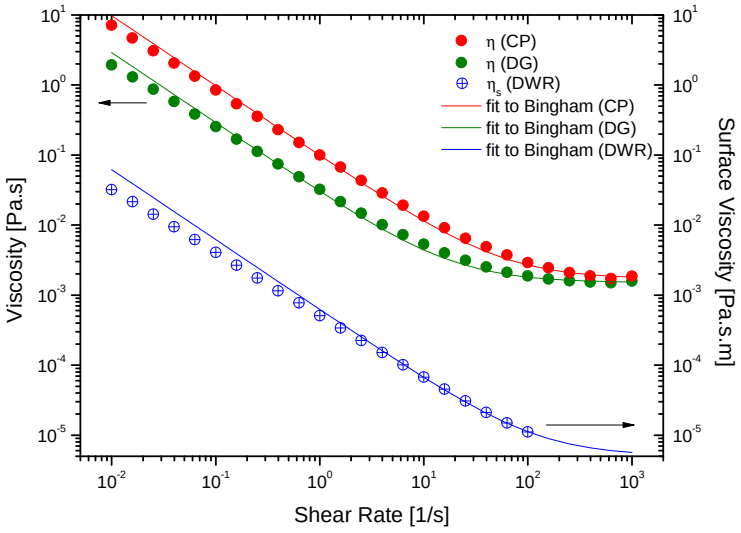

Figure 4.6: Flow and viscosity curves comparing bulk viscosity obtained by CP (red circles) and DG (green circles) with surface viscosity (blue circles) of a filtered 68 mg/mL β-LG solution. The lines represent respective fitting of data to the Bingham equation for yield stress (equation 4.1).

4.3.1.1 Air-water interfacial effects on conventional bulk rheology of β-LG solutions in excipient-free buffers

In many studies, excipient-free protein solution rheology has been measured using conventional (shear or stress-controlled) rheometers with geometries such as the CP. Sharma *et al.* (2011) combined analysis (bulk and interfacial rheology) of BSA in PBS lead to their suggestion that the apparent yield behaviour observed resulted from a protein film formed at the air-water interface. Indeed, β-LG is known to adsorb and form a film at the air-water interface [175] and its rheology at the interface has been extensively studied [167, 176–178]. Thus, our interpretation of bulk rheology results take on the suggestion that an apparent solid-like behaviour is inherently present in CP and DG bulk shear rheology of surfactant-free globular protein solutions. However, it is important to better understand which underpinning factors influence this behaviour and how do these interplay in protein solution rheology of surfactant-free samples. Therefore, the combination of rheological time sweep measurements and surface tension measurements were performed to seek if any correlations could be drawn.

A steady state time sweep rheological measurement of a β-LG $\sim$68 mg/mL (filtered solution with 0.1 μm pore-sized syringe filter) was performed on a CP to characterise the effect of time with continuous shearing (Figure 4.7(a)). The viscosity increased until it reached a maximum at a time point of approximately 1940 seconds (from the start of the second step). Viscosity then remained constant, and a rest period did not seem to affect the sample, since the viscosity values remained similar. The time point at which viscosity attained a steady state on the CP experiment, did not match the timescale measured from the tensiometry experiment shown in Figure 4.7(b). The latter experiment showed that surface tension reached an equilibrium (52.4 $\pm$ 0.37 mN/m) just after $\sim$1000 s. Filtered (0.22 μm) pure water and filtered (0.1 μm) sample buffer were measured as controls and had surface tension values of 72.9 $\pm$ 0.14 mN/m and

73.0 ± 0.34 mN/m.

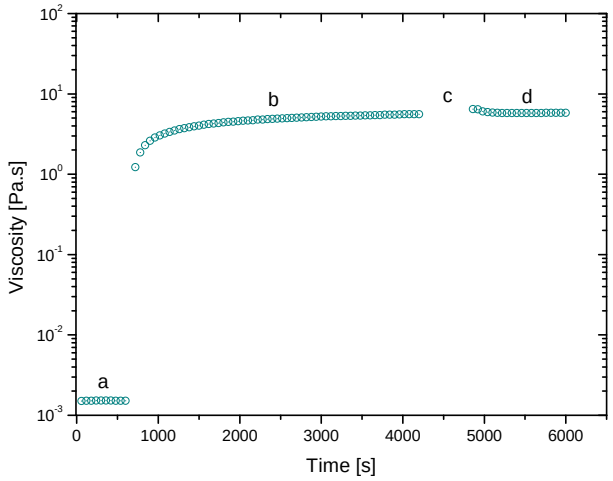

(a)

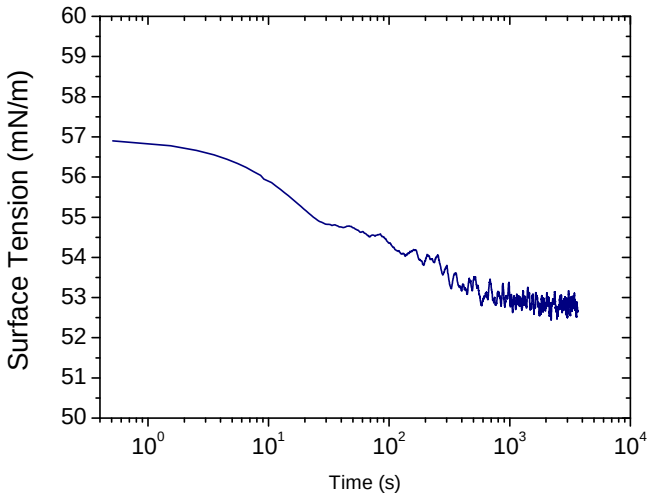

(b)

Figure 4.7: (a) Steady state time sweep with CP rheology and (b) a tensiometry curve for the β-LG 68 mg/mL filtered (0.1 μm) in 10 mM His-His.HCl pH 6.0. Stages for the time sweep (a) were: constant shear rate at 1000 s^{-1} for 10 min (**a**); $\dot{\gamma} = 0.01$ s^{-1} for 60 min (**b**); rest period (**c**); $\dot{\gamma} = 0.01$ s^{-1} for 20 min (**d**).

While the surface tension measurement was performed without shearing the air-

water interface, the CP rheological time sweep kept the sample volume with aid of an evaporation blocking system, to resemble the conditions of the tensiometry experiment. In the case of constant shearing, after the shear rate was dropped to 0.01 s^{-1}, the protein not likely formed the film at the air-water interface since the shear rate should be low enough to allow protein transport to the surface. The differences in methodology, inherent to the instrumentation, could explain why the timescales do not match between the different measurements. Nevertheless, the combination of these time-dependent experiments could represent, to different extents, the kinetics of protein transfer from bulk sub-phase to the air-water interface. Analogous time sweep experiments of BSA solutions and synovial fluid using bulk and interfacial shear rheology yielded similar results [63, 78].This suggests that the observed time and surface dependency is likely inherent to general surface activity properties of proteins.

In addition to timesweep results, consecutive rotational tests with the same sample (β-LG at ~68 mg/mL filtered) were performed with CP and DG (Figure 4.8). With both geometries, no hysterisis was observed when ramping down and up with no waiting time. However, between runs, resting for at least 5 minutes seemed to produce slightly lower viscosity values at the lower shear rates (<10 s^{-1}) while still presenting an apparent yield behaviour. This difference was clearer with the CP data than with the DG data. Interpretation of these results would require further tests to understand if the main reasons leading to the observed hysterisis relies solely upon surface activity. Although all the CP measurements were performed at a controlled environment with an evaporation blocking system, evaporation could still be possible, thus becoming another variable to consider as an influence to the changes observed at low stresses.

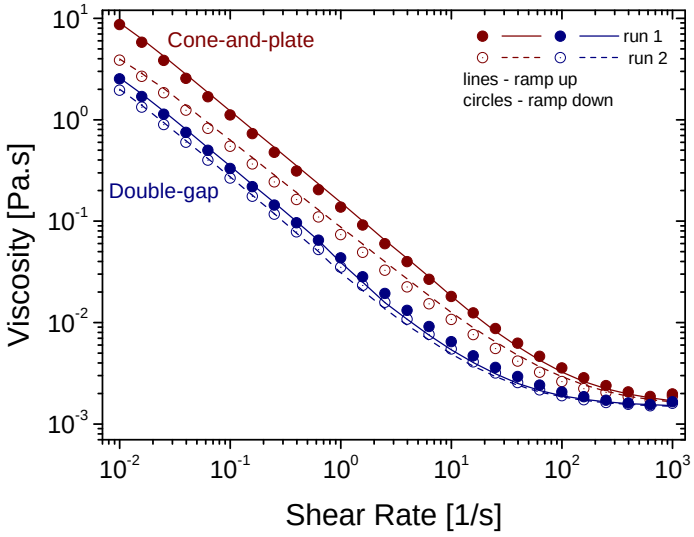

Figure 4.8: Viscosity curves of consecutive runs for βLG ~68 mg/mL comparison using CP and double gap. Circles (full or hollow) correspond to ramping down the shear rates, while lines (full or dashed) correspond to ramping up. CP data is represented in dark red, and DG is represented in blue. Time between runs was 5 minutes. Measurements taken at 25 °C.

These time-dependent results support the hypothesis that air-water interfacial effects need to be accounted for when measuring this type of fluid on a CP and DG geometries, since these are not free of an air-water surface area. Therefore, when using such geometries care needs to be taken to avoid unreliable readings for excipient-free protein solutions, particularly at the lower shear rates.

4.3.1.2 Air-water interface-free bulk rheological measurements of β-LG solutions and extrapolation of surface viscosity from CP and DG rheology

Having established that the air-water interface may influence the conventional bulk measurements, a comparison to air-water interface-free bulk measurements was needed as a control. Therefore, measurements at the higher shear rates ($\dot{\gamma} > 1000$ s^{-1}) using

a mVROC were performed (Figure 4.9 and Figure A.3 in Appendix A). The flow behaviour observed with the mVROC showed constant viscosities along the shear rates, suggesting that the samples had a Newtonian-like flow, comparable to a purely viscous liquid. Superimposition of mVROC data with CP and DG data at high shear ($\dot{\gamma}$ >10 s^{-1}) showed that the DG data matched better with the mVROC viscosity values. This has been observed by Sharma *et al.* (2011) with BSA solutions.

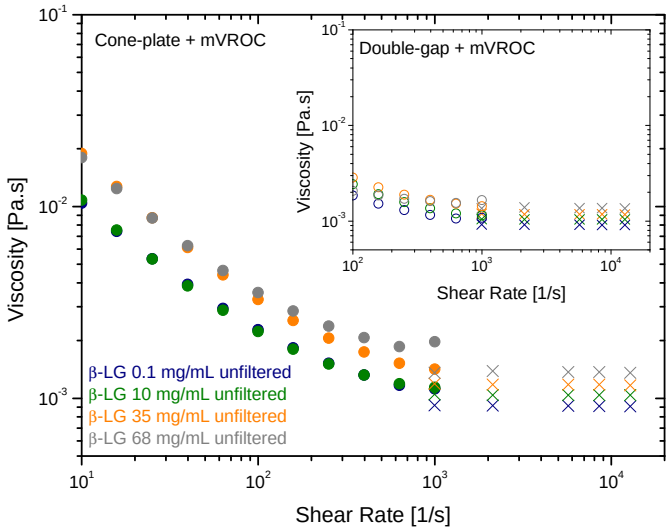

Figure 4.9: Rheology profiles of β-lactoglobulin samples comparing CP and DG data of unfiltered samples, with mVROC data (filtered samples). mVROC data are the crosses, CP data are the full circles and DG data are the hollow circles. Data shown only for higher shear rates of CP data. Measurements with mVROC were taken using the A05 chip. All data was taken at 25 °C.

A falling ball viscometer was also used for comparison, since the shearing rates applied by the falling ball to the fluid produce much lower shear rates than those imposed by the mVROC [49]. The viscosity values measured per solution were similar to those measured at $\dot{\gamma}$ = 1000 s^{-1} with both the CP and the DG (Table 4.1).

Table 4.1: Comparison between the viscosity values of β-LG filtered (0.1 μm) samples obtained using the CP and DG geometries, and the mVROC and falling ball viscometers. The results shown are mean and standard deviation of three separate measurements from each instrument.

β-LG concentration [mg/mL]	Viscosities [Pa.s]			
	Cone-and-plate	Double-gap	Falling ball viscometer	mVROC
	$\eta(\dot{\gamma} = 1000$ 1/s)			$\eta(\dot{\gamma} = 933$ 1/s)
0.1	$1.0\times10^{-3} \pm 6.2\times10^{-5}$	$1.1\times10^{-3} \pm 2.1\times10^{-5}$	$0.9\times10^{-3} \pm 2.3\times10^{-6}$	$0.9\times10^{-3} \pm 4.0\times10^{-6}$
10	$1.1\times10^{-3} \pm 2.0\times10^{-5}$	$1.2\times10^{-3} \pm 2.1\times10^{-5}$	$1.0\times10^{-3} \pm 1.2\times10^{-5}$	$1.0\times10^{-3} \pm 5.8\times10^{-5}$
35	$1.3\times10^{-3} \pm 1.5\times10^{-5}$	$1.3\times10^{-3} \pm 7.6\times10^{-5}$	$1.1\times10^{-3} \pm 1.0\times10^{-6}$	$1.2\times10^{-3} \pm 5.8\times10^{-6}$
68	$1.8\times10^{-3} \pm 1.1\times10^{-4}$	$1.5\times10^{-3} \pm 4.4\times10^{-5}$	$1.3\times10^{-3} \pm 4\times10^{-7}$	$1.4\times10^{-3} \pm 3.8\times10^{-7}$

Both AMVn and mVROC results demonstrated that applying high shear rates ($\dot{\gamma}$ = 1000 s^{-1}) using a CP or DG would be approximate to a bulk viscosity measurement performed with an air-water interface-free viscometer or rheometer. Although mVROC data did not allow measurements at the lower shear rates, it can be suggested that extrapolation to zero-shear viscosity ($\eta_0(\dot{\gamma} \rightarrow 0)$) would yield values similar to those measured at the higher shear rates. As seen from previously discussed results (e.g. Figure 4.6), the same extrapolation to zero-shear rate cannot be made with CP and DG data without accounting for the yield-like behaviour [78].

The suggestion that bulk viscosities measured with CP and DG are not true bulk viscosities implies that it is important to understand how the interface can influence the measurements. A rheometer fitted with a CP or a DG geometry will measure the torque as response of all the fluid in contact with the moving geometries, i.e. the cone and the bob, respectively. Therefore, if a surface active molecule forms a film at the air-water interface, the torque response will depend of the film's response to shear as well as the bulk's deformation. Calculating the surface area exposed to the air-water interface present in a CP and a DG system, we conclude that these areas are roughly

similar (73 mm^2 and 71 mm^2 for the CP50-1 and DG26.7, respectively). This could explain why the viscosities with CP are only just above to those obtained with the DG.

The Boussinesq number (Bo) is a dimensionless parameter that allows the calculation of the contribution of surface drag (η_s) relative to the bulk (η_b).

$$Bo = \frac{surface\ drag}{sub-phase\ drag} = \frac{\eta_s}{\eta_b\ l_s} \tag{4.2}$$

Bo depends on l_s, which is the geometry's characteristic length scale, where $l_s \approx A_b/P_i$. l_s depends on the geometry's dimensions, since A_b is the contact area between the geometry and the bulk sub-phase and P_i is the perimeter of wetted geometry in contact with the interface. From Equation 4.2, $Bo \gg 1$ when the interfacial stresses contribute more to the flow than the bulk stresses, while the contrary happens when $Bo \ll 1$. A geometry with a maximised wetted perimeter also contributes to high Bo values. This is the case of the DWR where $l_s = 0.7$ mm allows it to have higher sensitivity for interfacial measurements [94, 179]. The l_s for CP and DG were calculated considering the geometry's dimensions and are $l_s(CP) \approx 12.5$ mm and $l_s(DG) \approx 40.5$ mm, respectively (details are shown in Appendix A).

Figure 4.10 represents the calculated Bo for these three geometries using the measured interfacial shear viscosities and assuming $\eta_\infty = \eta_b$ from mVROC data.

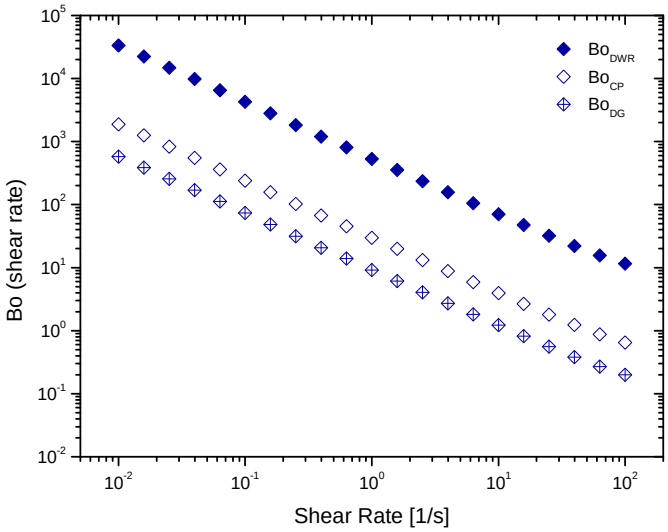

Figure 4.10: Boussinesq parameter dependent of shear rate calculated for DWR, CP and DG geometries using respective steady state shear rheology data, interface and bulk, from a filtered ~68 mg/mL β-LG solution.

These results showed that $Bo_{DWR} \gg Bo_{CP} > Bo_{DG}$ at the shear rates studied, and that $Bo \gg 1$ for these geometries, particularly at the lower shear rates ($\dot{\gamma}$ <10 s^{-1}). It showed that the bulk stresses started matching the interfacial stresses on the DG and the CP only when $\dot{\gamma}$ >16 s^{-1} and >63 s^{-1}, respectively. This also coincided to when viscosity values of the ~68 mg/mL sample reached constant values (cf. Figure 4.6). Our results were similar to those observed for BSA solutions from ref. [78], although in that study a CP of smaller dimensions (40 mm diameter) and a DG with a l_s of 59.5 mm were used. These differences in geometry were reflected in the Bo values, their DG provided lower Bo values at lower shear rates, thus measuring viscosities free from interfacial effects from slightly lower shear rates [78]. The opposite was reflected with the CP of their choice, which explained why our mVROC data superimpose better to our CP50-1 viscosity data at the higher shear rates (> 100 s^{-1}) (cf. Figure 4.9).

Following the proposal of Sharma *et al.* (2011), it was possible to quantify the

connection between these interfacial contributions and the torsional rheometry bulk measurement. The authors proposed the Equations 4.3 and 4.4, from which is possible to estimate bulk viscosities for a DG and CP from interfacial shear and a interface-free bulk measurements (e.g. mVROC, where $\eta_b \approx \eta_\infty \approx \eta_0(\dot{\gamma} \rightarrow 0)$). Assumptions have to be taken in account, such as the thickness of the surface active component is assumed to be smaller compared to the bulk geometry's effective characteristic length l_G. In addition, these derivations were made assuming that the measured torque ($M(\dot{\gamma})$) has contributions from the bulk sub-phase shear stress ($\tau_b = \eta_b \dot{\gamma}$) and the surface shear stress ($\tau_s = \eta_s \dot{\gamma}$). Finally, these contributions are calculated for the simple case where the surface is sheared without coupling with its bulk sub-phase [78].

$$\begin{aligned} \eta(\dot{\gamma}) &= \frac{M^{DG}(\dot{\gamma})}{4\pi R^2 L \dot{\gamma}} \\ &\approx \eta_b + l_G^{-1}\eta_s(\dot{\gamma}) \\ &\approx \eta_\infty + l_G^{-1}(\tau_s/\dot{\gamma}) \end{aligned} \qquad (4.3)$$

$$\begin{aligned} \eta(\dot{\gamma}) &= \frac{M^{CP}(\dot{\gamma})}{(2\pi R^3/3)\dot{\gamma}} \\ &\approx \eta_b + \frac{3\eta_s(\dot{\gamma}}{R} \\ &\approx \eta_\infty + l_G^{-1}\eta_s(\dot{\gamma}) \end{aligned} \qquad (4.4)$$

The effective characteristic length scales for each geometry, l_G, were also derived from the torque expressions and calculated to be $l_G(DG) = L$ and $l_G(CP) = R/3$, for the DG and CP, respectively [78]. Note that both equations (4.3 and 4.4) can be generalised to the same format (since $\eta_s(\dot{\gamma}) = \tau_s/\dot{\gamma}$).

Conversely, it was possible to estimate the surface viscosities extracted from the bulk measurements with CP and DG, based in a general equation derived similarly and assuming the same scenarios (Equation 4.5).

$$\eta_s(\dot{\gamma}) \approx l_G\,(\eta(\dot{\gamma}) - \eta_\infty) \qquad (4.5)$$

All results related to the extrapolation of surface viscosity from the bulk measurements and estimation of CP and DG data from surface measurement were based on

filtered (0.1 μm) β-LG ~68 mg/mL (Figures 4.11(a) and 4.11(b)).

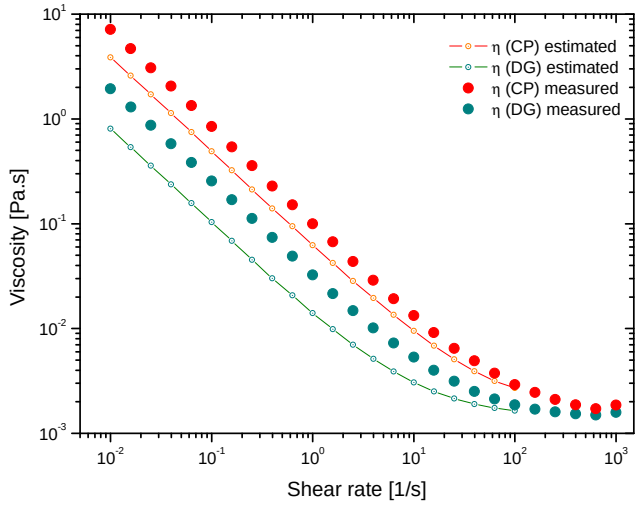

(a) Estimation of bulk viscosities from CP and DG experimental data

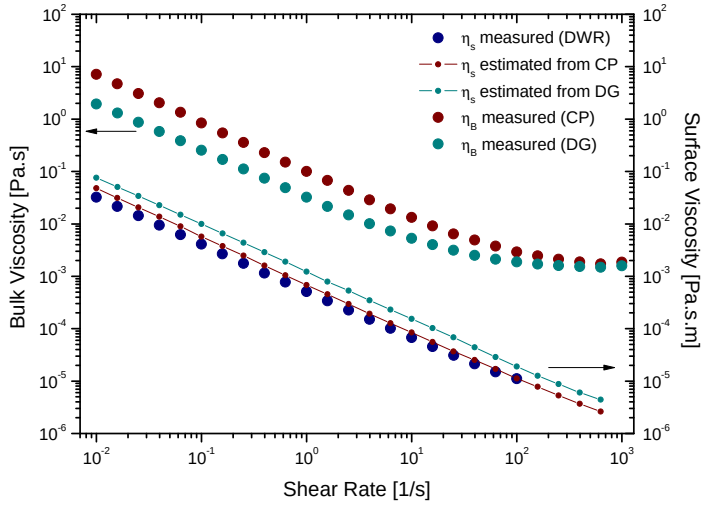

(b) Estimation of surface viscosity from CP and DG experimental data

Figure 4.11: (**a**) Bulk viscosity for CP and DG rheology estimated from interfacial rheology measurements. Measured data from CP and DG are shown for comparison. (**b**) Estimation of surface viscosity from CP and DG rheology. Measured data from DWR is plotted for comparison. All experimental data was obtained at 25 °C.

Estimation of bulk viscosity from the interfacial data (Figure 4.11(a)) resulted

in slightly underestimated values, particularly for the DG geometry. However, the estimated values for surface viscosity (Figure 4.11(b) seem to closely agree with the measured η_s using the DWR, especially for the CP data. The discrepancies here found may be due to the assumed scenario avoiding a coupling between sheared surface and sub-phase, i.e. the interfacial contributions from a CP or DG most likely come from a length larger than the film thickness, thus including a small proportion of bulk sub-phase [78]. Beyond these discrepancies, these latter calculations, in addition to the Boussinesq calculations, helped understand how the CP measurements were subject to higher influence of air-water interface, compared to the DG.

Since our results generally compare well to literature [78], even though when obtained from solutions of a different protein and using slightly different bulk geometries, they show that the air-water interface influence is inherent to CP and DG rheology of globular protein solutions. This also reinforces the importance of a better understanding of what happened at the lower shear rates of flow and viscosity curves of such samples.

4.3.2 Studying the influence of protein aggregates in bulk rheology of β-LG solutions

If protein solution viscosity is expected to be a function of volume fraction of the solutes present, it would be expected that all particles in a protein solution would also contribute to its viscosity proportionally to its concentration. Thus, it was hypothesised that the presence of insoluble aggregates could be a reason why the non-monotonic dependence appeared particularly at low shear rates. For this study, a comparison of rheological behaviour was made between unfiltered and filtered (0.1 μm) solutions, as well as an aggregate characterisation of the particles present in the samples. A further characterisation of the protein was made to understand its level

of aggregation and self-associative tendency at the solution conditions used in this study.

β-LG is known to be self-associative with the level of self-association dependent on the solution pH. At pH 6.0 β-LG was expected to be present mostly as a dimer, since pH 6.0 is higher than it's reported pI (5.2) and the dimers can associate further at between pH 5 - 8 [169]. In our case, a measurement with CG-MALS allowed characterisation of the associative state that β-LG was in the sample buffer at pH 6.0 (Figure 4.12). The MW was estimated to be 33.4 $\pm$ 0.14 kDa, which is close to the expected β-LG dimer MW of $\sim$36 kDa. The calculated self-virial coeffcient was -1.46$\times10^{-4}\pm$ 4.9$\times10^{-6}$ mol.mL/g^2. The negative value reflected the overall attractive self-interactions that can explain the self-associative characteristics of this protein at low ionic strength and close to physiologic pH [169]. CG-MALS data therefore showed that this protein was present mostly as a dimer at the solution conditions used throughout this study.

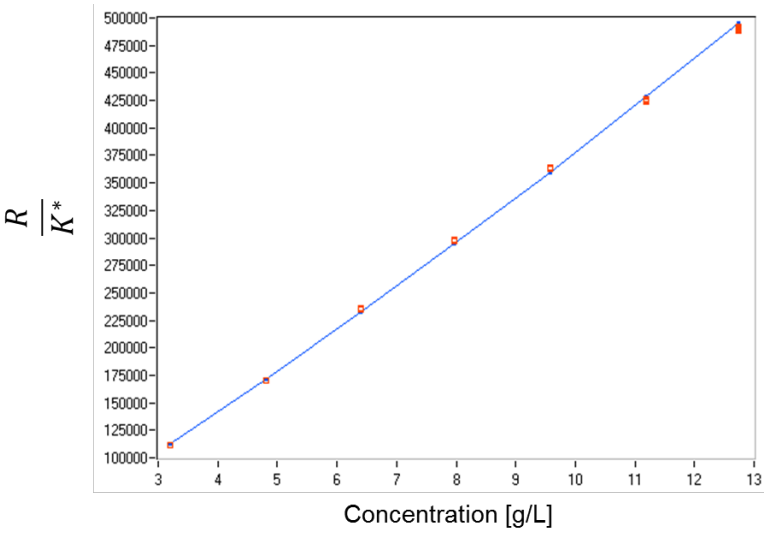

Figure 4.12: Static light scattering data (R/K*) versus concentration of β-LG starting at a stock concentration of 12.7 mg/mL and diluted with 10 mM His-His.HCl pH 6.0 buffer. The red squares represent the data and the line is for guidance only.

An analysis with HPSEC showed no difference in the number of peaks (species)

detected and respective elution times, between the unfiltered and the filtered samples (see Figure A.1 in Appendix A for an example of a chromatogram). Filtration of β-LG solutions did not affect the peak areas, as these remained essentially the same as seen with the unfiltered samples (Figure 4.13).

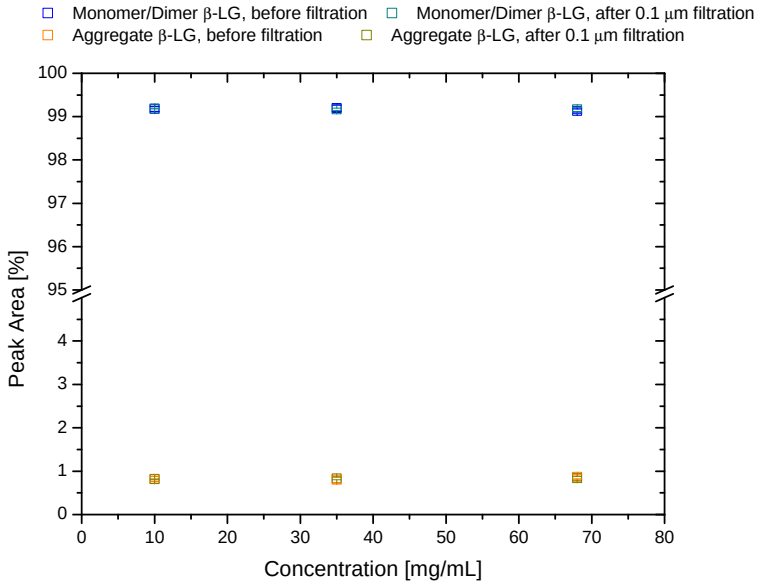

Figure 4.13: HPSEC chromatography data of β-LG species present in unfiltered and filtered solutions.

On microfluidics SDS-PAGE analysis, both unfiltered and filtered β-LG samples showed one band on both reducing and non-reducing conditions, identified to have a molecular weight of approximately 19 and 16 kDa, respectively (Figure 4.14). Considering the self-associative tendency of this protein, and due to successive dilutions used in this technique, all dimer dissociated into monomer. It was not possible to resolve the two variants A and B from this analysis. The purity of the material was confirmed, since no other MW band of a potential protein contaminant was identified [100, 169]. Although the MW obtained from this analysis were slightly lower than expected for the β-LG monomer, similar results were obtained in literature [121].

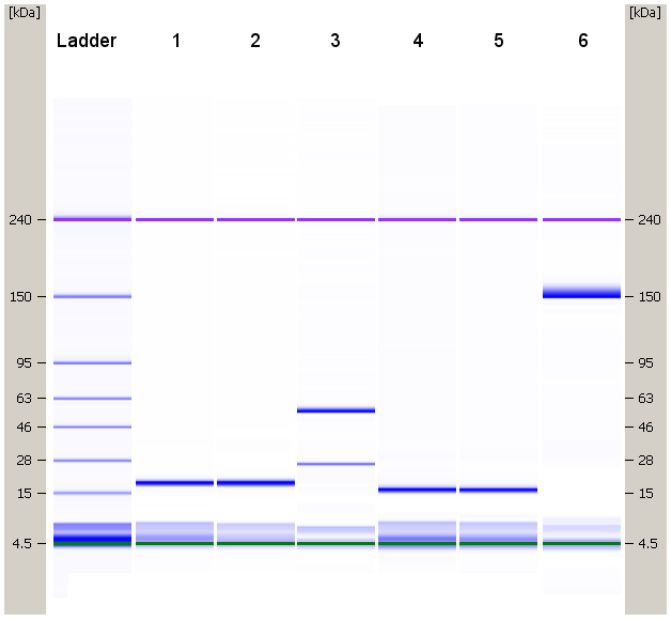

Figure 4.14: A microfluidics protein electrophoresis gel image for reduced and non-reduced conditions of β-LG samples. All samples diluted to 4 mg/mL with PBS. Lanes are: protein ladder, 1 - reduced β-LG unfiltered sample, 2 - reduced β-LG filtered 0.1 μm sample, 3 - reduced standard mAb sample (control), 4 - non-reduced β-LG unfiltered sample, 5 - non-reduced β-LG filtered 0.1 μm, 6 - non-reduced standard mAb sample (control).

After dialysis of several batches of β-LG stock, typically of ~80 mg/mL, these samples were always found to have visible particles. A qualitative characterisation of the prepared unfiltered samples was made via visual inspection (Table 4.2) regarding visible particles, opalescence and colour. After filtration into a clean vial, all samples were free of visible particles, showed no colour and were non opalescent (Figure 4.15).

The undialysed and dialysed β-LG stocks solutions were assessed on its osmolality with a calibrated freezing-point osmometer. A typical β-LG undialysed batch had an average of 55 $\pm$ 0.001 mOsmol/kg, whereas the dialysed batch would be 21 $\pm$ 0.002 mOsmol/kg which was similar to the value found for the filtered sample buffer (15 $\pm$ 0.001 mOsmol/kg). All batches of β-LG showed a similar osmolality value. pH measurements also showed that the samples retained their pH to 6.0.

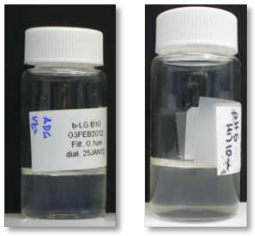

Figure 4.15: Image of β-LG solutions (∼68 mg/mL) before (right) and after (left) filtration using a 0.1 μm pore-sized syringe filter.

Table 4.2: Visual inspection classification for β-LG unfiltered samples. The material was assessed based on its colour, opalescence and visible particles content against a black and white screen with aid of a white light. Values or codes in parenthesis correspond to the standard to which the sample was similar.

Unfiltered β-LG sample concentration [mg/mL]	Colour	Opalescence	Particles
0.1	Colourless	Slightly opalescent (I)	Practically free of particles (1)
10	Slightly yellow (Y7)	Slightly opalescent (II)	Practically free of particles (4)
35	Slightly yellow (Y6)	Opalescent (IV)	Contains particles (5)
68	Slightly yellow (Y5)	Opalescent (V)	Contains particles (5)

Unfiltered samples were measured on the rheometer using both the CP and the DG geometries, as shown on Figures 4.2(a) and 4.2(b) in section 4.3.1. These samples exhibited a non-monotonic concentration dependence at the low shear rates ($< 10\ s^{-1}$). It was expected that filtration would yield lower viscosities, reduce the influence to the flow of larger insoluble particles (visible and sub-visible) and thus restore a monotonic concentration dependence at the lower shear rates. The results suggest that this was the case for the CP data, but not with the DG data (Figures 4.16(a) and 4.16(b)). Filtration could change slightly the concentration of material, where some monomer/dimers of β-LG could be adsorbed to the filter while the larger protein aggregates were filtered out. However, the difference between unfiltered and filtered solution concentrations

was lower than the accepted instrumental error for determination of concentration (10 %), except in the case of β-LG at 0.1 mg/mL (Table 4.3), while still being close to this error percentage. This slight drop in concentration can explain these differences between the viscosities at the higher shear rate (1000 s^1). Nevertheless, the larger differences between unfiltered and filtered samples were detected within the lower shear rates $\dot{\gamma}$ <10 s^{-1}, particularly and consistently with the CP data. One possible reason for disagreement with the DG data might be due the difficulty of loading the sample onto the cylinder gap, especially immediately after filtration where it is possible to inadvertently introduce micro-air bubbles that can further influence this measurement.

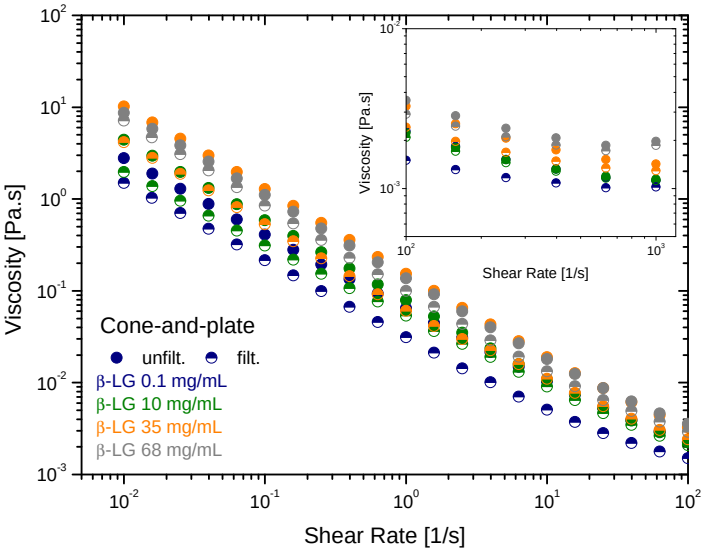

(a) CP

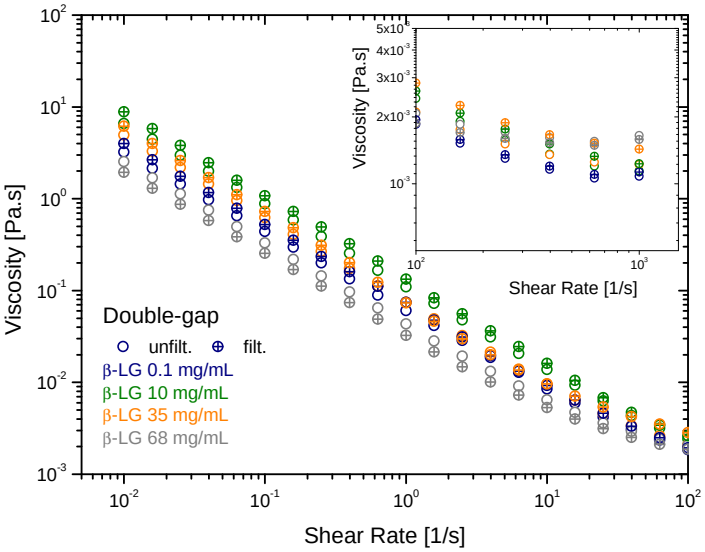

(b) DG

Figure 4.16: (a) CP data and (b) DG data of viscosity curves for samples of β-LG of different concentrations, comparing between the unfiltered and filtered (0.1 μm) solutions. Larger plots show the data at the lower shear rates (<100 s^{-1}) and the inset graphs show the data at the higher shear rates > 100 s^{-1}. All measurements taken at 25 °C.

Table 4.3: Measured concentrations via UV-Vis spectroscopy, of β-LG before and after filtration. Results are showed as an average and standard deviation of three separate measurements. [1] - $\Delta_{concentration}$ was calculated from $\frac{[Unfilt.]-[Filt.]}{[Unfilt.]} \times 100$.

β-LG sample	**Unfiltered** Measured concentration **[mg/mL]**	**Filtered (0.1 µm)** Measured concentration **[mg/mL]**	$\Delta_{concentration}$ [1] **[%]**
0.1	$0.12 \pm 4.4\times10^{-6}$	0.10 ± 0.01	16.7
10	$9.97 \pm 1.78\times10^{-2}$	9.97 ± 0.02	0
35	35.21 ± 0.32	35.15 ± 0.16	0.2
68	67.80 ± 0.88	63.85 ± 0.99	5.8

A comparison between the mVROC data superimposed with the CP and DG data of equally filtered samples, highlighted the similarity at the higher shear rates of viscosity values between the DG data and mVROC, with a slightly larger difference between CP and mVROC data (Figure 4.17).

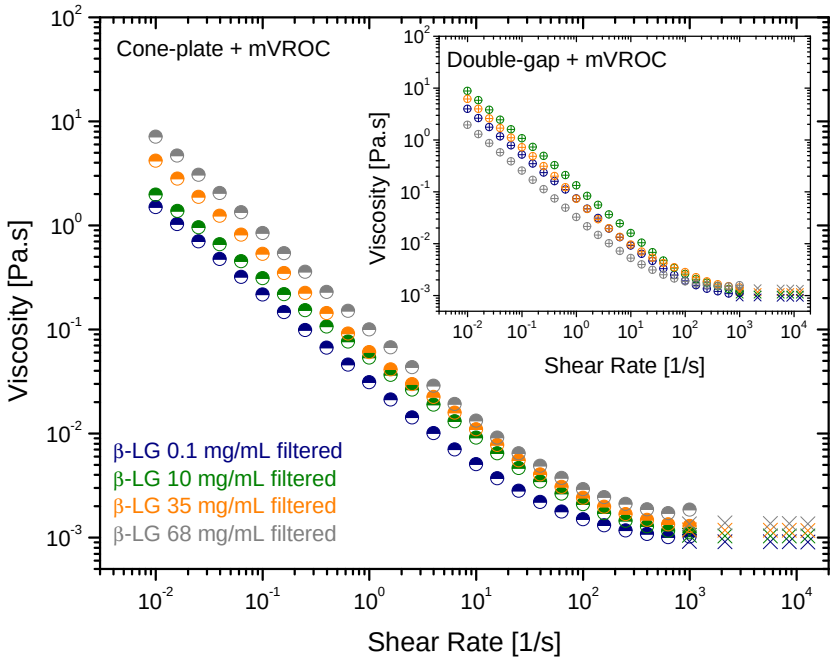

Figure 4.17: Rheology profiles of β-LG samples comparing mVROC, CP and DG data. Protein samples were all previously filtered with 0.1 μm pore-size syringe filters. Measurements were all taken at 25 °C.

It was necessary to identify what type of aggregates (soluble or insoluble) would influence this protein's solution rheology. The DLS correlation function data showed two steps, reflecting the existence of two different-sized populations (Figure 4.18). After filtration, slightly faster diffusion times were noted for the second population, while the first population remained unaltered (see Table A.1 in Appendix A). Size distribution by intensity (Figure 4.18, see inset graph) showed that apart from a main peak with a mean hydrodynamic diameter (H_D) of ~6 nm, these solutions presented a second peak with a $D_h > 100$ nm. According to literature, the typical hydrodynamic diameter of β-LG dimers in physiological pH conditions is around 5.2 - 5.8 nm [100, 180] assuming a thin hydration layer. Our DLS data was similar, taking in account differences in pH and ionic strength referred in literature, but also confirmed with the data obtained by

CG-MALS.

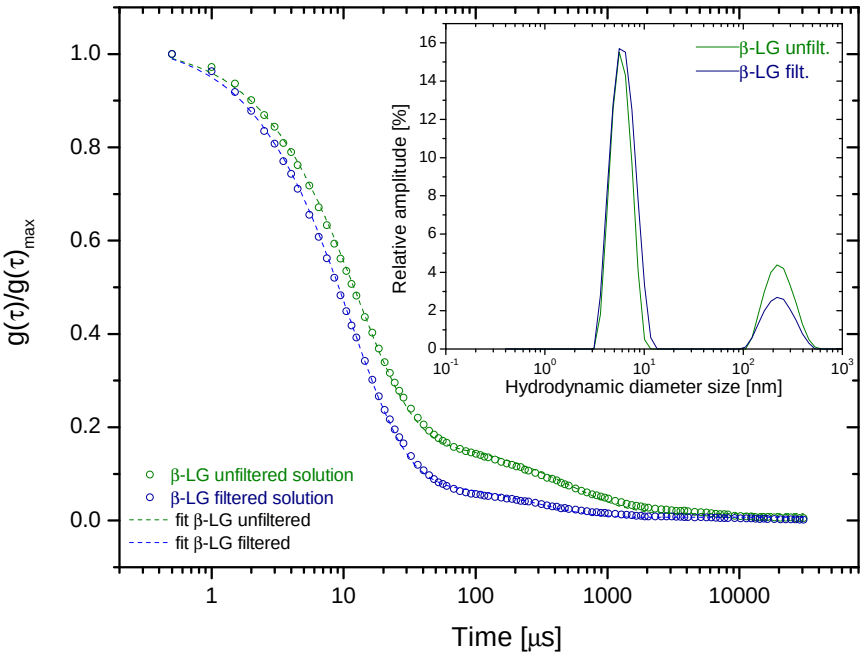

Figure 4.18: Size distribution by intensity of β-LG 68 mg/mL before and after filtration. Large graph corresponds to the normalised correlation function data versus decay times (hollow circles), as well as the fit to an exponential decay curve (dashed lines) for the before and after filtration β-LG 68 mg/mL samples. For both fits, the good-fitting parameter of r^2 was larger than 0.99. The inset graph shows the size distribution by intensity of the same samples shown on the correlation data.

It was expected that after filtering the solutions, the second population would have lower hydrodynamic size (H_D) or disappear altogether. However, filtration could generate new protein aggregates [127]. Other authors have also found that β-LG has an ability of forming aggregates (of diameter between 100 - 800 nm) quickly after being filtered, even when filtered directly to the DLS clean cuvette which was also our case [169]. This particular spontaneous clustering (or aggregation) of β-LG, particularly of variant A, has been addressed regarding the protein's specific surface

charge distribution [180, 181].

A time-sweep DLS measurement was done for a 1 mg/mL β-LG sample freshly filtered into the cuvette to investigate if this was the case, or if the equipment could detect the time point where the β-LG protein soluble aggregates would appear. Results showed that as soon as the sample was filtered and measured, it demonstrated a second peak with a mean H_D of between 200 - 500 nm, which fluctuated towards 1000 or higher nm with time (Figure 4.19). Although the populations with $H_D > 1000$ nm should not be considered due to the instrument's limit of detection [110], this was a sign that the monomers/ dimers could be clustering into aggregates of higher diameters shortly after filtration, in agreement to literature [169].

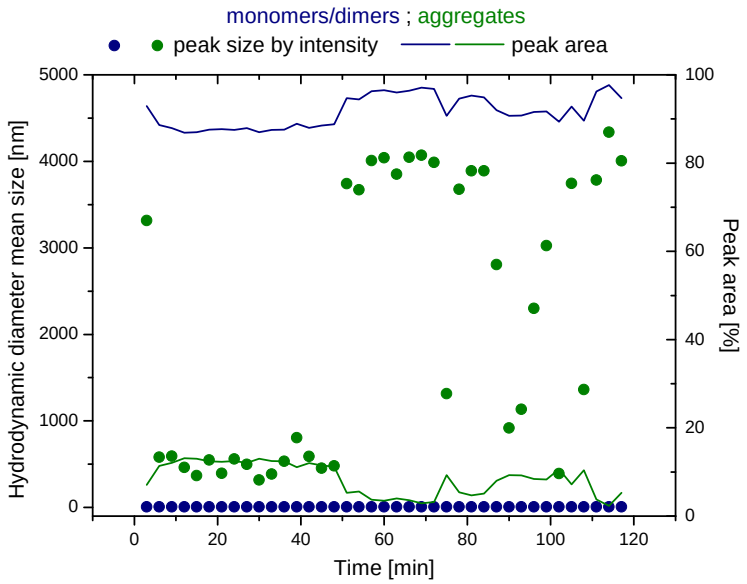

Figure 4.19: DLS time sweep of filtered 1 mg/mL β-lactoglobulin solution. The hydrodynamic diameter size by intensity for monomer/dimer (blue circles) and for aggregates (green circles). The lines correspond to their relative peak areas, also by intensity (monomer/dimer - blue; soluble aggregates - green).

A comparison with DLS and HPSEC analysis was also made between unsheared samples ('before rheology') and after being sheared ('after rheology'). DLS data is shown

in Appendix A (see Figures A.6(a) and A.6(b), and Table A.1). On HPSEC there was no difference detected on the chromatographic profiles and relative peak areas between before/after rheology on both unfiltered and filtered samples. With the 'after rheology' samples, there was a tendency towards larger aggregates detected by DLS. This could be have been an effect of shearing and the presence air-water interface on CP and DG measuring systems. Moreover, the possibility of shearing conditions and the adsorption to stainless-steel surfaces, such as those from CP and DG geometries, could contribute to the observed increase of soluble aggregates [29, 30]. Nevertheless, further investigations would be needed to determine the exact origin of these aggregates, taking in account the specific physical-chemical properties of β-LG.

To allow for a quantitative measurement and characterisation of sub-visible particles with a circular diameter (ECD) between 1 - 150 μm, all samples were analysed with micro-flow imaging. Filtration considerably reduced the number of sub-visible particles detected by micro-flow imaging (Figures 4.20(a) and 4.20(b)).

It would be assumed that after filtration, the material would be free from sub-visible particles, since the pore-size was of 0.1 μm. However, literature has shown that proteinaceous particles can remain even after filtration [127], where particles which have an axis length < 0.1 μm can still go through the membrane's pores. It can also be the case of filtered-induced protein aggregation [127]. As a control, 0.1 μm filtered sample buffer was measured in triplicate and repeatedly presented less than 10 particles per mL (see Table A.2 and Figures A.7 and A.8 in Appendix A). Therefore, when working with the MFI one has to consider the cleanliness of the environment, tubes or vials used, and be aware that there will be a residual number of sub-visible particles still present even after sample filtration.

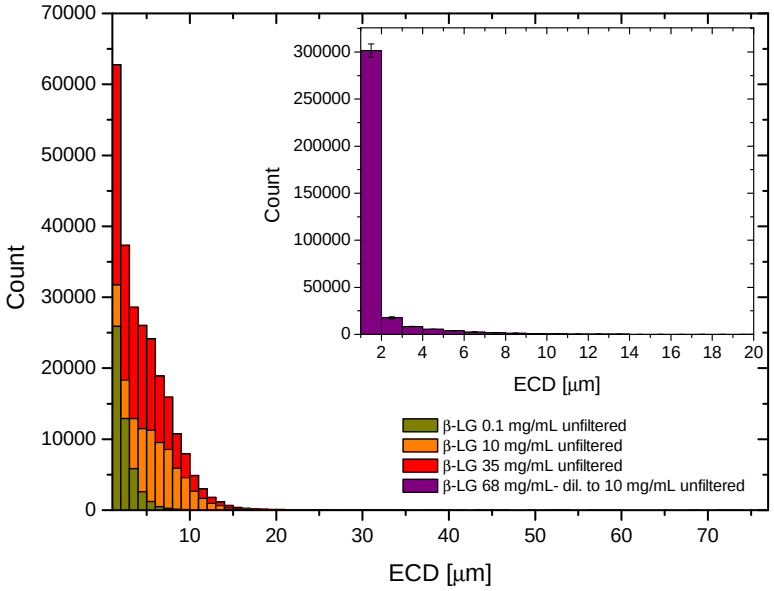

(a)

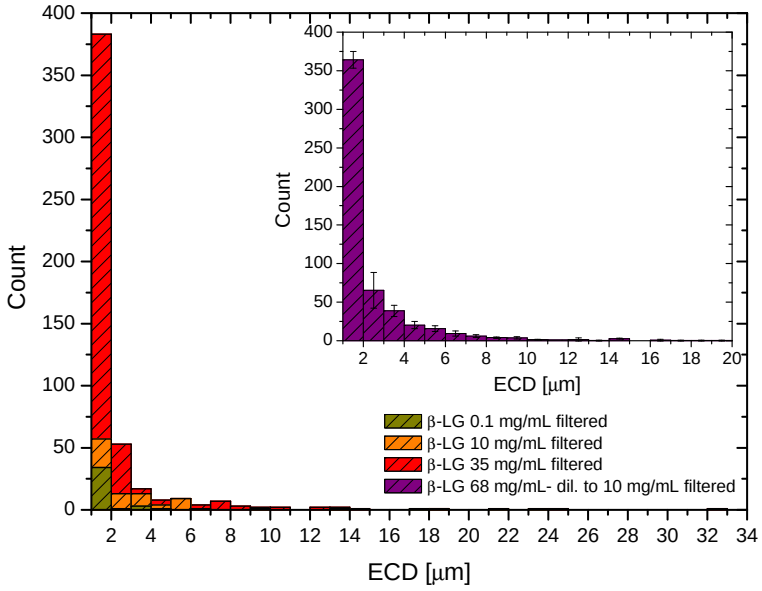

(b)

Figure 4.20: MFI sub-visible frequency histograms of (a) unfiltered and (b) filtered (0.1 μm) β-LG samples. Samples at ~68 mg/mL were diluted to 10 mg/mL to avoid clogging of the flow cell with visible particles present. The diluted 68 mg/mL unfiltered and filtered β-LG samples were measured in triplicate. Other concentrations (~0.1, ~10 and ~35 mg/mL) were measured with no further dilution and only once.

From MFI characterisation one concludes that these insoluble sub-visible proteinaceous particles were not only of different shapes, sizes and opacity (see Figures A.7 and A.8 in Appendix A), but also when under shear these aggregates were suspended in the sample. Therefore, to explain the differences seen between the rheology of unfiltered and filtered β-LG samples, especially with the CP data, it could be possible that these insoluble particles were contributing to increased viscosities at the shear rates applied. To estimate impact of this, the use of a rheological dimensionless parameter, the dressed Péclet number was calculated assuming a simple scenario. The dressed Péclet number is defined by:

$$Pe^* = \frac{\tau a^3}{k_B T} = \frac{\eta \dot{\gamma} a^3}{k_B T} \tag{4.6}$$

Pe^*, also known as reduced stress, measures whether the applied stress (in this case, shear stress τ) is large or small relative to the characteristic stress arising from Brownian motion (since k_B is Boltzmann's constant and T the fluid's temperature). Thus, equation 4.6 is dependent of the particle size, where a corresponds to the particle's characteristic length scale. Equation 4.6 is a ratio between the rate of advection imposed to the flow and the rate of the particle's relaxation by Brownian motion [48]. When $Pe^* \gg 1$, the shear stress effects overcome the particle's Brownian motion, whereas if $Pe^* \ll 1$, the opposite occurs [48].

The calculations of $Pe^*(\dot{\gamma})$ shown in Figures 4.21(a) and 4.21(b) represent the simplified situation where $Pe^*(\dot{\gamma})$ was in order of each of the sizes assumed to be present in a $\sim$68 mg/mL β-LG solution. In this case, it is considered only for the case of a monodispersed suspension composed of those separate sizes only. Besides polydispersity being a problem in calculating true Péclet numbers, the interparticle interactions also play an important role in colloidal suspensions, therefore interfering in the hydrodynamics of the suspension [48]. Finally, it was also assumed that the applied shear stresses were not disturbing the sizes of the protein soluble and insoluble species.

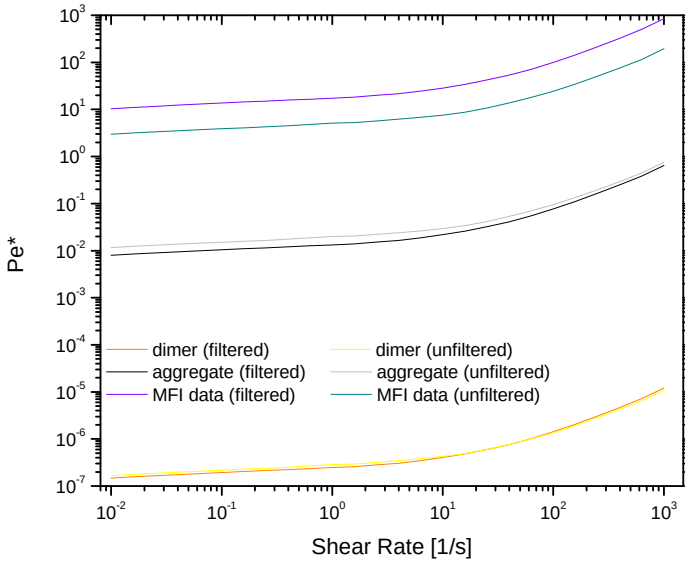

(a)

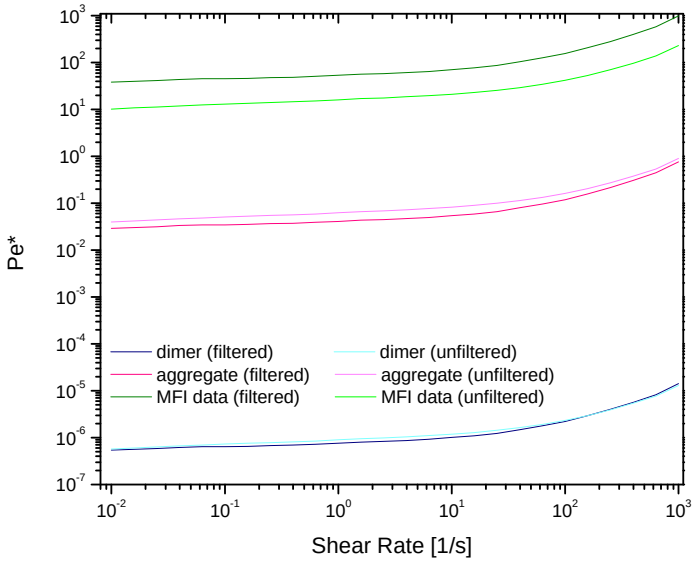

(b)

Figure 4.21: Comparison of Péclet number dependent on shear rate using different size data between unfiltered and filtered ∼68 mg/mL β-LG sample. (**a**) Calculations using DG shear rheology data. (**b**) Calculations using CP shear rheology data.

Nevertheless, these simplified calculations of $Pe^*(\dot{\gamma})$ highlighted that the larger the sizes of proteinaceous particles in a protein sample, the higher their influence the shear rheology particularly at low shear rates. For the CP and DG, only the Pe^*(MFI ECD data) >1. This meant that the stresses imposed to the fluid influenced the way these larger particles flowed, while the soluble aggregates and dimers flowed due to their Brownian motion. For both geometries the $Pe^*_{unfiltered} < Pe^*_{filtered}$ from the MFI data, when we should expect the opposite and as it is seen from the aggregate data. This discrepancy can be explained by the constant presence of large (ECD > 10 μm) sub-visible particles in the filtered samples, therefore skewing the mean ECD used for Pe^* calculations (Table A.2 in Appendix A).

4.4 Conclusions

In this chapter a detailed evaluation of the rheology of excipient-free β-LG solutions was made, where this protein served as a model for globular proteins. By collecting data from different types of rheometric instrumentation and comparing these, it was possible to identify that these solutions had a complex flow behaviour dependent on the shear rates applied. At low shear rates the flow properties of these samples seemed to be similar to solid-like flow, with a corresponding yield behaviour observed. Further analysis and close agreement of the data to a simple yield-stress Bingham model, supported our findings. At the higher shear rates, achieved with both the conventional torsional rheometers (CP and DG geometries) and a microfluidic rheometer (mVROC), these solutions produced a Newtonian-like flow, i.e. characteristic of a purely viscous fluid.

The origin of this yield-behaviour was also studied and suggested to be related to the surface activity of the protein and its time dependent formation of a protein film at the air-water interface. Comparison between interfacial rheology, tensiometry and

time-dependent bulk measurements with CP, although not reflecting matched timescales between measurements, further highlighted the importance of the presence of the air-water interface in the rheology of excipient-free protein solutions. Complementary data obtained from mVROC and AMVn provided evidence that when lacking this influence, protein solutions seem to show low viscosities and with constant values (e.g. mVROC).

Further analysis of this apparent change in regime between low and high shear showed that it was dependent, in an simple additive way, on contributions from surface effects and bulk sub-phase to the measured torque. Although our calculations included a few simplistic assumptions, these highlighted the fundamental hypothesis that a protein film at the air-water interface present in CP or DG experiments will be detected and translated in high viscosities at low shear rates.

Our detailed results add to recent findings in the literature [78] to the extent that this hypothesis was applied to another globular protein model. This brings emphasis to the broad application of this knowledge to protein solution rheology, in particular by applying to the study of therapeutically relevant proteins such as monoclonal antibodies.

We also hypothesised that the rheological properties depended on the soluble and insoluble protein species present in these samples. Even though filtration could have limitations, it was shown that the presence of sub-visible proteinaceous particles had an impact on the sample rheology, particularly at the lower shear rates. Small differences in rheology were detected, between the unfiltered and filtered samples, but this could be due to the small proportion of sub-visible particles (and visible, although not quantified) on the sample's total solids content. These findings highlight that the contents and size of protein species within a protein solution are key factors to understand in order to correctly and realistically evaluate its rheology.

Chapter 5

The rheology of a monoclonal antibody solution: a case study on the effect of aggregation of a model monoclonal IgG_1 on its solution rheology

5.1 Introduction

It is known that protein solutions will inherently contain different associative species that are formed with time, solution conditions, temperature, and/or dependent on other physical-chemical factors [28]. For the perspective of biopharmaceutical formulations, determination of stability is therefore an important part of development to ensure that the right conditions are chosen to prevent any loss of protein monomer, which in the case of antibodies, is the pharmacologically active substance [1, 44].

The generation of protein associative species can be lead by several pathways from which a protein monomer can degrade [28, 43]. The consequence of these pathways can ultimately lead to proteinaceous aggregates that vary in its size, morphology, reversibility properties, secondary and/or tertiary structure, and if cross-linked by covalent bonds [85]. In the protein formulation, it is important to understand the mechanisms that may lead to protein aggregation, in order to inhibit these as much as possible. Characterisation of proteinaceous associative species and their quantification

is therefore necessary to account for the stability and safety of the formulated drug product [10].

For colloidal suspensions, it is known that viscosity is a physical parameter connected to the suspension's content, to the particle morphology and the inter-particle interactions present [48]. This has been discussed in literature [182], and was discussed in the previous chapters of this thesis (Chapters 3 and 4) as a concept that should be addressed when understanding the rheology of protein solutions. Moreover, the importance of influence of the air-water interface in conventional rheology measurements of protein solutions was highlighted in Chapter 4 [74, 78, 143]. Therefore, the work in this chapter focused on extending these concepts to mAb solution rheology.

The mAb used for the studies presented in this thesis was a humanised IgG_1, provided as a lyophilised product containing stabilising additives. It was necessary to remove these excipients to generate the excipient-free mAb solution needed for this study. The first section of this chapter accounts for the physico-chemical comparisons of the different batches obtained after this removal procedure. This mAb has been characterised in literature, for its engineered ADCC enhancement via three mutations which were introduced to its C_H2 domain [183].

The general aim of this work was to understand if and how protein aggregation influenced the solution viscosity of this mAb. Thermal stressing over defined periods was the chosen method to promote the protein aggregation process. The solutions were characterised using several biophysical techniques to help understand the level of aggregation, the size, morphology, and quantity of the aggregates. In addition, by extending this case to the complexity of monoclonal antibody aggregation, we aimed to understand the effects of aggregation on the yield-like behaviour typically observed in excipient-free protein solutions. The ultimate aim of this chapter was, in light of the discusssions concerning the effect of concentration on the viscosity of protein solutions

(Chapter 3), if it was possible to relate the volume fractions of protein aggregates, as well as their size and shape to the solution' viscosities. An achievement in that regard, could help the development of future biopharmaceutical formulations in predicting mAb solution viscosity based on the physico-chemical characterisation of the protein aggregates generated during stability test.

5.2 Materials and Methods

5.2.1 Materials

5.2.1.1 Protein sample

The humanised monoclonal antibody studied was provided by MedImmune, LLC. (Gaithersburg, Maryland, USA). It is an IgG_1 of 145.461 kDa. The protein was supplied in a lyophilised formulation containing other additives, including a surfactant. The formulation additives were removed by purifying the reconstituted material, as described in section 2.2.3 of Chapter 2.

5.2.1.2 Sample preparation

After purification, diafiltration and concentration steps were performed to collect the mAb solutions (section 2.2.3 in Chapter 2). Three batches were obtained depending on the processing step and concentration: batch 1, 2a and 2b.

Independent of the diafiltration/ concentration method used, all mAb batches were checked for concentration, pH, osmolality, and their aggregation level by HPSEC. Additionally, all batches were checked for presence of the non-ionic surfactant which was an additive in the original lyophilised formulation (this procedure was performed

at and by MedImmune, Gaithersburg, MD, USA).

mAb solutions were prepared in a histidine buffer containing L-Histidine and L-Histidine monohydrochloride at 10 mM in ultrapure water, with a pH of 6.0 ± 0.2 at room temperature. L-Histidine salts were obtained from J.T. Baker Chemicals (Pennsylvania, USA) and were of analytical grade.

For circular dichroism analysis, a 10 mM sodium phosphate buffer pH 6.5 was prepared using monosodium phosphate monohydrate and dibasic sodium phosphate heptahydrate in ultrapure, both purchased from J.T. Baker Chemicals and of analytical grade. Ultrapure water was obtained from a water cleaning resin system from NANOpure Diamond, Barnstead, USA, with water quality of 18.0 mΩ-cm, and 0.22 μm filtered (EMD Millipore, USA). All buffers were filtered using 0.22 μm vacuum-driven filter units (Nalgene, USA), unless when 0.1 μm pore-size filtering was necessary (using PDVF syringe-filters Millex-VV from EMD Millipore, USA).

Filtration of mAb samples, using syringe filters, was done under a vertical laminar-flow fumehood to avoid any contamination by dust particles (LabCaire fumehood VLF6 Clean Air, PuriCore, Inc., USA).

Thermal stress aggregation study

After filtration of batches 2a (∼100 mg/mL) and 2b (∼17 mg/mL), the samples were left at 40 °C and 5 °C (control) for 6 weeks. Aliquots of the samples were analysed at 2 week intervals. The samples were typically taken out of the incubator and left at room temperature to equilibrate (∼30 minutes), since most of the experiments required readings at room temperature.

Dilution and temperature study of reversible aggregates

The sample used was stored at 40 °C for 7 weeks. Dilutions of 10 and 50 mg/mL of this sample were analysed on DLS and on HPSEC (with a sample tray temperature) either at 25 °C or 5°C. Injection concentration was kept 10 and 50 mg/mL, therefore the injection volume was changed according to keep constant the protein load in the chromatography column. For the HPSEC experiment at 5 °C, injections were made over a period of time of 7 days, whereas the experiment at 25 °C took a total of 21 hours. The DLS experiments lasted 25 hours.

For the rheology and HPSEC parallel studies of the effect of reversible aggregates, a mAb sample of 100 mg/mL left at 40 °C for 2 weeks was used. After the first measurement, for rheology and HPSEC, the original sample was stored at 5 °C. Fresh aliquots were measured on HPSEC as well as on the double-gap rheometer 24 hours later.

5.2.2 Methods

5.2.2.1 Quantification of protein concentration by UV spectroscopy

A calculated percent extinction coefficient ($A^{1\%}_{1cm}$) of 1.45 was used for mAb solutions. The concentrations reported were calculated as an average of measurements of 3 separate dilutions prepared from each sample. An error of up to 10 % was accepted for this measurement. All details related to this method are described in section 2.2.7 in Chapter 2.

5.2.2.2 Freezing-point osmometry

The osmotic strength of buffers and samples was measured. A freezing-point osmometer Osmomat O30-D (Gonotec GmbH, Germany) was used, zeroed with ultrapure water and calibrated with a 300 mOsmol/kg NaCl aqueous solution (Gonotec GmBH, Germany).

5.2.2.3 Differential scanning calorimetry

All details related to this method are described in section 2.2.12.1 in Chapter 2.

5.2.2.4 Isoelectric Focusing

All details related to this method are described in section 2.2.13.2 in Chapter 2.

5.2.2.5 Circular Dichroism

All details related to this method are described in section 2.2.14 in Chapter 2. The far-UV data collected was processed and fitted using the CONTINLL, SELCON3 and CDSSTR algorithms available on with the CDPRO software. The protein base reference used for these computations was reference set SP43. The data shown in this work is obtained from using the CDSSTR algorithm, since it was the best fit, having the lowest root mean squared (RMS) values compared to the other fits.

5.2.2.6 Bulk Rheology

The rheometer used was Anton-Paar (Graz, Austria) MCR 301 model. A cone-and-plate geometry was a stainless steel CP50-1 (diameter = 50 mm and cone angle = 1 °; Anton-Paar). To prevent evaporation of sample and to keep constant temperature of 25°C ± 0.1°C throughout the measurements, an evaporation blocking system equipped with a peltier unit was used. A double gap concentric cylinder geometry (DG26.7) was also used. The rheometer was calibrated with hydrocarbonate standard oils (N1.0 and N14) from Cannon Instruments (USA) using the same method for data collection. Prior to measurements, all samples were allowed to equilibrate to room temperature (∼ 23°C) for at least 30 minutes.

The reconstituted mAb formulation was analysed on the TA AR-G2 rheometer (TA

Instruments, USA), using a CP40-1 (40 mm diameter, 1 ° cone angle; TA Instruments). This measurement was performed at 25 °C.

Rotational tests (flow curves and viscosity curves) were performed by controlling the shear rate typically from 0.01 to 1000 s^{-1}. Each shear-rate step had a 60 second duration time during which the instrument was averaging over the collected data. For the TA AR-G2 rheometer, the shear-rate step had a 45 second duration time. Typically, two shear-rate sweeps (ramping down and up) were performed per sample, without waiting time between sweeps.

5.2.2.7 Micro-viscometer/rheometer on-a-chip

The microviscometer/ rheometer on-a-chip (mVROC), by Rheosense, Inc. (San Ramon, California, USA) was also used to measure the bulk viscosity of filtered (0.1 μm pore size) mAb solutions only. For these measurements, the A05 chip was used and temperature was kept constant at 25°C ± 0.1°C using a water circulation system (ThermoCube, SS cooling systems, USA) (for additional information, see section 2.2.6.2 in Chapter 2).

5.2.2.8 High performance size exclusion chromatography for determination of level of protein aggregation

All the details related to this method are described in section 2.2.9.2 in Chapter 2.

5.2.2.9 Static light scattering - HPSEC-MALS and CGMALS

For the HPSEC-MALS experiments, the system was an Agilent Technologies chromatography system as that described in section 2.2.9.2 of Chapter 2, adding an Optilab REX refractive index detector and an on-line DAWN-HELEOS II multi-angle light scattering detector. Details on both these detectors can be found in section 2.2.8.2 in Chapter 2. The method details were kept constant as stated for the HPSEC method.

Calibration of this experimental setup was made using a BSA standard at 2 mg/mL

in phophate buffer and sodium azide 0.2 %, obtained from Pierce Labs (Thermo Scientific, UK). Analysis and integration of the chromatograms was performed using Astra 6 software (Wyatt Corporation Technologies, Santa Barbara, California, USA). The dn/dc (refractive increment) used for this experiment was set at 0.185 mL/g [142].

The mAb samples analysed were: a non-stressed 100 mg/mL samples (stored at 5 °C); a 17 mg/mL sample stored at 40 °C for 2 weeks; and two 100 mg/mL samples stressed at 40 °C for T= 2 and T= 6 weeks, respectively. All the 100 mg/mL mAb samples were injected at 10 mg/mL dilutions and the 17 mg/mL samples were injected neat.

For the CGMALS experiment see details on section 2.2.8.2 of Chapter 2. The analysed mAb solution was a 5 mg/mL dilution from batch 2a, doubly filtered with 0.1 μm pore-size syringe filters. The sample was in 10 mM His-His.HCl pH 6.0 buffer and the successive dilutions were analysed with the filtered sample buffer (0.1 μm pore size). Data analysis was performed using Calypso software (Wyatt Corporation Technologies, Santa Barbara, California, USA).

5.2.2.10 Dynamic light scattering (DLS)

All details related to this method are described in section 2.2.8.1 in Chapter 2. mAb samples were measured at 1 mg/mL to reduce non-linearity effects on measurements due to increased viscosity of the samples at higher concentrations. Measurement settings for size readings were at a constant temperature of 25°C ± 0.1°C, performing 20 runs of 20 seconds duration each. Sample equilibration for 5 minutes was done at the same temperature. Size measurements were made in triplicate with fresh aliquots for each reading.

For time sweeps, the samples were also measured at 1 mg/mL and set up for

continuous readings for 24 hours. The number of runs were 20, with 20 seconds duration each. The temperature was either at 5 °C or 25 °C. With the sample measurement at 5 °C, a nitrogen gas flow was run through the sample compartiment at sufficient pressure to prevent condensation on the cuvette's sides.

5.2.2.11 Microfluidic chip sodium-dodecylsulfate polyacrylamide gel electrophoresis (SDS-PAGE)

All details related to this method are described in section 2.2.13.1 in Chapter 2. A gel was run to compare the dilutions of the three batches of excipient-free mAb solutions (batch 1, 2a and 2b). Another μ-SDS-PAGE experiment was performed to check the purity of thermally-stressed mAb samples. A comparison was made between samples at the last time point of the study with those at T=0. For the 100 mg/mL mAb samples, this experiment was performed after the study had finished, due to lack of timing before completion of the study. Therefore, about 250 μL of the samples at T=0 and T= 6 weeks were frozen at -80 °C and then thawed for the preparation of the gel electrophoresis test. Concerning the 17 mg/mL mAb samples, the comparison made was between the last time point (T=6 weeks) at 5 and 40 °C and the frozen sample at T= 0 at 5 °C (Figure 5.14(b)).

5.2.2.12 Flow imaging microscopy for sub-visible particle counting

All details related to this method are described in section 2.2.15 in Chapter 2. The mAb samples chosen for MFI analysis were, for both ∼100 and ∼17 mg/mL, unfiltered and filtered (0.1 μm) solutions. During the thermal stress study, aliquots from these two dilutions were measured at each time point (T= 0, 2, 4 and 6 weeks). Aliquots from

stressed samples at 40 °C and 5 °C were measured. The samples (100 and 17 mg/mL) at T= 0 corresponded to the initially filtered material. After the first filtration, no other filtration step was performed before measuring the solutions at the remaining time points.

5.2.2.13 Visual inspection of protein solutions

All details related to this method are described in section 2.2.16 in Chapter 2. Unfiltered and filtered (0.1 μm) samples of ∼100 and ∼17 mg/mL mAb solutions were visually inspected regarding their colour, opalescence and visible particle content.

5.3 Results and Discussion

5.3.1 Excipient removal and mAb characterisation

In order to explore the effects of aggregation on viscosity, this study utilised an excipient-free solution. To guarantee that none of the additives remained in solution, affinity chromatography followed by diafiltration/ concentration steps were employed. mAb batch 1 was obtained using a stirred-cell diafiltration-concentration method, while mAb batch 2 was obtained via a tangential flow filtration (TFF) method. Batch 2 was divided into 2a and 2b, and the solutions were kept separate, since batch 2b corresponded to the washings of the TFF membrane. All mAb batches were diafiltered in 10 mM His-His.HCl pH 6.0 buffer. These were characterised to confirm that, despite the different diafiltration-concentration methods used, the protein remained the same in its physical-chemical characteristics.

mAb Batch 1 had a total volume of ∼35 mL at a concentration of ∼88 mg/mL. Batch 2a had a total volume of ∼180 mL at ∼100 mg/mL, while batch 2b had a total volume of ∼140 mL at ∼17 mg/mL. After extracting the excipients, the mAb solutions were checked for osmolality. The excipients were clearly removed from the original

solution, since the purified mAb solutions presented an osmolality of ∼26 mOsmol/kg, comparable to the buffer (15 ± 2 mOsmol/kg) and much lower than the value measured for the formulation (896 ± 19 mOsmol/kg). The consistency of these solutions' pH was also checked and it remained to pH 6.0 at room temperature. Additionally the batches were checked for the non-ionic surfactant additive present in the original formulation. The gas chromatography method demonstrated that this additive was not detectable in the excipient-free material. The batches were submitted to circular dichroism, micro-differential scanning calorimetry, capillary isoelectric focusing, HPSEC, and microfluidics SDS-PAGE. Flow and viscosity plots of each batch were obtained using a cone-and-plate geometry and compared to the formulated material.

Since the diafiltration/concentration methods are a processing step common in mAb solution preparations, it has been discussed in literature its role in influencing the protein's structure and level of insoluble and soluble aggregates due to the high fluid shear rates involved [5]. As an initial characterisation, the circular dichroism technique was used to confirm the secondary and tertiary structures of the mAb remained unaltered. Figure 5.1 summarises the obtained circular dichroism scans made at far and near UV wavelengths. Figure 5.1(a) includes a table that shows the relative content of secondary structures present in this mAb. Between batches, no evident change was observed in the secondary structure, although the spectra were not super-imposable. The goodness of fit values of the CDSSTR algorithm fit to the experimental data represent these subtle differences between spectra at far UV wavelengths, though producing similar relative percentages of each secondary structure present in this macromolecule. The negative peak at ∼217 nm and a positive peak at ∼203 nm, as well as the resulting relative percentages high percentage (total ∼70 %) in β-sheet and low percentage of α-helix showed agreement with the expected results for a IgG_1 mAb [184, 185]. For the near UV wavelengths (Figure 5.1(b)), there was no major difference between the spectra

collected showing that the tertiary structure remained similar across the batches. The near UV spectra showed peak values slightly shifted to lower wavelengths, compared to literature [184–186]. A positive peak at ∼285 nm (related to tryptophan residues), followed by a negative band with a range between 270-250 nm, were still observed and considered to be typical to IgG near UV dichroisms. In summary, there was no evident difference found between the batches collected and, although this CD analysis had to be made at a different non-chiral buffer than in which the mAb was originally diluted, the macromolecule seemed to retain its structure.

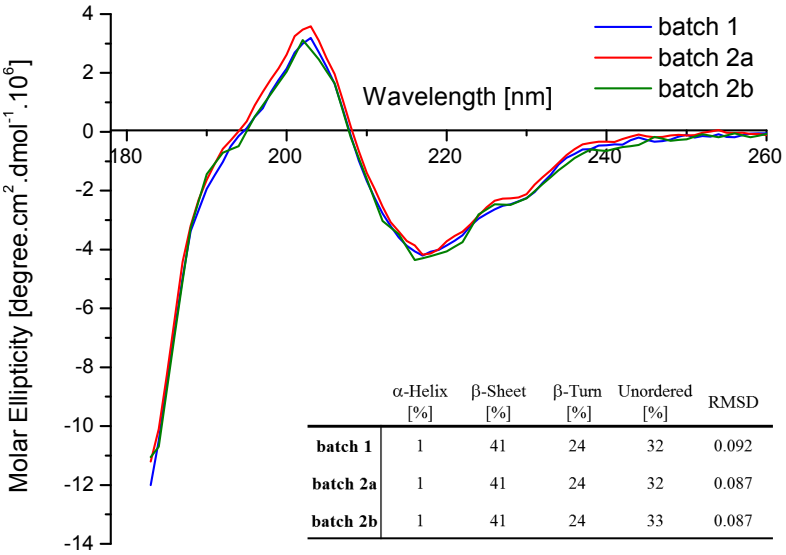

	α-Helix [%]	β-Sheet [%]	β-Turn [%]	Unordered [%]	RMSD
batch 1	1	41	24	32	0.092
batch 2a	1	41	24	32	0.087
batch 2b	1	41	24	33	0.087

(a) Far UV spectra

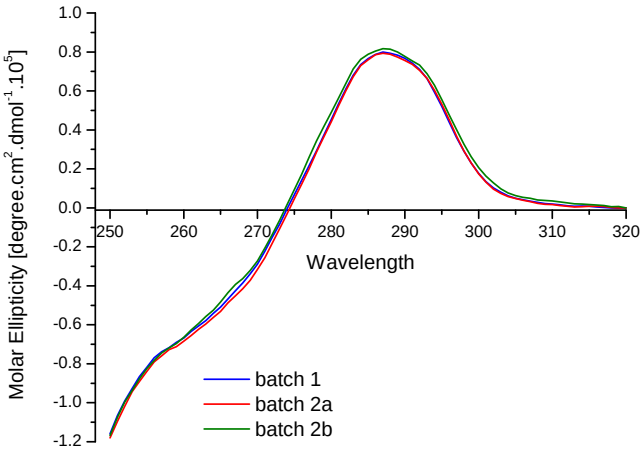

(b) Near UV spectra

Figure 5.1: Circular dichroism spectra for the three batches of excipient-free mAb in a 10 mM phosphate buffer pH 6.5: **a)** Far UV from 180 - 260 nm, including a table showing the relative percentages of each secondary structure present in the studied monoclonal antibody (results obtained from CDSSTR algorithm fitting and showing the calculated RMSD (root mean square deviation) as a measure of accuracy of the fit; **b)** Near UV spectra from 250 - 320 nm

CD data suggested that the mAb would be structurally similar throughout the solutions, however for an additional check and related to future studies (see following

section in this chapter), a calorimetry scan was obtained. Figure 5.2 shows that there were no evident differences in the identified melting temperatures (positive peaks in the spectra) between the different batches. Three peaks were found, corresponding to the melting temperatures of specific domains of the mAb. Throughout the solutions, these melting temperatures presented consistency in their values and were as follows: Tm_1 ~48.5 °C; Tm_2 ~72.4 °C; and Tm_3 ~83.7 °C. Correspondence of these peaks to the mAb's domains was as follows: Tm_1 was attributed to the C_H2 domain; Tm_2 to the F(ab')$_2$ domain; and the Tm_3 to the C_H3 domain [183]. This mAb was originally studied for its engineered 3-point mutation in the Fc region, more specifically in the C_H2 domain. It was found that this change was sufficient to produce an additional melting temperature at a lower value (~48.5 °C), than the commonly main peak typically around 72-73 °C, attributed to melting of both C_H2 and F(ab)'$_2$, found in non-mutated IgG_1 [183, 187]. It is noted that μ-DSC is also a commonly used technique for excipient screening, since the Tm values can shift due to the presence of several additives at different content [44]. The agreement of our measured Tm values with literature available about this mAb, studied in the same solution conditions as in our case, were a guarantee that the different process steps to obtain an excipient-free mAb solution were successful.

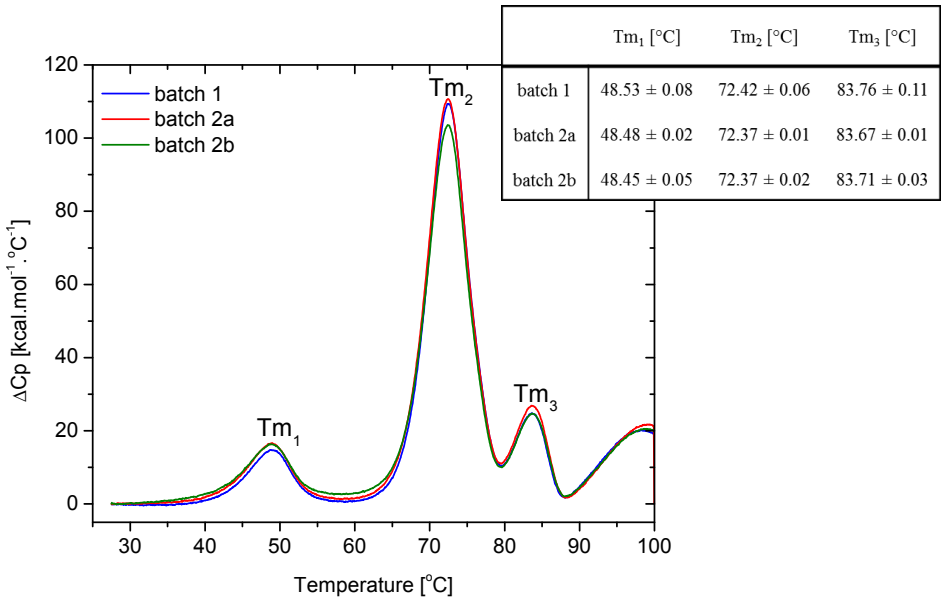

	Tm_1 [°C]	Tm_2 [°C]	Tm_3 [°C]
batch 1	48.53 ± 0.08	72.42 ± 0.06	83.76 ± 0.11
batch 2a	48.48 ± 0.02	72.37 ± 0.01	83.67 ± 0.01
batch 2b	48.45 ± 0.05	72.37 ± 0.02	83.71 ± 0.03

Figure 5.2: Micro differential scanning calorimetry data for the three batches of excipient-free mAb in 10 mM His-His.HCl pH 6.0 buffer. The melting temperatures were attributed to the different mAb domains as follows: Tm_1 = C_H2 domain; Tm_2 = F(ab')$_2$ domains; Tm_3 = C_H3 domain.

Capillary isoelectric focusing was performed to verify that the batches of mAb were similar in their charge heterogeneity. cIEF is a commonly used technique to help identify batch-to-batch consistency between the same macromolecule submitted to several processing steps [123]. As with CD and μ-DSC, the cIEF results showed that there were no evident differences between batches of this mAb (Figure 5.3). The cIEF electropherogram of this mAb had a main peak of pI = 8.94. Two acidic isoforms were detected, as well as one basic isoform. The acidic species are often related to sialylation and deamidation reactions which generate acidic isoforms of the mAb, due to storage or processing steps [125]. On the other hand, the basic isoforms can be due to a C-terminal lysine at the heavy chain [124].

	No. of peaks detected	Main peak pI (Area [%])	Acidic species: pI (Area [%])	Basic species: pI (Area [%])
batch 1	6	8.94 (56)	8.79 (17) 8.81 (10)	9.06 (5)
batch 2a	6	8.94 (56)	8.79 (17) 8.81 (8)	9.05 (5)
batch 2b	6	8.94 (57)	8.80 (16) 8.82 (9)	9.06 (5)

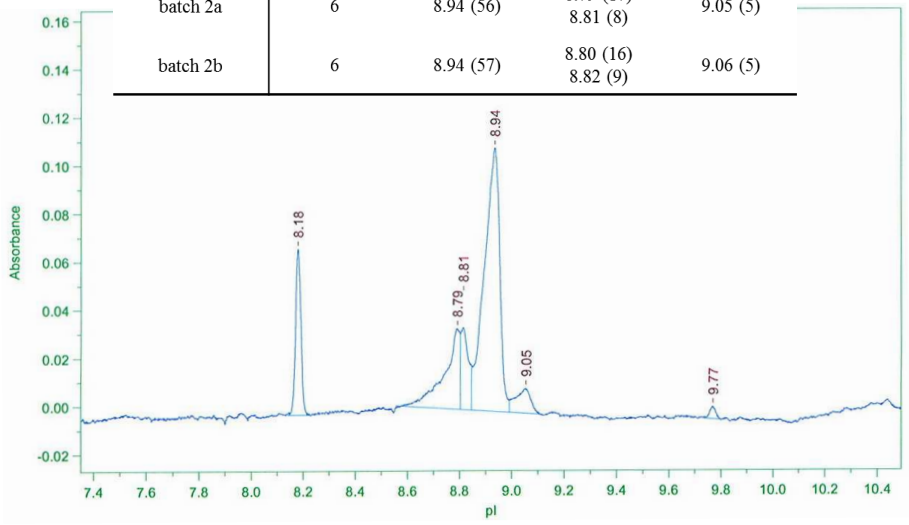

Figure 5.3: Example of capillary isoelectric focusing electropherogram showing the isoforms for batch 2b of the excipient-free mAb. All batch samples were analysed in a Pharmalyte composition between pI 8 and 10.5, with the pI markers 8.18 and 9.77. Each sample was analysed in duplicate. The summarised cIEF results for the three batches are shown in the table.

The mAb batches was checked for its level of aggregation by HPSEC. In general, all batches had a monomer content of >98 % (with a retention time of ∼8.7-8.9 min), a small presence of higher molecular weight species (HMWS, eluting at ∼7.4 min) and a low percentage of lower molecular weight species (LMWS, eluting at 10.8-10.9 min) (Table 5.1). For an example of a chromatogram of a non-stressed mAb sample, see Figure B.1 in Appendix B. By comparing these batches, the only difference is with batch 2a where there was a slightly lower content of monomer. As this material was concentrated to the highest value of concentration (∼100 mg/mL) and that step was performed with TFF, the slight increase in HMWS could be a result of the effect of shear and high concentration [5]. In fact, during TFF it is common to concentrate to higher values than intended, only to dilute it to the actual target concentration.

Table 5.1: Table showing the relative peak area for the species detected by HPSEC analysis of the three batches of mAb. Each batch was analysed in triplicate. Data is shown as average and its standard deviation.

	Peak Area [%]		
	Monomer	High MW	Low MW
batch 1	99.10 ± 0.015	0.75 ± 0.006	0.16 ± 0.009
batch 2a	98.63 ± 0.005	1.20 ± 0.006	0.17 ± 0.002
batch 2b	99.18 ± 0.005	0.66 ± 0.001	0.16 ± 0.005

The microfluidics SDS-PAGE gel image shown in Figure 5.4 compared the mAb present in these three solutions. Lanes 1 to 3 show these samples after exposure to reducing-conditions. The two typical strong bands at ∼56 kDa and ∼25 kDa, correspond to the expected heavy and light chains present in a IgG_1, respectively [186]. These bands are in agreement with the those observed for the other mAb in lane 4, also an IgG_1, used here for control and system suitability purposes. Under non-reducing conditions (lanes 5 - 7), the samples had a strong band at ∼145 kDa, in agreement with the control sample. The high purity of these samples, with > 98 % relative presence of monomer, was highlighted with the HPSEC and the μ-SDS-PAGE results.

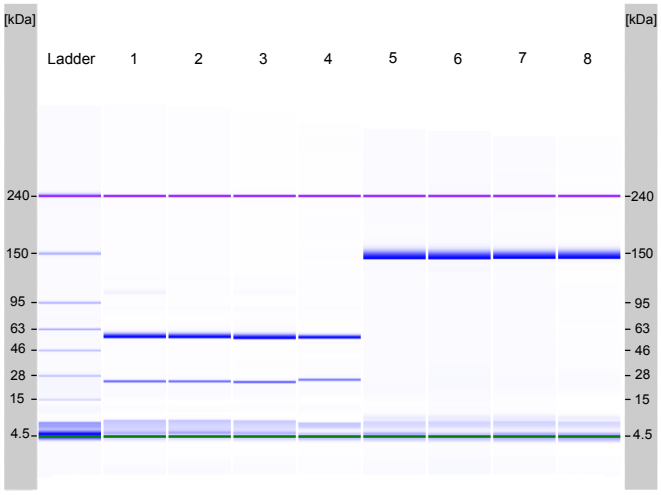

Figure 5.4: Microfluidics SDS-PAGE gel image of non-reduced and reduced samples of each of the three batches of the excipient-free mAb. Legend to the lane number is as follows: 1) reduced - batch 1; 2) reduced - batch 2a; 3) reduced - batch 2b; 4) reduced control mAb; 5) non-reduced - batch 1; 6) non-reduced - batch 2a; 7) non-reduced - batch 2b; 8) non-reduced control mAb. The control mAb was a different IgG_1 from the mAb in our study, and was used for this technique's system suitability check.

The three batches of excipient-free mAb were compared to the formulated material in terms of its rheological response. Figures 5.5(a) and 5.5(b) represent the viscosity curves and the flow curves, respectively. In Figure 5.5(a), a striking difference between the formulated mAb and the additive-free solutions was observed, where the former showed a Newtonian-like behaviour, while the latter had a change of viscosity throughout the applied shear rates. As with what was discussed in Chapter 4, the viscosity profiles of the additive-free mAb samples had an apparent yield-like behaviour. In Figure 5.5(b), the linear decrease of shear stress with shear rates, for formulated mAb solution, was a marked difference in comparison to the almost shear-rate independent shear stress values at lower shear rates seen on the additive-free mAb solutions. Since the formulation included a non-ionic surfactant, the data suggested that the yield behaviour seen on the other mAb solutions was a result of the lack of competitive surface active molecules such as the surfactant. This comparison has been observed in literature and similar results

to ours were obtained [74, 143]. However, as the formulation contained other additives apart from the non-ionic surfactant it is was not clear if the surfactant's presence was solely responsible for this Newtonian-like effect. On the other hand, this experiment emphasised that conducting the previous 'purification' with affinity chromatography was a successful method for eliminating the formulation additives from the original mAb solution.

In detail, at the higher shear rates the additive-free material showed that its viscosities were monotonically dependent of concentration (see inset of Figure 5.5(a)). The formulated material had a slightly higher viscosity ($\sim$5 mPa.s) compared to the $\sim$100 mg/mL solution. This could be due only to its concentration $\sim$120 mg/mL, or a combination of that with the presence of additives in solution. At a lower shear rate ($\dot{\gamma}$= 0.01 s^{-1}, the batches of mAb demonstrated viscosities decreasing with the solution concentration (see inset of Figure 5.5(a)).

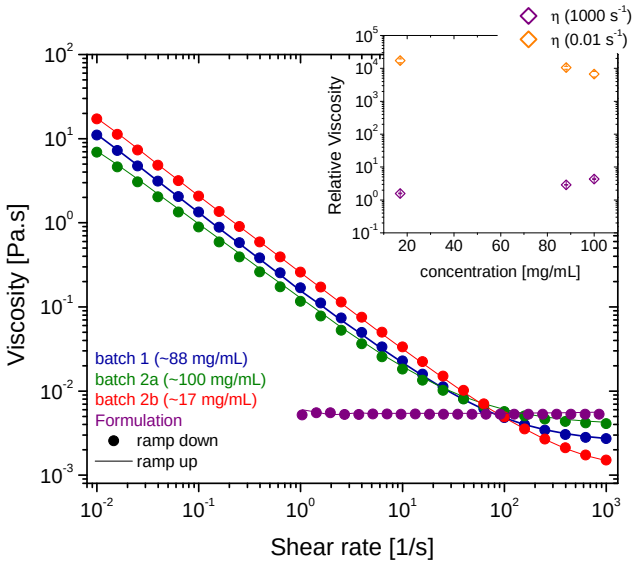

(a) Viscosity curves

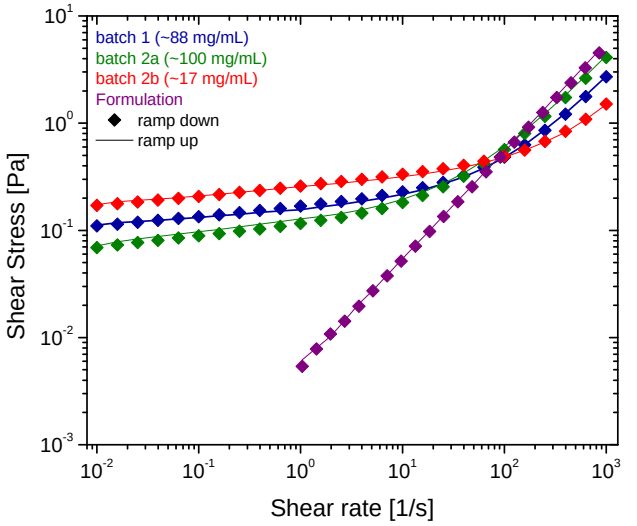

(b) Flow curves

Figure 5.5: Experimental rheology data showing **a)** viscosity and **b)** flow curves comparing the three excipient-free mAb batches and the formulated mAb sample, all prior any filtration. Inset graph in **a)** is the relative viscosity at low shear ($\eta(0.01\ s^{-1})$) and at high shear ($\eta(1000\ s^{-1})$) versus the concentrations of three batches of non-formulated mAb.

In summary, throughout this batch characterisation, the material was similar in its phyiscal-chemical properties even though it suffered different post-processing steps. The

additives present in the original mAb formulation were efficiently removed. Nevertheless, for future studies discussed in this chapter and the following chapter, these batches were not combined into one. Since batch 2a had the largest volume and highest concentration, it was chosen for the studies regarding the effect of thermal stress on its solution rheology. For this study, the comparison with a diluted mAb sample was made using batch 2b. Batch 1 was used solely for the results presented and discussed in Chapter 6.

5.3.2 mAb solution rheology: a case study on the effect of aggregates

This section is focused on the effect of aggregation on the mAb's solution rheology. Since the mAb had a melting temperature of about ∼48 °C, it was expected that its stability at this buffer conditions would be compromised by thermal stressing at 40 °C. Thus, this was the chosen method to force protein aggregation. However, before starting this study, large particles (of size > 0.1 μm diameter) were filtered out to reduce a possible nucleation effect influencing the generation of further protein aggregation. Therefore, the time point when filtration occurred was considered the initial time point (T= 0) for the aggregation study that lasted for 6 weeks.

For the study of filtration and aggregation of the mAb solutions, the rheology was measured with cone-and-plate and double-gap geometries, and characterisation of the protein oligomers was performed by HPSEC, MFI, DLS, and μ-SDS-PAGE. Microfluidics rheometry with mVROC was used to measure only the filtered mAb solutions. The sample's concentration was also monitored during the study. Also, a study was done on the potential effect of CP and DG rheology on these samples, focusing on the relative quantity and/or size of the aggregates before and after the rheology experiments.

5.3.2.1 Effect of insoluble particles on the mAb solution rheology

The unfiltered ∼100 and ∼17 mg/mL mAb solutions were visually inspected before filtration with 0.1 μm pore-size membrane syringe filters. The results are shown in Table 5.2. Although the ∼100 mg/mL sample was practically free of particles, these usually formed a dust-like spiral from the bottom of the vial after swirling the sample for inspection. The 17 mg/mL sample did not show this. The sample at 100 mg/mL presented higher degree of opalescence and colour than the diluted mAb solution. This could be related to the concentration effect. After filtration both samples showed to be free of particles, the colour was maintained respective to each concentration, while the 100 mg/mL mAb solution showed slight opalescence (score: III).

Table 5.2: Visual inspection score for mAb unfiltered samples at 100 and 17 mg/mL. The material was assessed based on its colour, opalescence and visible particles content against a black and white screen with aid of a white light. Values or codes in parenthesis correspond to the standard to which the sample was similar.

mAb sample, unfiltered [mg/mL]	Colour	Opalescence	Particles
100	Slightly yellow (Y6)	Opalescent (V)	Practically free of particles (4)
17	Slightly yellow (Y7)	Slightly opalescent (III)	Practically free of particles (4)

Since visual inspection is a qualitative analysis, a quantitative evaluation of filtration efficiency was performed with micro-flow imaging. Figure 5.6 shows the comparison of particle count frequency histograms along the equivalent circular diameters between the unfiltered and filtered mAb samples. As expected from visual inspection analysis, the ∼100 mg/mL sample showed higher particle count, mostly concentrated towards smaller sizes. This was a feature also seen with the diluted mAb solution, however its

total particle count was lower (2213 particles) compared to the higher concentration (43987 particles) (see Table B.2 in Appendix B). Both filtered samples showed an evident decrease of particle count per size class and in the analysed volume. Filtered sample buffer was also measured, as a control sample. Sub-visible particles were present in the filtered buffer although to a much reduced level compared to the filtered mAb solutions (Table B.2 in Appendix B). As discussed in the previous chapter, although MFI allowed a quantitative analysis of sub-visible size range proteinaceous particles (1 - 100 μm), it still drew uncertainties regarding the effectiveness of filtration since filtered solutions always presented some sub-visible particles.

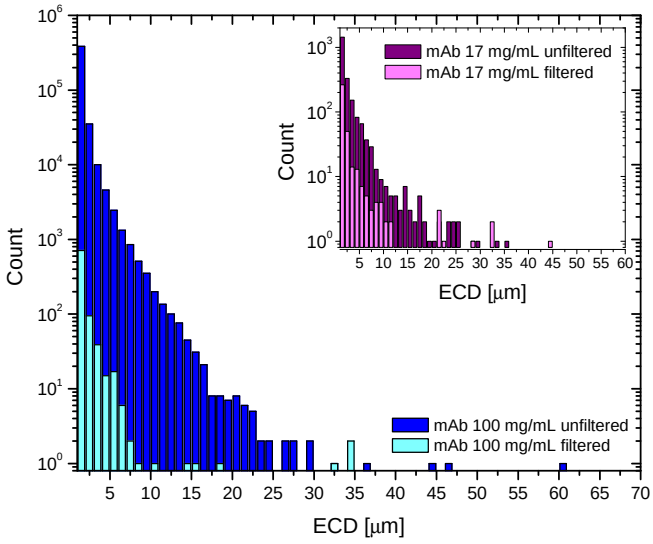

Figure 5.6: MFI sub-visible protein aggregates frequency histograms comparing between unfiltered and filtered 100 mg/mL mAb solutions (large graph) and 17 mg/mL mAb solutions (inset graph).

For HPSEC data, no change was observed between unfiltered and filtered mAb solutions (Table 5.3). Since the HPSEC technique allows the detection of soluble aggregates only up to a certain MW size (~600 kDa, in this case), and the unfiltered

solutions had over 98 % relative amount of mAb monomer, it was expected that filtration would not affect the sample's HPSEC profiles.

Table 5.3: Table with the relative peak area for the species detected by HPSEC analysis comparing unfiltered and filtered 100 mg/mL and 17 mg/mL mAb solutions. Data is represented as average and standard deviation of three measurements of each sample.

	100 mg/mL		17 mg/mL	
	Unfiltered	Filtered	Unfiltered	Filtered
Low MW	$0.10 \pm 1.29\times10^{-3}$	$0.09 \pm 8.14\times10^{-4}$	$0.13 \pm 5.03\times10^{-3}$	$0.13 \pm 1.78\times10^{-3}$
Monomer	$98.56 \pm 1.27\times10^{-2}$	$98.57 \pm 7.69\times10^{-3}$	$99.25 \pm 1.57\times10^{-2}$	$99.25 \pm 2.85\times10^{-3}$
High MW	$1.35 \pm 6.24\times10^{-3}$	$1.36 \pm 2.52\times10^{-3}$	$0.62 \pm 1.60\times10^{-2}$	$0.62 \pm 2.92\times10^{-3}$

On the DLS analysis of the unfiltered mAb samples a main peak was identified by intensity distribution with a mean H_D of ∼11 nm (Figure 5.7). The values agreed with the commonly reported hydrodynamic diameter corresponding to an equilibrium between IgG_1 monomer and dimer [104], where monomer content is much larger than the dimer's.

Only the unfiltered 100 mg/mL mAb sample showed two peaks by intensity distribution. The relative amplitude of the second population with larger diameters (∼1000 nm) was lower (∼3 %). The likelihood that these particles were present in such low number was evidenced by volume distribution showing only one peak (∼11 nm) (values on Table 5.4 in section 5.3.2.2). After filtration, a slightly narrower monomer/dimer peak was observed on the intensity distribution plot, corresponding to a slight difference in the H_D and relaxation times (Figure 5.7(a) and Table 5.4). For the 17 mg/mL mAb unfiltered/ filtered samples, the slight change to a narrower main peak (at ∼11 nm) after filtration could be representative of the loss of proteinaceous material to the filter's membrane (Figure 5.7(b) and Table 5.4).

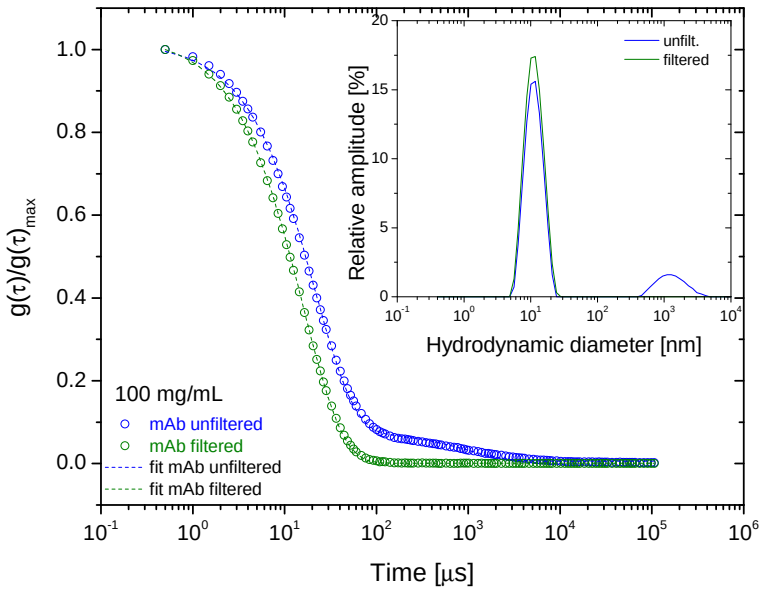

(a)

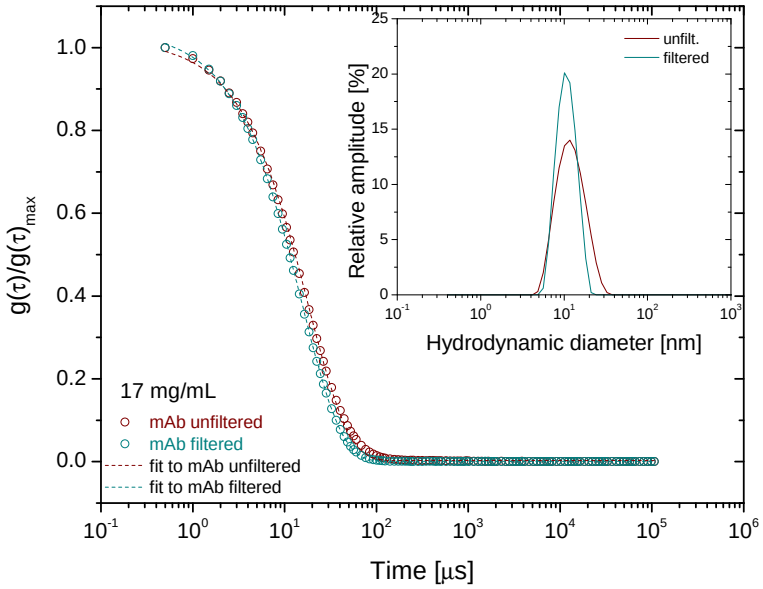

(b)

Figure 5.7: Comparison of DLS data for unfiltered and filtered samples (1 mg/mL dilutions) from **a)** 100 and **b)** 17 mg/mL mAb solutions. For both **a)** and **b)**: the large graph represents the normalised correlation data (circles) and the lines are the fit to the exponential decay curve; and the inset graph shows the same data presented as hydrodynamic diameter size distribution by intensity.

Evaluation of both MFI and DLS results suggested that the 100 mg/mL unfiltered solution had a larger heterogeneity in particle size. However, analysis by HPSEC showed that most of the soluble proteinaceous material was in the monomeric state. Moreover, from the MFI analysis reports, for both filtered and unfiltered samples, the insoluble particles had a volume fraction of <1 % of total sample volume.

The results discussed above, along with the previous chapter's conclusions, helped to understand that the rheology could still be affected by presence of these larger particles related to their actual volume fraction in suspension (Figure 5.8). The DG rheology data demonstrated a smaller difference in the viscosities between the unfiltered and filtered samples, when compared to those differences in the CP rheology data. Other similarities were found in these solutions to the results discussed for the β-LG data. On both mAb concentrations, the unfiltered samples measured with CP had higher viscosities throughout the applied shear rates, compared to the DG data. The mVROC data of filtered mAb solutions, shown in Figures 5.8(a) and 5.8(b), demonstrated the Newtonian-like behaviour at the higer shear rates ($\geq$1000 s^{-1}). The viscosities measured with mVROC were almost superimposed with the filtered sample CP and DG data.

In addition, at all instances, the data obtained with CP and DG geometries always demonstrated a yield-like behaviour at low shear rates such as also observed for β-LG solutions. The rheological data was fitted to the Bingham equation for yield stress for viscoelastic samples (Equation 5.1), resulting in good correlation to the experimental data (all $r^2 > 0.97$).

$$\tau = \tau_{BY} + \eta_{BY}\dot{\gamma} \tag{5.1}$$

where τ_{BY} represents the yield point value. An example of how τ_{BY} is extrapolated when plotting the $\tau(\dot{\gamma})$ to the zero shear rate value ($\dot{\gamma} = 0$ s^{-1}), is shown in Figure B.3, and the computed τ_{BY} values are shown in Table B.3, both in Appendix B.

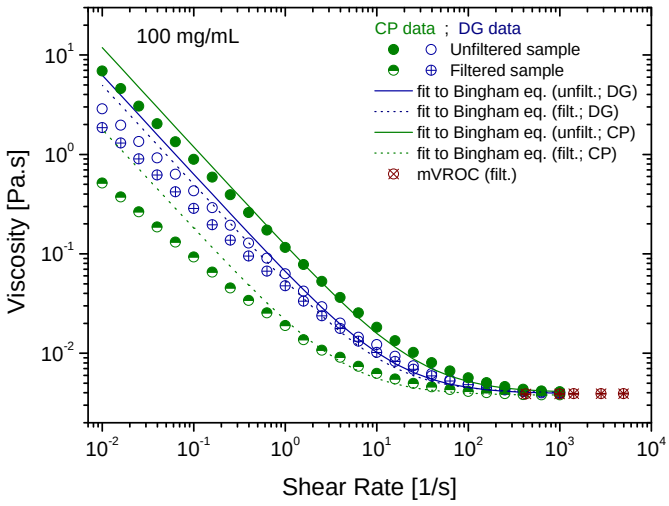

(a)

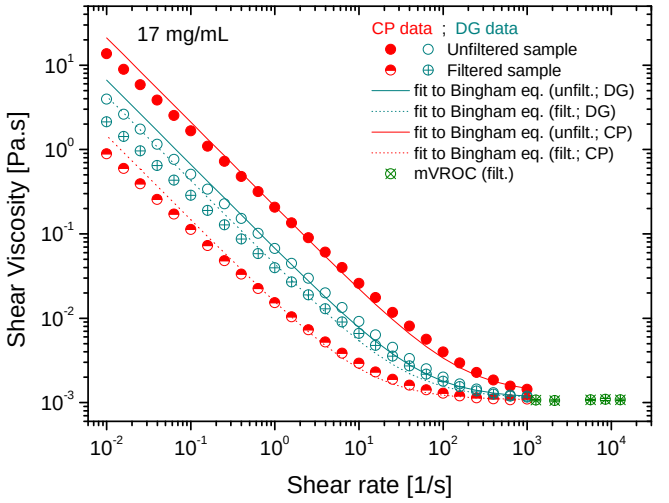

(b)

Figure 5.8: Rheology data for unfiltered and filtered **a)** 100 mg/mL and **b)** 17 mg/mL mAb solutions, comparing results obtained from CP and DG geometries. The experimental data was fitted to the Bingham equation (lines - full and dashed). On both plots, mVROC data is represented for the filtered samples. All measurements were made at 25 °C.

The similarities in the rheological observations between the IgG and β-LG protein studies, and comparison to literature [74, 78, 143, 182], suggests that in this case it could also be assumed an air-water interface influence on the conventional rheology

measurements. Moreover, these observations point towards the hypothesis that protein species contribute to the rheology as a response of their own surface activity at the air-water interface during these measurements.

After filtration, the CP data presented lower viscosities than the DG rheology data. This was in disagreement to similar data obtained with β-LG filtered solutions. The Bousssinesq parameter, accounting for the influence of surface effects compared to bulk sub-phase contributions, was calculated to better understand this case (Figure 5.9). With the mAb filtered samples, $Bo_{CP} > Bo_{DG}$. Since Bo was computed using the data provided in Figure 5.8, and $\eta_{CP,filt.} < \eta_{DG,filt}$ these results suggested that the mAb CP data was influenced more by the bulk flow contributions than the DG data. The reason why this was observed may well be related to the surface activity of the macromolecular species present in solution. It could be possible that this mAb had less air-water surface activity, compared to β-LG. Time restraints did not allow a tensiometry study to be performed for mAb solutions which would allow us to ascertain this.

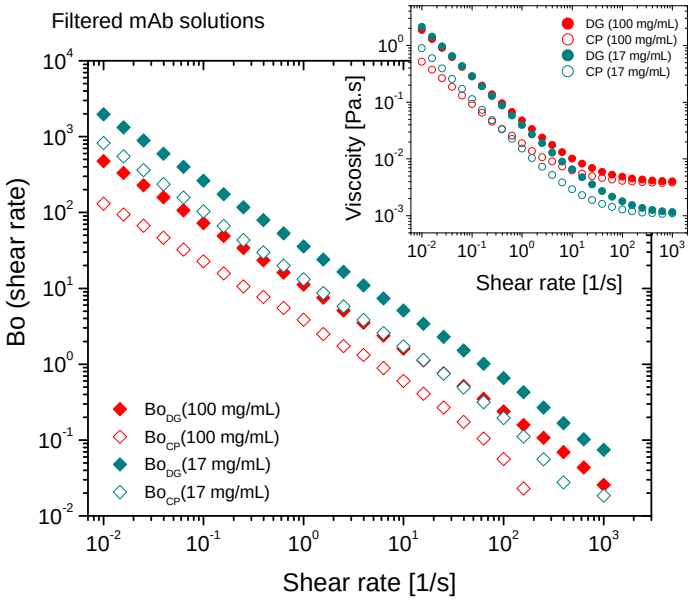

Figure 5.9: Boussinesq parameter (shear-rate dependent) calculated for CP (hollow diamonds) and DG (full diamonds) rheology of filtered 100 (red) and 17 mg/mL (blue) solutions. The inset graph shows the viscosity curves correpondent to the data used to calculate the Boussinesq number (full circles - DG; hollow circles - CP).

The estimated surface viscosity was calculated using on the filtered mAb viscosities, based on the same arguments in section 4.3.1.1 in Chapter 4. As seen in Figure 5.10, for both concentrations, CP and DG rheology data suggested that these samples' estimated surface viscosity would be similar with the exception of the higher shear rates. Unfortunately, it was not possible to perform any interfacial rheology measurements using the DWR with these mAb solutions.

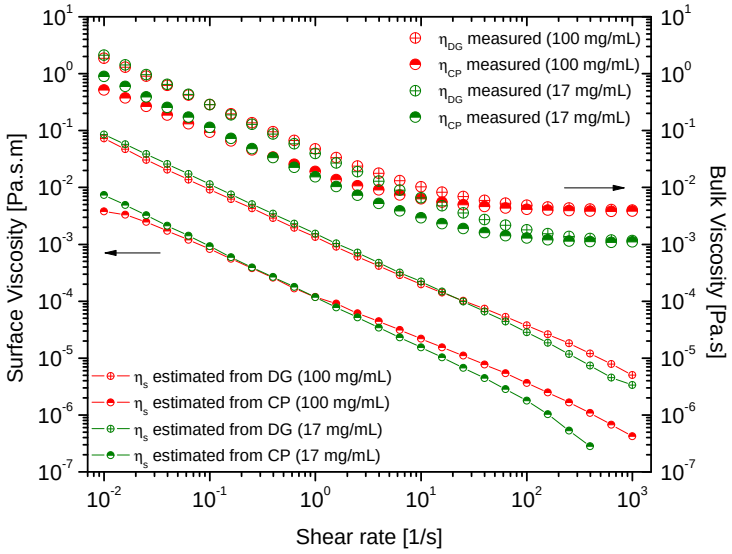

Figure 5.10: Estimated surface viscosity from the measured CP and DG rheology for 100 and 17 mg/mL filtered (T= 0) mAb solutions. The calculations are made using the average η_{bulk} obtained from measurements of these samples with mVROC.

5.3.2.2 Effect of thermal stress on the mAb solution rheology

After the previous assessment, the filtered mAb material at 100 and 17 mg/mL was left at 40 °C for 6 weeks and its level of aggregation and rheology were characterised every 2 weeks.

Figures 5.11(a) and 5.11(b) represent the relative peak areas for monomer, total high MW and low MW species from 100 and 17 mg/mL mAb samples at each time point, respectively. Samples at the same concentration were stored at 5 °C and also characterised on HPSEC for control purposes. Results from the 100 mg/mL mAb samples showed a steep decrease of monomer through time, with a corresponding increase of high MW species, while the low MW species remained the same (Figure 5.11(a)). Total monomer loss after 6 weeks for this sample was ∼40 %. Soluble aggregates were observed for the 17 mg/mL sample, with a total monomer loss of ∼10 % after 6 weeks. It is important to remember that the 100 mg/mL samples were

diluted to 10 mg/mL prior HPSEC analysis, while the 17 mg/mL samples were injected neat. Therefore, it was expected that these relative peak areas from the analysis of the dilution would be representative of the original sample. Peak area values are summarised in Table B.1 in Appendix B.

Examples of chromatograms throughout the time points are shown in Figure B.1 in Appendix B. From the 2 weeks time point onwards, the chromatograms of the 100 mg/mL samples had four peaks corresponding to high MW samples. For clarity, the level of aggregation relative to high MW species was chosen to be represented as sum of the four peak areas. Chromatograms of the 17 mg/mL sample had two peaks corresponding to the HMWS. At 6 weeks, for both concentrations of mAb, a shoulder peak with retention time ∼9.3 min was detected. This shoulder peak was inconsistently detected by the analysis software, therefore it was counted as part of the monomer peak for comparison with the remaining time points.

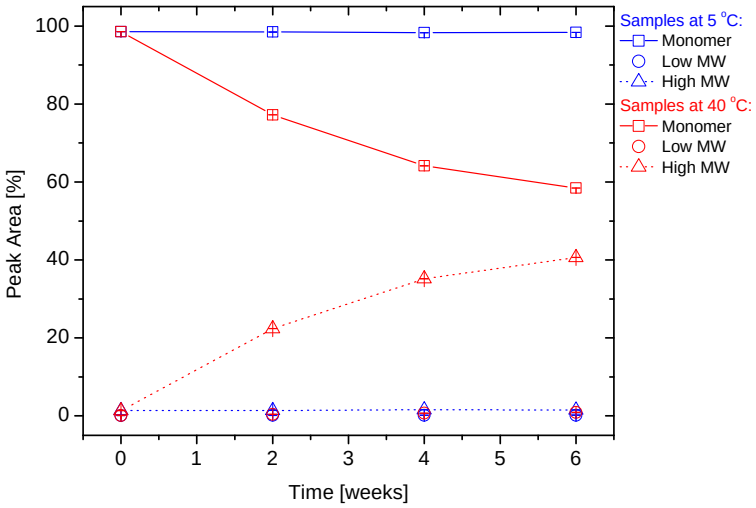

(a)

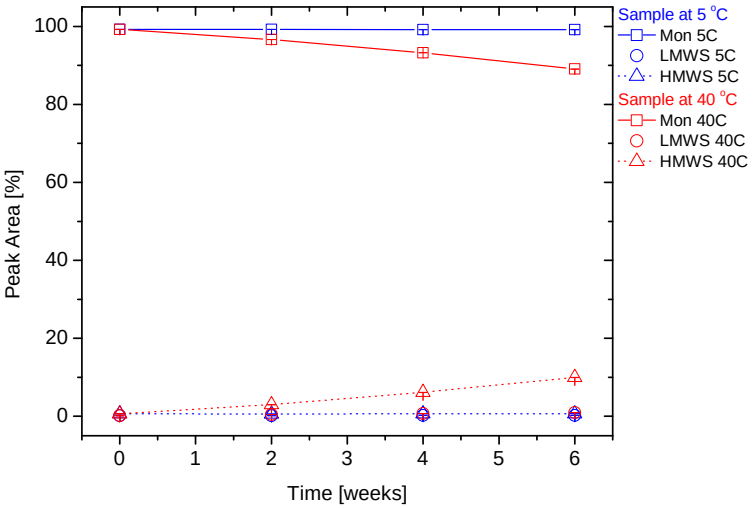

(b)

Figure 5.11: Relative peak percentage of monomer, fragment and total aggregates detected by HPSEC for **a)** 100 mg/mL (injected at 10 mg/mL) and **b)** 17 mg/mL (injected neat) at 40 °C and 5 °C during 6 weeks. Error bars are standard deviation of three measurements per sample.

Figure 5.12 shows the sub-visible particle count throughout time and for each of the studied samples. An increase in the particle count between time points indicated that besides the increase of soluble aggregates with temperature stress, a small percentage

of sub-visible particles was generated. From the MFI reports, the volume fraction of these particles although increasing, was still $< 1\%$ of total sample volume. It was noted that, in comparison to the previously discussed unfiltered mAb samples, the aggregated materials did not reach such high particle counts even at the end of this study.

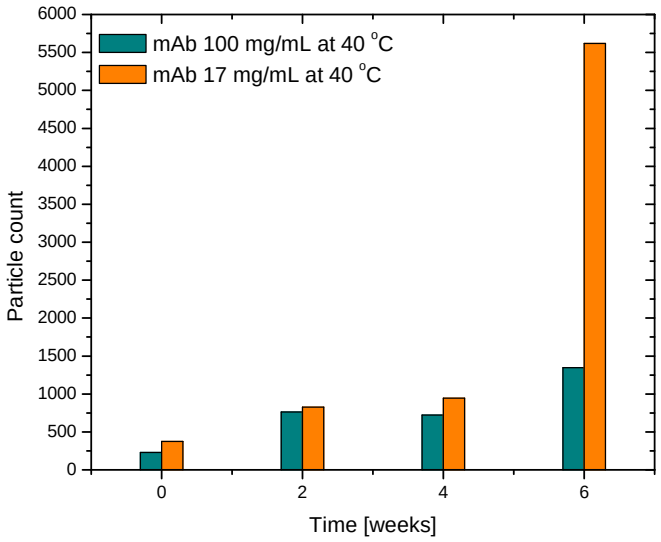

Figure 5.12: MFI sub-visible particle count comparing 100 and 17 mg/mL mAb samples at different time points after aggregation at 40 °C.

The DLS analyses showed the increased aggregation of mAb along the study. However, the peaks obtained by this technique did not allow any resolution by intensity or volume distribution between the possible sizes of the aggregates. Figure 5.13(a) shows results for the 1 mg/mL dilutions from 100 mg/mL mAb samples throughout the time points. By intensity, the peak clearly shows a mean hydrodynamic diameter size changing to higher values (> 20 nm). The detected peak was wider with time, corresponding to the known increase of soluble aggregates' volume fraction in the samples. By volume distribution, the increased tailing of the peak towards higher diameters confirmed the increase in soluble aggregate volume fraction. For $\sim$17 mg/mL

samples very slight changes to the hydrodynamic sizes were noted (Figure 5.13(b)). This corresponded well with the small changes in monomer loss/ increase of high MW species observed with HPSEC. DLS confirmed that protein aggregation was occurring with exposure at 40 °C, generating soluble aggregates of $H_D < 100$ nm. However, in correlation to the collected HPSEC data, DLS did not allow any resolution between this IgG monomer and its oligomers sizes. Table 5.4 summarises the size differences for the mAb samples measured by DLS. The DLS intensity distribution data was also fitted to exponential decay functions in order to determine the relaxation times of the detected size-populations. In general, these relaxation times increased, reflecting the presence of soluble species of higher sizes. The lack of resolution between mAb monomer and protein oligomers yielded one computed relaxation time.

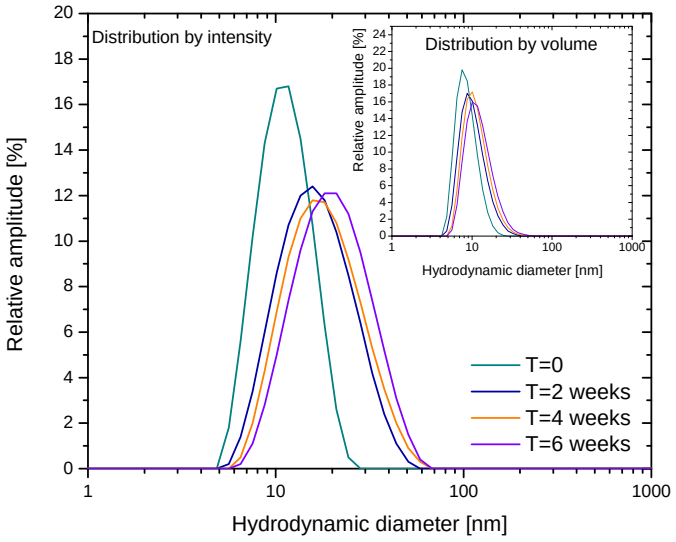

(a) 100 mg/mL mAb samples

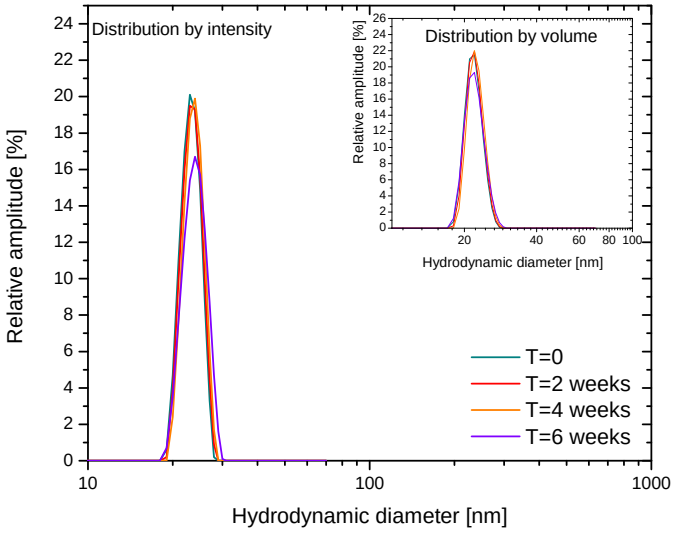

(b) 17 mg/mL mAb samples

Figure 5.13: Comparison of hydrodynamic diameter size by intensity and by volume distribution, for **a)** 100 and **b)** 17 mg/mL mAb samples stressed for 6 weeks at 40 °C. For both **a)** and **b)**, the large graph represents the size distribution by intensity and the inset graph corresponds to the size distribution by volume.

Table 5.4: Mean hydrodynamic size and relaxation times obtained by DLS for the 100 and 17 mg/mL mAb samples (unfiltered, filtered and aggregated at 40 °C). [1] - Data was obtained by diluting samples to 1 mg/mL; [2] - the dilution from 100 mg/mL mAb unfiltered solution was the only sample to present two peaks in size distribution by intensity; [3] - mean hydrodynamic size by intensity distribution and standard deviation of three measurements; [4] - mean hydrodynamic size by volume distribution and standard deviation of three measurements; [5] - relaxation time obtained by fitting the correlation data with exponential decay equations, showing the standard error from fit.

mAb sample		Mean Hydrodynamic Diameter Size by Intensity [nm] [3]	Mean Hydrodynamic Diameter Size by Volume [nm] [4]	Relaxation time [µs] [5]
100 mg/mL [1]	Unfiltered [2]	11.59 ± 0.10; 1078 ± 379	9.44 ± 0.25	21.2 ± 0.1; 993 ± 65.3
	Filtered (0.1 µm)	11.90 ± 0.28	9.02 ± 0.08	15.9 ± 0.02
	T=2	17.40 ± 0.33	11.06 ± 0.19	23.3 ± 0.1
	T=4	19.70 ± 0.10	12.03 ± 0.19	24.5 ± 0.1
	T=6	21.94 ± 0.39	13.15 ± 0.16	28.1 ± 0.1
17 mg/mL [1]	Unfiltered	14.32 ± 1.43	8.91 ± 0.15	18.2 ± 0.09
	Filtered (0.1 µm)	11.37 ± 0.95	9.09 ± 0.07	15.4 ± 0.02
	T=2	12.24 ± 0.78	8.78 ± 0.50	16.7 ± 0.04
	T=4	12.48 ± 0.55	9.29 ± 0.40	16.5 ± 0.02
	T=6	12.68 ± 0.16	9.38 ± 0.09	17.2 ± 0.03

μ-SDS-PAGE was used for evaluation of sample degradation products. Figure 5.14(a) shows the gel corresponding to the non-reduced and reduced samples of 100 mg/mL mAb at T=0 , T= 6 weeks, at 5 and 40 °C, respectively, compared to the T=2.5 months samples at 5 and 40 °C (as controls). The controls in this experiment were both the frozen samples at T=0 but also the aggregated mAb sample after 2.5 months exposure to 40 °C. At non-reducing conditions, samples exposed to 40 °C showed extra bands at lower MW than the main monomer band (∼150 kDa), typically at ∼143 kDa and ∼137 kDa. This could correspond the lower MW species corresponding to the shoulder-peak observed with HPSEC.

The 100 mg/mL mAb samples exposed to reducing conditions showed a consistent

break-down between heavy (∼60 kDa) and light (∼27 kDa) chains (Figure 5.14(a)). Extra bands were observed at ∼121 kDa and ∼93 kDa, which could correspond to other reductions at different dissulfide bond locations in the original monomer, such as producing a half-IgG or F(ab)'$_2$ fragments [188]. Reduced samples at 5 °C did not show extra bands, supporting the conclusion that these bands are most likely products of mAb degradation.

As seen previously via HPSEC and DLS results, the 17 mg/mL samples stored at 40 °C suffered degradation to a lower extent to that observed with the higher concentration. This was observed with μ-SDS-PAGE, where extra bands of lower MW than monomer (non-reducing conditions) and higher MW than the heavy chain (at reducing conditions), were detected. This indicated the mAb had similar degradation products and degradation mechanisms independent of concentration.

Those samples exposed at 40 °C showed bands with lower relative intensity compared to the non-aggregated mAb samples. This was another indication of the loss of monomer throughout the time exposure at 40 °C. In summary, μ-SDS-PAGE analysis provided further information regarding mAb degradation products. It addition, these observations added evidence to the heterogeneity of protein species present in solution of these thermally stressed mAb samples.

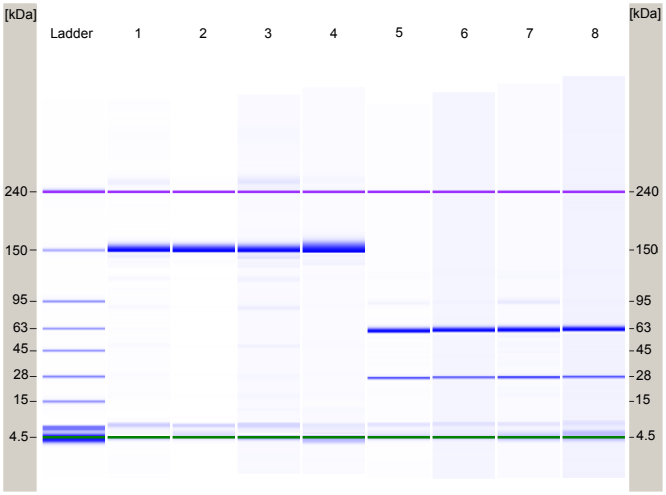

(a) 100 mg/mL mAb samples

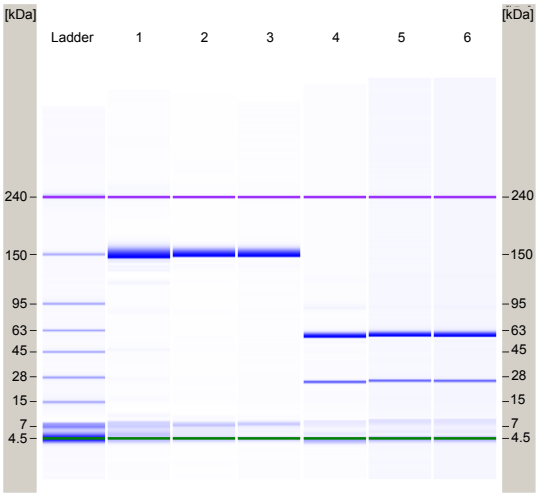

(b) 17 mg/mL mAb samples

Figure 5.14: Microfluidics SDS-PAGE gel images for **a)** 100 mg/mL and **b)** 17 mg/mL mAb samples, comparing stressed samples at 40 °C with those at 5 °C at different time points. For **a)**, dilutions from 100 mg/mL mAb solutions, lanes are: 1) non-reduced - 40 °C, T= 6 weeks; 2) non-reduced - 5 °C, T= 0; 3) non-reduced - 40 °C, T= 2.5 months; 4) non-reduced - 5 °C, T= 2.5 months; 5) reduced - 40 °C, T= 6 weeks; 6) reduced - 5 °C, T= 0; 7) reduced - 40 °C, T= 2.5 months; 8) reduced - 5 °C, T= 2.5 months. For **b)**, dilutions from 17 mg/mL mAb solutions, lanes are: 1) non-reduced - 40 °C, T = 6 weeks; 2) non-reduced - 5 °C, T= 0; 3) non-reduced - 5 °C, T= 6 weeks; 4) reduced - 40 °C, T= 6 weeks; 5) reduced - 5 °C, T= 0; 6) reduced - 5 °C, T= 6 weeks.

So far, one can conclude that this is a very complex model in terms of its components. It has also been demonstrated that there could be an increase of insoluble particles as result of this thermodynamic stress. As the materials change in its composition of monomer, dimers and other oligomers, soluble or insoluble, and even mAb fragments, it would be expected that the viscosity of this mAb's aggregated material would be affected.

The measurements on double-gap and cone-and-plate geometries demonstrated that, in general, the viscosities were increasing with exposure time at 40 °C (Figure 5.15). This trend was more visible with the 100 mg/mL mAb samples than with the samples at 17 mg/mL and particularly looking at the high shear viscosities ($\dot{\gamma}$ = 1000 s^{-1}) (Figure 5.16(a)). However, at lower shear rates, for time points such as the CP data of 100 mg/mL at T= 6 weeks, the viscosities were lower than the material had showed at previous time points. Superimposition of the CP and DG viscosities showed that, at the higher shear rates, the CP data was generally slightly higher than the viscosities measured by DG rheology (Figure B.2 in Appendix B).

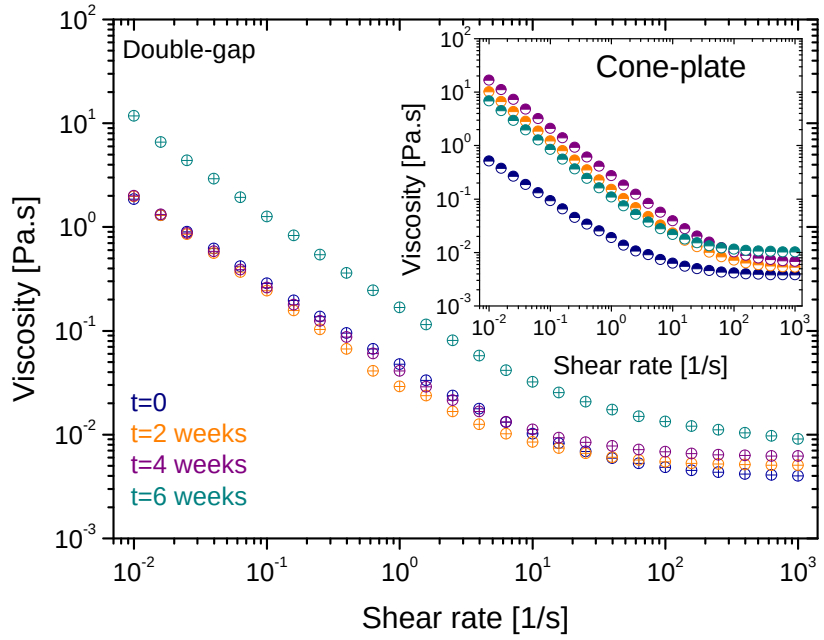

(a) 100 mg/mL mAb samples

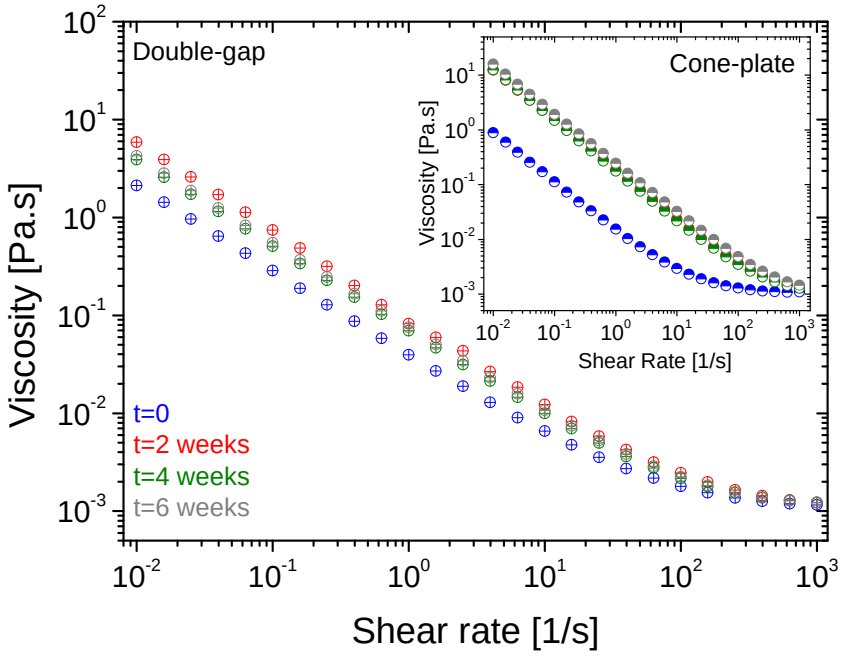

(b) 17 mg/mL mAb samples

Figure 5.15: Rheology data obtained for both cone-and-plate and double-gap geometries of **a)** 100 mg/mL and **b)** 17 mg/mL mAb solutions left for 6 weeks at 40 °C and analysed at room temperature (25 °C).

The rheological profiles of these protein solutions, even though of altered contents, did not change its flow behaviour. The data showed no hysteresis between sweeping up and down the shear rates. The profiles remained with yield-behaviour characteristics, and the experimental data was fitted with the Bingham model (Equation 5.1) to find if the yield points would follow a similar trend as the high-shear viscosities (Figure 5.16(b)). Yield points and r^2 values from corresponding fits are represented in Table B.3 in Appendix B.

Figure 5.16(b) showed that throughout the time points, yield values for each sample were not consistently increasing. It was inconclusive if the increase of aggregation had an impact on the yield behaviour of these samples. The hypothesis would be that the proteinaceous aggregates generated would potentially contribute to this yield-behaviour as it is known that the increase of solid content in dispersions that demonstrate yield-like behaviour originate higher yield points [48]. If the contents would be solely involved in contributions to the air-water interface protein films hypothetically present in these geometries would be another point to investigate. Presumably, part of the monomers here present could be in a partially unfolded state, where hydrophobic areas of the protein would be exposed and therefore more air-water surface active [189].

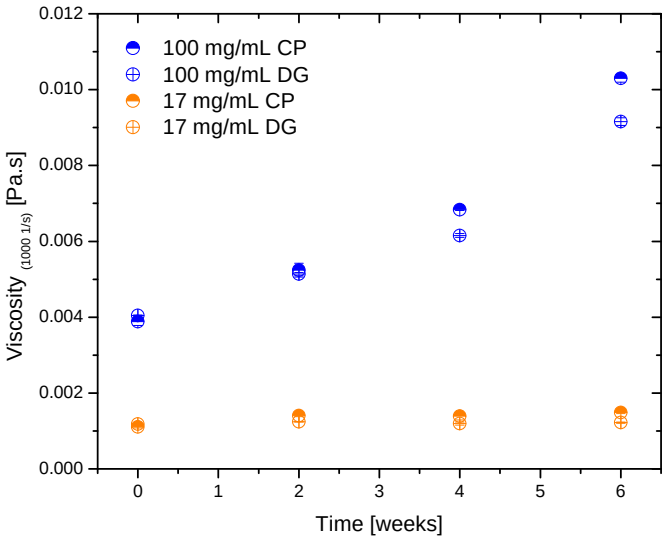

(a)

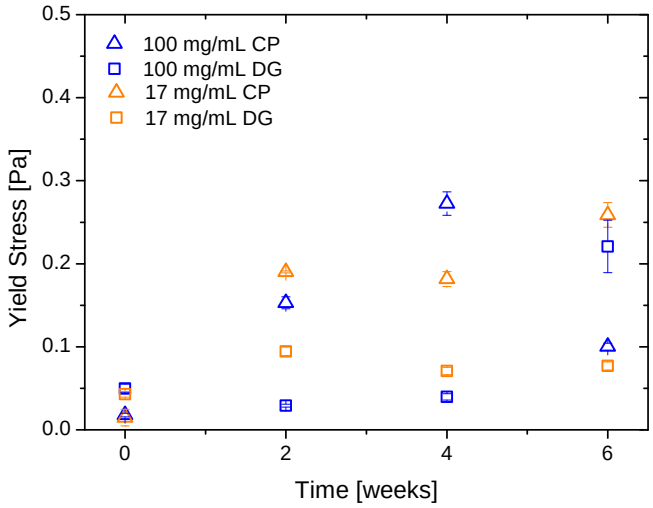

(b)

Figure 5.16: a) High shear viscosity (η = 1000 s^{-1}) of mAb samples stressed at 40 °C for 6 weeks (from CP and DG data). Data points are average of three readings at 1000 s^{-1}. Error bars represent the standard deviation. **b)** Yield point values of the same mAb solutions stressed at 40 °C for 6 weeks. Yield points were obtained by fitting the Bingham model to the CP and DG rheology experimental data. Error bars correspond to the standard error given by the linear regression.

On a detailed note, the CP rheology data suffered irreproducibility within repeating samples, such as what is demonstrated in Figure 5.17. At times, a Newtonian-like behaviour was observed, whereas a new loading from the same sample would have a yield-like behaviour at low shear rates. Double-gap rheology presented reproducibility across mAb samples at all the time points/ conditions of sample. It could be possible that the same events observed here were related to those described with reference to the rheology of unfiltered and filtered mAb solutions. In light of our hypothesis discussed so far, and what recent literature has proposed [74, 78], the Newtonian-like behaviour observed in protein solutions would be related to a lack of protein-film formation at the air-water interface present in these measurements. However, since both measuring systems used here were shown to have a similar air-water interface surface area (73 mm^2 and 71 mm^2 for the CP50-1 and DG26.7, respectively), it was interesting to observe that the DG did not show inconsistencies similar to those from the CP geometry.

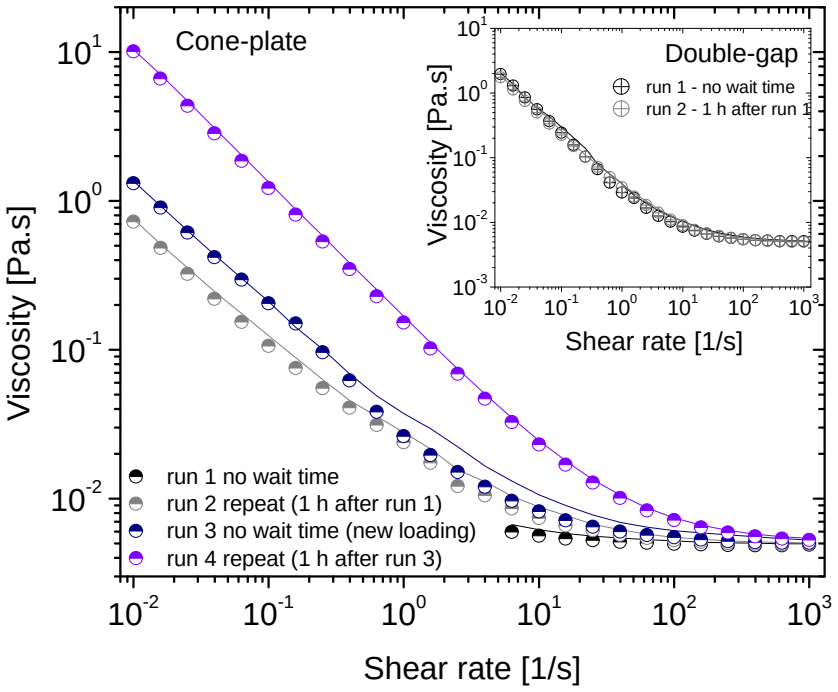

Figure 5.17: Comparison between waiting times before measurements of a 100 mg/mL mAb sample thermally stressed at 40 °C after 2 weeks, with CP and DG geometries. Circles - data ramping down shear rates; lines - data sweeping up shear rates. On CP rheology, run 1 and run 2 were obtained from the same sample, while run 3 and run 4 were another aliquot, both from 100 mg/mL T= 2 weeks at 40 °C sample. Run 1 and 2 for DG rheology data were performed on the same loaded sample. All measurements performed at 25 °C.

5.3.2.3 Analysis of level of aggregation of recovered mAb solutions after cone-and-plate and double-gap rheology

The CP and DG geometries are made of stainless steel, which is a material that has been shown to cause aggregation of mAbs, suggested to be via an oxidation mediated degradation pathway [30]. Therefore, there was an interest in understanding if this surface in conjugation to shearing, would evidence any signs of change in aggregation pattern.

Aliquots of mAb samples ran on the cone-and-plate and double-gap geometries were

recovered and analysed for its level of aggregation by DLS and HPSEC. Table 5.5 shows a summary of the concentrations measured for all the samples analysed throughout this study. There was a slight increase within the material that was stored for 6 weeks at 40 °C. This variation in concentration was within the 10 % error allowed for the UV-vis spectroscopy method. Despite this, a larger difference was identified between mAb samples after the CP rheology experiments and the same samples before that experiment. Although the technique used the evaporation blocking system, evaporation seemed to be inevitable, probably due to the lower sample volume (675 μL) when compared to the double-gap (3.8 mL).

Table 5.5: Table summarising the concentrations of mAb for its different batches, and in different conditions (when applicable): before and after filtration with 0.1 μm pore-size syringe filter, before and after the rheology experiments, and along the time at 40 °C.

mAb sample		Sample concentration		
		Before rheology [mg/mL]	After CP rheology [mg/mL]	After DG rheology [mg/mL]
Batch 1		88.52 ± 0.10	-	-
100 mg/mL	Unfiltered	108.31 ± 0.44	-	-
	Filtered (0.1 µm) T=0	103.42 ± 0.53	113.34 ± 0.48	111.95 ± 0.62
	T=2	108.78 ± 0.06	115.86 ± 0.70	117.51 ± 0.99
	T=4	113.51 ± 0.23	126.22 ± 0.79	111.64 ± 1.74
	T=6	119.62 ± 0.47	123.71 ± 0.93	115.29 ± 0.48
17 mg/mL	Unfiltered	17.69 ± 0.16	-	-
	Filtered (0.1 µm) T=0	17.43 ± 0.10	-	-
	T=2	17.13 ± 0.41	18.89 ± 0.05	18.70 ± 0.07
	T=4	18.19 ± 0.11	18.90 ± 0.16	18.31 ± 0.16
	T=6	18.62 ± 0.15	16.36 ± 0.08	18.97 ± 0.07

On HPSEC analysis, comparing before/after rheology sample from 17 mg/mL mAb samples did not show any differences (Figure 5.18(b)). Results derived from the 100 mg/mL mAb samples showed differences at 4 weeks and 6 weeks data with

contradicting tendencies. The apparent lack of any consistent deviation of 'after CP' or 'after DG' data from 'before rheology' data suggests that these differences could be minor. Therefore, no change of aggregate content could be conclusively related to be due to rheological experiments only. In all of these samples, the low MW species presented superimposed data suggesting that these were not changed (not shown in the figures, to improve graphical clarity).

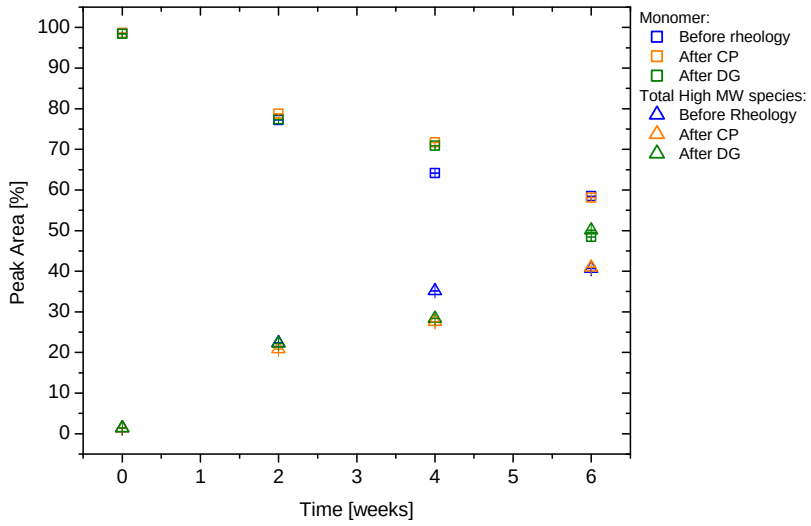

(a) 100 mg/mL mAb samples

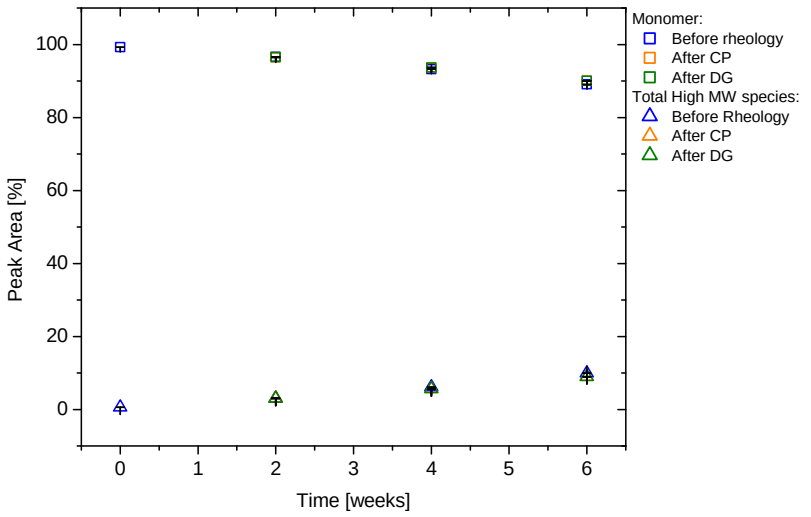

(b) 17 mg/mL mAb samples

Figure 5.18: Comparison of level of aggregation by HPSEC between the same samples before and after the rheology experiments. **a)** corresponds to data from 100 mg/mL mAb samples, and **b)** corresponds to data from 17 mg/mL mAb samples, all stressed at 40 °C for 6 weeks. Low MW species not represented since all data points were superimposed for both concentrations.

For the DLS analysis of these samples, similar observations were made (Figure

5.19). In general, for the 17 mg/mL samples no change between 'after' and 'before' hydrodynamic diameter sizes (by volume distribution) was observed. The 100 mg/mL sample set showed slight variation on the data although no evident trend was found.

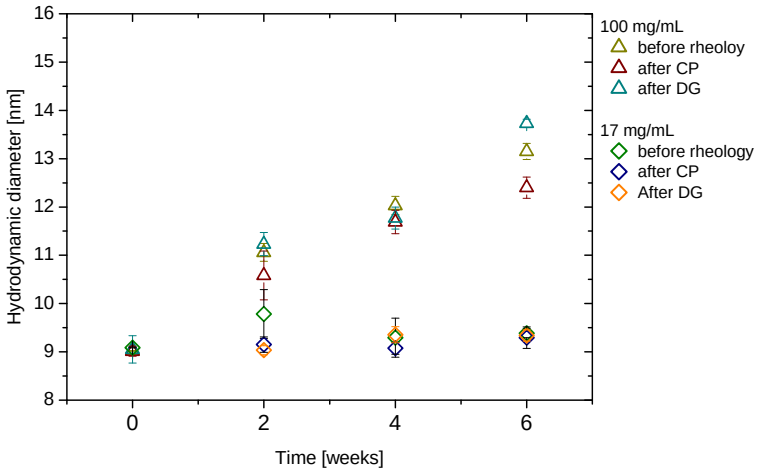

Figure 5.19: Hydrodynamic diameter by volume distribution comparison between before and after rheology for dilutions of 100 and 17 mg/mL mAb samples stressed at 40 °C for 6 weeks.

Based on these observations, even though the 'after rheology' samples generally had increased concentrations when compared to the 'before rheology' solutions, the evaporation of sample and use of these geometries did not seem to influence the mAb's level of aggregation. However, HPSEC and DLS were the only techniques used here, leaving unanswered questions regarding if changes to the mAb's tertiary or secondary structure occurred.

The importance of investigating the effect of shearing on the studied mAbs, during these rheological experiments, became clear when it was detected that thermally stressed mAb samples that had undergone rheology showed a slight change of colour between yellow and brown. This was found for the 100 mg/mL solutions stressed at 40 °C at T= 2 weeks and T= 4 weeks, for CP and DG rheology. After analysis, these

recovered samples were restored to the incubator at 40 °C . The change of colour was noticed 2 months after the study had started. HPSEC analysis revealed that the coloured samples had an extra low MW species peak compared to the control sample (100 mg/mL mAb at 40 °C for T= 2 months, not undergone the rheology experiment). Due to a lack of time further investigations were not pursued. This could have been result of further chemical degradation due to the degraded mAb being in contact with stainless steel leading to protein oxidation [30]. In addition, it was noted that the control sample did not show any change of colour. Moreover, non-thermally stressed mAb samples that had been previously analysed on the rheometer, recovered and stored at 5 °C, did not have any colour change.

5.3.3 Soluble reversible aggregates: biophysical characterisation and effect on the viscosity of the mAb solution

It was important to understand if the analysis of the diluted aggregated mAb samples would be a good representation of the original content of soluble aggregates. It is known that reversible self-association can occur with proteins and due to various reasons, such as changes in pH or ionic strength [6, 51].

The IgG_1 studied here was characterised by CG-MALS to measure its self-virial coefficient and determine if the monomer would show reversible self-associative properties in 10 mM His-His.HCl pH 6.0. The mAb was found to have an estimated $A_2 = 3.97\times10^{-4}\pm 5\times10^{-6}$ mol.mL/g^2 and a MW = 150.02 ± 0.6 kDa. The MW estimate was close to the actual predicted MW. The positive self-virial coefficient value suggested that there would be mainly repulsive interactions between the monomers in the studied conditions. This information suggested that the mAb monomer would not be expected to show signs of reversible self-association at these conditions.

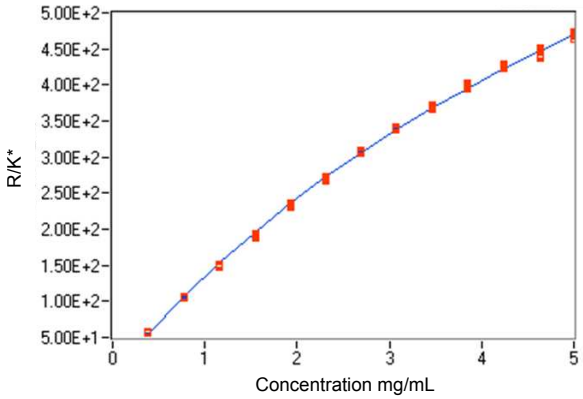

Figure 5.20: Static light scattering data (R/K*) versus concentration of mAb solution starting at a stock concentration of ∼5 mg/mL and diluted with 10 mM His-His.HCl pH 6.0 buffer. The red squares represent the light scattering data and the line is for guidance only.

The question remained whether the relative quantification of the level of aggregation by size-exclusion would be representative of the total soluble aggregates after stressing at 40 °C. Therefore, a dilution and temperature study were performed. Dilutions of 10 and 50 mg/mL from a 100 mg/mL mAb sample at 40 °C were analysed on HPSEC, keeping the auto-sampler tray temperature either at 25 °C or 5°C. The results are shown in the two following sets of Figures 5.21 and 5.22.

Figure 5.21 shows the first analysis of 10 and 50 mg/mL dilutions at a constant temperature of 5 °C, which is the typical auto-sampler tray temperature of the HPLC system used throughout our work. A difference of 3 to 4 % was observed for the peak areas for total high MW species and monomer between the 10 and 50 mg/mL dilutions. There was no change in the low MW species relative content. Between the first measurement and the last, there was a 'gain' in monomer peak area of ∼9 and ∼7 % for 10 and 50 mg/mL dilutions, respectively (Figure 5.21(a)). Figure 5.21(b) shows the different relative peak areas versus time, discriminated by each of the identified high MW species peaks. It was observed that only the peak area corresponding to the retention time at ∼7.5 min remained almost constant. Peaks with retention times at ∼6.6 and ∼7.0 min evidenced a descending trend on their relative area.

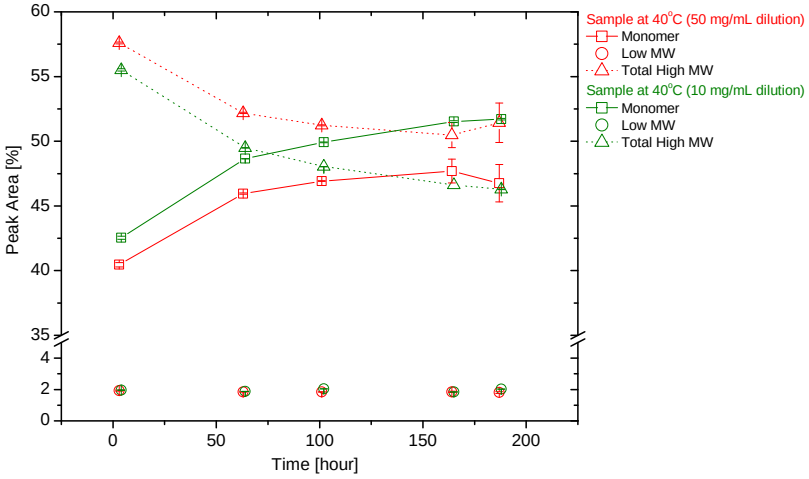

(a)

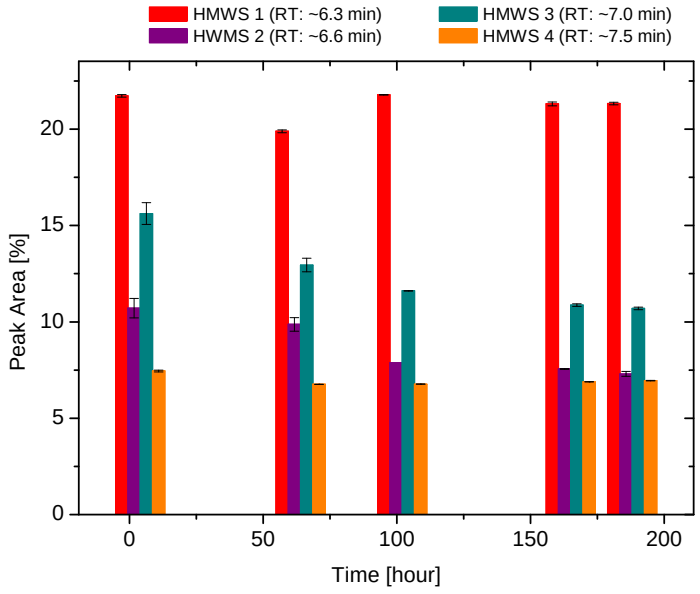

(b)

Figure 5.21: Level of aggregation along a 5 day period of 10 and 50 mg/mL dilutions from 100 mg/mL mAb sample that was at 40 °C for 7 weeks. **a)** corresponds to the global level of aggregation, where total HMWS is represented. **b)** shows the detailed peak areas correspondent to the eluted HMWS only. Graph **a)** and **b)** represent the HPSEC study performed leaving the analysed dilutions at 5 °C (HPSEC tray temperature).

A similar experiment was performed, with the auto-sampler tray at 25 °C (Figure 5.22). Since the previous experiment showed a large decrease in total aggregate species during the first 50 hours, this experiment had a total time of 21 hours. At 25 °C, the monomer increase was not as sharp, with a difference of ∼4 and ∼3 % for 10 and 50 mg/mL dilutions, respectively. The difference in peak area between the dilutions at each time point remained at 3 - 4 ∼ (Figure 5.22(a)). Within each of the detected high MW species peaks, the peak area corresponding to the retention time at ∼7.4 min remained constant (Figure 5.22(b)).

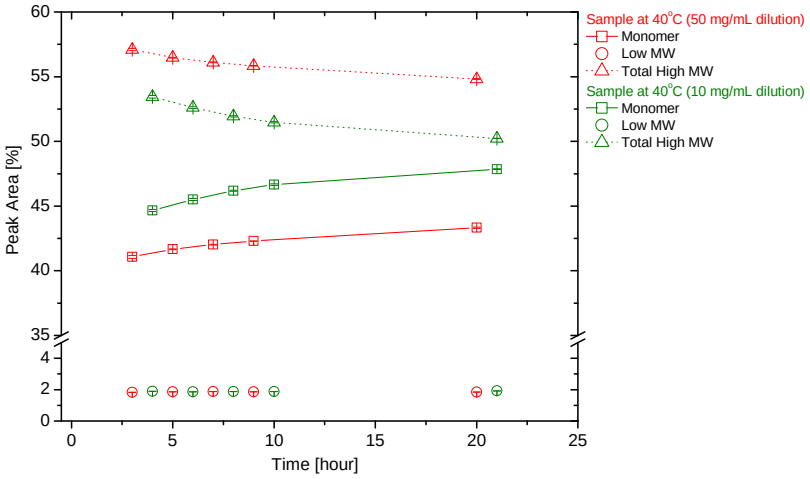

(a)

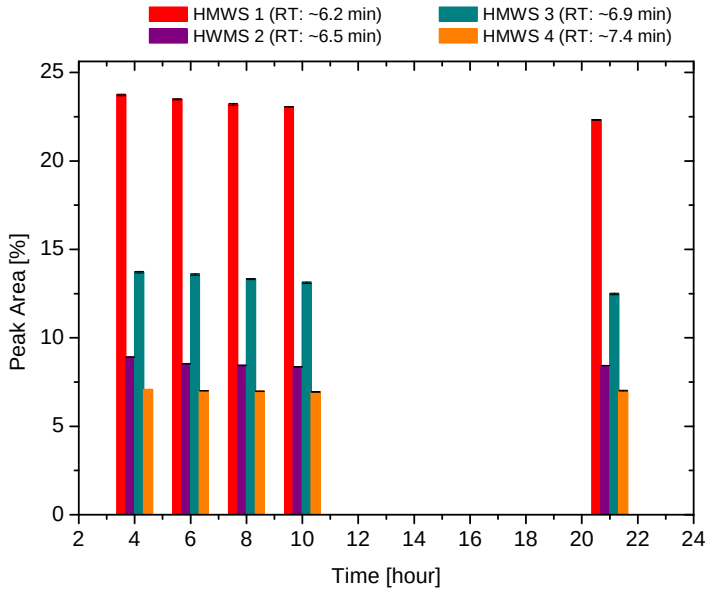

(b)

Figure 5.22: Level of aggregation along a 24 hour period of 10 and 50 mg/mL dilutions from 100 mg/mL mAb sample that was at 40 °C for 7 weeks. **a)** corresponds to the global level of aggregation, where total HMWS is represented. **b)** shows the detailed peak areas correspondent to the eluted HMWS only. Graph **a)** and **b)** represent the HPSEC study performed leaving the analysed dilutions at 25 °C (HPSEC tray temperature).

A quick analysis with DLS was performed measuring H_D sizes at 5 and 25 °C for 24 hours (Figure 5.23). By diluting to 1 mg/mL, the potential 'break-up' of aggregates is most likely higher than when diluting to 10 mg/mL, leaving less larger sized species in solution.

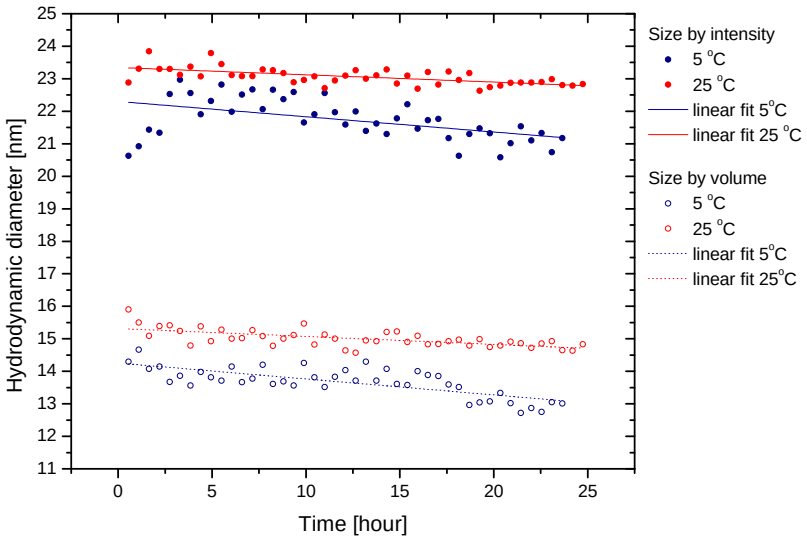

Figure 5.23: Time sweep of measured hydrodynamic size of 1 mg/mL dilution from 100 mg/mL mAb sample stressed at 40 °C for 2.5 months. The full circles represent the diameter size by intensity distribution and the open circles are correspondent to the hydrdynamic size by volume. The data is also comparing the difference in size along time when performing the measurement at 5 °C (blue) and 25 °C (red).

In summary, it was demonstrated that once this mAb presented soluble aggregates, a part of these species could dissociate into monomer. This suggested that this percentage of aggregates were most likely formed by non-covalent bonds, thus suggesting their reversible nature. It was observed that dilution and low temperature (5 °C), promoted this aggregate dissociation to monomer. These findings were most evident with the sample at 100 mg/mL, whereas the sample at 17 mg/mL also studied for its rheology did not show such a significant change on its aggregate relative content, while still

demonstrating signs of the same phenomenon (Figure B.5(b) in Appendix B).

The impact of these observations reflect on the quantitative and qualitatitive analysis of the thermally stressed mAb samples studied so far. In this mAb's specific case, it could impact its rheology measurements. Attempting at quantitatively relating the level of aggregation of these samples to their viscosity at 100 mg/mL would not be accurate, since HPSEC was typically conducted with 10 mg/mL dilutions and the samples left at the auto-sampler at 5 °C until analysed.

5.3.3.1 Evaluation of the effect of soluble aggregate reversibility on rheological measurements

A rheology experiment alongside HPSEC analysis was performed with a 100 mg/mL mAb solution stressed at 40 °C for 2 weeks, to understand the implications of these findings in the viscosity measurements of this IgG_1 in this buffer. After the first measurement, the original sample was stored at 5 °C. Fresh aliquots were measured on HPSEC as well as on the double-gap rheometer 24 hours later, for comparison. A slight drop in viscosities across the shear rate range was observed between the time points, e.g. at 1000 s^{-1} the difference was ∼0.15 mPa.s (Figure 5.24). This difference in viscosities was too small (<1 mPa.s) to be considered significant. This suggests that the percentage of aggregates that dissociate to monomer, at this stage, would not likely affect the rheological measurements of this mAb solution, not only in terms of its flow (as it was not changed) but also in terms of the viscosity values.

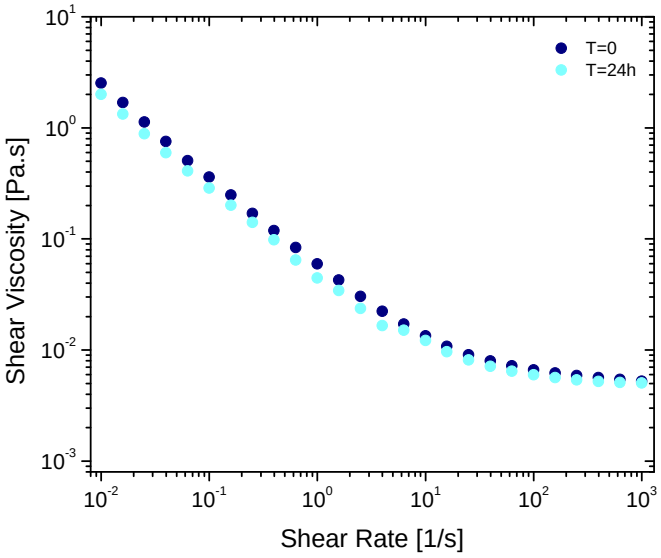

Figure 5.24: Double-gap rheology of a 100 mg/mL mAb sample stressed at 40 °C for 2 weeks measured with a 24 hour interval. After the first rheological measurement (T= 0), the mAb solution was stored for 24 hours at 5 °C and another aliquot was analysed on the DG geometry when T= 24 hours. Measurement temperature was 25 °C.

With the HPSEC results, similar results were found to those previously described in this section. A difference of about 3 % was seen between the 10 and 50 mg/mL injections at each time point; and an increase of monomer/ decrease of total high MW species of ∼3 and 2 % was found for the 10 and 50 mg/mL injections, respectively (Figure 5.25). Such low percentage of reversible soluble aggregates could well explain the small differences measured with DG rheology.

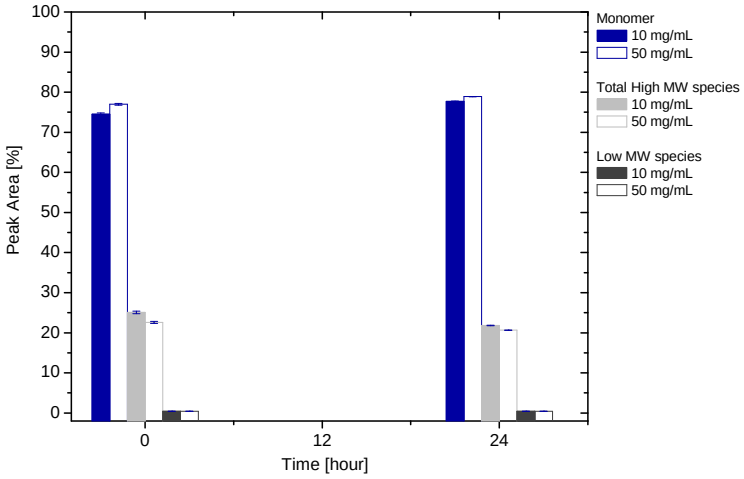

Figure 5.25: Level of aggregation of a 40 °C stressed T=2 weeks 100 mg/mL mAb sample, diluted and analysed at 10 and 50 mg/mL, measured with a 24 hour interval. This experiment was performed at the same time the rheology experiment was conducted. The mAb solution was stored for 24 hours at 5 °C and another aliquot was analysed on HPSEC when T= 24 hours. HPSEC tray temperature was 5 °C.

5.3.3.2 HPSEC-MALS analysis of mAb solutions: calculation of the MW

Static light scattering analysis was performed to obtain information of MW of HMWS and monomer peaks. Figure 5.26 represents examples of one injection per each of the analysed samples. These plots correspond to the computed (fitted) molecular weight for each of the peaks identified and analysed, versus the elution time. Note that the lower molecular weight species (at 10.9 min, with the UV-detector) were not fitted. This is because of their small size yielding that their relative signal in light scattering data was poor and thus making its analysis difficult [102]. Therefore, the peaks that were analysed were those with relevant light scattering signal (full line in the figure), and corresponded to the monomer peak (∼8.9 min), and aggregates at ∼7.5 min, ∼6.9 min, ∼6.5 min and ∼6.1 min.

Analysis of these samples was made by applying the Debye formalism to each of the peaks detected. The degree of fitting of each of the peaks experimental data was changed accordingly to achieve higher R^2. Note that the fittings were done for a particular elution volume slice and checked if adequate for the remaining slices. An example of this analysis are Figures 5.27(a) and 5.27(b) which show the Debye plots - light scattering data versus $\sin^2(\theta/2)$ - corresponding to a specific elution volume slice of peak 1 and peak 2, respectively, from different samples. Included in these figures are the summary data obtained from this fitting.

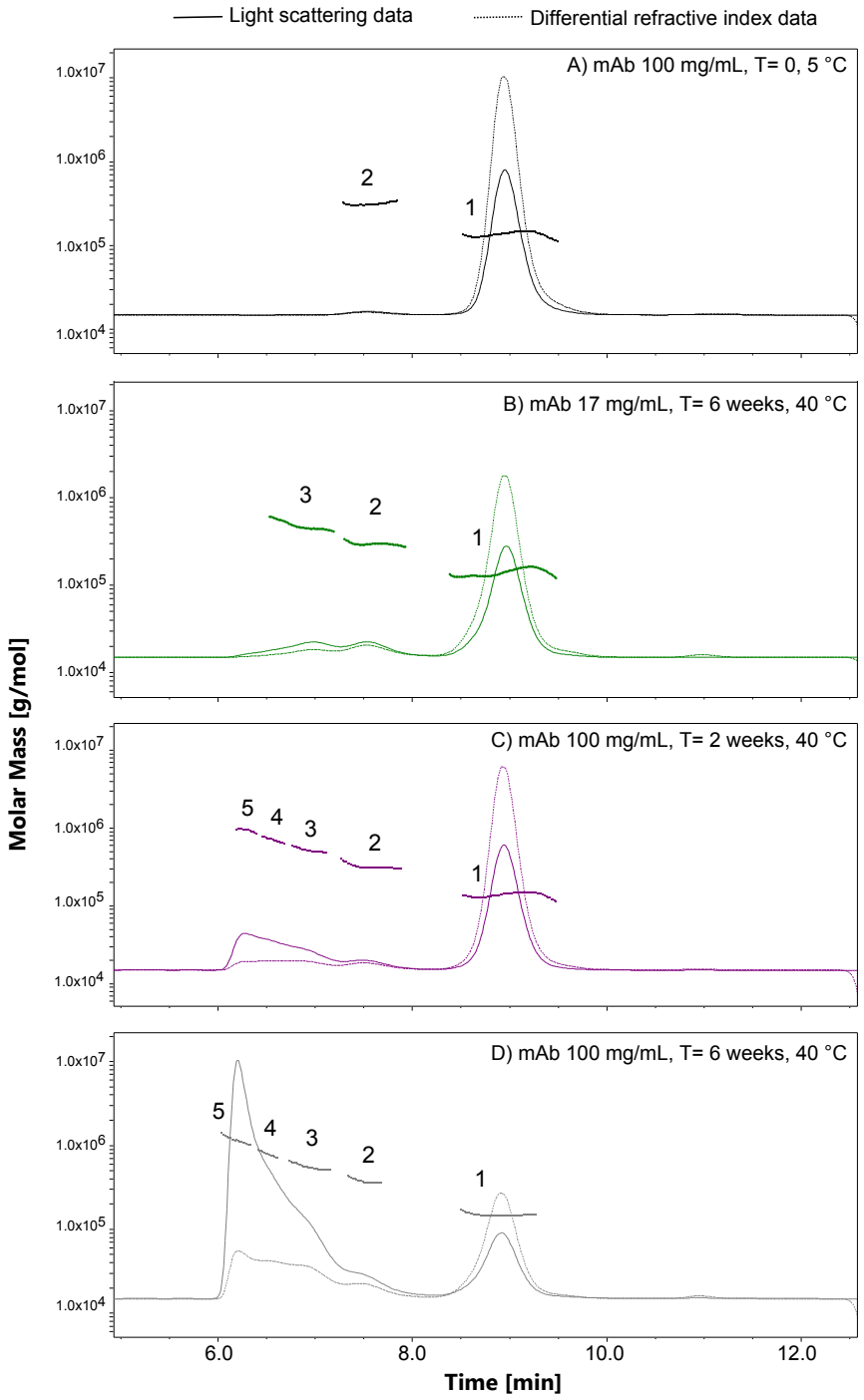

Figure 5.26: HPSEC-MALS experiments showing light scattering (full line), differential refractive index data (dotted line), and calculated molecular weight (circles) for each detected peak from mAb solutions at different time points during thermal stressing at 40 °C: **A)** unstressed mAb solution; **B)** 17 mg/mL mAb sample that was stressed for 6 weeks at 40 °C; **C)** 100 mg/mL mAb after 2 weeks at 40 °C; **D)** 100 mg/mL mAb solution after 6 weeks at 40 °C. The 100 mg/mL mAb solutions here presented were diluted to 10 mg/mL, while the 17 mg/mL mAb solution was injected neat.

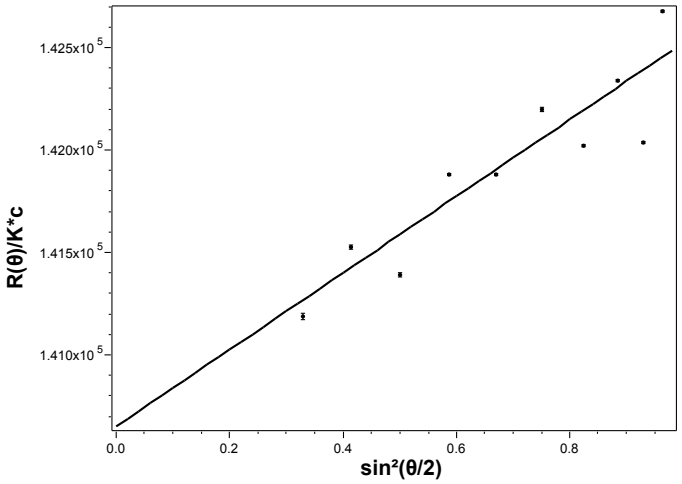

mAb 100 mg/mL, T= 0, 5 ºC	
Peak; slice	1; 537
Elution time [min]	8.939
MW [g/mol]	$140.7\times10^3 \pm 0.003$
Model	Debye
R^2	0.8651
Fit degree	1

(a)

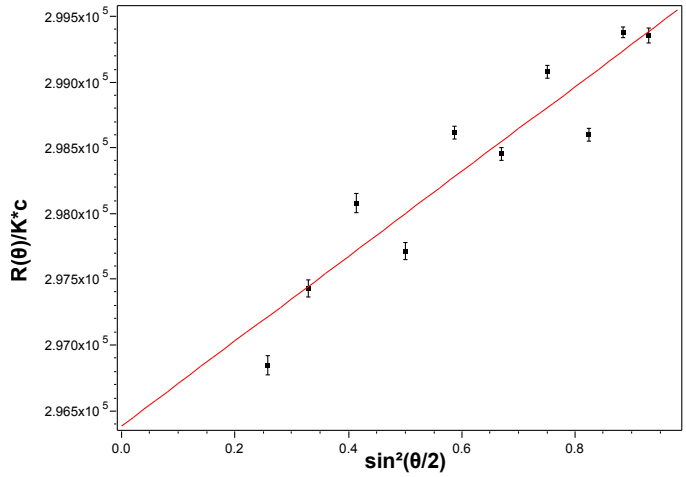

mAb 17 mg/mL, T= 6 weeks, 40 ºC	
Peak; slice	2; 456
Elution time [min]	7.576
MW [g/mol]	$296.4\times10^3 \pm 0.003$
Model	Debye
R^2	0.8882
Fit degree	1

(b)

Figure 5.27: Debye plots for two of the analysed peaks of the mAbs samples, along with the data respective to each of the analysed elution volume slices . **a)** Debye plot for 100 mg/mL mAb sample at T= 0, 5 °C; **b)** Debye plot for 17 mg/mL mAb sample at T= 6 weeks, 40 °C. Raleigh ratio experimental data are represented in full circles, and the fit corresponds to the line. Data analysed using the Debye formalism.

From this analysis, the molecular weights were computed as a sum per peak for each sample. Table 5.6 summarises these results showing the weight-averaged molecular weight. The root mean square radius is not reported since these scatterers, including

the higher MW oligomers, had a radius $< 1/20^{*}\lambda$ of the incident light used in the instrument, thus disabling computation of the RMS radius for these macromolecules

Table 5.6: Molecular weight (weight-averaged) (M_w) for each peak identified from mAb samples exposed to 40 °C, compared to storage at 5 °C. Each sample was analysed in triplicate. Molecular weight reported is the average, and the standard error is from the 3 measurements.

Sample	Peak (Mw ± st dev [kDa])				
	1	2	3	4	5
mAb 100 mg/mL, T= 0, 5 °C	139.8 ± 0.4	352.9 ± 51.9	-	-	-
mAb 17 mg/mL, T= 6 weeks, 40 °C	141.1 ± 0.1	298.5 ± 0.7	468.5 ± 4.1	-	-
mAb 100 mg/mL, T= 2 weeks, 40 °C	141.6 ± 0.6	362.7 ± 61.4	577.9 ± 84.2	773.8 ± 114.2	1024.0 ± 156.8
mAb 100 mg/mL, T= 6 weeks, 40 °C	146.3 ± 0.1	388.4 ± 6.4	572.1 ± 7.0	805.8 ± 6.6	1096.6 ± 28.6

From the data in Table 5.6, and knowing that the predicted MW of this mAb was ∼145.46 kDa, a correspondence of these calculated MW with the number of associated monomers for each peak, was made. Peak 1 was attributed to the mAb monomer since the calculated MW was within 5 % of the predicted monomer's MW. A dimer, trimer, tetramer and pentamer of this mAb would be expected to have the following molecular mass: ∼290; ∼435; ∼580; and ∼725 kDa. Our data suggested that the only plausible correlation to dimers and trimers, could be for peak 2 and peak 3, respectively. As for peaks 4 and 5, the calculated MW indicated that these eluted volume fractions were composed of mAb oligomers of higher order than pentamers. Even though the calculated polydispersity for each of these peaks was ∼1, it is noted that for the highly aggregated samples (100 mg/mL after T= 2 and T= 6 weeks), fitting of these peaks to the Debye model required higher order fit degrees. This was a consequence of higher error in light scattering data, due to the species of higher mass and possibly of irregular shape. Peak 3

was better analysed from the 17 mg/mL mAb sample, since its chromatographic profile showed better separating resolution.

Relating the MALS data to the detailed study of the reversible high MW species, indicated that the n^{th}-oligomers' dissolution was mostly directly to monomer, without including a gradual step dissociation into dimer. Therefore, it is likely that this IgG's dimers were not the 'reactive species' for n^{th}-oligomer formation.

Judging by the DLS data and the close MW values calculated for these aggregates, it is expected that its aspect ratios would be very similar. This would likely yield a very small difference between the aggregates' intrinsic viscosities, explaining how although the relatively high percentage present of these aggregates after 6 weeks at 40 °C, the increase in viscosity at high shear remained a difference of ∼5-6 mPa.s for the 100 mg/mL mAb sample.

5.4 Conclusions

In the first section it was shown that the mAb material purified and concentrated was free of previously added excipients. It was also shown that the different processing steps did not influence the physico-chemical properties of the mAb. All the batches were of high monomer content (>98 %), revealing the material's high purity.

A comparison between the flow and viscosity curves of these batches and the original formulation suggested that the original formulation additives had an effect on the rheology of this mAb. Removing the excipients contributed to a yield-like behaviour at low shear rates, regardless of the mAb concentration. The rheology data observed with the excipient-free material had similar features to those previously observed with β-LG solutions and discussed in literature [78, 182]. This indicated that similar factors were underpinning this type of sample's flow properties.

A comparison between unfiltered and filtered mAb solutions was made to understand

the influence of visible and sub-visible particles in the flow behaviour. A drop in the viscosities was detected, although more marked at the lower shear rates and particularly with the CP geometry. Further characterisation suggested that, by filtering out most of the insoluble visible and sub-visible particles, lead to this reduction of viscosities at the lower shear rates.

The filtered material was then studied during thermal stress at 40 °C for 6 weeks. Results obtained from HPSEC, μ-SDS-PAGE, DLS, and MFI provided information on the type of aggregates formed, their relative quantification and size. DLS did not allow a resolution in sizes between the IgG monomer and any possible oligomers, showing that the mean H_D sizes were increasing slightly. HPSEC results were advantageous for determining the level of aggregation, although it demonstrated that the oligomers formed were most likely of similar MW. μ-SDS-PAGE and HPSEC were particularly useful to emphasize other products of degradation where possible fragmentation could have occurred, although further analysis would be needed to clarify this.

In general, the thermally stressed material showed increased viscosities throughout the time of exposure, while the increasing amount of oligomers dominated. The evident differences were detected with samples at the highest mAb concentration (100 mg/mL). The 40 °C stressed ∼17 mg/mL mAb solution also demonstrated loss of monomer, although to much lower extent (∼10 %, after 6 weeks), when compared to the higher concentration (∼40 %), the latter being an effect of high concentration. This increase of aggregates did not seem to change whatsoever their flow behaviour at low shear rates, remaining as a yield-like behaviour at that shear rate range (0.01 - 10 s^{-1}). At the highest shear rates, the difference in viscosities between time points was evident and did follow a increasing trend. However, there was no evident increase of yield values with time at stressing conditions. The increase of viscosity observed in these samples was suggested to be mostly due to the increase in soluble aggregates. Even though there was

an increase in the sub-visible particle content, these were calculated to be <1 % of total sample volume.

Tests on the level of aggregation comparing samples before and recovered from rheology experiments showed that, in our case, no obvious tendencies were detected. The case of 'after rheology' degraded mAb material had a change in colour towards brown could not be conclusively attributed to the effect of shear stress and stainless steel on these samples.

In addition, it was shown that a percentage of these aggregates were dissolving to monomer after dilution (10 mg/mL) and at lower temperatures (5 °C). This phenomena was as a drawback for the accurate quantification of soluble aggregates via HPSEC. Implications of this aggregate-to-monomer reversibility in the accuracy of the viscosity measurements performed during the study, were however likely to be negligible.

Finally, mAb samples were submitted to HPSEC-MALS analysis to calculate the MW of the detectable protein species. Poor resolution between the high MW species did not allow a accurate measurements for the highest MW oligomers, but it was possible to compute that this IgG monomer tended to aggregate in dimers and trimers, and other oligomers.

This mAb was a case study to demonstrate that protein degradation, by entailing a complex interpretation and quantification of different protein species, makes the interpretation of its solution rheology difficult. In this case, the non-static protein species content, due to soluble aggregate reversibility, adds to this complexity. However, our aim of studying the rheology of this mAb solutions using orthogonal characterisation biophysical techniques, allowed an analysis at the molecular level to a detail that shed light into variables commonly dismissed in study of protein solution rheology.

Chapter 6

Exploring the impact of surface active macromolecular excipients on the flow properties of protein solutions

6.1 Introduction

In the previous two chapters, the rheology of globular proteins was studied using β-LG and mAb as model proteins in additive-free solutions. The discussion of factors likely influencing the flow properties observed, particularly at the low shear rates, reflected the concept that the macromolecules' surface-activity was underpinning the materials' rheology [78]. Moreover, our studies of formulated rAlbumin and mAb solutions contributed to the argument, as without a surfactant additive, the rheology of this protein solution also demonstrated a tendency towards a yield stress.

Therefore, to further this knowledge, for the work in the present chapter two studies were envisioned. The first focussed on further understanding the rAlbumin solution rheology, exploring further the role of polysorbate-80 in the case of thermal stressing. The second part of this chapter refers to the synthesis and study of amphiphilic brush-like poly(ethylene glycol) methacrylate polymers as potential additives to biopharmaceutical formulations as modifiers of rheology.

6.1.1 The use of polysorbate-80 in biopharmaceutical formulations

Polysorbates are compounds frequently used in pharmaceutical, cosmetic and food products for their properties as non-ionic amphiphilic surfactants [190]. A polysorbate is a viscous liquid that is composed of fatty acid esters of poly(oxyethyelene) sorbitan, where in the case of polysorbate 80 the fatty acid ester is octadecenoic ester (Figure 6.1) [191]. However, polysorbates are known to contain a variety of derivatives of sorbitan poly(oxyethylene) fatty acid esters [192].

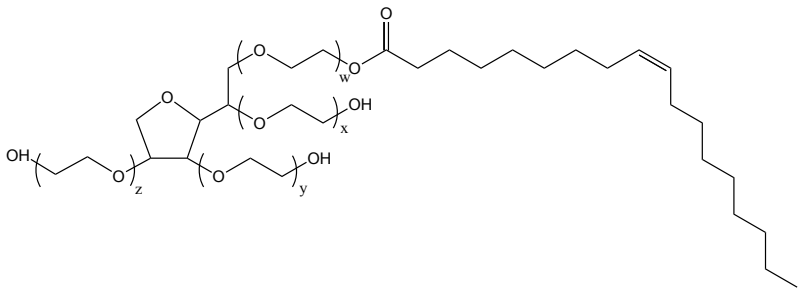

Figure 6.1: Structure of polysorbate-80, where w+x+y+z= 20, referring to the total number of oxyethylene groups.

Specifically in biopharmaceutical formulations, the use of polysorbate (e.g. polysorbate 20 and 80) has been due its capabilities in preventing protein aggregation and potential interactions of the biomacromolecule with interfaces (solid and/or liquid) [33, 193]. Since there are numerous processes that biopharmaceutical solutions are subjected to where interface cannot be avoided, the use of polysorbates in monoclonal antibody drug products is predominant [194].

The reason why these surfactants are very successful in biopharmaceutical formulations lies in their low critical micelle concentrations [195], thus enabling the use of low amounts of the compound. The mechanism of how polysorbates interact with proteins is attributed to their capability to slowly competitively displace the adsorption of proteins at interfaces [37, 163]. It has been found that this mechanism in protein-surfactant

mixtures, denominated as orogenic displacement, occurs with an increase of surfactant in solution resulting in a decrease of protein absorption, even if the molar ratios between both are fixed [37]. This mechanism is suggested to be complex involving not only interfacial adsorption, but also interactions between protein-surfactant. The free surfactant molecules are suggested to interact hydrophobically with the hydrophobic 'patches' of an absorbed protein at the interface, forming protein-surfactant complexes which will lead to a less surface active protein. When higher surfactant concentrations are present, free molecules will therefore gradually displace these hydrophilic protein-surfactant complexes, thus displacing completely the protein from the hydrophobic interface [34,163,196]. This theory has been verified through various techniques, such as surface tension [163, 166, 189], interfacial dilatational and shear rheology [143, 176, 196], and using atomic force microscopy [176, 177]. Recently, theoretical models have been developed to describe this mechanism [163].

The use of polysorbates in biopharmaceutical industry, can however come with the risk of adding degradation reactions to protein formulations. It has been shown that these surfactants can induce protein aggregation if stored for long periods of time at high temperature [32, 197]. Protein degradation by oxidation has also been demonstrated to occur via peroxide contamination of the surfactant [198]. Recently, assessment of polysorbate degradation under similar conditions to those imposed in biopharmaceutical studies has revealed that an increased presence of peroxides leads to an auto-oxidation degradation mechanism of the surfactant [189]. For these reasons, it remains highly important that the addition of surfactants such as polysorbates needs to be at as low concentration as possible, so to reduce its effects on the drug product degradation [197].

In the context of the work presented here, the use of polysorbate 80 in the rAlbumin formulation was investigated for its rheological effects, in conjugation with thermal

stressing at 60 °C. The study involved characterisation of the solution's rheology with CP measuring system, and characterisation of level of protein aggregation, by DLS, HPSEC and gel electrophoresis.

6.1.2 Exploring the effect of brush-like PEG methacrylate amphiphilic polymers as excipients in protein formulations

Applications of synthetic polymers spans a large range of areas, from nanoelectronics, cosmetics, healthcare, biomedical to biotechnology processes [199], particularly with the advent of polymerisation processes allowing versatile synthesis of materials [200].

One particular class of polymeric materials that stands out in its applications in biotechnology and biomedical purposes, are stimuli-responsive polymer brushes [201]. This type of polymer, of varying architecture and composition, can be prepared by grafting polymers into a linear polymer chain ('backbone') or grafted from a surface [201]. Various types of stimuli-responsive molecular brushes have been developed, with changes in their properties that are dependent on their surrounding environment, such as temperature, pH, type of ion or magnetic field [201–203]. When present in a specific stimuli-predominant environment this type of polymers typically undergoes conformational changes such as collapse of the brushes' linear chains into globules, yielding reversible changes in solubility and a tendency to self-assemble into micelles or vesicles [201, 203, 204].

The development of versatile polymerisation processes, such as controlled/living radical polymerisation techniques (LRP), were key to advancing the synthesis and application of such polymers [199, 201, 205]. These techniques include atom transfer radical polymerisation (ATRP), reversible addition fragmentation chain transfer (RAFT), and nitroxide-mediated radical polymerisation (NMRP), among other types

of processes [205]. Since in this work we used the ATRP technique to synthesise poly[poly(ethylene glycol) methyl ether methacrylate] homopolymers, an explanation of its mechanism will follow.

Figure 6.2 summarises the mechanism of ATRP, which is a catalytic reaction that uses a metal-ligand complex. The radicals ($R^{\cdot}$) are generated by reaction of the ATRP initiator ($R-X$, an alkyl halide) with the transition metal complex ($M_t^y \,/\, L$, where L is the ligand) at its lower oxidation state (y). This reaction yields the radical and increases the transition metal's oxidation state, coupling it to the halide ($X-M_t^{y+1} \,/\, L$). This is denominated the activation reaction (with rate constant k_{act}). The generated radicals $R^{\cdot}$ can polymerise with the (macro)monomer, in a propagation reaction with rate constant of k_p. However, the transition metal complex can also transfer the halide to the $R^{\cdot}$ regenerating the original alkyl halide compound, which corresponds to a deactivation reaction (k_{deact} originating a dormant polymer chain capped with the halide. In parallel, the radicals can undergo other termination reactions (rate constant k_t), reacting with each other ($R-R$), or by disproportionation (generating $R-H$, $R-HC=CH_2$) [200, 205].

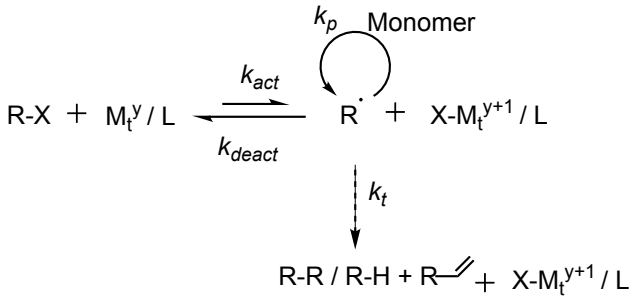

Figure 6.2: Scheme for general ATRP reaction. Adaptaed from [205].

Polymerisation by ATRP is therefore a catalytic process where the persistent radical effect self-regulates the reaction's equilibrium between activation and deactivation by transfering the atom between the growing chains and the transition metal catalyst.

For this reason, the equilibrium is shifted towards the deactivation reaction producing dormant polymerised chains [200, 205].

In the case of poly[poly(ethylene glycol) methyl ether methacrylate] polymers, ATRP gives a good control in polymerisation and molecule architecture, producing polymers of narrow molecular weight distribution [205]. The reaction can be conducted in organic solvents and high temperature [199], although it has also been performed under aqueous and room temperature conditions [203, 204].

In the case of the study presented here these polymer brushes were synthesised by grafting through, i.e. by polymerising macromonomers (Figure 6.3). Other possible ways of constructing brush-like polymers in general consist of coupling individual side chains to a common backbone, and polymerising the side chains from a backbone chain [199, 201]. In our case, the chosen method proves simple particularly since the ether-capped poly(ethylene glycol) methacrylates used (PEGMA) were commercially available, needing only the synthesis of the ATRP initiator. Provided a high purity of the original macromonomer, the technique exemplified in the scheme of Figure 6.3 can provide 100 % density of brushes up to a limit where steric hinderance can disable further polymerisation [201].

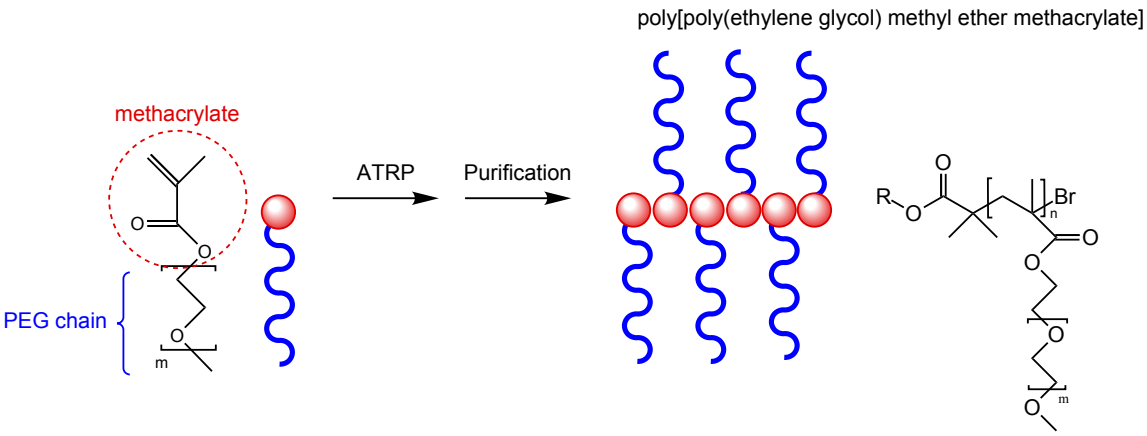

Figure 6.3: General schematics of poly[poly(ethylene glycol) methyl ether methacrylate] brush polymers. The PEGMA is the functional (methacrylate) macromonomer that was polymerised, thus creating a homopolymer with a brush-type structure.

The choice for the synthesis and use of PEGMA brushes in their effect on protein rheology laid also with their suggested biocompatibility [204], good solubility in aqueous media [199, 201], amphiphilic properties [202, 204, 206], and capacity to micellise [199]. Other uses of PEGMA brushes have been on protein-resistant antifouling membranes or films [204, 207]. The latter reason has large potential in the biopharmaceutical industry since, as mentioned above, they may be useful in preventing interaction with different interfaces along the biopharmaceutical processing steps which can lead to protein degradation [194]. Other authors have developed techniques to conjugate PEGMA brushes to proteins, proving an alternative to linear PEG conjugation [208, 209].

As a starting point, the work shown in this chapter focused only on the synthesis of homopolymers of PEGMA, using ATRP as the polymerisation technique. The materials recovered were then characterised by ^{1}H-NMR and HPSEC with triple detection. The polymers were assessed for their capability of micellisation and their molecular crowd-inducing properties in the presence of proteins. These experiments were prepared in order to help detect any possible limit in concentration of these materials when blending with proteins. The chosen proteins were again β-LG and the mAb, the same proteins de-

scribed in the previous chapters of this thesis. Once the protein-polymer mixtures were prepared, measurements with cone-and-plate rheology and mVROC were performed, as well as characterisation with HPSEC and DLS for the level of aggregation.

6.2 Materials and Methods

6.2.1 Materials

6.2.1.1 Protein samples

The monoclonal antibody studied was provided by MedImmune, LLC. (Gaithersburg, Maryland, USA). It is an IgG_1 of 145.461 kDa. The protein was supplied in a lyophilised formulated format containing other additives, including a surfactant. The formulation additives were removed by purifying the reconstituted material, as per description in section 2.2.3 of Chapter 2.

The protein β-LG was obtained from Sigma-Aldrich (product L3908, batches 097K7012 and 080M7312V) as a mixture of bovine variants A and B, in a lyophilised powder containing approximately 10% w/w of sodium chloride.

rAlbumin used in this work was kindly donated by Novozymes Biopharma UK Ltd. (Nottingham, UK). The original sample was formulated at 200 mg/mL concentration. For rAlbumin samples, the formulation buffer was composed of NaCl (145 mM), Polysorbate-80 (15 mg/L) and sodium octanoate (32 mM) in ultrapure water (pH = 7.0 $\pm$ 0.3 at room temperature).

6.2.1.2 Reagents

All reagents used for the rAlbumin formulation buffer preparation were obtained from Sigma-Aldrich and were of analytical grade. Polysorbate-80 used for the rAlbumin buffer

and its determination of critical micellar concentration by fluorescence was obtained from Fluka and of grade meeting the standards from the European Pharmacopoeia. PEG 8000 for the protein solubility test was purchased from Alpha-Aesar.

All the chemicals used for polymer synthesis were purchased from Sigma-Aldrich or Acros. All the solvents used for polymer synthesis, purification and analysis (size exclusion chromatography and nuclear magnetic ressonance) were purchased from Sigma-Aldrich or Fisher Scientific and were of HPLC grade, and used without further purification.

The histidine buffer was prepared containing L-Histidine and L-Histidine monohydrochloride at 10 mM in ultrapure water (pH = 6.0 ± 0.2 at room temperature). Histidine salts were purchased from J.T. Baker Chemicals (Pennsylvania, USA) and were of analytical grade.

All prepared buffers had a 2-month expiry date and were kept at 5 °C. Ultrapure water was obtained from a water cleaning resin system from NANOpure Diamond (Barnstead, USA) with water quality of >18.0 mΩ-cm, and 0.22 μm filtered (PVDF membrane, EMD Millipore, USA). All buffers were filtered using 0.22 μm vacuum-driven filter units (Nalgene, USA), unless when 0.1 μm pore-size filtering was necessary (using PDVF syringe-filters Millex-VV from EMD Millipore, USA).

6.2.1.3 Sample preparation

(a) rAlbumin thermal stress study

For the thermal stress study of rAlbumin, samples at 200 mg/mL and at 20 mg/mL were used. The 20 mg/mL sample was prepared by 1:10 dilution of original stock sample in rAlbumin formulation buffer. Samples were stored in closed glass vials at 60 °C and 5 °C (control samples). Aliquots of thermally-stressed and non-stressed samples were

analysed at the following time points: T= 0, T= 3 days, T= 7 days, T= 14 days, T= 28 days. If sample dilution was needed, these were prepared into formulation buffer.

(b) mAb and β-LG blends with polyPEGMAs

For the work described in this chapter, mAb batch 1 was used. This batch (~89 mg/mL) was concentrated to ~100 mg/mL using centrifugal concentrators Millipore MW cut-off 30 kDA (Millipore EMD) by following the manufacturer's protocol. The final mAb sample was then filtered with 0.22 μm pore-size syringe filters.

Sample preparation for β-LG is described in section 2.2.2 in Chapter 2. For the work presented in this chapter, a fresh batch of dialysed β-LG solution in 10 mM His-His.HCl pH 6.0 was prepared at a stock concentration of ~79 mg/mL after filtration (0.22 μm).

Any dilution of either mAb or β-LG samples was prepared in 10 mM His-His.HCl pH 6.0 buffer.

Blends of β-LG and mAb samples were prepared individually with each of the synthetic polyPEGMAs. All β-LG samples were at ~68 mg/mL, while all mAb samples were used at ~100 mg/mL. Each of the polyPEGMAs were added to each of the protein solutions at the following concentrations: 0.1, 1, 2.5 % w/v. A total of 7 samples were prepared per protein solution: 3 with increasing concentrations of polyPEGMA$_{475}$ and 3 with increasing concentrations of polyPEGMA$_{1100}$, and one control protein sample without any added polymer. All samples were prepared in 10 mM His-His.HCl pH 6.0 buffer, into sterile glass vials with a rubberised cap. All sample preparation and any filtration of mAb or β-LG solutions, using syringe filters, was done under a vertical laminar-flow fumehood to avoid any contamination by dust particles (LabCaire fumehood VLF6 Clean Air, PuriCore, Inc., USA). After preparation, to ensure full mixing of the materials, all samples were subjected to a gentle oscillatory shake (~50 rpm) for at least 5 hours. The materials were then left for 24 hour at

5 °C to before being analysed. All samples were checked for the pH at room temperature.

6.2.2 Methods

6.2.2.1 Protocol for ATRP pPEGMA synthesis

(1) Synthesis of ATRP initiator

The ATRP initiator 2-bromo-2-methylpropionic benzyl ester (**3**) was synthesised in the following conditions and used for synthesis of both pPEGMAs studied in this work. The commercially available phenylmethanol ((**2**), 50 g, 0.462 mol) was dissolved in dicloromethane (DCM ~ 200 mL) in a 1 L round-bottom flask with a magnetic stirrer bar under argon gas. Triethylamine (97 mL, 0.694 mol) was added with a syringe, and the flask was put over ice (0-5 °C). Attached to the flask was a closed glass ampoule that was filled with 2-bromoisobutyrylbromide (**1**) (86 mL, 0.692 mol) which was slowly added dropwise to the solution in the flask, over a 1 hour period. After this addition, the reaction was left overnight at room temperature remaining under argon. The precipitate formed (triethylammonium bromide) was removed by filtration twice and discarded. All filtrate was collected and the solvent removed by rotary evaporation. The product was then put through a basic alumina column with DCM, consecutively until the extracted fraction was a yellow coloured liquid. This fraction was collected, the DCM evaporated, and the product was dried over phosphorus pentoxide in a vacuum desiccator.

The initiator (2-bromo-2-methylpropionic benzyl ester) (**3**) was characterised by ^{1}H-NMR to ensure its purity.

(2) Synthesis by ATRP and purification of polyPEGMA-475 and polyPEGMA-1100

Prior to the synthesis of polyPEGMA homopolymers, each of the commercially available monomers PEGMA-475 and PEGMA-1100 were separately dissolved in DCM and passed through a neutral alumina column to remove the inhibitor present in solution. The monomers were collected and the recovered after evaporation of solvent. Then the respective monomer (PEGMA-475 or PEGMA-1100), along with PMDETA (N,N,N',N",N"-pentamethyldiethylenetriamine) and 2-bromo-2-methylpropionic benzyl ester were added to a two-neck round-bottom flask with a magnetic stirrer and dissolved with toluene (see Table 6.1 for the reagents' quantities used per reaction). The flask was sealed with rubber septums and degassed with argon for at least 20 minutes. Cu(I)Br was added under argon atmosphere, the mixture was continually stirred and put at 60 °C under continuous argon bubbling. The polymerisation was stopped after 1 hour by removing the flask from the heat, cooling it on ice and immediately exposing its contents to air.

The unreacted PEGMA monomer was precipitated in petroleum ether, recovering the supernatant. The solvents were then evaporated, and the resulting product was dissolved in DCM and passed through an alumina column at least three times to remove the copper catalyst. The excess DCM was removed by evaporation. The polymer was further dissolved in purified water (∼500 mL) and Na_2S was added to react with any remaining copper (II). This reaction was left stirring overnight at room temperature. The precipitate was filtered out (0.22 μm pore-size nylon membrane, Millipore) by vacuum-driven filtration. The aqueous polymer solution was dialysed in purified water (1000 Da cut-off membrane, Spectra/Por-6). The final dialysed solution was freeze-dried.

The polyPEGMA-475 and polyPEGMA-1100 resulting polymers were further dried

under vacuum for several days, and kept at 2-5 °C, under argon atmosphere when not in use. The polymers were characterised by ^{1}H-NMR and HPSEC.

	Compund	g or mL	mmol
pPEGMA-475	2-bromo-2-methylpropionic benzyl ester	1.53 g	5.9
	PEGMA-475	0.026 mL	59
	PMDETA	1.2 mL	5.8
	Cu(I)Br	0.832 g	5.8
	Toluene	78 mL	-
pPEGMA-1100	2-bromo-2-methylpropionic benzyl ester	0.815 g	3.2
	PEGMA-1100	17.4 g	15.8
	PMDETA	0.660 mL	3.2
	Cu(I)Br	0.454 g	3.2
	Toluene	52 mL	-

Table 6.1: Quantities of the reagents used for the synthesis of polyPEGMA-475 and polyPEGMA-1100.

6.2.2.2 Quantification of protein concentration by UV spectroscopy

The calculated percent extinction coefficient ($A^{1\%}_{1cm}$) was of 1.45 for mAb solutions. For β-LG $A^{1\%}_{1cm}$= 9.6 [100], and for rAlbumin $A^{1\%}_{1cm}$ = 5.8 [99]. The protein and polyPEGMA blends, as well as the controls (polyPEGMA in buffer) were also analysed on Nanodrop without diluting to obtain a UV-Vis scan from 200 - 800 nm. All details related to this method are described in section 2.2.7 in Chapter 2.

6.2.2.3 Bulk Rheology

The rheometer used was an Anton-Paar (Graz, Austria) modular compact rheometers (MCR) 301. For the rheology measurements of rAlbumin solutions, a cone-and-plate CP50-1 (diameter = 50 mm and cone angle = 1 °) was used. For the analysis of

polymer-protein blends a cone-and-plate CP40-0.3 was used (diameter = 40 mm, cone angle = 0.3 °). To prevent evaporation of sample and to keep constant temperature of 25°C ± 0.1°C, an evaporation blocking system equipped with a peltier unit was used. Prior to measurements, all samples were allowed to equilibrate to room temperature (∼ 23°C) for at least 30 minutes.

Rotational tests (flow curves and viscosity curves) were performed by controlling the shear rate typically from 0.01 to 1000 s^{-1}, and measuring torque, shear viscosity and shear stress. To increase data validity and sensitivity of the method, each shear-rate step had a 60 second duration time during which the instrument was averaging over the collected data. Typically, two shear-rate sweeps (ramping down and up) were performed per sample, without waiting time between sweeps.

6.2.2.4 Micro-viscometer/rheometer on-a-chip

The microviscometer/ rheometer on-a-chip (mVROC), by Rheosense, Inc. (San Ramon, California, USA) was used for measurement of bulk viscosity at high shear rates. All samples analysed with the mVROC were filtered with 0.1 μm pore-size syringe filters (Millex-VV Millipore filters). For these measurements, the A05 chip was used and temperature was kept constant at 25°C ± 0.1°C using a water circulation system (ThermoCube, SS cooling systems, USA) (for additional information, see section 2.2.6.2 in Chapter 2).

6.2.2.5 High performance size exclusion chromatography for determination of level of protein aggregation

rAlbumin samples were analysed for their level of aggregation on HPSEC. β-LG and mAb solutions only as well as the blends of these proteins with the synthetic polyPEGMAs were also analysed for their level of aggregation. Details related to method and equipment are described in section 2.2.9.2 in Chapter 2.

6.2.2.6 HPSEC for synthetic polymers

During and immediately after synthesis, aliquots of polyPEGMA homopolymers were characterised using a chloroform/ TEA 95/5 % v/v HPSEC (or GPC) system to check solely for their molar masses and purity. For this purpose, the system was calibrated for conventional calibration with a mixture of narrow MW polystyrene standards commercially available (EasiVial PS-M, Agilent Technologies, UK).

The synthesised polyPEGMAs and PEG 8000 were analysed for MW and intrinsic viscosity on a chloroform/ TEA 95/5 % v/v gel-permeation chromatography system calibrated for triple detection (refractive index, 90 ° light scattering detector, and differential pressure). A narrow polystyrene was used as standard for detector response and inter-detector delay. Polyethylene glycol standards from Polymer Labs (Agilent, UK) were also analysed for comparison. All PEG/PEO samples were injected only once at concentrations 3-5 mg/mL, while the polyPEGMAs were injected at ∼2.5 mg/mL and in triplicate. The refractive index increment used for analysis of all PEG or PEO polymers was dn/dc = 0.053 mL/g, while for the polyPEGMA analysis dn/dc = 0.057 mL/g.

All equipment and method details for both HPSEC/GPC systems are described in section 2.2.9.4 in Chapter 2.

6.2.2.7 ^{1}H-Nuclear magnetic resonance

^{1}H-Nuclear Magnetic Resonance (^{1}H-NMR) spectra were recorded on a Br*ü*ker 400 MHz spectrometer (Br*ü*ker, Germany). Chemical shifts are reported in ppm (δ units) downeld from internal tetramethylsilane standard. Polymer samples were dissolved (1:3 parts) in $CDCl_3$.

6.2.2.8 Dynamic light scattering

Details related to this method are described in section 2.2.8.1 in Chapter 2. Measurement settings for rAlbumin size readings were at a constant temperature of 25 °C, performing 15 runs of 10 seconds each. For the β-LG, a total of 10 runs of 10 seconds each were performed. For mAb solution size measurements, 20 runs of 20 seconds each were collected. For β-LG and for IgG samples, measurements were performed at 25 °C. Analysis of polyPEGMA and protein blends were measured at the same conditions as those chosen for each protein, respectively. The polyPEGMA solutions (in buffer) were analysed at their original concentration (1, 10 and 25 mg/mL), while the protein and polyPEGMA mixtures were measured at a protein concentration of ∼1 mg/mL. An equilibration time of at least 5 minutes was set before the measurement started. For all protein samples, size measurements were made in triplicate with fresh aliquots for each reading.

6.2.2.9 Microfluidic chip sodium-dodecylsulfate polyacrylamide gel electrophoresis (SDS-PAGE)

Details related to this method are described in section 2.2.13.1 in Chapter 2. rAlbumin samples used for this experiment were: 200 and 20 mg/mL at 5 °C T= 4 weeks; and

200 and 20 mg/mL at 60 °C at T= 4 weeks.

6.2.2.10 Tensiometry

All the detailes referring to this technique are described in section 2.2.10 in Chapter 2. A freshly prepared filtered solution (0.1 μm pore-size syringe filters, Millex-VV, EMDMillipore, USA) of polyPEGMA-475 in buffer at 1 mg/mL was analysed.

6.2.2.11 Detection of critical micellar concentration by fluorescence spectroscopy

Polysorbate-80 (PS-80) and polyPEGMA solutions were prepared in 10 mM His-His.HCl pH 6.0 buffer, by dissolving the materials in purified water to prepare stock concentrations (100 μM for PS-80, and 5 mg/mL for polyPEGMAs) and diluting with water to achieve all concentrations for the experiment.

A stock solution of pyrene (Sigma-Aldrich) in acetone was prepared at a concentration of 0.05 mg/mL. Aliquots of 24 μL from the pyrene stock solution were transferred to capped clean glass vials, and left to evaporate the acetone. After solvent evaporation, surfactant and polymer dilutions were individually added to each of the vials yielding a final concentration of 6×10^{-7} M of pyrene (each vial containing 10 mL of solution). This procedure was done in triplicate for each dilution per studied compound. The samples were shaken well and then incubated at 25 °C overnight away from light in a water bath with a gentle oscillatory shake (∼70 rpm). After this, the samples were measured on a Varian Cary Eclipse fluorescence spectrophotometer with an excitation wavelength of 342 nm. The emission spectra was collected at a scan rate of 10 nm/s, emission slit of 2.5 nm, from 350 to 400 nm. The pyrene fluorescence peaks between 373-374 nm

(peak I) and 383-385 nm (peak III) were obtained and its ratio ($I_{peakI}/\ I_{peakIII}$) was calculated per sample.

6.2.2.12 Protein solubility assay using polymers

Polymer solutions were prepared at 40% w/w in separate acidic and basic buffer components. In this study, the sample buffer was 10 mM His-His.HCl pH 6.0. The basic polymer solution was titrated with the acidic polymer solution while being thoroughly stirred. Protein samples were prepared in 10 mg/mL stock solutions in the same buffer.

In a 96-well plate (UV-Vis clear plates, Greiner Bio-One, Ltd., UK) the buffer was loaded, followed by the protein sample and then the polymer solution, mixing well. Each protein-polymer blend was prepared in triplicate. The microplate was covered and left in an incubator at 25°C overnight. After this time, the microplate was centrifuged (Heraeus Megafuge 11R, Thermo Fisher Scientific, UK) at the temperature of the assay at 338 g for up to 2 hours at a time, until a precipitation or distinct phase-separation was observed. Subsequently, 70 μL of supernatant from each well were transferred to a new UV-Vis clear 96-well plate. These solutions were then measured for absorbance at 280 nm on a UV-Vis plate reader (FluoStar Optima, BMG Labtech, Germany). A UV-visible scan was obtained from these solutions, including for the polyPEGMA solutions only, without any protein added (considered as control solutions). The absorbance at 280 nm data was converted to calculate the concentration of protein present in each well. The logarithm of protein concentrations were plotted versus % w/w of polymer present in solution. The slope of the graph was reported as the apparent solubility for the studied protein in the tested buffer containing the selected polymer. The reported solubility values for the proteins tests were used for relative comparison only, therefore being denominated as 'apparent' solubility.

This method was used with the commercially available polymer polyethylene glycol (PEG) with molecular weight of 8 kDa (Alfa Aesar, UK) as well as the poly-poly(ethylene glycol)methyl ether methacrylates (polyPEGMAs) prepared in this work. The % w/w of polymer used had to be changed between the different proteins and when using different polymers.

6.3 Results and Discussion

6.3.1 Part I - The effect of thermal stressing of rAlbumin solutions on its solution rheology

Vials of rAlbumin at two concentrations (200 and 20 mg/mL) were left at 60 °C for 28 days to thermally stress the protein into forming higher order aggregates. From literature, the melting temperatures of human serum albumin have been reported to be a two-state transition with Tm_1 of ∼56 °C and Tm_2 of ∼63 °C, due to the sequential unfolding of the protein's domains [27, 210, 211]. Since rAlbumin solutions were biopharmaceutical preparations formulated to withstand stresses and prevent protein agregation, the chosen temperature to thermally stress this protein had to be approximate to the monomer's 'melting' temperature.

From the evaluation by HPSEC, those samples at 200 mg/mL showed clear signs of loss of monomer, with increasing presence of dimers, trimers and evidence of higher MW species. Figure 6.4 shows a drop in monomer peak area of ∼7 %, with the corresponding increase of higher MW species distributed between dimer, trimer and other oligomers, but no evidence of lower MW species. At the last time point, it was noticed an increase of monomer, contradicting the previously seen tendency of monomer loss. This sudden increase in monomer content, was most likely related to a large fraction of proteinaceous

material that was retained on the 0.45 μm pore-size membrane centrifuge filters, since it was noticed that it took longer time to fully centrifuge the samples from this time point. Therefore, with much of the protein aggregates retained at the filter's membrane, it reduced the quantity of soluble protein aggregates present in solution which most certainly did not correspond to the material's true level of aggregation.

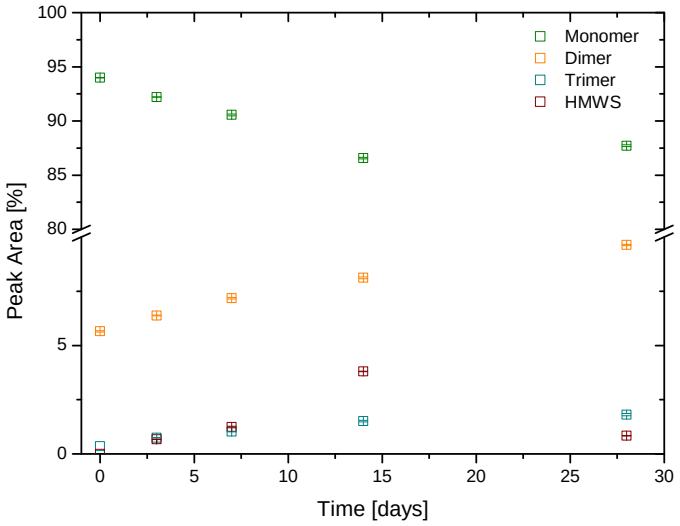

Figure 6.4: Level of aggregation of 200 mg/mL rAlbumin sample after 4 weeks at 60 °C for 4 weeks. Results shown are average values of analysis in triplicate, with error bars corresponding to the standard deviation of these measurements.

Examples of HPSEC chromatograms are shown on Figure 6.5, for both dilutions of 200 and 20 mg/mL of rAlbumin. The 20 mg/mL sample at T=0 weeks evidenced the typical rAlbumin chromatogram with monomer, dimer and trimer peaks, but for the remaining time points, the trimer peak was not observed. The assessment of this sample's aggregation level by HPSEC suggested that the aggregation was occurring at a lower rate than that experienced by the higher concentration.

Control samples, at the same concentrations, were also analysed by HPSEC and showed a very slight decrease of monomer with corresponding increase in dimer content,

generally showing that the samples were stable at this concentration (detailed data is shown in Tables C.1(a) and C.1(b), in Appendix C).

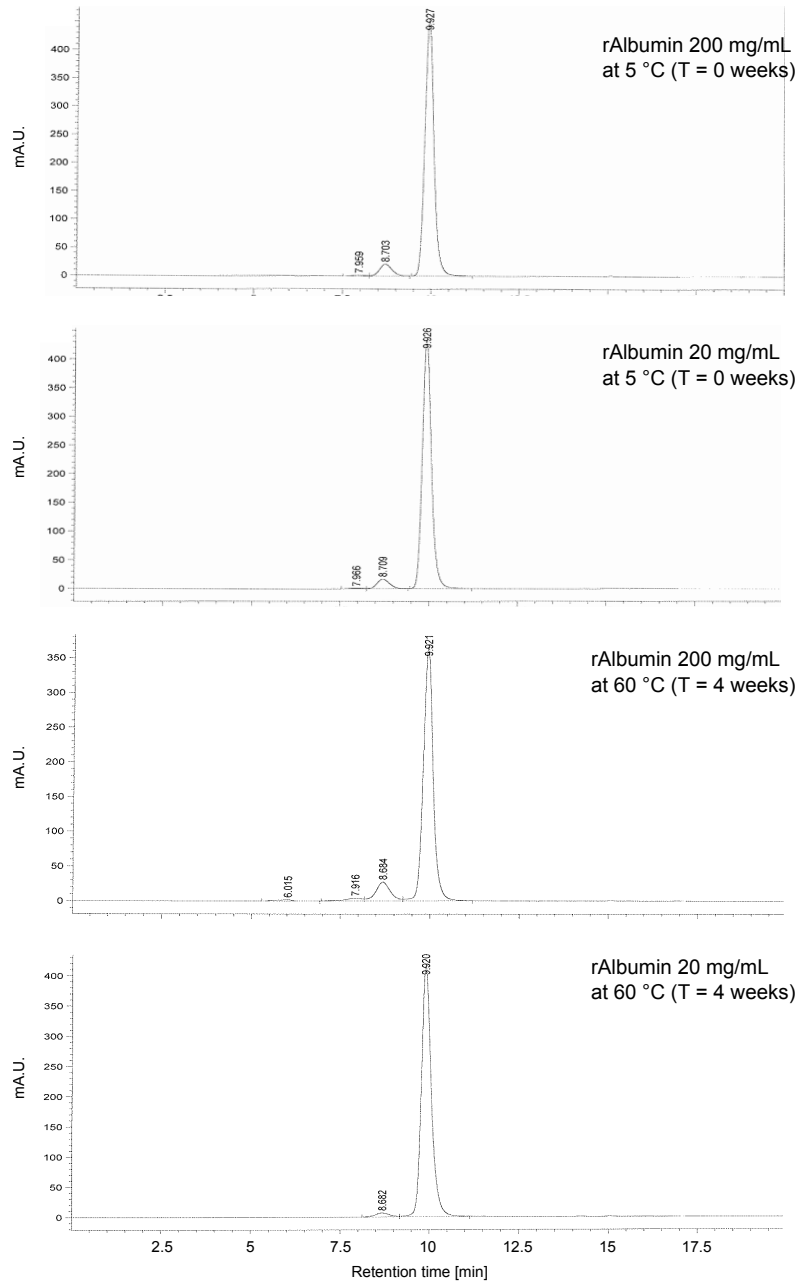

Figure 6.5: Example of HPSEC chromatograms from rAlbumin samples at 200 and 20 mg/mL exposed to 60 °C for 4 weeks. A comparison between chromatograms shown for the 200 and 20 mg/mL at 5 °C, T= 0 weeks (control) is shown against samples at the same concentration but after study completion (at 60 °C, T= 4 weeks). All samples subjected to HPSEC analysis were diluted to ∼10 mg/mL and filtered with 0.45 μm centrifuge-filters.

The data observed after DLS analysis of these same samples at the chosen times points for the HPSEC study, demonstrated further evidence of protein aggregation occurring with time exposure at 60 °C. Those dilutions obtained from 200 mg/mL sample showed larger difference compared to the samples analysed from 20 mg/mL of rAlbumin.

With the 200 mg/mL samples, an increase in protein aggregate species were observed by the presence of the second peak which had increasingly higher peak area with time. Comparatively, the analyses from 20 mg/mL of rAlbumin also showed peaks at higher mean hydrodynamic diameter but at lower intensities. By volume distribution, these samples evidenced less influence of these larger scatterering species, since the only peak detected did not seem to trend to much higher hydrodynamic diameters. However, the changes observed on intensity plot for samples diluted from 200 mg/mL rAlbumin, had a marked deviation to higher H_D of the peak detected by volume distribution. Detailed data are shown in Table C.2 in Appendix C.

All samples were analysed after preparing fresh dilutions at 1 mg/mL, without any further filtration. However, the rHA sample originally at 200 mg/mL after 4 weeks at 60 °C had to be filtered using 0.45 μm centrifugal concentrators to remove large proteineaceous particles to record feasible DLS measurements.

These results, confirmed the tendency seen with the HPSEC results. Both of these experiments showed that, with time, the protein aggregates formed at 200 mg/mL of rAlbumin monomer were demonstrating higher sizes towards 1 μm of diameter and were becoming insoluble.

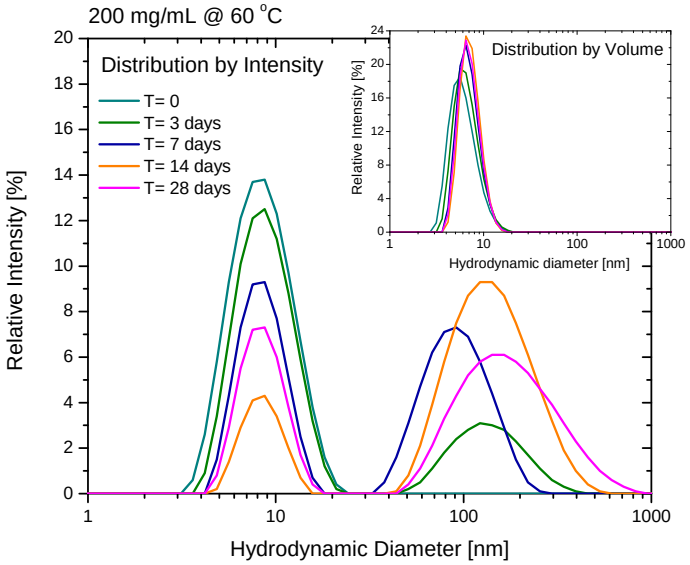

(a)

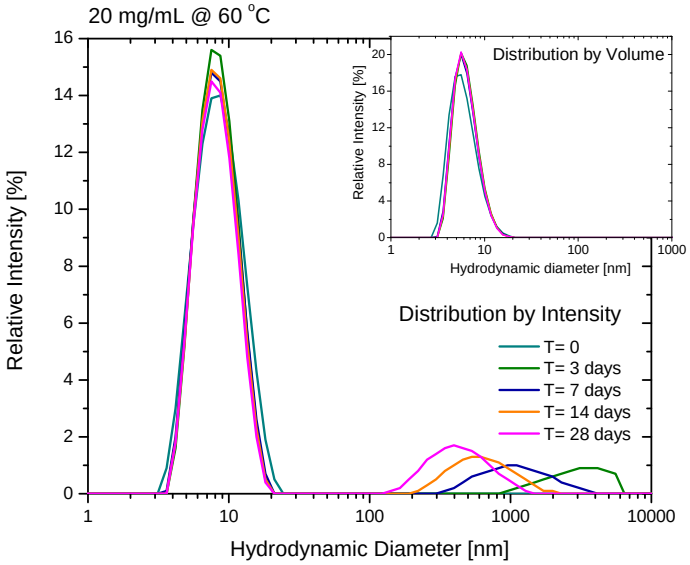

(b)

Figure 6.6: DLS data of rAlbumin samples thermally stressed for 28 days at 60 °C, showing hydrodynamic diameter of detected peaks by intensity (large graph) and volume (inset graph) distributions. **(a)** Samples diluted from 200 mg/mL rAlbumin. **(b)** Samples diluted from 20 mg/mL.

μ-SDS-PAGE analysis comparing dilutions from each concentration of rAlbumin

after 4 weeks at 60 and 5 °C was performed. The comparison with samples at 5 °C served as control, where samples where not expected to show any signs of aggregation (as demonstrated by HPSEC). As discussed previously in Chapter 3, the correspondence to albumin monomer was attributed to the band at ∼53-54 kDa. A slight band at ∼110 kDa observed with the non-reduced 200 mg/mL T= 28 days at 60 °C corresponded to the increase of dimerisation of rAlbumin after thermal stressing. The remaining analysed non-reduced samples also demonstrated a peak/ band at this MW, having a peak area of ∼3 %, compared to the ∼10 % observed for the fully aggregated sample. At reducing conditions the band at ∼60 kDa was present in all samples with peak areas of >96 %, indicating an almost full reduction of the dimers detected in non-reducing conditions.

Although the 200 mg/mL sample presented higher aggregation levels and contained species of higher oligomeric association than trimers (in HPSEC and DLS), both these nor trimers were not detected with μ-SDS-PAGE. Species of higher MW than 240 kDa would not be detected with this system, and the trimers were most likely present at too low concentration to be detected - note that even with the samples at 5°C, trimers were not detected.

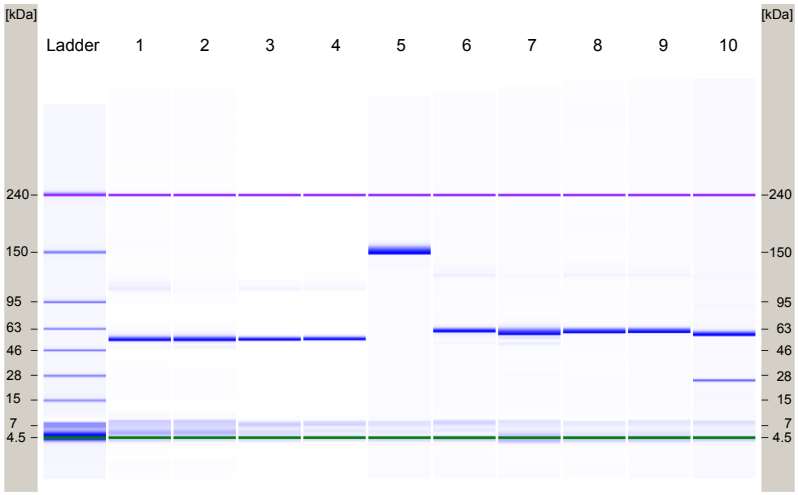

Figure 6.7: Gel image for rAlbumin samples after storage at 60 °C for 28 days. At non reducing conditions, lanes: 1) 200 mg/mL dilution, at 60 °C, T= 28 days; 2) 20 mg/mL dilution, at 60 °C, T= 28 days; 3) 200 mg/mL dilution, at 5 °C, T= 28 days; 4) 20 mg/mL dilution, at 5 °C, T= 28 days; 5) non-reduced control mAb sample. At reducing conditions, lanes: 6) 200 mg/mL dilution, at 60 °C, T= 28 days; 7) 20 mg/mL dilution, at 60 °C, T= 28 days; 8) 200 mg/mL dilution, at 5 °C, T= 28 days; 9) 20 mg/mL dilution, at 5 °C, T= 28 days; 10) reduced control mAb solution. The mAb sample was used for system suitability purposes.

Up to 28 days the samples had a constant visual appearance where those solutions with 200 mg/mL of rAlbumin had a light yellow colour, whereas the 20 mg/mL solution presented no colour, and both typically did not show any signs of opalescence nor visible insoluble particles. However, after the fourth week at 60 °C, the samples at 200 mg/mL had a gel-like viscous residue formed at the bottom of its vials. These samples were opalescent but did not have any visible particulates or fibers.

The rheology profiles of these samples at each of the time points are shown in Figures 6.8(a) and 6.8(b). At the initial time point, before submitting the samples to high temperatures, the solutions at both concentrations showed a Newtonian-like behaviour, with constant shear viscosities along the applied shear rates. This had been observed previously for the formulated rAlbumin solutions addressed in Chapter 3. However, the rheological behaviour of those samples at 200 mg/mL exposed to 60 °C

changed with time. After 3 and 7 days, the samples exhibited increased viscosities at low shear rates, resembling an apparent yield-stress behaviour. The material exposed to 60 °C after 14 days showed signs of transition in its profile. At 28 days, the sample clearly had signs of shear thinning, that of a gel-like fluid (slope <-1).

Apart from these changes in behaviour, particularly at low shear rates, the samples seemed to show constant viscosities at the higher shear rates ($> 100\ s^{-1}$), with exception of the sample at T= 28 days.

Those samples at 20 °C did not show signs of change in their rheological profiles nor a significant variation of their shear viscosities. This correlated well with the data shown for HPSEC, DLS and μ-SDS-PAGE, where it was proven that the degree of rAlbumin aggregation was much lower when compared to the solutions at 200 mg/mL also at 60 °C. Particularly from the DLS data, it was seen that the 20 mg/mL samples had an increasingly higher level of aggregation but of low relative volume fraction in the solutions. Therefore, the small amount of protein aggregates present did not affect these samples' rheological behaviour, at least at a level detectable by CP rheology and at these conditions.

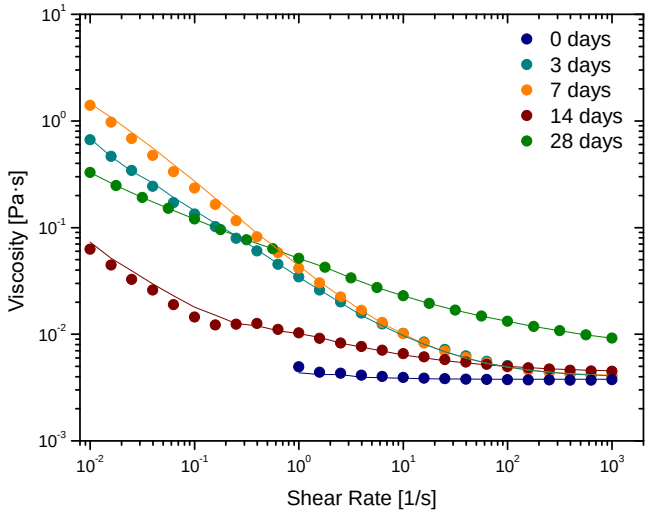

(a)

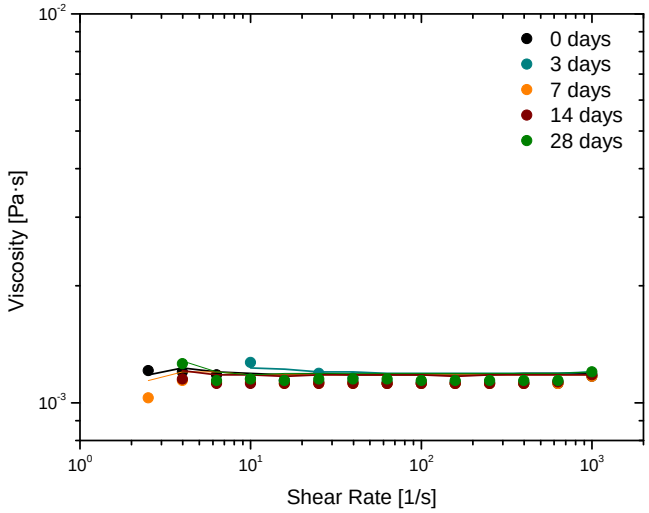

(b)

Figure 6.8: Cone-and-plate rheology data for rAlbumin samples along the time exposed to 60 °C, up to 28 days. **(a)** 200 mg/mL rAlbumin samples. **(b)** 20 mg/mL rAlbumin samples.

Following from the discussions and conclusions of the previous chapters in this thesis, and from literature evidencing the effect of PS-80 in the rheology of globular protein solutions [74, 143], the results shown here point to the fact that this non-ionic surfactant was responsible for the Newtonian-like behaviour observed for the rAlbumin

samples at the initial time point. In the case presented here and based on the literature, we assumed that the PS-80, being a surface active molecule, would out-compete the albumin species to the air-water interface present when using the cone-and-plate. In our data, after protein aggregation was induced by increased temperature, the fact that the rheological profile showed a change to an apparent yield stress behaviour could be an indication that the surfactant was not enough to prevent the protein species from reaching the air-water interface. It remained uncertain whether this change was caused from presence of protein aggregates or solely albumin species partially unfolded, exhibiting higher areas of hydrophobic patches. Further studies should follow in order to determine this effect.

The change in rheological behaviour, from the apparent yield stress behaviour to a shear thinning behaviour was attributed to the higher levels of aggregation. Visually, the samples exposed to 60 °C after 28 days did evidence signs of gelation. From the literature, it is known that albumin can create gels after thermal stressing [61, 212]. These properties have been discussed to originate from the formation of aggregates, which create an inter-particle network [210].

Also present in this formulation buffer was NaCl, at 145 mM, which could also impact on the rheological results. Recalling results from Chapter 3 regarding the dilution of rAlbumin solutions provided from the commercially available stock into a 145 mM NaCl only buffer, showed that the apparent yield stress properties were increasingly evident with higher dilution of these solutions. As the concentration of salt was maintained in the studies in that chapter, the presence of PS-80 and protein were gradually reduced as the dilutions progressed. It was clear that there was tendency towards an apparent yield stress rheological profile at the lower shear rates in these solutions, and it was suggested that it was this difference that mainly contributed to the changes observed in rheology. The study shown in the present chapter aims to support

this suggestion, by showing that after a 3 days at extreme thermal stress, the effect of PS-80 on surface activity was no longer seen on the rheology of such rAlbumin samples.

6.3.2 Part II - Novel use of polyPEGMA brush-type polymers as additives in protein solutions and their effect in rheology

In this section we describe the synthesis and use of polyPEGMA brush-type polymers as additives in protein solutions. As mentioned earlier, the aim was to synthesise homopolymers poly[poly(ethylene glycol) methyl ether methacrylate]. Two compounds were synthesised aiming for a 10 000 Da molecular weight each, using as macromonomers the PEGMA-475 and PEGMA-1100, both commercially available PEG-methacrylates, differing only in the chain length.

It was discussed earlier that brush-like polymers based on PEGMAs can be stimuli-responsive, with temperature as an example of a stimulus [201, 213]. The PEG chain length has been shown to impart solubility limitations when it comes to temperature response in aqueous environment, i.e. beyond a lower critical solution temperature (LCST) the materials tend to precipitate [201]. This is an important factor to consider for our purposes, since biopharmaceutical formulations are typically tested for protein stability at high temperature (40 °C) and for long periods of time. Therefore, it was important to avoid phase transitions that could affect the protein's native state even though it is a reversible event [201]. The macromonomers chosen here are known to have a high LCST in aqueous conditions, well above 40 °C. The LCST of these compounds tends to increase with chain length, e.g. LCST of PEGMA-475, estimated to be ∼90 °C [199, 201]. In the case of PEGMA-1100, as it comprises 22-23 units of PEG versus its methacrylate backbone, it remains soluble in water even at temperatures ∼ 100 °C [213].

6.3.2.1 Synthesis and characterisation of polyPEGMAs

The synthesis of the brush-type PEG based polymers was performed by controlled ATRP. The initiator for this synthesis, 2-bromo-2-methylpropionic benzyl ester (**3**), was synthesised as shown in Figure 6.9, by acylation of benzyl alcohol (**2**) with 2-bromo-2-methylpropionyl bromide (**1**) at freezing conditions, as per similar reactions described in literature [214]. The yield obtained was ∼63 %. Compound 3 was further purified and dried to ensure it was free of solvents and at high purity. Its ^{1}H-NMR spectrum in $CDCl_3$ is shown in Figure C.1 with its description in Appendix C.

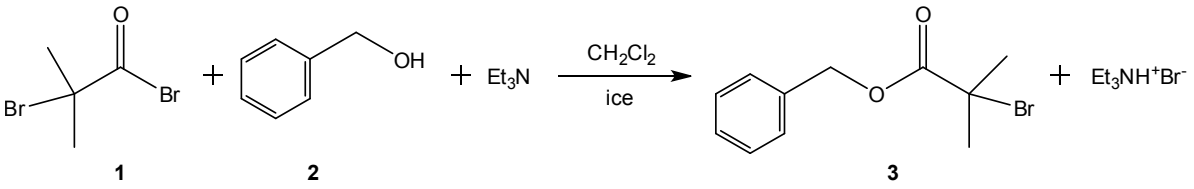

Figure 6.9: Scheme for the synthesis of ATRP initiator. **1** - 2-bromo-2-methylpropionyl bromide; **2** - benzyl alcohol; Et_3N - triethylamine; reaction conditions were dichloromethane (CH_2Cl_2) and ∼0 °C; **3** - 2-bromo-2-methlypropionic benzyl ester; Et_3NHBr - triethylammonium bromide.

The homopolymers poly[poly(ethylene glycol) methyl ether methacrylate] (**5a** and **5b**) were synthesised in presence of Cu(I)Br catalyst and the ligand PMDETA (N,N,N',N',N"-pentamethyldiethylenetriamine) from polymerisation of monomers PEGMA-475 (**4a**) or PEGMA-1100 (**4b**) [203, 208, 214]. The products were isolated and purified as described in the methods, yielding highly pure homopolymers corresponding to compounds **5a** (yellow viscous liquid) and **5b** (white powder). For simplicity, the two poly[poly(ethylene glycol) methyl ether methacrylate] polymers synthetised will be referred in this work as polyPEGMA-475 or pPEGMA-475, and polyPEGMA-1100 or pPEGMA-1100, respectively corresponding to products **5a** and **5b**.

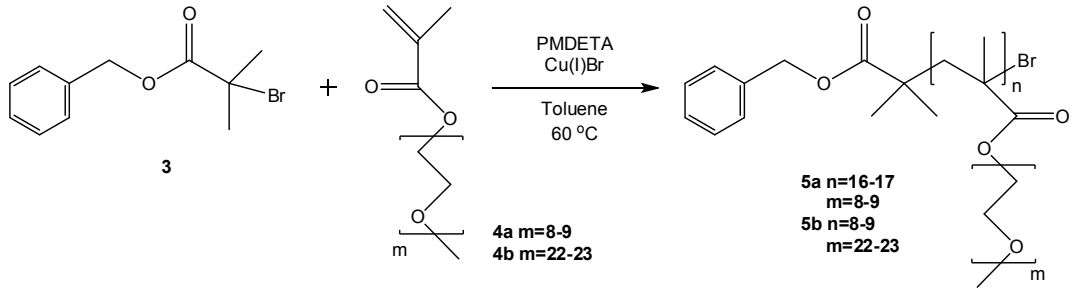

Figure 6.10: Scheme for the synthesis of poly[poly(ethylene glycol) methyl ether methacrylate] by ATRP. **3** - 2-bromo-2-methlypropionic benzyl ester; **4a** - PEGMA monomer 475 g/mol; **4a** - PEGMA monomer 1100 g/mol; reaction conditions were PMDETA (N,N,N',N',N"-pentamethyldiethylenetriamine), Cu(I)Br, in toluene at 60 °C; **5a** - polyPEGMA-475; **5b** - polyPEGMA-1100.

Synthesis of these brush-like homopolymers was carried out up to one hour, yielding ∼90 % conversion of monomer to polymer. Monomer conversion was calculated via ^{1}H-NMR analysis of aliquots during synthesis. This estimation was made by comparing the integration of the vinyl protons present in the monomer (δ = 5.71 and 6.31 ppm, corresponding to one proton each) to the overall integration of protons corresponding to the ester protons of monomer (δ = 4.41 ppm) and polymer (δ = 4.27 ppm).

^{1}H-NMR analysis of both polymers evidenced peaks characteristic to the PEG pendant chains (brush) of the polymer, at δ = 3.37 ppm (methoxyl protons, **g**) and δ ∼ 3.64 ppm (methylene protons, **f** (Figure 6.11) [204]. Another signal corresponding to protons present in the PEG brush were δ = 4.07 ppm (**e**), the ester protons. From the methacrylate backbone, the group of peaks in the range ∼0.6 - 1.2 ppm were assigned to the methyl protons (**d**), and the range ∼1.78 - 2.1 ppm to the methylene protons (**c**). The remaining peaks at δ = 7.30 ppm and 5.05 ppm, correspond to the aromatic (**a**) and the benzyl protons (**b**), present in the end group present in each homopolymer.

The degree of polymerisation could be estimated from the ^{1}H-NMR analysis of these polymers. This was estimated by fixing the integration of the aromatic protons (**a**, in

Figure 6.11) to 5, and integrating either the ester protons (**e**) or methoxyl protons (**g**). By dividing integrations of **e** or **g** by 2 or 3, respectively, it was estimated that for the polyPEGMA was constituted by polymerisation of 8-9 monomer units, and that polyPEGMA-475 was constituted of 16-17 monomer units (Figure C.2 in Appendix C).

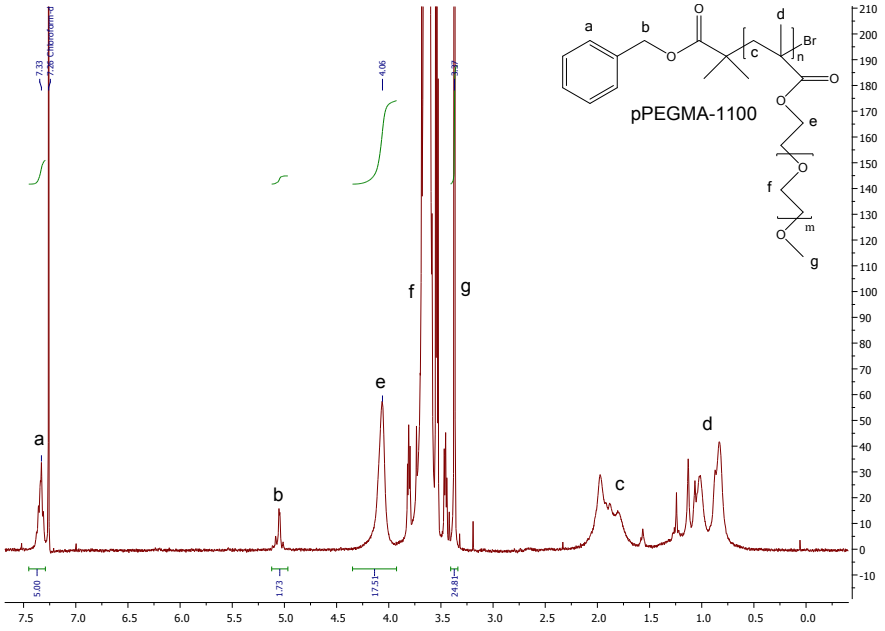

Figure 6.11: NMR spectra for poly[poly(ethylene glycol) methyl ether methacrylate]-1100. Sample was dissolved in $CDCl_3$.

The target MW for these homopolymers was at 10 kDa. HPSEC analysis, with triple detection, was performed to characterise these polyPEGMAs in terms of their purity, weight and intrinsic viscosity. Table 6.2 compares the calculated peak MW (Mp), number-averaged MW (Mn), weight-averaged MW (Mw), polydispersity index (PDI = Mw/Mn), and calculated intrinsic viscosity for the polymers analysed. The synthesised polyPEGMAs were analysed on the same HPSEC system along with linear PEG or PEO of Mp ranging from 1970 Da to 43580 Da. These linear PEG polymers were compared to the polyPEGs regarding the intrinsic viscosity and MW.

From triple detection HPSEC analysis, the calculated MW for the polyPEGMAs

was revealed to be quite similar, with the polyPEGMA-475 having slightly lower Mn (∼10709 Da) compared to the poly-PEGMA1100 (∼10973 Da). This corresponded to the expected MW target. The polydispersity index was relatively low for both polymers, indicating a narrow range of polymer sizes. Since the PEG/ PEOs chosen for analyses were of high purity grade for standard purposes (except for PEG 8000), it was expected that these materials would exhibit a PDI of ∼1.0.

Table 6.2: Data obtained from HPSEC calibrated for triple detection with PEG/ PEOs of standard quality (range 1970 - 43580). Mp - peak MW; Mn - number-averaged MW; Mw - weight-averaged MW; PDI - polydispersity index, corresponding to Mw/Mn. [1] - PEG 8000 of analytical grade, was the linear PEG used for protein solubility studies; [2] - polyPEGMAs were analysed in triplicate, where data is reported as average and standard deviation; [3] - [η] values obtained from analytical specifications of the PEG/PEO standards; [4] - [η] values calculated from this analysis.

Sample	**Mp** [g/mol]	**Mn** [g/mol]	**Mw** [g/mol]	**PDI** (= Mw/Mn)	**Lit. [η]** [3] [dL/g]	**Calculated [η]** [4] [dL/g]
PEG 1970	1441	1439	1439	1.00	0.0770	0.1014
PEG 3930	4803	4801	4802	1.00	0.1242	0.1046
PEG 6430	6425	6331	6350	1.00	0.1658	0.1747
PEO 12140	13474	13468	13468	1.00	0.2571	0.2793
PEO 20000	22176	22215	22225	1.00	0.3594	0.4100
PEO 26840	31385	31383	31504	1.00	0.4553	0.5784
PEO 43580	46790	46795	46796	1.00	0.6125	0.7337
PEG 8000 [1]	9815.00	9655.00	9748.00	1.01	-	0.2371
pPEGMA-475 [2]	12241 ± 107	10709 ± 136	12250 ± 78	1.14 ± 0.01	-	0.0682 ± 0.001
pPEGMA-1100 [2]	12848 ± 276	10973 ± 360	12279 ± 317	1.12 ± 0.01	-	0.1096 ± 0.002

The intrinsic viscosities measured for polyPEGMA-475 and polyPEGMA-1100 were 0.0682 ± 0.001 and 0.1096 ± 0.002, respectively. In comparison to the linear PEG/PEO, the [η] measured showed a linear increase with MW. polyPEGMA-475, although having a similar molar mass to polyPEGMA-1100, was the analysed polymer which yielded

the lowest intrinsic viscosity. As this physical parameter is dependent on the shape and aspect ratio of the molecule, and in this case, all polymers were measured in a good solvent and at the same temperature (∼25 °C), the overall shape/aspect ratio was expected to be the variable changing between polymer. Although both polyPEGMAs had a Mn ∼10 kDa, which is larger than the first three analysed PEG standards, the brush-like shape of the synthesised polymers clearly translated in a difference in intrinsic viscosity. Between the polyPEGMAs, it was clear from its [η] value that the shorter PEG chains of 475 Da (brushes), would probably yield a compact molecule, compared to the longer chains of 1100 Da. Even though these calculations were performed in chloroform, a good solvent for these analysed polymers, it is assumed that the materials should have similar tendencies when dissolved in water, another good solvent for PEG and PEGMA polymers [199].

The relatively low MW and the lower intrinsic viscosities of the polyPEGMAs were two important properties sought after for this study. If using these amphiphilic polymers as potential additives in protein formulations, minor viscosity increase due to its addition would be critical.

6.3.2.2 Study of the required concentration of polyPEGMA for the protein-polymer blends

The study of a concentration range of polyPEGMAs to use with the protein solutions was an important issue to address. Macromolecules such as PEG based polymers are known to influence the solubility of biomacromolecules, such as globular proteins, particularly forcing protein precipitation due to polymer-protein interactions in crowding solution conditions [215, 216]. From another perspective, since homopolymers polyPEGMAs are known for its self-assembly properties at aqueous conditions [199, 204], our additional

criteria in terms of concentration limits was to prevent micellisation of this material in a protein solution. By keeping the polymer concentration lower than its potential critical micellar concentration, the single chain brush polymers would be available in solution for possible inter-particle interactions, or if solely acting as amphiphiles, to be free to interact with any potential interfaces. Moreover, this is a common practice when adding polysorbates in biopharmaceutical formulations. For these two reasons, a protein 'solubility' test was performed with the polyPEGMAs, as well as an indirect assessment of their potential critical micellar concentrations.

The technique chosen to determine the critical micellar concentration (CMC) was an indirect method utilising a hydrophobic molecule (pyrene), which should preferably stay at the hydrophobic core of a micelle once it is formed in an aqueous solution [190]. The guest probe pyrene has been studied for this purpose since changes in its polar enviroment can be easily measured through its fluorescence emission. The intensity of its peaks change accordingly to the change in pyrene's local environment, and the fluorescence intensity ratio between its first (λ ~373 nm) and third peak (λ ~383 nm) is typically reported. The higher the ratio (measuring in fluorescence emission intensity) the more polar the environment is. The hydrophobic cores of micelles should contribute to high solubility of pyrene therefore allowing detection of micellisation [190].

For comparison purposes and to guarantee that the chosen technique details were adequate, detection of polysorbate-80's CMC was made (Figure 6.12). From the figure, the data showed that at lower concentrations of polysorbate the intensity ratio of peaks I and III was higher, whereas from polysorbate concentrations higher than 10 μM the ratio was reduced. Polysorbate-80 reported CMC is ~10 μM, with which our data is in agreement [190]. The change in this ratio was visually detected in the fluorescence emission scans ($\lambda_{excitation}$ = 342 nm), where the third peak increased its emission intensity (Figure 6.12 inset graph, arrow pointing at ~383 nm).

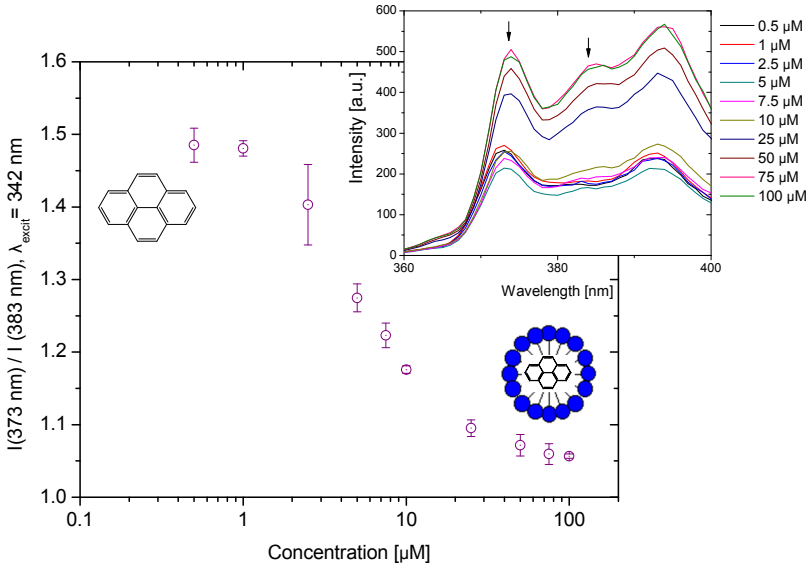

Figure 6.12: Determination of critical micellar concentration of polysorbate-80 by guest probe pyrene emission fluorescence intensity. The large graph refers to the ratio between intensities of peak I and III for pyrene, at λ ~373 nm and ~383 nm, respectively. The inset graph shows the fluorescence emission scans from 360 to 400 nm. Arrows are pointing to the peaks I and III.

The polyPEGMA polymers were also subjected to this experiment, but yielded completely different results. From Figure 6.13, it was concluded that these polymers did not seem to micellise at these experimental conditions (water, at room temperature). The intensity ratio measured, throughout the range of concentrations used (0.01 - 5 mg/mL), suggested that pyrene was always present in a polar environment. According to literature, micellisation of similar polyPEGMA homopolymers should occur promptly at aqueous environment and at room temperature [204]. However, the materials discussed in Hussain *et al.* (2008) although homopolymers composed of the same 475 and 1100 Da monomer units, and of similar MW, have a short chain poly(ethylene glycol) end group, which could contribute differently to its self-assembly.

From tensiometry studies, it was possible to measure the surface tension polyPEGMA-475 at 1 mg/mL, at the air-liquid interface. In a 1 mg/mL aqueous solution, polyPEGMA-475 at 1 mg/mL had a surface tension of 56.6 ± 0.18 mN/m,

having a similar surface tension at the same concentration in 10 mM His-His.HCl pH 6.0 buffer (55.6 ± 0.19 mN/m). Filtered (0.22 μm) pure water and filtered (0.1 μm) buffer had surface tension values of 72.9 ± 0.14 mN/m and 73.0 ± 0.34 mN/m, respectively. Since no significant change was observed in the polymer's surface tension in water vs. buffer, it was concluded that the polymer would not micellise at buffer conditions. The fluorescence emission spectra for this experiment is shown in Figure C.5 in Appendix C.

Therefore, these polymers were proven to be surface active at the air-liquid interface, but did not seem to micellise readily at room temperature in water. From this study a limitation in concentration could not be derived.

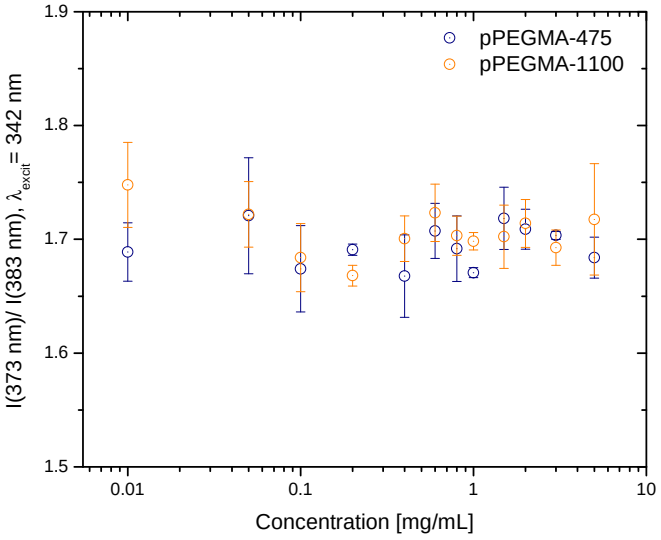

Figure 6.13: Determination of critical micellar concentration of polysorbate-80 by guest probe pyrene emission fluorescence intensity. The graph refers to the ratio between intensities of peak I and III for pyrene, at λ ~373 nm and ~383 nm, respectively, and compares data obtained for polyPEGMA-475 and polyPEGMA-1100.

The mAb and β-LG apparent solubilities were studied by testing if the protein would precipitate using a linear polymer (PEG 8000) and our synthetic polymers. In theory,

as the polymer concentration increases, the protein should have lower free volume and protein self-assembly should eventually lead to its own precipitation [215, 217]. A micro-plate technique adapted from ref. [217] was chosen for this assessment. Solutions were all in buffer conditions and the test was conducted at 25 °C, since these would be the same conditions for the rheology experiments.

As with the pyrene probe studies, apparent solubility of mAb and β-LG solutions were first prepared in presence of increasing concentrations (% w/w) of PEG 8000. From literature, it has been shown that using PEG of MW up to 6000 can yield different results, however from that MW onwards, the globular proteins seem to precipitate in presence of the same PEG concentration, regardless of chain length [215, 216]. When there a decrease of protein concentration, precipitation occurred and it is the slope of the linearity in that decrease which is often reported as the protein's 'apparent solubility' [215, 217].

Figure 6.14(a) shows this assessment for β-LG solutions. Comparing the results between the different polymers, it was observed that β-LG precipated at ∼8 % w/w of PEG 8000, while its concentration only started decreasing from ∼10 % w/w of polyPEGMA-1100 and from ∼13.2 % w/w of polyPEGMA-475. From Figure 6.14(b) this comparison did not produce significant changes across the polymers used, where these did not induce precipitation of the mAb.

The polymer concentrations identified to induce protein precipitation (or even just opalescence) were determined as a maximum polymer quantity in solution that could be used for further studies.

Although it is not reported that PEG and PEG-based materials should absorb at 280 nm, the solutions of polyPEGMA only were analysed for its UV-visible absorption and any residual absorbance at this wavelength was subtracted (see Figure C.4 in

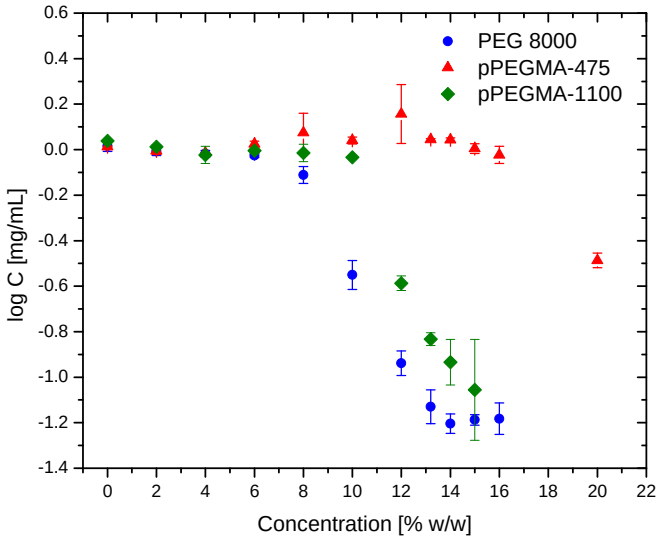

(a)

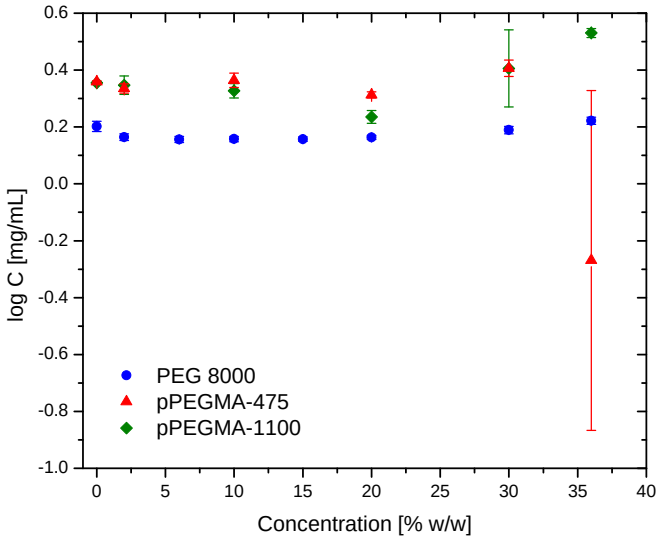

(b)

Figure 6.14: (**a**) β-LG and (**b**) mAb 'apparent solubility' assessment in the presence of increased concentrations (% w/w) of PEG 8000 and the synthesised polyPEGMAS (-475 and -1100). The experiment was conducted at 25 °C and all solutions were made in 10 mM His-His.HCl pH 6.0 buffer.

Appendix C).

6.3.2.3 Characterisation of protein-polyPEGMA blends

β-LG and mAb solutions, at ∼68 and ∼100 mg/mL concentrations respectively, were blended with three chosen concentrations of each polyPEGMA at: 1, 10 and 25 mg/mL. Even though the $[\eta]$ values of polyPEGMAs were demonstrated to be low in comparison to a linear polymer, there would be no interest in increasing its concentration in these blends to avoid the risk of increasing of overal sample viscosity.

The samples were prepared and characterised on basis of its size distribution by DLS, its level of aggregation by HPSEC, and for its rheology.

The polymer in buffer solutions were analysed upon UV-visible spectrometry to check for consistency in their preparation. Absorption maximum peaks at ∼230 and ∼258 nm were identified.

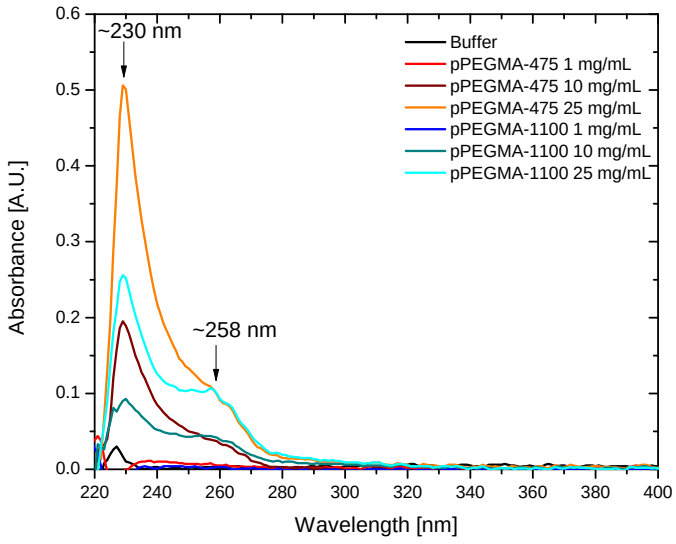

Figure 6.15: UV-Vis spectrum for polyPEGMA solutions in buffer.

In parallel to the DLS data measured from 1 mg/mL (to protein concentration) of each sample, the mean H_D were measured for each of the polymer only solutions (Figure 6.16). From both Figures 6.16(a) and 6.16(b) the data suggested that besides a main peak present in the intensity distribution, other populations of higher H_D were present at any of the concentrations studied. However, these larger sized populations constituted a low relative percentage of total sample, as per observed by volume distribution where the main peak had H_D towards the lower sizes ($\sim$4 - 5 nm).

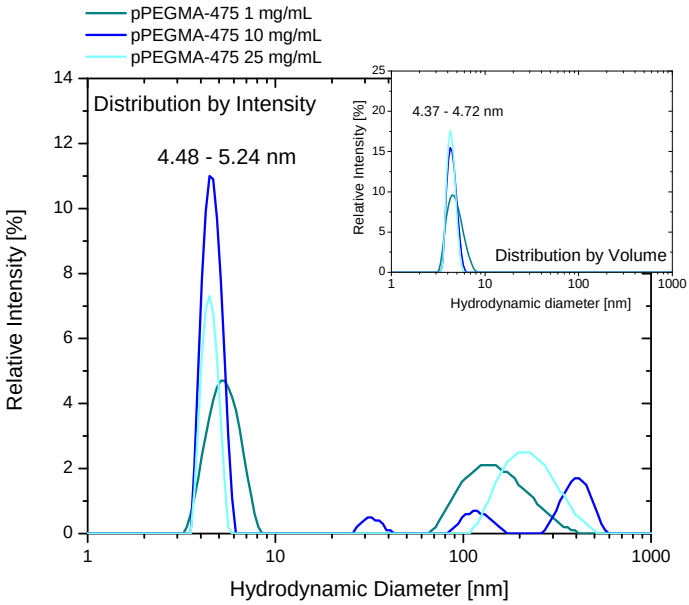

(a)

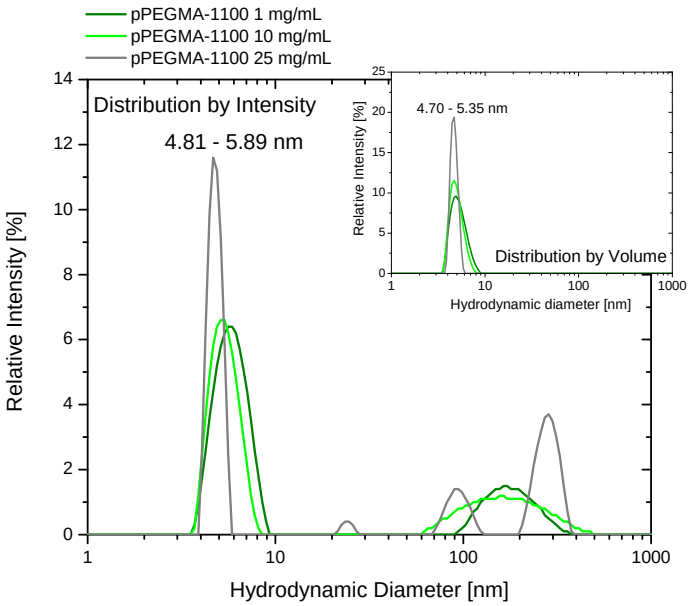

(b)

Figure 6.16: Hydrodynamic diameter size by intensity distribution (large graph) and volume distribution (inset graph) of polyPEGMA solutions in buffer. (**a**) DLS data for polyPEGMA-475 solutions; (**b**) DLS data for polyPEGMA-1100 solutions. All measurements taken at 25 °C.

A comparison of our data to the literature showed that the H_D at ∼4.48 - 5.24 nm and ∼4.81 - 5.89 nm, for polyPEGMA-475 and polyPEGMA-1100, respectively, corres-

ponded to the single chain sizes [204]. The larger sized scatterers detected by intensity distribution, were most likely self-assembled micelles of the polyPEGMAs [204]. Their heterogeneity and presence at low fraction in solution, would explain why it was not consistently possibly to detect these material's CMC by the guest probe technique.

Within each polyPEGMA's DLS data, the increase in concentration seemed to produce a narrower main peak at volume distribution suggesting lower presence of larger sized scatterers. Between the two polyPEGMAs, the hydrodynamic diameter size correspondent to single chain was slightly within the same range size, possibly due to similar MW even though the PEG-chain length was higher with polyPEGMA-1100.

The mAb-polymer blends presented consistent values for both intensity and volume distributions, where only the peak attributed to the mAb monomer-dimer equilibrium was detected at a $H_D \sim 11$ nm (by intensity distribution). By diluting the protein-polymer samples, the detection by light scattering of single chain polymers or possible self-associative polymer species was not possible. However, for the β-LG-polymer blends, higher diameter-sized populations were detected, although the original β-LG sample evidenced peaks at the similar size range. The results shown here were consistent to observations on DLS measurements of filtered (0.1 μm) β-LG samples discussed in chapter 4). These results also demonstrated that after filtration (0.22 μm) protein aggregates were always detected. DLS data are reported in tables summarising the mean peaks H_D by intensity and volume distribution measured for the polyPEGMA buffers and β-LG-polymer blends (Tables C.3 and C.4).

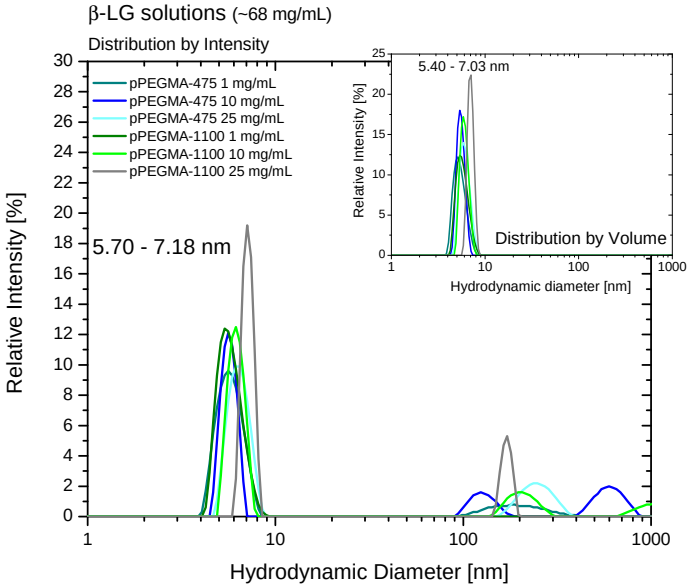

(a)

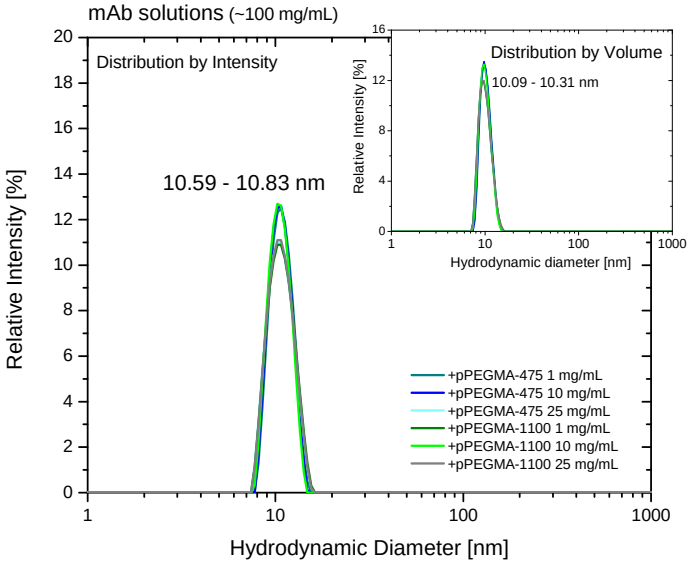

(b)

Figure 6.17: Hydrodynamic diameter size by intensity distribution and volume distribution of polyPEGMA and protien blends. (**a**) data for blends with polyPEGMA-475; (**b**) data for blends with polyPEGMA-1100. All measurements performed at 25 °C.

As well as with DLS data, the HPSEC analysis of these protein-polymer blends proved to show no differences between the blends and the protein only sample. The

chromatograms of β-LG and mAb blends with polymers showed the same peaks and at similar retention times. Examples of chromatograms for the studied blends are shown in Figure C.3 in Appendix C. Tables 6.3(a) and 6.3(b) summarise this HPLC data, where the relative mean peak areas (in %) showed consistency throughout the β-LG and mAb samples, respectively.

Table 6.3: Tables summarising the HPSEC peak area relative percentage for (**a**) β-LG and (**b**) mAb blends with polyPEGMAs.

(a)

		Peak Area [%]	
		Dimer	HMWS
β-LG		99.44 ± 0.01	0.56 ± 0.01
+ pPEGMA-475 [mg/mL]	1	99.40 ± 0.02	0.60 ± 0.02
	10	99.34 ± 0.17	0.66 ± 0.17
	25	99.47 ± 0.02	0.53 ± 0.02
+ pPEGMA-1100 [mg/mL]	1	99.29 ± 0.28	0.71 ± 0.28
	10	99.48 ± 0.22	0.52 ± 0.12
	25	99.48 ± 0.05	0.52 ± 0.05

(b)

		Peak Area [%]		
		Monomer	LMWS	HMWS
mAb		98.51 ± 0.04	0.21 ± 0.04	1.28 ± 0.00
+ pPEGMA-475 [mg/mL]	1	98.60 ± 0.05	0.14 ± 0.05	1.26 ± 0.00
	10	98.47 ± 0.18	0.26 ± 0.17	1.27 ± 0.01
	25	98.54 ± 0.06	0.17 ± 0.06	1.30 ± 0.01
+ pPEGMA-1100 [mg/mL]	1	98.57 ± 0.05	0.15 ± 0.04	1.29 ± 0.01
	10	98.56 ± 0.08	0.16 ± 0.07	1.28 ± 0.01
	25	98.51 ± 0.18	0.22 ± 0.20	1.26 ± 0.01

The protein-polymer blends, as well as the polymers solutions in buffer, were measured on a CP rheometer and on mVROC. The polyPEGMA solutions in 10 mM His-His.HCl pH 6.0 buffer had a Newtonian-like behaviour throughout the range of applied shear rates (Figure 6.18. The values measured with CP at shear rates ~600-1000

s^{-1} are close to the values measured with mVROC, with no significant change (see Table C.5).

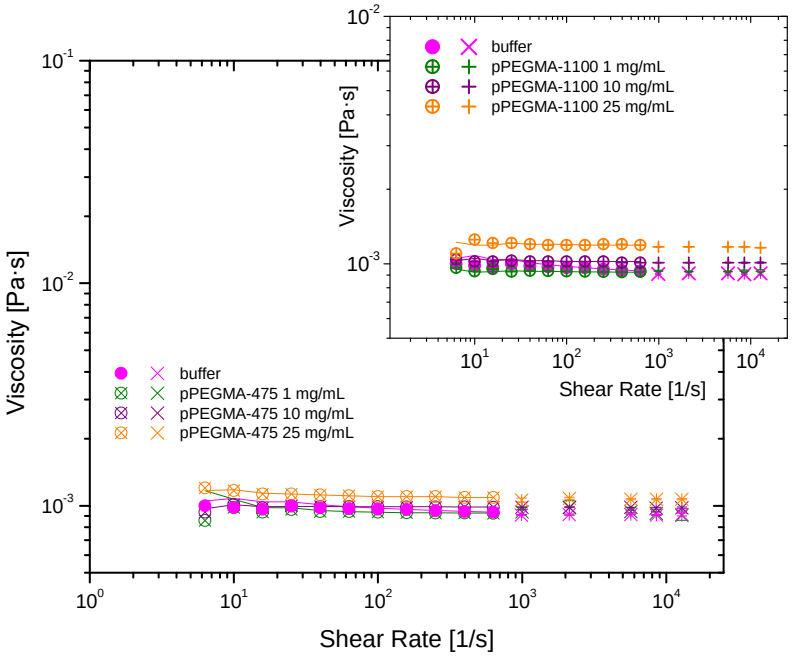

Figure 6.18: Cone-and-plate and mVROC rheology data for buffer and polyPEGMA solutions in buffer. Large graph - polyPEGMA-475 samples; inset graph - polyPEGMA-1100 samples. The cone-and-plate (CP) experimental data are circles (sweep down) and respective lines (sweep up). mVROC data are represented in crosses/pluses (average of triplicate measurements with error bars as standard deviation. Measurements performed at 25 °C.

Rheology data for the β-LG-polyPEGMA blends showed that adding these polymers to this protein solution (at ~68 mg/mL), did not change the protein's original rheological profile (Figure 6.19(a)). At low shear rates, yield-like behaviour was still dominant. With increased concentrations of added polyPEGMA-475, the viscosities at low shear rates (0.01 - 1 s^{-1}) had a slight decrease when compared to the protein only solution. However, the data with polyPEGMA-1100 did not show the same tendency.

At higher shear rates (>100 s^{-1}), the samples typically showed a tendency towards constant viscosity. The viscosity values at high shear rates (~600-1000 s^{-1}) were very

similar to the viscosities measured by mVROC, with the latter showing slightly lower values (∼0.2-0.3 mPa.s difference).

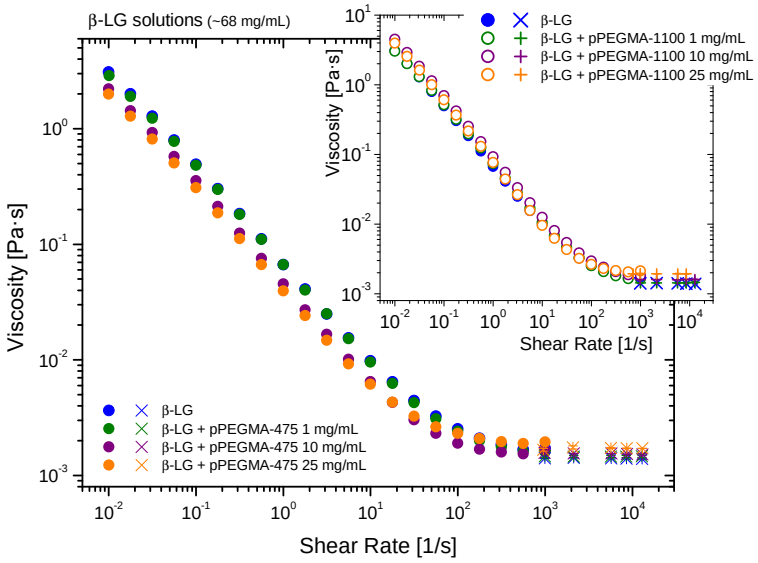

(a)

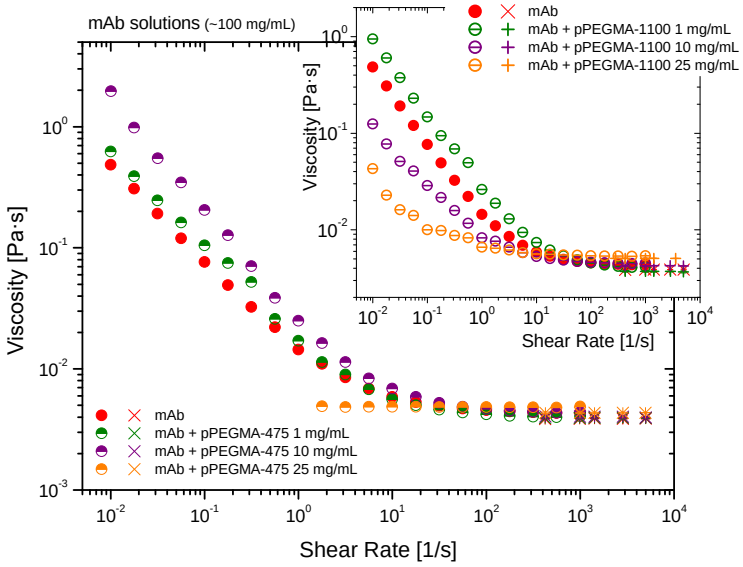

(b)

Figure 6.19: Cone-and-plate and mVROC rheology data for (**a**) β-LG and polyPEGMA blends, and (**b**) mAb and polyPEGMA blends, both in 10 mM His-His.HCl pH 6.0 buffer. Large graphs - polyPEGMA-475 samples; inset graphs - polyPEGMA-1100 samples. The cone-and-plate (CP) experimental data are circles (sweep down shear rates). mVROC data are represented as crosses/ pluses (average of triplicate measurements with error bars as standard deviation. All measurements were taken at 25 °C.

For the mAb-polymer blends, a noticeable change in these sample's rheological profiles was observed (Figure 6.19(b)). Between the mAb sample (∼100 mg/mL) and the mAb plus polyPEGMA at 1 mg/mL (both -475 and -1100), no major differences were observed at low shear rates, where a yield-like behaviour was prominent. However, for both polymers, the increase of its concentration to 25 mg/mL led to a change in the flow properties towards a Newtonian-like behaviour. This was evident with addition of polyPEGMA-475 at 25 mg/mL. The intermediate concentration of polyPEGMAs at 10 mg/mL produced different results at low shear rates. Nevertheless, the values of viscosities of the blends when the polyPEGMAs had their concentration increased, showed a tendency to increased viscosities. This was valid for all blends with each of the proteins.

In general, the rheology data showed that only when adding 25 mg/mL of polyPEGMAs, an effect could be observed on the rheology of the studied protein solutions. Considering the data discussed in previous chapters, and in the previous Part I of the present chapter related to the effects of polysorbate-80, we suggest that it is the surface tension of the solution's components what dominates the rheological response at the lower shear rates. The differences observed between the flow properties of β-LG and mAb to the presence of the amphiphilic polyPEGMAs may well be related to each of these protein's own surface-activity and its difference to the polymers surface tension at the air-liquid interface. However, possible interactions between the proteins and polymers could be considered, without involving the same thermodynamic mechanisms involved in surfactant-protein competition at air-liquid interfaces. Although it has been shown that brush-type copolymers of PEGMA have the tendency of repel interaction with proteins [207], to our knowledge no studies towards protein and homopolymer polyPEGMAs have not been made. Moreover, the PEG side-chain length could play an important role, since it confers higher hydrophilicity to the polymer [213]. This would

explain the difference in the behaviour noted between mAb + polyPEGMA-475 at 25 mg/mL and mAb + polyPEGMA-1100 at the same concentrations. Therefore, further work would be needed towards understanding what possible underpinning interactions could be involved between these chosen proteins and the polyPEGMAs synthesised here.

The effects of using relatively low MW brush-polymers, yielding low intrinsic viscosities compared to linear PEG polymers, were noted on the rheology since only at the highest concentration of polyPEGMAs a change in the flow behaviour was observed (difference $\sim$1 mPa.s). Protein samples (both β-LG and mAb) added with 1 mg/mL of either polyPEGMA had virtually no increase in solution viscosities (when $\dot{\gamma}$ $\sim$1000 s^{-1}), with an addition of 10 mg/mL yielding a viscosity difference of < 0.5 mPa.s.

6.4 Conclusions

This chapter presented studies with its aims following from the investigations discussed throughout this thesis. In the first part we aimed to further understand the role of PS-80 in protein solution rheology, by exploring the changes in flow behaviour along a time period after thermal stressing. In the second part, synthetic brush-type PEG-based polymers were used for their amphiphilic properties to explore their potential at reducing the yield behaviour exhibited by globular protein solutions, at low shear rates.

By stressing formulated rAlbumin solutions at 60 °C, it was observed that after 14 days, the protein had aggregated highly, culminating in formation of a gel after 28 days at 60 °C. Since gelation of albumin solutions have been demonstrated to happen at such temperature conditions but in faster rates [61, 210], it can be concluded that the additives present in this rAlbumin formulation were effective in delaying

the protein's degradation and aggregation, in agreement with literature [218]. In terms of the rheological aspects, this gradual protein degradation was observed by a change in flow properties which started as Newtonian-like fluids (non stressed samples), showing increased yield-like behaviours (after 7 days at 60 °C), followed by signs of shear-thinning.

To contribute to these findings, we recall the experiment in Chapter 3, where dilution of a stock formulation was made with 145 mM NaCl buffer. At these conditions, while the concentration of protein and polysorbate-80 were being diluted, its rheology showed that a yield-like behaviour was emerging, coinciding with reports in literature [143].

Again, as with the mAb solutions studied in Chapter 5, it is assumed that the aggregated material increases in its complexity throughout the time of the study, not only in terms of protein species contents, but also possible degradation products of the excipients involved could also influence the rheology data. As mentioned earlier, and according to literature, it was expected that at 60 °C polysorbate-80 would degrade by hydrolysis and oxidation, which could have effects on the rheology by consequently reducing the capability of this surfactant to out-compete the protein at the air-water interface [189]. Nevertheless, it is suggested that it was due to the level of rAlbumin aggregation that should have mostly contributed to the change of phase of this material, in agreement with other literature concerning human serum albumin [210].

Regarding the second part of this chapter, synthetic brush-type polyPEGMAs (polyPEGMA-475 and polyPEGMA-1100) were used as additives in protein solutions (β-LG and mAb, individually), with the aim of exploring their amphiphilic properties and effects on shear rheology. The study did not involve any thermal aggregation, instead it focused only on the use of these polymers in protein blends at room temperature. Following from the first part of this chapter, using conventional rheometry with

a cone-and-plate where an air-water interface is present, the rheology measurements revealed to be an indirect way to evaluate the surface activity of these polymers in comparison to polysorbate-80.

The polymers were studied for their capability of self-assembly, which was shown by DLS that it possibly occurs at low concentrations (1 mg/mL), although through indirect determination by fluorescence of pyrene as a guest probe, the CMC was not identified. Based on HPSEC triple detection, measurement of these polymers' intrinsic viscosity yielded low $[\eta]$ values when compared to linear PEGs of similar MW. For protein 'apparent solubility' studies, where it was expected that only excluded-volume play a role, the polyPEGMAs caused each of the proteins to precipitate at higher concentrations of polymer compared to PEG 8000. This corroborated with results from $[\eta]$ determination - lower aspect ratios would cause lower excluded volume effects. Finally, the analysis by aqueous HPSEC for protein purity showed that the presence of these materials did not alter the protein level of aggregation when compared to the polymer-free samples.

Rheology experiments showed that the increase of polymer, particularly at 25 mg/mL, did result in a slight increase of overall solution viscosity at the higher shear rates. At low shear rates, the three concentrations used of polyPEGMAs (1, 10 and 25 mg/mL), showed different results depending on the protein used in the mixture. For β-LG solutions, the rheological profiles remained to be yield-like, throughout the concentrations of added polyPEGMA. For mAb solutions, only the addition of 25 mg/mL of polyPEGMA-475 markedly changed the protein solution's flow behaviour from showing an apparent yield to constant viscosities throughout the applied shear rates. The polyPEGMA1100 at 25 mg/mL showed a similar result, although did not fully show a Newtonian-like behaviour.

We suggest that the reason for this could be with the different surface-activity of

each of the proteins, where it is known that β-LG forms strong elastic films at the air-water interface [167]. Therefore, although the polyPEGMAs are surface active amphiphilic materials, their surface activity might not reach such low surface pressure as those from these proteins, or even if compared to polysorbate-80.

Chapter 7

Conclusions and future work

7.1 Conclusions

7.1.1 The effect of protein concentration on the viscosity of a recombinant albumin solution formulation

In this work, a range of rAlbumin solutions, in a formulated buffer containing salt and a surfactant, were analysed for their rheological behaviour with the aim of understanding the effects of high protein concentration on the solution viscosity. Rheological measurements showed that the solutions (∼0.1 - 500 mg/mL) behaved as purely viscous fluids in the range of the applied shear rates. It was observed an increase in viscosity as the protein concentration was increased in solution.

Characterisation with regards the level of aggregation and species size proved that concentrating the rAlbumin had the effects of increasing solution viscosity and the change in relative composition of protein species.

The rAlbumin viscosity data was fitted using theoretical models known to predict suspension viscosity, which have been applied to protein solution rheology. Based on the shape or aspect ratio of particles and its packing fraction (or concentration), these equations are applied to hard spherical or quasispherical particles [153,159], and account

for interparticle distance [156]. However, these models did not predict successfully the viscosities for the entire range of rAlbumin concentrations.

The most successful viscosity predictions, up to 400 mg/mL, were obtained when using generalised versions of the original models [136, 137]. These revised equations introduce the concept of a weight-averaged intrinsic viscosity, allowing for its application to suspensions containing known concentrations of multiple particles of varying shape. Our results further highlighted the importance of considering this variation in composition within a protein solution, thus justifying its complete characterisation of oligomeric species. To our knowledge, no other analysis typically accounts for this variation within a sample containing one protein.

These recent generalised models assume that the jamming limit remains unaltered with changing composition. However, since the highest concentrations (450 and 500 mg/mL) were not computed with these fits, it may well be that at such concentrations this jamming limit may change. At such high concentrations, close to predicted jamming limits, other crowding effects such as protein-protein interactions should be also considered into these models. This possibly leaves space for these considerations to be accounted for in future theoretical models to be developed.

The simple model of rAlbumin was studied as an example of a 'real-life' biopharmaceutical formulation at high concentrations and to explore successful predictions of its solution viscosity. To be able to predict the effect of high concentrations (e.g. 400 mg/mL) of a monoclonal antibody based on species shape/ aspect ratio and its contents, is an ultimate goal in this field. However, this does not exclude the possibility of existing complex flow behaviours of protein solutions at high concentrations, or additional physicochemical variables related to protein degradation. Nevertheless, the application of these generalised models to biopharmaceutical formulation is important, as the need for developing protein drugs at high concentrations has been a demanding

parameter [5, 8]. Our results highlighted that the number of protein species, and its variation in composition, are key factors for predicting the solution viscosity of protein solutions.

7.1.2 The effect of insoluble protein aggregates on the rheology of beta-lactoglobulin solutions

β-LG excipient-free solutions were characterised by bulk and interfacial shear rheology. Solutions at various concentrations, characterised using conventional rheology instrumentation, evidenced an apparent yield stress behaviour at a low shear rate range (0.01 - 10 s^{-1}), whilst showing constant viscosities throughout higher shear rates. Comparing interfacial shear rheology, air-water interface-free bulk viscosity measurements, and tensiometry results, it was demonstrated that the observed yield-like behaviour was due to the formation of a protein viscoelastic film at the air-water interface, as present in conventional rheometry. Further application of theoretical equations to our data, concerning this yield-stress at lower shear rates, evidenced that our results were in agreement with literature. In addition, the results highlighted the importance of taking in account the presence of air-water interface in conventional rheology measurements of excipient-free protein solutions. In this practical perspective, the results contributed to a better understanding of rheological measurements of such samples, when using conventional rheometry (e.g. cone-and-plate), being such a commonly used instrumentation to evaluate the rheology of biopharmaceutical liquid formulations.

Our detailed results add to recent findings [78] in the extent that this hypothesis was applied to another globular protein model. This brings emphasis to the broad application of this knowledge to protein solution rheology, in particular by applying to the study of therapeutically relevant proteins such as monoclonal antibodies.

Further studies considered the effect of insoluble β-LG aggregates on the solutions' rheology, linking with their characterisation in size and quantification. The presence of insoluble proteinaceous particles was suggested to have an impact on the solution's flow behaviour, particularly at the lower shear rates. These findings highlighted that the content in protein species and their size characteristics of a protein solution are key factors to understand correctly and realistically evaluate its rheology. Moreover, the results emphasized the importance of understanding and interpreting better these measurements of protein solutions, looking at the widest range of shear rates possible, taking advantage of complementary rheometry instrumentation (e.g. mVROC besides the conventional rheometer), to extract useful information obtained throughout this range.

7.1.3 The rheology of a monoclonal antibody solution: a case study on the effect of aggregation of a model monoclonal IgG_1 on its solution rheology

Since the monoclonal antibody was provided formulated, several steps were performed not only to extract the excipients from this solution but to confirm similarity between batches of this macromolecule's excipient-free solutions. These were proved to have no evident difference between them.

The rheological response of the excipient-free mAb solutions, was similar to the response of β-LG samples: a yield-like behaviour at low shear rates was present, when using cone-and-plate or double-gap geometries. These observations highlighted the common features regarding this characterisation, observed across globular protein solution rheology, indicating that similar factors (e.g. macromolecule's surface-activity) were underpinning this type of sample's flow properties.

With the mAb solutions (not thermally stressed samples), the presence of insoluble protein particles was suggested to have a pronounced effect on the solution's flow behaviour at the lower shear rates, revealing a drop in viscosities. By thermally stressing the mAb samples at 40 °C, throughout a period of 6 weeks, the materials showed higher viscosities overall, but particularly was evident at the higher shear rates (∼600 - 1000 s^{-1}). However, their flow behaviour remained similar - still observing yield-stress at low shear rates (0.01 - 10 s^{-1}). Although relationships between computed yield values along sample time points were attempted, the hypothesis that the presence of generated protein aggregates (soluble and insoluble) do contribute to this yield-like behaviour remained unanswered. However, judging by quantifications made of the different types of aggregates (by size/ soluble/ insoluble), it was suggested that for this mAb, the large increase of soluble aggregates (detected by HPSEC and DLS) may have contributed the most to the increase of protein viscosity. Further analysis of the mAb's different species formed during this study revealed that for this particular case, its aggregation behaviour, i.e. aggregate reversibility, yielded implications in accurately quantifying these species.

The aim of studying mAb solution rheology under these extreme conditions, using orthogonal characterisation biophysical techniques, allowed an analysis at the molecular level to a detail that focused on variables commonly dismissed in the study of protein solution rheology.

7.1.4 Exploring the impact of surface active macromolecular excipients on the flow properties of protein solutions

Since it was observed, and supported by literature, that the yield-like behaviour at low shear rates on CP or DG rheology were likely to be related to protein surface-activity, it was then investigated the role of a non-ionic surfactant (polysorbate-80) commonly used in protein formulation. Indeed, the role of PS-80 in suppressing yield behaviour in

these measurements was observed in Chapter 3. In this chapter, however, formulated rAlbumin samples were stressed at 60 °C. In comparison to the previously discussed mAb study, thermally stressed rAlbumin samples evidenced a change of rheological behaviour throughout the period of time - starting as Newtonian-like fluids (non stressed samples), showing increased yield-like behaviours (after 7 days at 60 °C), and followed by signs of shear-thinning at the end of the study. This was suggested to be mostly related to the observed aggregation of albumin [212], and the loss of PS-80's competitive mechanisms at the air-water interface [189].

In another take of the findings reported so far, a study was also developed to use synthethic poly[poly(ethylene glycol) methyl ether methacrylate] polymers (polyPEGMA-475 and polyPEGMA-1100), with amphiphilic properties, to investigate their potential effects in protein solution rheology, in a similar perspective as the observed role of PS-80.

After polymer characterisation with ^{1}H-NMR and HPSEC, studies for polymer self-assembly and protein-polymer crowding effects were performed. The aim was to establish concentration limits when adding the synthetic macromolecules to the chosen protein solutions (β-LG and mAb). The physicochemical properties of the polymers, measured directly (MW and intrinsic viscosity) or indirectly (e.g. CMC determination), helped understanding the rheological results obtained for the studied protein-polymer blends. The results suggested that a change in flow behaviour, from the typical yield observed on excipient-free protein solutions, could only be suppressed towards a Newtonian-like behaviour if higher concentrations of the polymers were used - this was observed when mixing with a $\sim$100 mg/mL mAb solution. The almost unchanged yield-behaviour observed with the $\sim$68 mg/mL β-LG blends highlighted the importance of having sufficiently surface-active additives present in formulations to minimise the yield-like behaviour, since this protein is known to rapidly form strong elastic films at

the air-water interface [167].

Overall, this chapter's results highlighted the importance of understanding the underpinning molecular interactions governing protein solution rheology, by relating these to commonly used excipients in protein formulations and their possible mechanisms of action.

7.2 Future Work

Regarding the effect of concentration on the viscosity of protein solutions, it was clear that current theoretical models are simplified to a point which its applicability is no longer possible when concentrations reach higher values. Other factors at this range (in the case of rAlbumin, >400 mg/mL) are suggested to be implicated in the viscosities observed. These could involve protein-protein interactions, since the models are ideally applied to hard spherical or other-shaped particles, assuming interparticle repulsion [153, 159]. Further work should include investigations of the jamming limit variations at high concentrations, which could also help develop applicable equations. The study of mAb samples, in a way similar to ours, could also bring benefit particularly since mAb are typically relevant to biopharmaceutical formulations [5]. Direct quantifications should be performed of PS-80 in the highly concentrated rAlbumin solutions ($>$ 200 mg/mL), to understand if there could be any potential effect on these samples' viscosity, species distribution and inter-particle interaction.

Overall, for the remaining chapters of this thesis, it was evident that surface-activity of macromolecules (of bio or synthetic source) was an important parameter throughout the presented discussions. Although tensiometry data was initially developed for the β-LG samples, in parallel with interfacial shear rheology, further work would be necessary to complement the data regarding the mAb and the surfactant/ polymer

studies. In relation to β-LG and mAb data, one of the interests was to explore the effect of protein aggregates present in solution could contribute to the air-water interface. This would be most important regarding the mAb case-study and the effect of its increasing protein aggregates during thermal stressing, on the samples' interfacial properties.

It is important to highlight that the results observed regarding the mAb study were markedly related to this molecule's specific properties [183]. Knowing that mAbs are engineered for specific pharmacological targets this can yield individual particularities concerning their properties [1, 219]. Thus, it is largely assumed that studies concerning mAb samples are usually a case-to-case scenario. Based on the rationale presented here, studying other mAbs could be of benefit to explore common underpinning factors involving their aggregation behaviour and its effects on mAb solution rheology.

The results related to the role of PS-80 in biopharmaceutical formulations, in a rheological perspective, could be basis to investigations concerning therapeutic proteins formulated in other commonly used excipients. In the case of PS-80, due to its mechanism of action in competing with proteins at the air-water interface, this was indirectly observed via our data. Other excipients could also be of interest, such as arginine, shown to markedly reduce the viscosity of high concentration mAb solutions [6] and to be implicated on the protein's surface-activity via preferential hydration among other mechanisms of interactions [44]. Once more, it is emphasised the importance of studying throughout the largest shear rate range possible, preferably considering the lower shear rates (0.01 - 10 s^{-1}) where the yield-like behaviour observed for excipient-free protein solutions.

Suggested future work concerning the synthetic brush-like polyPEGMA homo-polymers, would be mostly focused on polymer structure. For example, still using PEG side-chains of low MW but taking into account the LCST of the monomer used,

would enhance the hydrophobicity of the polymer, but possibly restricting to the use of PEGMA-475 would be the best option. The initiator used could be changed towards fine tuning the surface-activity of the single-chain brush polymers [204]. In terms of polymer MW, keeping to low degrees of polymerisation, thus low MW (∼8 - 10 kDa) would be ideal to maintain the low intrinsic viscosity values observed here. However, the steric hindrance present in polyPEGMAs of low MW could be a problem [199]. Synthesis of PEG-brush copolymerised with other monomers containing different moieties or creating copolymer of mixed length PEG side-chains, could be considered to fine-tune the macromolecule's hydrophilic - hydrophobic balance. Desirably, these architectures should be designed to benefit of hydrophilicity, low MW, minimum steric hinderance between side chains, low intrinsic viscosity, non-ionic surface-activity yielding low CMC values, with high LCST, while still being biocompatible and biodegradable.

Appendix A

Appendix A

A.1 β-LG size exclusion chromatogram

Figure A.1 is an example of a size-exclusion chromatogram of a 10 mg/mL injection of β-LG. The peak at $\sim$ 10.4 minutes represents the dimer of β-LG at a approximate 98-99 % peak area and the peak at $\sim$9.2 minutes represents dimer aggregates at a roughly 1 % peak area [220]. The peaks shown between 12.5 and 15 minutes are correspondent to the His-His.HCl sample buffer.

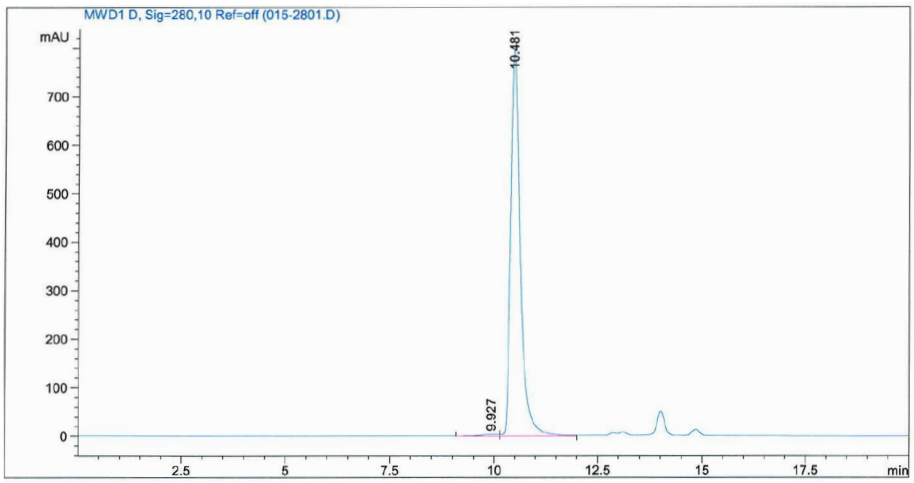

Figure A.1: β-LG high performance size-exclusion chromatogram. Peaks at 10.4 minutes and 9.2 minutes corresponded to β-LG species, respectively, dimers and aggregates. The peaks between 12.5 and 15 minutes were related to the sample's buffer.

A.2 mVROC data

Figure A.2 shows the shear stress values from a ∼68 mg/mL β-LG filtered solution versus the sensor's distance on the microfluidics channel of the chip used (A05) on the instrument. The linear decrease of shear stress along the microchannel was seen at all the flow rates (Q) applied to the sample and were considered valid measurements since it's $r^2 = 1.0$. This plot represents an example of the raw data that was measured for this sample and all samples while using the mVROC. Figure A.3 shows the mVROC results obtained from all β-LG filtered solutions, measured in triplicate.

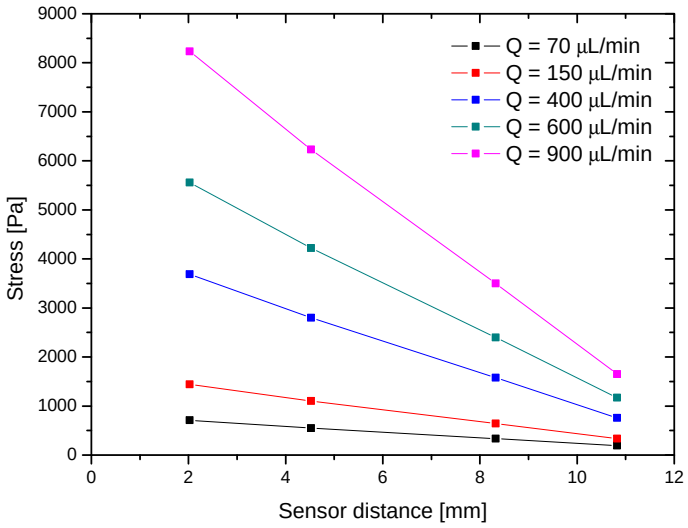

Figure A.2: Distance of the A05 chip's sensors versus the shear stress of a β-LG 68 mg/mL sample on the mVROC. Each line corresponded to a flow rate Q imposed to the sample in the syringe. The decrease in stress has a linear correlation of $r^2 = 1$.

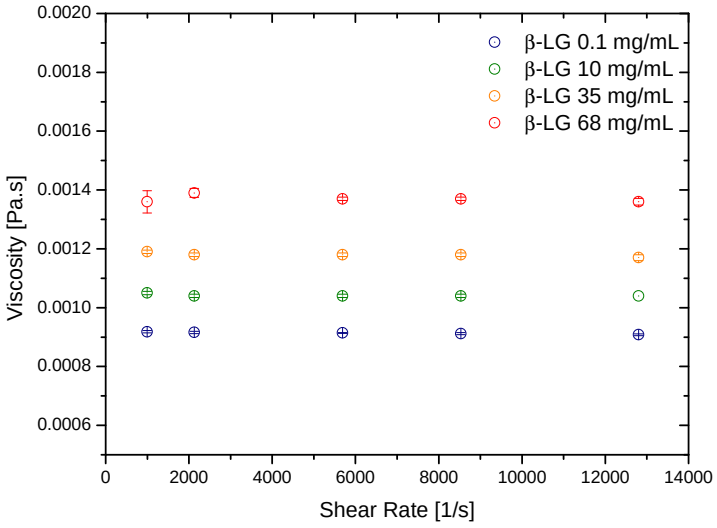

Figure A.3: Rheology profiles of β-lactoglobulin samples obtained from mVROC experiments. Protein samples were all previously filtered with 0.1 μm pore-size syringe filteres. Each sample was measured three times. Error bars represent standard deviation. Measurements taken using the A05 chip.

A.3 Calculation of l_s

In section 4.3.1.2, regarding the calculation of Boussinesq shear rate dependency for each measuring system, it was referred that the parameter l_s was needed (Equation A.3).

$$Bo = \frac{\eta_s}{\eta b \; l_s} \tag{A.1}$$

l_s depends on the dimensions of the measuring system since it is a ratio between A_b, the area of a geometry in contact with the bulk of the sample, and P_i, the perimeter of wetted geometry in contact with the interface. In the case of the cone-and-plate, A_s corresponded to the lateral surface area of the cone (Figure A.4(a)). This measuring system had a truncation, which was accounted for in our calculations shown below. The P_i of the CP corresponded to the perimeter of a circle. Consequently, the $l_s(CP)$ was

represented by the following equation:

$$l_s(CP) = \frac{\pi R^2 \sqrt{\tan^2(\theta) + 1} - \pi \frac{h_2^2}{\tan(\theta)} \sqrt{\frac{1}{\tan^2(\theta)} + 1}}{2\pi R} \tag{A.2}$$

The known dimensions of CP are the cone's angle (θ, 1°), the radius (R, 25 mm) and the truncation gap (h_2, 0.104 mm), therefore computing $l_s(CP) \approx 0.0125$ mm.

In the case of the double-gap, the A_s was a sum of the two lateral faces of the moving bob (hollow cylinder) and the area corresponding to the thickness of the hollow cylinder (Figure A.4(b)). The P_i was the sum of two perimeters, corresponding to the outer and inner radius of the bob (R_o and R_i, respectively). $l_s(DG)$ was therefore represented by the equation:

$$l_s(DG) = L + \frac{R_o^2 - R_i^2}{2(R_o + R_i)} \tag{A.3}$$

The dimensions of the double-gap were its immersed length (L, 40 mm), and the outer and inner radius of the bob (R_o and R_i, 13.334 mm and 12.333 mm, respecitvely). This yielded a $l_s(DG) \approx 40.5$ mm.

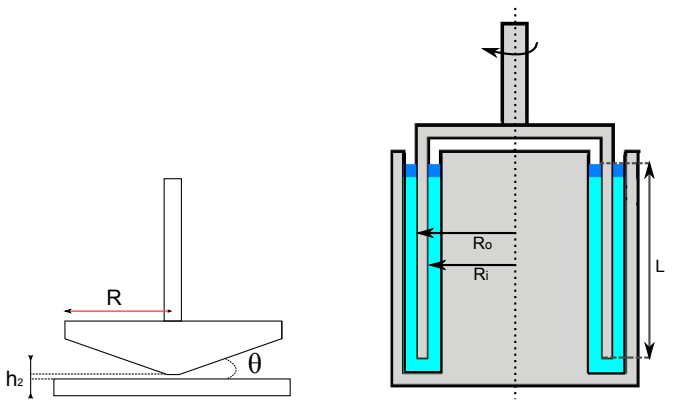

(a) (b)

Figure A.4: Schematic side-view of the (**a**) cone-and-plate and the (**b**) double-gap measuring systems. Dimensions correspondent to the letters in the figures are given in the text.

A.4 Additional DLS data

The following figures and table summarise the data obtained using dynamic light scattering to characterise various samples. In the main text, Figure 4.18 summarised the results for the β-LG 68 mg/mL. Here, the remaining results are shown. All samples suggest that filtration yielded a population of protein aggregates of lower hydrodynamic diameter compared to the unfiltered sample (Figure A.5 and Table A.1).

The β-LG sample at 68 mg/mL was also compared regarding its size characterisation between before and after the cone-and-plate and double-gap rheology. Results seen on Figures A.6(a) and A.6(b) correspond to the unfiltered and filtered ∼68 mg/mL only and respectively. Table A.1 shows the results for the relaxation times corresponding to each of the populations detected, obtained from fitting the 2-term exponential decay equation, which followed the data's tendency (Equation A.4). All the fits had a $r^2 > 0.99$.

$$g(\tau) = g_0 + A_1 \exp^{-x/t_1} + A_2 \exp^{-x/t_2} \tag{A.4}$$

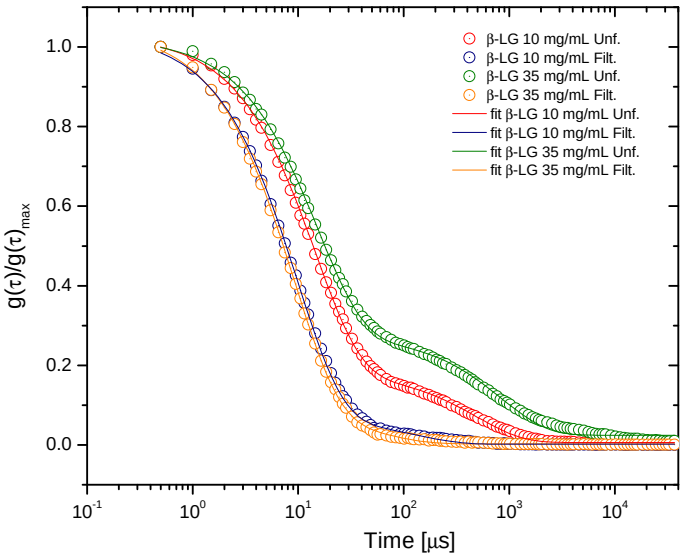

Figure A.5: Normalised correlation data from DLS for 10 and 35 mg/mL β-LG samples (hollow circles) comparing between unfiltered and filtered solutions, and its respective 2-term exponential decay fits (lines).

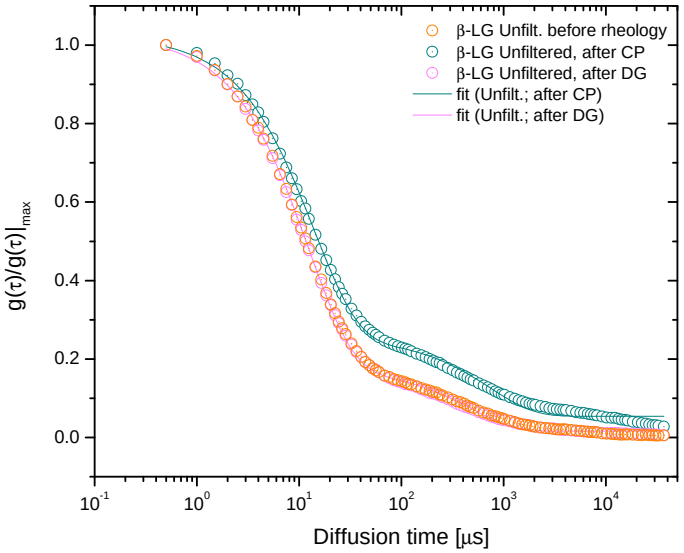

(a)

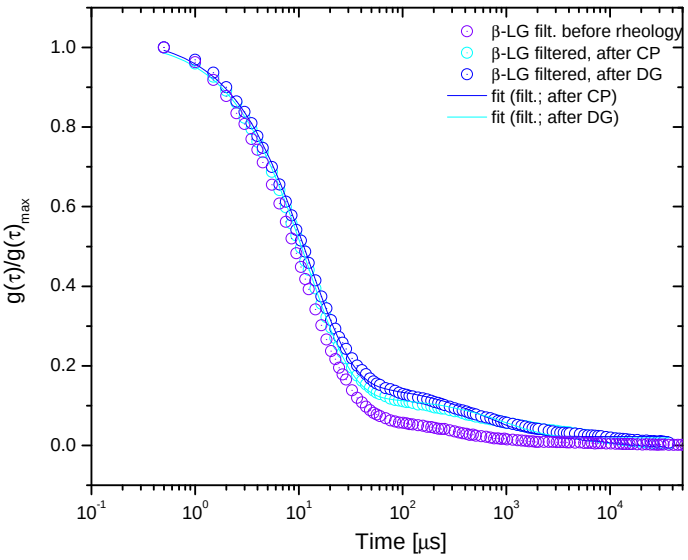

(b)

Figure A.6: Normalised correlation data from DLS for 68 mg/mL β-LG unfiltered and filtered solutions diluted to 1 mg/mL comparing between before and after rheology with cone-and-plate and double-gap. The shown data (hollow circles) were fitted to a 2-term exponential decay equation (lines).

Table A.1: Table summarising DLS results of β-LG samples. [1] - all samples were measured after dilution to 1 mg/mL and were not obtained after rheological measurements; [2] - results for 68 mg/mL sample (unfiltered and filtered) obtained after cone-and-plate rheology, and diluted to 1 mg/mL; [3] - results for 68 mg/mL sample (unfiltered and filtered) obtained after double-gap rheology, and diluted to 1 mg/mL; [4] - mean hydrodynamic diameter size and standard mean obtained by intensity results from the DTS software; [5] - relaxation times were obtained from fitting the 2-term exponential decay equations to the normalised correlation data, and are here reported as its value with standard error.

β-LG sample		Mean Hydrodynamic Diameter Size by Intensity [nm] [4]		Relaxation time [µs] [5]	
		Peak 1	Peak 2	Peak 1	Peak 2
Unfiltered [1]	10	6.9 ± 1.6	402 ± 164	14.4 ± 0.1	494 ± 11.6
	35	6.4 ± 1.3	322 ± 97	15.2 ± 0.2	849 ± 27.1
	68	6.0 ± 1.3	242 ± 76	12.6 ± 0.1	544 ± 22.6
Filtered [1] (0.1 µm)	10	6.1 ± 1.9	334 ± 144	9.7 ± 0.1	126 ± 9.5
	35	6.2 ± 2.2	436 ± 229	8.9 ± 0.1	60.4 ± 5.3
	68	6.3 ± 1.7	238 ± 79	11.2 ± 0.1	299 ± 19.9
After Cone-and-plate [2]	Unfiltered	5.9 ± 1.3	198 ± 54	13.9 ± 0.2	730 ± 37.0
	Filtered	5.9 ± 1.5	236 ± 70	12.2 ± 0.1	662 ± 40.0
After Double-gap [3]	Unfiltered	5.8 ± 1.5	220 ± 108	12.3 ± 0.1	473 ± 19.9
	Filtered	5.8 ± 1.6	217 ± 109	12.2 ± 0.1	1007 ± 73.5

A.5 Additional MFI data

Table A.2 summarises the reported results of β-LG samples and sample buffer in particle concentration (#/mL), particle count, equivalent circular diameter (in μm) mean size with standard deviation, and the size range of the detected particles. The samples were read as unfiltered solutions and after filtration with 0.1 μm pore-size syringe filters. The buffer was also analysed after filtration.

Table A.2: Table with the final reported results from micro-flow imaging analysis of unfiltered and filtered (0.1 μm) β-LG samples at 0.1, 10, 35 and 68 mg/mL. The table also includes data for three separate measurements of the sample buffer, also filtered with 0.1 μm syringe filters. Samples at 0.1, 10 and 35 mg/mL (unfiltered and filtered) were only read once. The unfiltered and filtered samples at 68 mg/mL were analysed in three separate runs. [1] - Particle concentration values were approximated to units; [2] - ECD is "equivalent circular diameter".

β-LG sample [mg/mL]		Particle concentration [1] [#/mL]	Particle Count [#]	ECD [2] mean size ± st. Deviation [µm]	ECD [2] size range of detected particles [µm]
Unfiltered	0.1	75736	49536	2.31 ± 1.53	1 – 59
	10	185457	121301	4.54 ± 3.17	1 – 74
	35	374671	245059	4.45 ± 3.04	1 – 73
	68	542404	354633	1.57 ± 1.46	1 – 77
		524450	342895	1.58 ± 1.47	1 – 56
		517443	338441	1.58 ± 1.47	1 – 67
Filtered (0.1 µm)	0.1	61	40	1.88 ± 2.66	1 - 18
	10	156	102	3.01 ± 3.70	1 – 24
	35	759	495	2.06 ± 2.65	1 – 33
	68	850	556	2.60 ± 4.18	1 – 77
		836	547	2.53 ± 3.72	1 – 51
		792	518	3.67 ± 2.48	1 – 40
Sample buffer (10 mM His-His.HCl pH 6.0, filtered 0.1 µm)		9	6	1.46 ± 0.58	1 – 3
		5	3	1.13 ± 0.00	1 – 2
		5	3	3.79 ± 3.40	1 – 8

The figures below are an example of one frame and a few examples of sub-visible particles detected for a unfiltered and a filtered ∼68 mg/mL β-LG (diluted to 10 mg/mL) (Figures A.7 and A.8, respectively). Included in the figures are also its respective particle size properties. Circularity represents the ratio of the circumference of an equivalent area circle over the measured perimeter. The intensity parameter of a particle is expressed in illumination intensity levels that are related to the bit depth supported by the digital camera on the instrument. Intensity is dependent of the difference in refractive index between formulation buffer and the particle. The aspect ratio is the ratio between the longitudinal and transversal axis of the particle [39, 127].

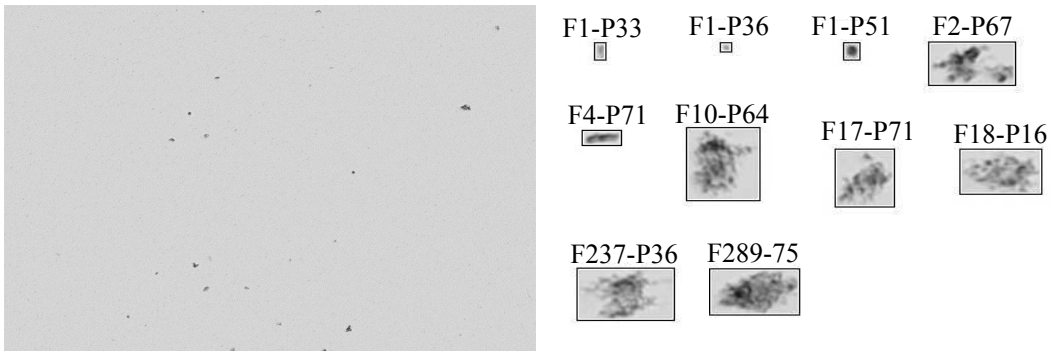

Particle	ECD [µm]	Circularity	Intensity mean	Aspect ratio
F1-P33	6	0.77	722	0.51
F1-P36	2	0.85	620	0.83
F1-P51	9	0.88	554	0.79
F2-P67	45	0.45	603	0.49
F4-P71	16	0.72	579	0.31
F10-P64	58	0.86	617	0.75
F17-P71	43	0.48	649	0.64
F18-P16	50	0.55	672	0.58
F237-P36	53	0.49	656	0.73
F289-P75	56	0.60	574	0.50

Figure A.7: Images and sizing properties of examples of particles detected with MFI for unfiltered ∼68 β-LG solution.

Particle	ECD [µm]	Circularity	Intensity mean	Aspect ratio
F32-P1	1	0.85	800	0.72
F597-P1	52	0.80	248	0.91
F868-P1	15	0.74	465	0.56
F1396-P1	18	0.75	716	0.54
F1890-P1	13	0.87	600	0.64

Figure A.8: Images and sizing properties of examples of particles detected with MFI for filtered ∼68 β-LG solution.

Appendix B

Appendix B

B.1 Additional data on HPSEC

Table B.1 summarises the values obtained from HPSEC analysis of the 100 and 17 mg/mL mAb samples stressed at 40 °C and, as a control, from samples stored at 5 °C.

Figure B.1 represents some examples for the chromatograms obtained from the 100 and 17 mg/mL mAb. Typically, a non stressed mAb sample would elute such as what is represented in the first chromatogram of this figure. After 2 weeks storage at 40 °C, the 100 mg/mL mAb sample showed four peaks of high MW species (chromatogram B, in the figure). The difference between the sample after 2 weeks and 6 weeks not only was the increase in peak area of the higher MW species (with respective drop for the monomer), but a shoulder peak on the tail of the monomer peak. This shoulder was not always detected by the software. An example of this shoulder peak is given on chromatogram D, from the sample 17 mg/mL at 40 °C after 6 weeks. Here, the high MW species were only detected as two small peaks.

Table B.1: Relative peak percentage of monomer, fragment and total aggregates detected by HPSEC for **a)** 100 and **b)** 17 mg/mL at 40 °C and 5 °C during 6 weeks. Each sample was measured in triplicate. Results are reported as average and standard deviation.

(a)

		Time [weeks]			
100 mg/mL		0	2	4	6
5 °C	Monomer	98.57 ± 0.002	98.48 ± 0.08	98.29 ± 0.01	98.40 ± 0.002
	High MW	1.36 ± 0.002	1.39 ± 0.04	1.55 ± 0.01	1.48 ± 0.002
	Low MW	0.08 ± 0.001	0.13 ± 0.05	0.16 ± 0.003	$0.12 \pm 6\times10^{-4}$
40 °C	Monomer	98.57 ± 0.01	77.22 ± 0.03	64.14 ± 0.06	58.45± 0.01
	High MW	1.34 ± 0.01	22.38 ± 0.04	35.16 ± 0.06	40.64 ± 0.02
	Low MW	$0.09 \pm 8\times10^{-4}$	0.40 ± 0.02	0.69 ± 0.01	0.91 ± 0.01
	Monomer loss	-	21.35 ± 0.04	34.43 ± 0.07	40.12 ± 0.02

(b)

		Time [weeks]			
17 mg/mL		0	2	4	6
5 °C	Monomer	99.25 ± 0.003	$99.27 \pm 5\times10^{-4}$	99.18 ± 0.002	99.17 ± 0.002
	High MW	0.62 ± 0.003	$0.60 \pm 6\times10^{-4}$	0.63 ± 0.002	0.62 ± 0.001
	Low MW	0.13 ± 0.002	$0.13 \pm 2\times10^{-4}$	0.19 ± 0.003	0.21 ± 0.001
40 °C	Monomer	99.25 ± 0.003	96.62 ± 0.002	93.25 ± 0.019	89.08 ± 0.032
	High MW	0.62 ± 0.003	2.96 ± 0.003	6.11 ± 0.05	9.95 ± 0.029
	Low MW	0.13 ± 0.002	$0.43 \pm 9\times10^{-4}$	$0.67 \pm 4\times10^{-4}$	0.96 ± 0.004
	Monomer loss	-	2.6 ± 0.004	6.0 ± 0.02	10.2 ± 0.03

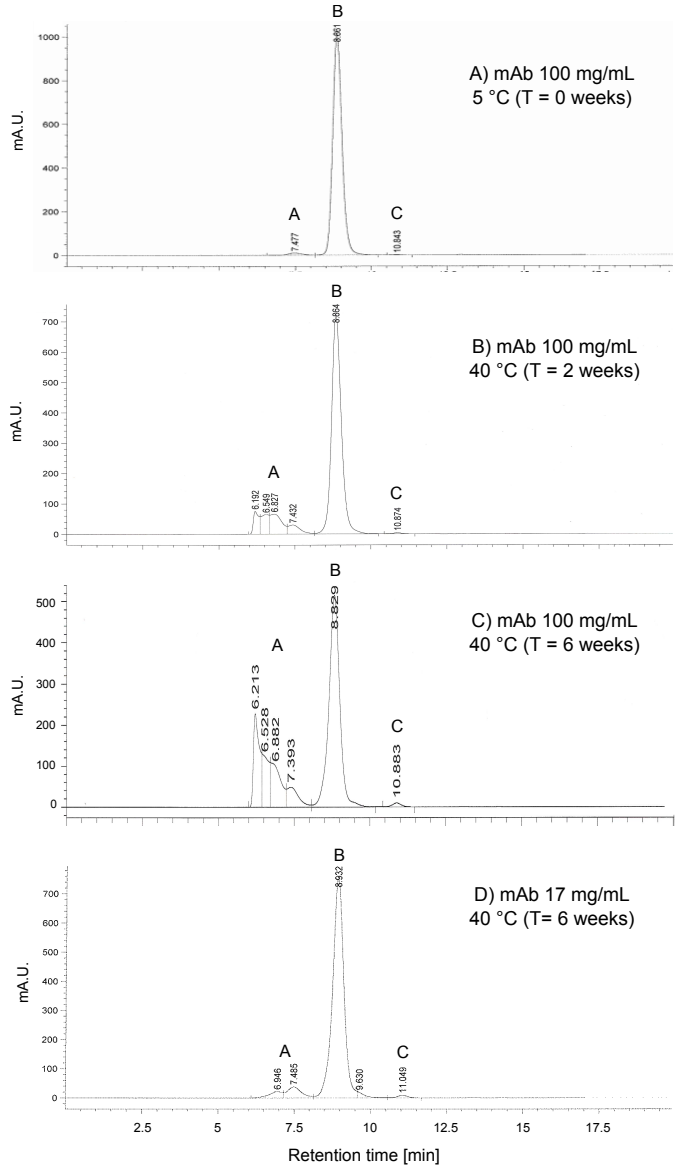

Figure B.1: HPSEC chromatograms of mAb solutions at different time points during thermal stressing at 40 °C: **A)** represents the typical chromatogram of unstressed mAb solution, showing a monomer peak (B), the higher molecular weight species (HMWS) peak (C), and a lower molecular weight species (LMWS); **B)** corresponds to the 100 mg/mL mAb sample that was stressed for 2 weeks at 40 °C, where peaks B and C remained similar to T=0 but more HMWS peaks (A) were identified; **C)** 100 mg/mL mAb after 6 weeks at 40 °C showing higher peak area percentage for all detected HMWS (A); **D)** a 17 mg/mL mAb solution after 6 weeks at 40 °C, where only two peaks of HMWS were detected but another LMWS peak was identified. The 100 mg/mL mAb solutions here presented were diluted to 10 mg/mL, while the 17 mg/mL mAb solution was injected neat.

B.2 Additional MFI data for the mAb samples

Table B.2 gives the particle concentration, particle count, ECD mean size and its standard deviation and the range of detected sizes per mAb sample analysed with the MFI. Note that control mAb samples at both concentrations stored at 5 °C were measured at the same time points. Also included in the table are the data for three separate measurements of the sample buffer (10 mM His-His.HCl at pH 6.0).

Table B.2: Table with the final reported results from micro-flow imaging analysis of 100 and 17 mg/mL mAb solutions for: unfiltered and filtered material; as well as a comparison between aggregated and non-aggregated material along a 6 week period time. The table also includes data for three separate measurements of the sample buffer, also filtered with 0.1 μm syringe filters. mAb samples were only read once. [1] - Particle concentration values were approximated to units; [2] - ECD is "equivalent circular diameter".

mAb Sample			Particle concentration [1] [#/mL]	Particle Count [#]	ECD [2] mean size ± st. deviation [µm]	ECD [2] size range of detected particles [µm]
100 mg/mL	Unfiltered		672186	43987	1.49 ± 0.96	1 – 61
	Filtered (0.1 µm)		1370	896	1.86 ± 2.31	1- 35
	5 °C	T=0	80	52	2.69 ± 4.88	1 – 27
		T=2	2518	1545	2.19 ± 2.35	1 – 24
		T=4	1558	1019	2.33 ± 3.09	1 – 30
		T=6	-	-	-	-
	40 °C	T=0	353	231	2.02 ± 2.88	1 – 37
		T=2	1302	764	2.07 ± 2.63	1 – 33
		T=4	1102	721	1.88 ± 3.64	1 – 80
		T=6	2062	1347	2.29 ± 4.34	1 – 108
17 mg/mL	Unfiltered		3383	2213	2.49 ± 3.21	1 – 69
	Filtered (0.1 µm)		573	375	2.65 ± 4.35	1 – 45
	5 °C	T=2	418	273	2.24 ± 2.80	1 – 32
		T=4	813	532	3.47 ± 6.42	1 – 96
		T=6	2667	1744	2.54 ± 3.54	1 – 44
	40 °C	T=2	1263	826	1.96 ± 3.03	1 – 53
		T=4	1294	846	1.79 ± 1.74	1 – 24
		T=6	8588	5617	2.00 ± 1.85	1 – 28
Sample buffer (10 mM His-His.HCl pH 6.0, filtered 0.1 µm)			9	6	1.46 ± 0.58	1 – 3
			5	3	3.79 ± 3.40	1 – 8
			5	3	1.13 0.00	1 – 2

B.3 Additional data on the mAb rheology

The figures below show the superimposed CP and DG rheology data of mAb samples through the time points after storage at 40 °C for 6 weeks. The larger graphs are focused at the lower shear rates up to 100 s^{-1}, whereas the inset graphs show the viscosities of

these samples at the higher shear rates (Figures B.2(a) and B.2(b)).

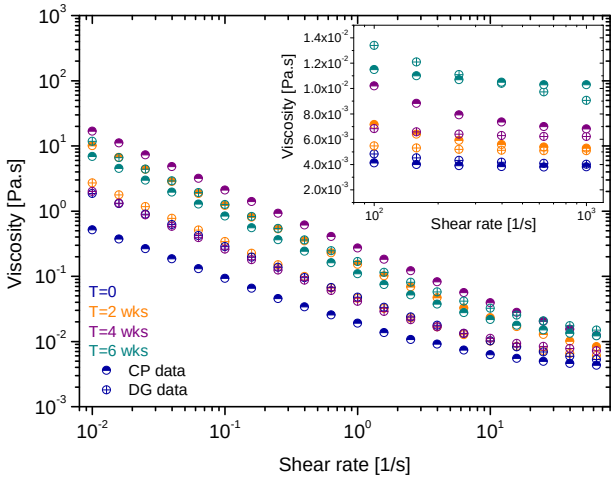

(a) 100 mg/mL mAb samples

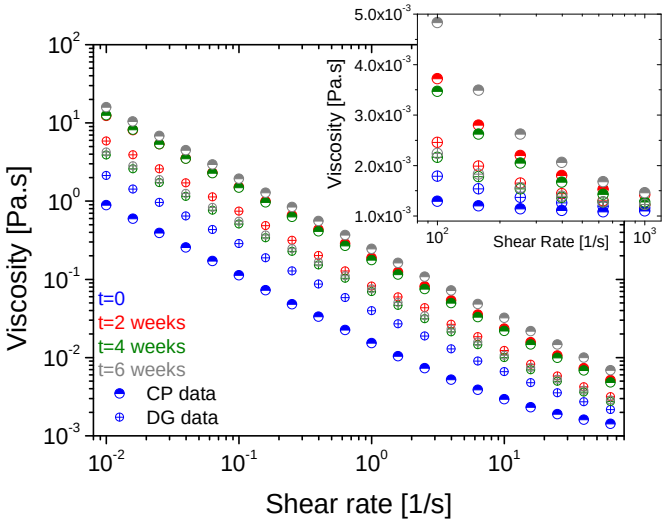

(b) 17 mg/mL mAb samples

Figure B.2: Superimposition of cone-and-plate and double-gap rheology data looking in detail at low and high shear rates of **a)** 100 mg/mL and **b)** 17 mg/mL mAb solutions aggregated for 6 weeks at 40 °C and analysed at 25 °C.

Figure B.3 is an example for fitting the Bingham model for yield-stress to the experimental flow data (shear stress versus shear rate). Here represented are the cone-and-plate and double-gap data from 100 mg/mL mAb solution after storage at

40 °C at T=0 and T= 6 week. The yield points correspond to the y-axis intercepts of the fitted linear functions. The calculated yield points and r^2 values to the respective regressions are summarised in Table B.3.

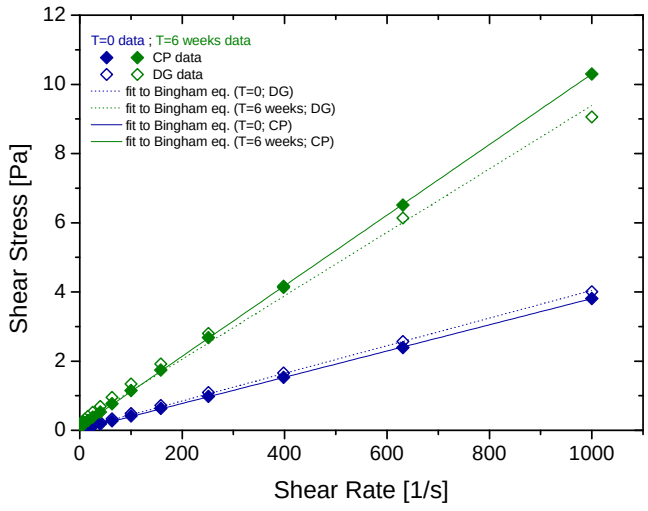

Figure B.3: Example of fitting to Bingham equation for yield stress, for flow curves comparing T= 0 and T= 6 weeks time point samples of 100 mg/mL mAb solution after thermal stressing at 40 °C. Data obtained using both CP and DG geometries, and measured at 25 °C.

Table B.3: Yield stress values calculated from fitting the Bingham equation for yield stress to the experimental flow curves of mAb samples at 100 and 17 mg/mL, unfiltered and filtered, and after thermally stressing these samples at 40 °C for 6 weeks. The yield stress values are reported with its standard error from the linear regression. The values in brackets represent the fitting's adjusted R-squared.

			Time [weeks]			
		Unfiltered	0	2	4	6
100 mg/mL	**Cone-and-plate**	$0.119 \pm 7.1\times10^{-3}$ (0.9938)	$0.018 \pm 2.3\times10^{-3}$ (0.9999)	$0.153 \pm 7\times10^{-3}$ (0.9993)	$0.272 \pm 1.4\times10^{-2}$ (0.9982)	$0.100 \pm 4.3\times10^{-3}$ (0.9999)
	Double-gap	$0.063 \pm 5\times10^{-3}$ (0.9994)	$0.050 \pm 5.1\times10^{-3}$ (0.9994)	$0.029 \pm 1.8\times10^{-3}$ (0.9999)	$0.039 \pm 3.8\times10^{-3}$ (0.9999)	$0.221 \pm 3.2\times10^{-2}$ (0.9954)
17 mg/mL	**Cone-and-plate**	0.210 ± 0.01 (0.9762)	$0.015 \pm 1.1\times10^{-3}$ (0.9996)	$0.190 \pm 8.9\times10^{-3}$ (0.9809)	$0.182 \pm 8\times10^{-3}$ (0.9811)	$0.259 \pm 1.5\times10^{-2}$ (0.9497)
	Double-gap	$0.066 \pm 3.5\times10^{-3}$ (0.9963)	$0.043 \pm 3.3\times10^{-3}$ (0.9966)	$0.094 \pm 5.2\times10^{-3}$ (0.9919)	$0.071 \pm 4.5\times10^{-3}$ (0.9944)	$0.077 \pm 4.8\times10^{-3}$ (0.9934)

B.4 Additional data on DLS

The correlation data for the mAb samples at 100 mg/mL and 17 mg/mL (after dilution to 1 mg/mL) analysed on DLS are shown on Figure B.4. The data was fitted with an exponential decay function (of one term only) and the relaxation time values obtained from these fits are shown in Table 5.4 in the main text. For all the fits to the correlation data, the $r^2 > 0.97$.

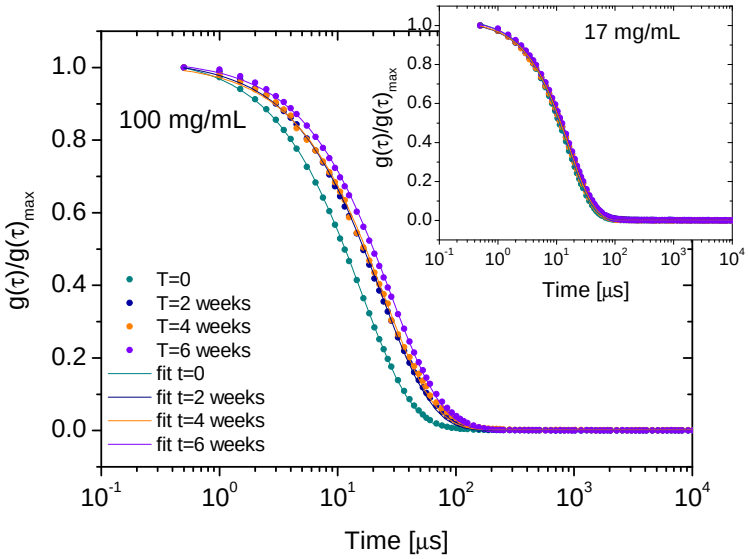

Figure B.4: DLS correlation data for the 100 and 17 mg/mL mAb solutions, diluted to 1 mg/mL for analysis, after aggregation at 40 °C for 6 weeks. The large graph shows data related to the samples diluted from 100 mg/mL mAb solution, and the inset graph corresponds to data from 17 mg/mL mAb solution. For each time point, the correlation data (circles) was fitted with an exponential decay curve (lines) to find the correspondent relaxation times.

The data shown on Tables B.4(a) and B.4(b) correspond to the mean hydrodynamic size by intensity and by volume for the mAb samples recovered after CP and DG rheology, respectively. This data is represented on Figure 5.19 in the main text.

Table B.4: Mean hydrodynamic size obtained by DLS for the 100 and 17 mg/mL mAb samples (aggregated at 40 °C) after **a)** cone-and-plate and **b)** double-gap rheology. [1] - Data was obtained by diluting samples to 1 mg/mL; [2] - mean hydrodynamic size by intensity distribution and standard deviation of three measurements; [3] - mean hydrodynamic size by volume distribution and standard deviation of three measurements.

(a)

mAb sample – After cone-and-plate		Mean Hydrodynamic Diameter Size by Intensity [nm] [2]	Mean Hydrodynamic Diameter Size by Volume [nm] [3]
100 mg/mL [1]	T=0	11.53 ± 0.48	9.01 ± 0.10
	T=2	17.16 ± 0.37	10.58 ± 0.35
	T=4	19.83 ± 1.28	11.69 ± 0.24
	T=6	20.83 ± 0.60	12.40 ± 0.22
17 mg/mL [1]	T=2	11.43 ± 0.36	9.15 ± 0.16
	T=4	12.22 ± 0.24	9.08 ± 0.12
	T=6	12.60 ± 0.32	9.29 ± 0.22

(b)

mAb sample – After double-gap		Mean Hydrodynamic Diameter Size by Intensity [nm] [2]	Mean Hydrodynamic Diameter Size by Volume [nm] [3]
100 mg/mL [1]	T=0	12.25 ± 0.32	9.05 ± 0.28
	T=2	16.33 ± 0.21	11.23 ± 0.24
	T=4	20.77 ± 1.10	11.77 ± 0.22
	T=6	23.02 ± 0.43	13.73 ± 0.09
17 mg/mL [1]	T=2	11.52 ± 0.32	9.03 ± 0.09
	T=4	12.08 ± 0.38	9.36 ± 0.17
	T=6	12.50 ± 0.44	9.34 ± 0.12

Figure B.5(a) represents the HPSEC data of 10 mg/mL dilutions from the 100 mg/mL mAb sample (40 °C, T= 2.5 months) that was collected in parallel to the DLS time sweep study of the same stock sample (see Figure 5.23). This was related to the study of reversible aggregates present in the thermally stressed mAb samples at 5 °C and 25 °C conditions. Note that at this point in time (2.5 months), the total HMWS was ∼60 %, while monomer peak area was ∼40 %. This data is also a reference for the μ-m-SDS-PAGE experiment, which made use of an aliquot of this aggregated material for one of its control samples.

Figure B.5(b) summarises the data obtained for the neat injections of 17 mg/mL at 40 °C at T= 7 weeks. The red data points were obtained while leaving the samples on the HPSEC auto-sampler tray at 5 °C; while the green data points correspond to the 25 °C conditions.

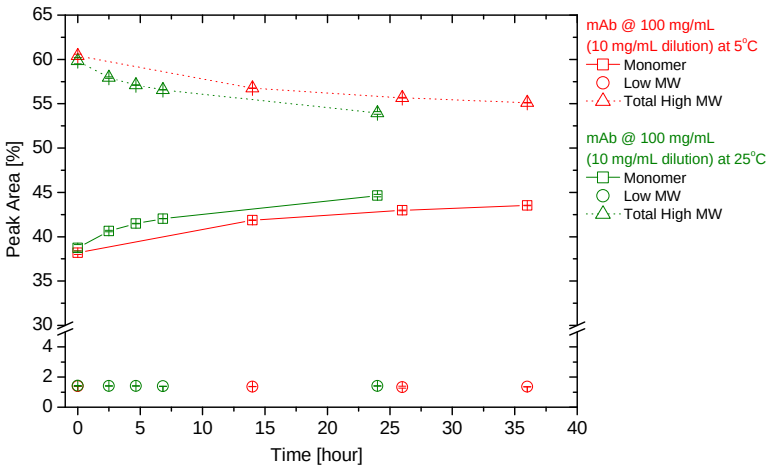

(a)

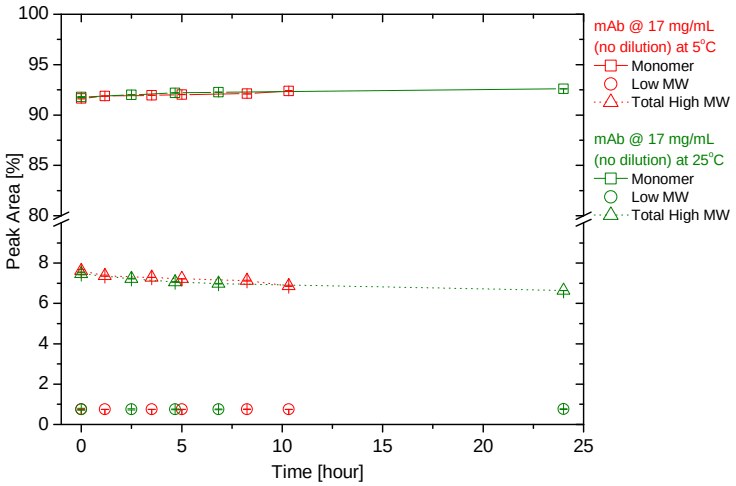

(b)

Figure B.5: Time sweeps relating the level of aggregation of diluted mAb solutions and the effect of temperature - experiment conducted in parallel to similar time sweep performed with DLS (dilution of 100 mg/mL mAb solution only). **a)** Corresponds to dilutions made from 100 mg/mL mAb sample, thermally stressed after T= 2.5 months at 40 °C. **b)** Corresponds to 17 mg/mL mAb sample (not diluted), thermally stressed after T= 7 weeks at 40 °.

Appendix C

Appendix C

C.1 Part I - The effect of thermal stressing of rAlbumin solutions on its solution rheology

The following tables summarise the relative peak areas for the detected protein species of rAlbumin samples exposed to 60 °C throughout a 4 week study (Table C.1(a) and C.1(b)). Samples at 200 and 20 mg/mL of rAlbumin were also left at 5 °C for control purposes. In the case of thermally stressed 200 mg/mL rAlbumin samples, these evidenced a third peak corresponding to high molecular weight protein species that increased in peak area with time. Presence of trimers or high MW species were not detected for 20 mg/mL as early as at the 3rd day after the start of the study.

Table C.1: Relative peak areas of protein species detected by HPSEC of rAlbumin samples at 5 and 60 °C, during a time period of 28 days. **(a)** Refers to data for 200 mg/mL rAlbumin solutions. **(b)** Refers to data for 20 mg/mL rAlbumin solutions. These samples were all diluted to 10 mg/mL and analysed in triplicate. The values presented are averages with respective standard deviations.

(a)

		Time [days]				
200 mg/mL		0	3	7	14	28
5 °C	Monomer	94.00 ± 0.03	93.91 ± 0.01	93.85 ± 0.01	93.87 ± 0.02	93.71 ± 0.05
	Dimer	5.65 ± 0.03	5.74 ± 0.005	5.79 ± 0.01	5.78 ± 0.02	5.92 ± 0.04
	Trimer	0.35 ± 0.005	0.35 ± 0.001	0.36 ± 0.002	0.35 ± 0.005	0.37 ± 0.01
	High MW species	-	-	-	-	-
60 °C	Monomer	94.00 ± 0.03	92.21 ± 0.02	90.56 ± 0.08	86.57 ± 0.07	87.71 ± 0.08
	Dimer	5.65 ± 0.03	6.38 ± 0.02	7.18 ± 0.03	8.12 ± 0.04	9.63 ± 0.03
	Trimer	0.35 ± 0.005	0.74 ± 0.01	1.03 ± 0.01	1.51 ± 0.04	1.81 ± 0.05
	High MW species	-	0.67 ± 0.004	1.24 ± 0.03	3.80 ± 0.01	0.84 ± 0.01

(b)

		Time [days]				
20 mg/mL		0	3	7	14	28
5 °C	Monomer	94.45 ± 0.004	-	-	93.87 ± 0.02	93.71 ± 0.05
	Dimer	5.26 ± 0.01	-	-	5.78 ± 0.02	5.92 ± 0.04
	Trimer	0.29 ± 0.003	-	-	0.27 ± 0.01	0.26 ± 0.005
60 °C	Monomer	94.45 ± 0.004	97.08 ± 0.003	97.40 ± 0.01	97.63 ± 0.01	97.74 ± 0.01
	Dimer	5.26 ± 0.01	2.92 ± 0.003	2.60 ± 0.01	2.37 ± 0.01	2.26 ± 0.013
	Trimer	0.29 ± 0.003	-	-	-	-

DLS results for the analysis of rAlbumin at 60 °C for 28 days are shown on Table C.2. The protein samples were analysed after dilution to ∼1 mg/mL and the data shown are the mean hydrodynamic diameter sizes by intensity and volume. The relaxation times were obtained by fitting the experimental correlation data to a one or two step decay exponential function. All samples were analysed directly after dilution, without any filtration, except for the 200 mg/mL T= 28 days sample, where a filtration (0.45 μm)

was needed to allow a reading on the instrument.

Table C.2: DLS results for the rAlbumin samples stressed at 60 °C for 28 days. [1] - Data was obtained by diluting samples to 1 mg/mL; [2] - mean hydrodynamic size by intensity distribution and standard deviation of three measurements; [3] - mean hydrodynamic size by volume distribution and standard deviation of three measurements; [4] - relaxation times were obtained by fitting an exponential decay curve (1 or 2 step) to the experimental data.

rAlbumin sample		Mean Hydrodynamic Diameter Size by Intensity [nm] [2]	Mean Hydrodynamic Diameter Size by Volume [nm] [3]	Relaxation time [µs] [4]
200 mg/mL [1]	T= 0	8.78 ± 0.10	6.80 ± 0.11	15.7 ± 0.1
	T= 3 days	9.32 ± 0.37; 159 ± 32	6.83 ± 0.12	16.4 ± 0.1; 106 ± 2.7
	T= 7 days	8.61 ± 0.04; 92.7 ± 4.37	7.04 ± 0.18	19.8 ± 0.1; 136 ± 1.3
	T= 14 days	8.67 ± 0.10; 156 ± 7.09	7.49 ± 0.22	26.5 ± 0.3; 238 ± 1.2
	T= 28 days	8.71 ± 0.10; 197 ± 0.92	7.65 ± 0.33	23.6 ± 0.2; 286 ± 2.6
20 mg/mL [1]	T= 0	8.50 ± 0.59	6.62 ± 0.21	14.9 ± 0.1
	T= 3 days	8.64 ± 0.15; 1381 ± 1564	6.61 ± 0.46	14.0 ± 0.1; 84.3 ± 3.6
	T= 7 days	8.59 ± 0.10; 1325 ± 452	6.80 ± 0.05	14.1 ± 0.1; 90.1 ± 4.6
	T= 14 days	8.41 ± 0.22; 1203 ± 1297	6.88 ± 0.19	14.3 ± 0.1; 99.2 ± 4.6
	T= 28 days	8.48 ± 0.16; 941 ± 991	6.66 ± 0.10	14.9 ± 0.1; 149 ± 7.8

C.2 Part II - Novel use of polyPEGMA brush-type polymers as additives in protein solutions and their effect in rheology

Figures C.1 and C.2 refer to the ^{1}H-NMR spectra of 2-bromo-2-methylpropionic benzyl ester and poly[poly(ethylene glycol)methylether methacrylate]-475, respectively.

NMR characterisation of the synthesised initiator yielded three peaks at δ = 7.38 ppm (**a**), 5.22 ppm (**b**) and 1.96 ppm (**c**), corresponding respectively to the aromatic

protons, the benzylic protons and the protons of the two methyl groups present in the molecule (Figure C.1).

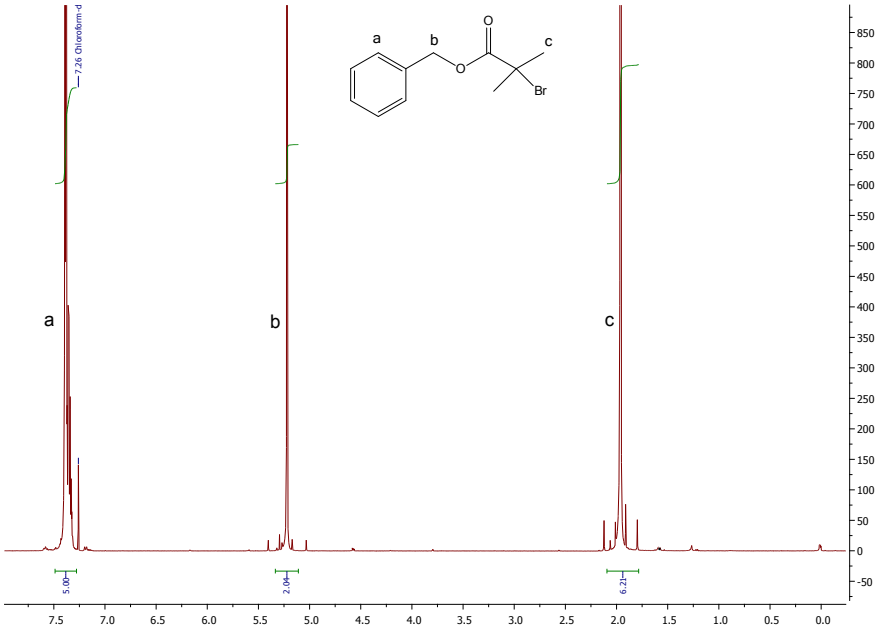

Figure C.1: NMR spectra for 2-bromo-2-methylpropionic benzyl ester. Sample was dissolved in $CDCl_3$.

The NMR spectra for polyPEGMA-475 (Figure C.2) has the same peaks at the approximately the same chemical shifts as the NMR results found for polyPEGMA-1100 (Figure 6.11). The difference between these spectra has to do with the integration for most of its peaks, corresponding to the less number of protons present in the polyPEGMA-475 molecule. The peaks that remain with equal integration are for those protons present in the end group at chemical shifts $\delta = 7.33$ ppm and $\delta = 5.05$ ppm, corresponding to the aromatic protons (**a**) and the benzylic protons (**b**), respectively.

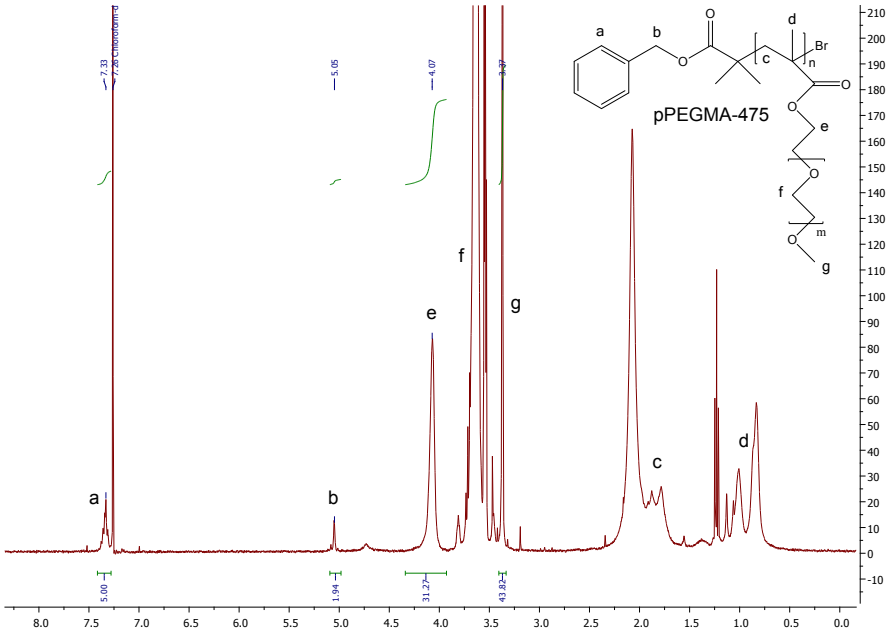

Figure C.2: NMR spectra for poly[poly(ethylene glycol)methylether methacrylate]-475. Sample was dissolved in $CDCl_3$.

Figure C.3 shows the calculated molar mass after analysis of the polyPEGMAs on HPSEC calibrated with triple detection. The polymers were injected in triplicate and represented here is an example of one analysis per polymer.

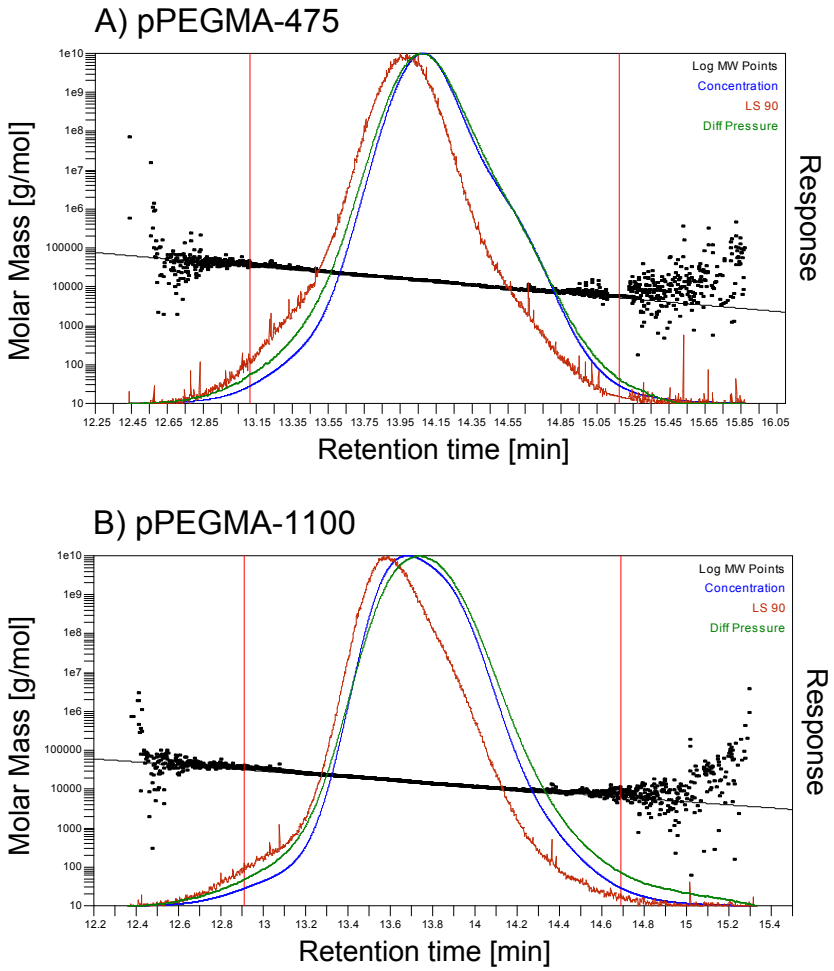

Figure C.3: Example of chromatograms for polyPEGMA analysis on HPSEC calibrated with triple detection. (**A**) pPEGMA-475 (**B**) pPEGMA-1100. Black points represent the calculated molar mass per peak; blue line refers to the refractive index signal (concentration); red line corresponds to the light scattering (90 °) detector; and green line corresponds to the differential pressure signal from the viscometer.

Figure C.4 represents the UV-visible absorbance spectra of the polyPEGMA solutions (in % w/w) used for the protein solubility studies. Aliquots of these samples were analysed to ensure the correct increase of polyPEGMA presence in each sample. These were also measured for any possible absorbance at 280 nm, useful when determining the protein concentration of the protein in the blends prepared for this experiment. The arrows on the graph are pointing at the two maximum peaks of UV absorbance for polyPEGMAs (at this buffer conditions): at ∼230 nm and ∼258 nm. The third arrow

points at $\lambda = 280$ nm, where it can be observed that there was an increase of absorption at this wavelength, with an increase of polymer concentration.

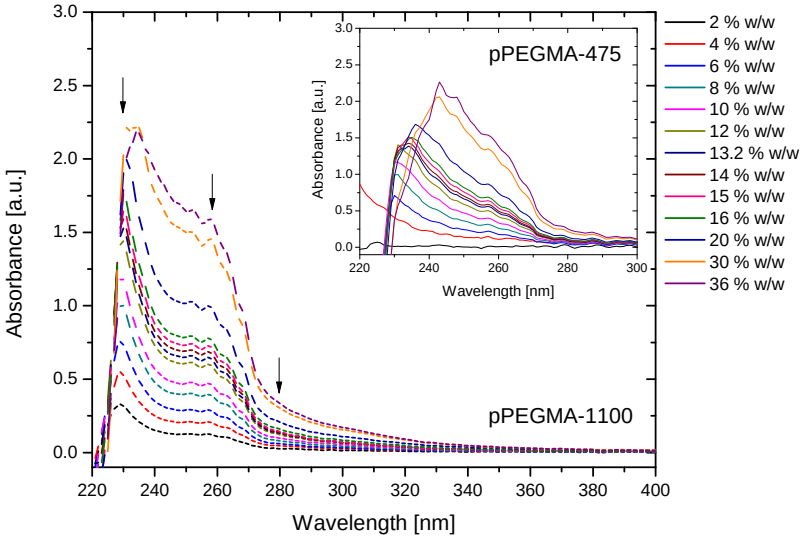

Figure C.4: UV-Visible absorption spectra of polyPEGMA solutions in buffer, in the concentrations used for the protein solubility test. The larger graph corresponds to data of polyPEGMA-1100 dispersions, while the polyPEGMA-475 data is represented on the inset graph. The three arrows are pointing to the following wavelengths: ∼230 nm, ∼258 nm and 280 nm.

The figures below represent the emission spectra for pyrene fluorescence a probe for micellisation occurrence on polyPEGMA solutions (in the range of 0.01 to 5 mg/mL) (Figures C.5(a) and C.5(b)). Although there was an increase of emission with the increase of the polymer concentrations, on each of the cases, the increase in intensity of peak III ($\lambda \sim 384$ nm) was not observed.

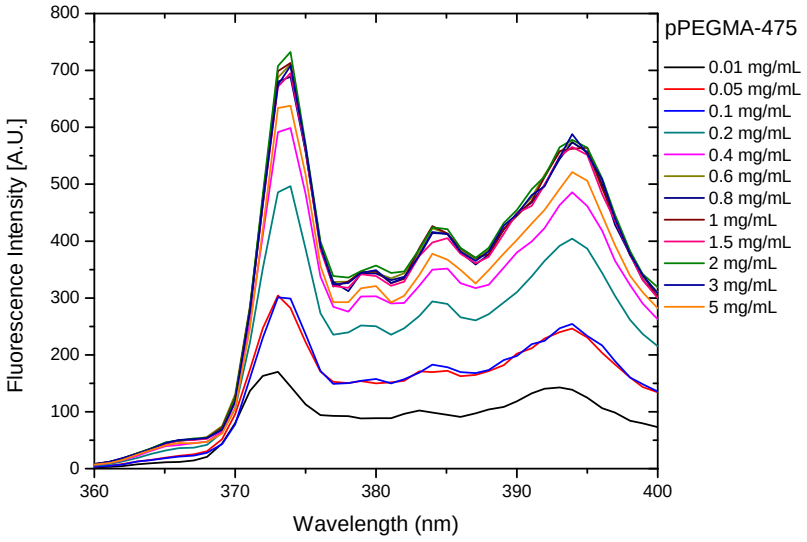

(a)

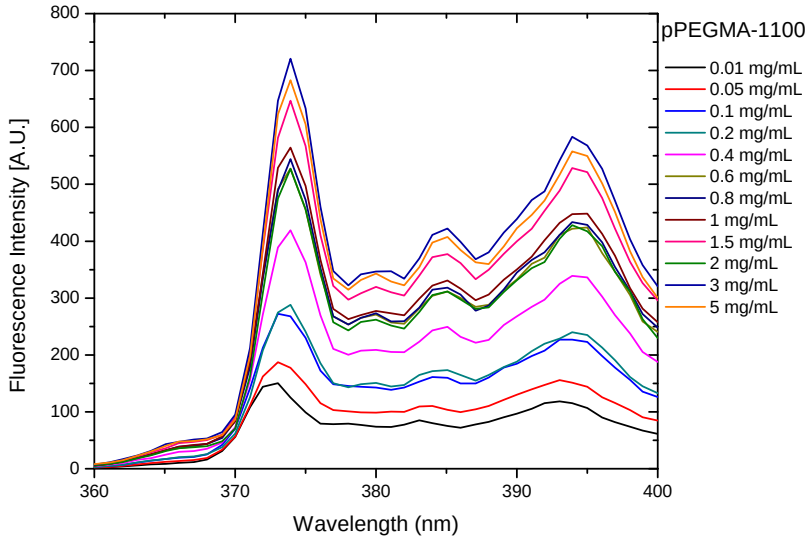

(b)

Figure C.5: Emission spectra for fluorescence of pyrene probe on the micellisation studies with polyPEGMA solutions. **a)** polyPEGMA-475 solutions, and **b)** polyPEGMA-1100 solutions.

The tables below summarise the measured hydrodynamic diameter (H_D) in nm measured by intensity and volume distribution for the polyPEGMA solutions and the β-LG samples (Tables C.3 and C.4). The polymer solutions in buffer (10 mM His-

His.HCl pH 6.0) were analysed at their actual concentration, without further dilution. The protein-polymer blends were diluted to 1 mg/mL (of protein concentration, at 280 nm), so to allow a comparison to the previous results of protein only DLS measurements (discussed in the other chapters of this thesis).

Table C.3: Table with the hydrodynamic diameter sizes by intensity and volume distribution of the polyPEGMA samples. [1] - polymer samples were measured at the stated concentrations; [2] - mean hydrodynamic size by intensity distribution and standard deviation of three measurements; [3] - mean hydrodynamic size by volume distribution and standard deviation of three measurements.

Sample		Mean Hydrodynamic Diameter Size by Intensity [nm] [2]	Mean Hydrodynamic Diameter Size by Volume [nm] [3]
pPEGMA-475 [mg/mL] [1]	1	5.24 ± 0.13; 175 ± 37	4.74 ± 0.13
	10	4.48 ± 0.06; 273 ± 63	4.37 ± 0.05
	25	4.61 ± 0.01; 23.8 ± 7.8; 107 ± 11; 430 ± 24	4.46 ± 0.02
pPEGMA-1100 [mg/mL] [1]	1	5.89 ± 0.32; 70 ± 7.2; 162 ± 280	5.35 ± 0.19
	10	5.35 ± 0.05; 186 ± 12	5.09 ± 0.08
	25	4.81 ± 0.03; 21.5 ± 3.9; 114 ± 17; 363 ± 80	4.70 ± 0.01

Table C.4: Table with the hydrodynamic diameter sizes by intensity and volume distribution of of β-LG and polyPEGMA blends. [1] - Data was obtained by diluting samples to 1 mg/mL; [2] - mean hydrodynamic size by intensity distribution and standard deviation of three measurements; [3] - mean hydrodynamic size by volume distribution and standard deviation of three measurements.

Sample		Mean Hydrodynamic Diameter Size by Intensity [nm] [2]	Mean Hydrodynamic Diameter Size by Volume [nm] [3]
β-LG + pPEGMA-475 [mg/mL] [1]	1	5.79 ± 0.04; 191 ± 27	5.47 ± 0.08
	10	5.70 ± 0.07; 370 ± 222	5.53 ± 0.08
	25	6.94 ± 0.58; 283 ± 31	6.74 ± 0.62
β-LG + pPEGMA-1100 [mg/mL] [1]	1	6.18 ± 0.12; 219 ± 56	5.80 ± 0.07
	10	6.27 ± 0.22; 208 ± 61	6.04 ± 0.15
	25	7.18 ± 0.25; 199 ± 28	7.06 ± 0.23

Figure C.6 shows examples of HPSEC chromatograms obtained from β-LG and mAb blends with polyPEGMA at 25 mg/mL. The samples were all diluted to 10 mg/mL (at protein concentration), prior HPSEC analysis. These chromatograms are examples representative for all the blends analysed, since there was no difference between samples, within the same protein type of sample.

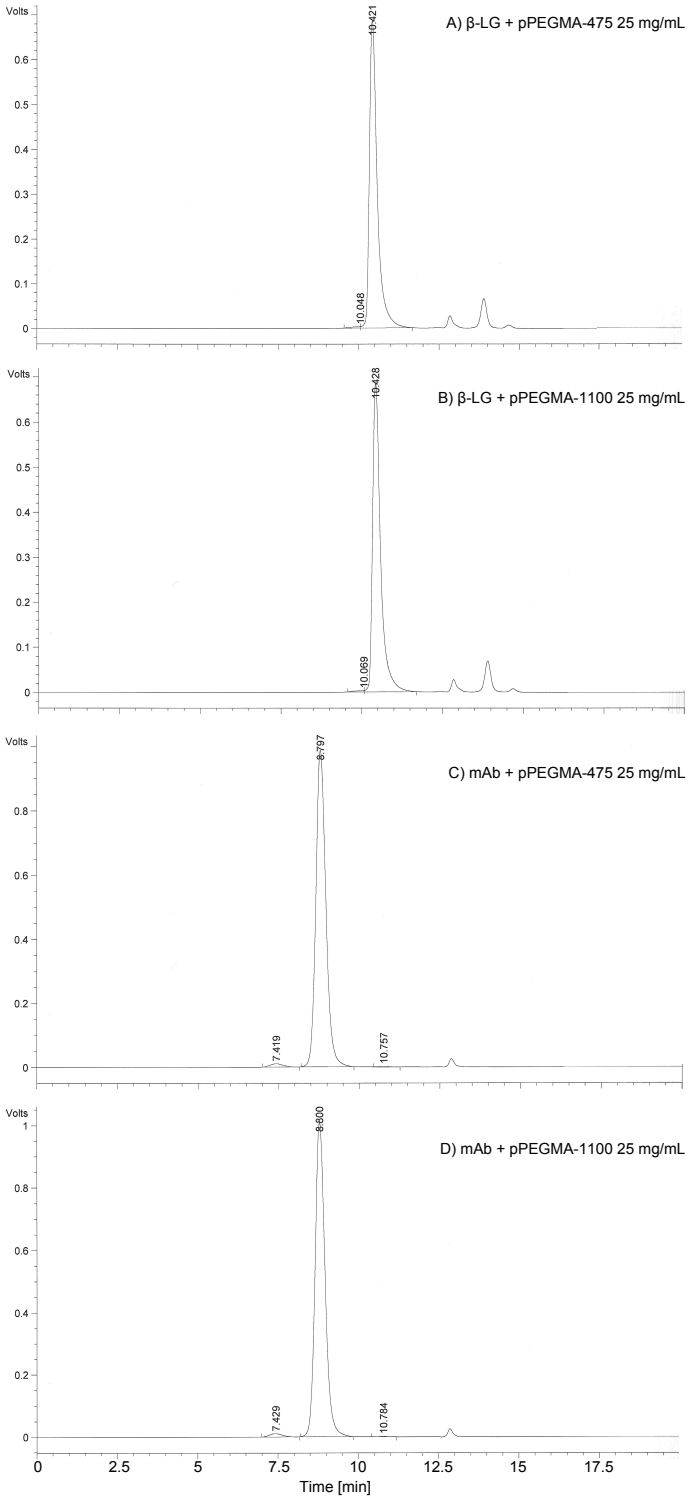

Figure C.6: HPSEC chromatograms for polyPEGMA and protein blends. **A** and **B** - ∼68 mg/mL of β-LG solution with 25 mg/mL polyPEGMA-475 or polyPEGMA-1100, respectively. **C** and **D** - ∼100 mg/mL of mAb solution with 25 mg/mL of polyPEGMA-475 or polyPEGMA-1100, respectively. Samples were analysed on HPSEC after dilution to 10 mg/mL of protein.

The following tables C.5, C.6 and C.7 list the average values and standard deviation of three readings of each sample from the cone-and-plate rheology experiments and the mVROC experiments. For the CP rheology data, the represented viscosity values were those at 1000 s^{-1} and for the mVROC experiments, those at 990-1000 s^{-1}. As the sample's viscosities vary slightly, the calculated true shear rates applied on the mVROC measurements varied correspondingly still being close to 990 - 1000 s^{-1}.

Table C.5: High shear rate viscosities measured with cone-and-plate and mVROC for buffer and polyPEGMA solutions.

Sample		η [Pa.s] Cone-and-plate (shear rate = 1000 s^{-1})	η [Pa.s] mVROC (shear rate ~ 1000 s^{-1})
Buffer – 10 mM His-His.HCl pH 6.0		$9.38\times10^{-4} \pm 5.7\times10^{-6}$	$9.09\times10^{-4} \pm 4.2\times10^{-6}$
pPEGMA-475 [mg/mL]	1	$9.26\times10^{-4} \pm 2.6\times10^{-6}$	$9.38\times10^{-4} \pm 2.6\times10^{-5}$
	10	$9.85\times10^{-4} \pm 1.5\times10^{-6}$	$9.85\times10^{-4} \pm 1.6\times10^{-6}$
	25	$1.05\times10^{-3} \pm 6.1\times10^{-5}$;	$1.06\times10^{-3} \pm 2.3\times10^{-5}$
pPEGMA-1100 [mg/mL]	1	$9.24\times10^{-4} \pm 1.5\times10^{-6}$	$9.35\times10^{-4} \pm 5.8\times10^{-6}$
	10	$1.01\times10^{-3} \pm 5.8\times10^{-6}$	$1.01\times10^{-3} \pm 2.7\times10^{-6}$
	25	$1.19\times10^{-3} \pm 5.8\times10^{-6}$	$1.17\times10^{-3} \pm 7.2\times10^{-6}$

Table C.6: High shear rate viscosities measured with cone-and-plate and mVROC for β-LG solution and its blends with polyPEGMAs. β-LG solution was at ∼68 mg/mL in all samples, while the concentrations of polyPEGMA-475 and polyPEGMA-1100 were varying.

Sample		η [Pa.s] Cone-and-plate (shear rate = 1000 s^{-1})	η [Pa.s] mVROC (shear rate ~ 1000 s^{-1})
β-LG (~68 mg/mL)		$1.67\times10^{-3} \pm 7.1\times10^{-5}$	$1.41\times10^{-3} \pm 1.3\times10^{-5}$
β-LG + pPEGMA-475 [mg/mL]	1	$1.66\times10^{-3} \pm 6.4\times10^{-5}$	$1.47\times10^{-3} \pm 4.3\times10^{-5}$
	10	$1.73\times10^{-3} \pm 1.1\times10^{-4}$	$1.57\times10^{-3} \pm 2.9\times10^{-5}$
	25	$1.91\times10^{-3} \pm 5.7\times10^{-5}$	$1.67\times10^{-3} \pm 4.4\times10^{-5}$
β-LG + pPEGMA-1100 [mg/mL]	1	$1.68\times10^{-3} \pm 5.7\times10^{-5}$	$1.43\times10^{-3} \pm 2.6\times10^{-5}$
	10	$1.91\times10^{-3} \pm 8.5\times10^{-5}$	$1.60\times10^{-3} \pm 4.2\times10^{-6}$
	25	$2.24\times10^{-3} \pm 1.5\times10^{-4}$	$1.94\times10^{-3} \pm 2.0\times10^{-5}$

Table C.7: High shear rate viscosities measured with cone-and-plate and mVROC for mAb solution and its blends with polyPEGMAs. The mAb solution was at ∼100 mg/mL in all samples, while the concentrations of polyPEGMA-475 and polyPEGMA-1100 were varying.

Sample		η [Pa.s] Cone-and-plate (shear rate = 1000 s^{-1})	η [Pa.s] mVROC (shear rate ~ 1000 s^{-1})
mAb (~100 mg/mL)		$4.22\times10^{-3} \pm 1.6\times10^{-4}$	$3.86\times10^{-3} \pm 8.8\times10^{-6}$
mAb + pPEGMA-475 [mg/mL]	1	$4.21\times10^{-3} \pm 2.0\times10^{-4}$	$3.93\times10^{-3} \pm 1.3\times10^{-5}$
	10	$4.56\times10^{-3} \pm 2.3\times10^{-4}$	$4.06\times10^{-3} \pm 1.0\times10^{-4}$
	25	$4.80\times10^{-3} \pm 7.5\times10^{-5}$	$4.35\times10^{-3} \pm 6.2\times10^{-5}$
mAb + pPEGMA-1100 [mg/mL]	1	$4.25\times10^{-3} \pm 1.4\times10^{-4}$	$3.7\times10^{-3} \pm 6.8\times10^{-5}$
	10	$4.66\times10^{-3} \pm 1.6\times10^{-4}$	$4.22\times10^{-3} \pm 3.3\times10^{-5}$
	25	$5.52\times10^{-3} \pm 1.8\times10^{-4}$	$5.1\times10^{-3} \pm 2.2\times10^{-5}$

Bibliography

[1] W. Wang. Antibody structure, instability and formulation. *Journal of Pharmaceutical Sciences*, 96:1–26, 2007.

[2] A. L. Daugherty and R. J. Mrsny. Formulation and delivery issues for monoclonal antibody therapeutics. *Advanced Drug Delivery Reviews*, 58(5-6):686–706, 2006.

[3] S. Stolnik and K. Shakesheff. Formulations for delivery of therapeutic proteins. *Biotechnology Letters*, 31(1):1–11, 2009.

[4] D. Filpula. Antibody engineering and modification technologies. *Biomolecular Engineering*, 24(2):201–215, 2007.

[5] S. J. Shire, Z. Shahrokh, and J. Liu. Challenges in the development of high protein concentration formulations. *Journal of Pharmaceutical Sciences*, 93(6):1390–1402, 2004.

[6] J. Liu, M. D. H. Nguyen, J. D. Andya, and S. J. Shire. Reversible self-association increases the viscosity of a concentrated monoclonal antibody in aqueous solution. *Journal of Pharmaceutical Sciences*, 94(9):1928–1940, 2005.

[7] S. Matheus, H. C. Mahler, and W. Friess. A critical evaluation of T-m(FTIR) measurements of high-concentration IgG(1) antibody formulations as a formulation development tool. *Pharmaceutical Research*, 23(7):1617–1627, 2006.

[8] J. Jezek, M. Rides, B Derham, J. Moore, E. Cerasoli, R. Simler, and B. Perez-Ramirez. Viscosity of concentrated therapeutic protein compositions. *Advanced Drug Delivery Reviews*, 63(13):1107–1117, 2011.

[9] A. Saluja and D. S. Kalonia. Nature and consequences of protein-protein interactions in high protein concentration solutions. *International Journal of Pharmaceutics*, 358(1-2):1–15, 2008.

[10] J. den Engelsman, P. Garidel, R. Smulders, H. Koll, B. Smith, S. Bassarab, A. Seidl, O. Hainzl, and W. Jiskoot. Strategies for the assessment of protein aggregates in pharmaceutical biotech product development. *Pharmaceutical Research*, 28(4):920–933, 2011.

[11] H-C. Mahler. Protein aggregation: pathways, induction factors and analysis. *Journal of Pharmaceutical Sciences*, 1:1–25, 2008.

[12] I. Roitt, J. Brostoff, and D. Male. *Immunology*. Mosby, London, UK, 7th edition, 2006.

[13] M. Cox and D.L. Nelson. *Lehninger Principles of biochemistry*. W.H. Freeman and Co., 5th edition, 2008.

[14] A. Tramontano, V. Morea, M. Rustici, C. Chothia, and A. M. Lesk. Antibody structure, prediction and redesign. *Progress in Biophysics and Molecular Biology*, 65(SUPPL. 1):5, 1996. XIIth International Biophysics Congress August 11-16, 1996 Amsterdam, Netherlands.

[15] V. H. Lee. *Peptide and Protein Drug Delivery*. Marcel Dekker, Inc, New York, USA, 1st edition, 1990.

[16] A. A. Wakankar and R. T. Borchardt. Formulation considerations for proteins susceptible to asparagine deamidation and aspartate isomerization. *Journal of Pharmaceutical Sciences*, 95(11):2321–2336, 2006.

[17] H. T. Wright. Nonenzymatic deamidation of asparaginyl and glutaminyl residues in proteins. *Critical Reviews in Biochemistry and Molecular Biology*, 26(1):1–52, 1991.

[18] J. L. Cleland, M. F. Powell, and S. J. Shire. The development of stable protein formulations: a close look at protein aggregation, deamidation and oxidation. *Critical Reviews in Therapeutic Drug Carrier Systems*, 10(4):307–377, 1993.

[19] A. B. Robinson, J. H. McKerrow, and P. Cary. Controlled deamidation of peptide and proteins - an experimental hazard and a possible biological timer. *Proceedings of the National Academy of Sciences of the United States of America*, 66(3):753–&, 1970.

[20] E. J. McNally and J. E. Hastedt. *Protein Formulation and Delivery*. Informa Healthcare, New York, USA, 1st edition, 2008.

[21] W. E. Riha, H. V. Izzo, and J. Zhang. Nonenzymatic deamidation of food proteins. *Critical Reviews in Food Science and Nutrition*, 36(3):225–255, 1996.

[22] J. Cacia, R. Keck, L. G. Presta, and J. Frenz. Isomerization of an aspartic acid residue in the complementarity-determining regions of a recombinant antibody to human IgE: Identification and effect on binding affinity. *Biochemistry*, 35(6):1897–1903, 1996.

[23] L. W. Dick Jr, D. Qiu, R. B. Wong, and K-C. Cheng. Isomerization in the CDR2 of a monoclonal antibody: Binding analysis and factors that influence the isomerization rate. *Biotechnology and Bioengineering*, 105(3):515–523, 2009.

[24] G. Gaza-Bulseco and H. Liu. Fragmentation of a recombinant monoclonal antibody at various pH. *Pharmaceutical Research*, 25(8):1881–1990, 2008.

[25] L. J. Brady, T. Martinez, and A. Balland. Characterization of nonenzymatic glycation on a monoclonal antibody. *Analytical Chemistry*, 79(24):9403–9413, 2007.

[26] A. Beck, M. C. Bussat, N. Zorn, V. Robillard, C. Klinguer-Hamour, S. Chenu, L. Goetsch, N. Corvaa, A. Van Dorsselaer, and J. F. Haeuw. Characterization by liquid chromatography combined with mass spectrometry of monoclonal anti-IGF-1 receptor antibodies produced in CHO and NSO cells. *Journal of Chromatography. B, Analytical Techniques for Biomedical Life Sciences*, 819(2):203–218, 2005.

[27] W. Wang. Instability, stabilization, and formulation of liquid protein pharmaceuticals. *International Journal of Pharmaceutics*, 185(2):129–188, 1999.

[28] W. Wang and C.J. Roberts. *Aggregation of Therapeutic Proteins*. John Wiley & Sons, Inc., New Jersey, 1 edition, 201.

[29] J.S. Bee, J.L. Stevenson, B. Mehta, J. Svitel, J. Pollastrini, R. Platz, E. Freund, J.F. Carpenter, and T.W. Randolph. Response of a concentrated monoclonal antibody formulation to high shear. *Biotechnology and Bioengineering*, 103(5):936–943, 2009.

[30] J.S. Bee, M. Davis, E. Freund, J.F. Carpenter, and T.W. Randolph. Aggregation of a monoclonal antibody induced by adsorption to stainless steel. *Biotechnology and Bioengineering*, 105(1):121–129, 2010.

[31] J. Bee, S. Schwartz, S. Trabelsi, E. Freund, J.L. Stevenson, J.F. Carpenter, and T.W. Randolph. Production of particles of therapeutic proteins at the air-water interface during compression/dilation cycles. *Soft Matter*, 8(40):10329–10335, 2012.

[32] M. J. Treuheit, A. A. Kosky, and D. N. Brems. Inverse relationship of protein concentration and aggregation. *Pharmaceutical Research*, 19(4):511–516, 2002.

[33] S. Rudiuk, L. Cohen-Tannoudji, S. Huille, and C. Tribet. Importance of the dynamics of adsorption and of a transient interfacial stress on the formation of aggregates of IgG antibodies. *Soft Matter*, 8(9):2651–2661, 2012.

[34] A. Mackie and P. Wilde. The role of interactions in defining the structure of mixed protein-surfactant interfaces. *Advances in Colloid and Interface Science*, 117(1-3):3–13, 2005.

[35] M.A. Bos and T. van Vliet. Interfacial rheological properties of adsorbed protein layers and surfactants: a review. *Advances in colloid and interface science*, 91(3):437–471, 2001.

[36] V. Fainerman, E.H. Lucassen-Reynders, and R. Miller. Adsorption of surfactants and proteins at fluid interfaces. *Colloids and Surfaces*, 143(2-3):141–165, 1998.

[37] V. Fainerman, S.A. Zholob, M. Lese, M. Michel, and R. Miller. Competitive adsorption from mixed nonionic surfactant / protein solutions. *Journal of Colloid and Interface Science*, 274(2):496–501, 2004.

[38] J. S. Philo and T. Arakawa. Mechanisms of protein aggregation. *Current Pharmaceutical Biotechnology*, 10(4):348–351, 2009.

[39] C-T. Huang, D. Sharma, P. Oma, and R. Krishnamurthy. Quantitation of protein particles in parental solutions using micro-flow imaging. *Journal of Pharmaceutical Sciences*, 98(9):3058–3071, 2009.

[40] R.L. Wiseman, E.T. Powers, and J.W. Kelly. Partitioning conformational intermediates between competing refolding and aggregation pathways: Insights into trans-thyretin amyloid disease. *Biochemistry*, 44(50):16612–16623, 2005.

[41] W. F. Weiss, T. M. Young, and C. J. Roberts. Principles, approaches, and challenges for predicting protein aggregation rates and shelf life. *Journal of Pharmaceutical Sciences*, 98(4):1246–1277, 2009.

[42] J.M. Andrews and C.J. Roberts. Non-native aggregation of alpha-chymotrypsinogen occurs through nucleation and growth with competing nucleus sizes and negative activation energies. *Biochemistry*, 46(25):7558–7571, 2007.

[43] C.J. Roberts. Non-native protein aggregation kinetics. *Biotechnology Bioengineering*, 98(5):927–938, 2007.

[44] T. Kamerzell, R. Esfandiary, S. Joshi, C.R. Middaugh, and D.B.. Volkin. Protein-excipient interactions: Mechanisms and biophysical characterization applied to protein formulation development. *Advances in Drug Delivery Reviews*, 63(13):1118–1159, 2011.

[45] S. R. Trevino, J. M. Scholtz, and C. N. Pace. Measuring and increasing protein solubility. *Journal of Pharmaceutical Sciences*, 97(10):4155–4166, 2008.

[46] S. Timasheff. Protein-solvent preferential interactions, protein hydration, and the modulation of biochemical reactions by solvent components. *Proceedings of the National Academy of Sciences*, 99(15):9721–6, 2002.

[47] S. Shimizu and D.J. Smith. Preferential hydration and the exclusion of cosolvents. *Journal of chemical physics*, 121(2):1148–54, 2004.

[48] J. Mewis and N. Wagner. *Colloid Suspension Rheology*. Cambridge University Press, UK, 1 edition, 2012.

[49] T. G. Mezger. *The Rheology Handbook*. Vincentz Network GmbH and Co., Hannover, Germany, 2 edition, 2006.

[50] A. Saluja, A. V. Badkar, D. L. Zeng, S. Nema, and D. S. Kalonia. Application of high-frequency rheology measurements for analyzing protein-protein interactions in high protein concentration solutions using a model monoclonal antibody (IgG2). *Journal of Pharmaceutical Sciences*, 95(9):1967–1983, 2006.

[51] S. Kanai, J. Liu, T. W. Patapoff, and S. J. Shire. Reversible self-association of a concentrated monoclonal antibody solution mediated by Fab-Fab interaction that impacts solution viscosity. *Journal of Pharmaceutical Sciences*, 97(10):4219–4227, 2008.

[52] A. Saluja, A. V. Badkar, D. L. Zeng, and D. S. Kalonia. Ultrasonic rheology of a monoclonal antibody (IgG2) solution: Implications for physical stability of proteins in high concentration formulations. *Journal of Pharmaceutical Sciences*, 96(12):3181–3195, 2007.

[53] H. X. Zhou, G. Rivas, and A. P. Minton. Macromolecular crowding and confinement: biochemical, biophysical, and potential physiological consequences. *Annual Reviews of Biophysics*, 37:375–397, 2008.

[54] R. J. Ellis and A. P. Minton. Join the crowd. *Nature*, 425:27–28, 2003.

[55] A. Minton. The influence of macromolecular crowding and macromolecular confinement on biochemical reactions in physiological media. *Journal of Statistical Mechanics: Theory and Experiment*, 276(14):10577–10580, 2001.

[56] A. P. Minton. Effective hard particle model for the osmotic pressure of highly concentrated binary protein solutions. *Biophysical Journal*, 94(7):L57–L59, 2008.

[57] V.L. Vilker, C.K. Colton, and K.A. Smith. The osmotic pressure of concentrated protein solutions: effect of concentration and pH in saline solutions of bovine serum albumin. *J. Colloid Interface Sci*, 79(2):548–566, 1981.

[58] H. Wada. Electroviscous effects of simple electrolytes under shear. *Journal of Statistical Mechanics: Theory and Experiment*, 0(1):P01001, 2005.

[59] C.W. Macosko. *Rheology Principles, Measurements, and Applications*. VCH, New York, 1st edition, 1994.

[60] S. Ikeda and K. Nishinari. Intermolecular forces in bovine serum albumin solutions exhibiting solidlike mechanical behaviors. *Biomacromolecules*, 1(4):757–763, 2000.

[61] S. Ikeda and K. Nishinari. On solid-like rheological behaviors of globular protein solutions. *Food Hydrocolloids*, 15(4-6):401–406, 2001.

[62] S. Ikeda and K. Nishinari. Solid-like mechanical behaviors of ovalbumin aqueous solutions. *International Journal of Biological Macromolecules*, 28(4):315–320, 2001.

[63] K. Oates, W. Krause, R.L. Jones, and R.H. Colby. Rheopexy of synovial fluid and protein aggregation. *Journal of the Royal Society, Interface*, 3(6):167–174, 2006.

[64] C. Picart and Galliard H. Piau, J-M. Human blood shear yield stress and its hematocrit dependence. *Journal of Rheology*, 42(1):1–12, 1998.

[65] C. G. Hall and G. N. Abraham. Reversible self-association of a Human Myeloma Protein: Thermodynamics and relevance to viscosity effects and solubility. *Biochemistry*, 23(22):5123–5129, 1984.

[66] Y. Zhang and P. S. Cremer. Interactions between macromolecules and ions: the Hofmeister series. *Current Opinion in Chemical Biology*, 10:658–663, 2006.

[67] B. A. Salinas, A. S. Hasige, S. M. Bishop, N. Harn, and J. F. Carpenter. Understanding and modulating opalescence and viscosity in a monoclonal antibody formulation. *Journal of Pharmaceutical Sciences*, 99(1):1–12, 2009.

[68] M. Sukumar, B. L. Doyle, J. L. Combs, and A. H. Pekar. Opalescent appearance of an IgG1 antibody at high concentrations and its relationship to noncovalent association. *Pharmaceutical Research*, 21(7):1087–1093, 2004.

[69] Her Majesty's Stationary Office British Pharmacopoeia commission. *British Pharmacopoeia 2010*, volume IV, chapter Appendix IV A: Clarity of Solution. TSO, London, 2010.

[70] S. Yadav, S.J. Shire, and D.S. Kalonia. Factors affecting the viscosity in high concentration solutions of different monoclonal antibodies. *Journal of Pharmaceutical Sciences*, 99(12):4812–4829, 2010.

[71] S. Yadav, S. Shire, and D. Kalonia. Viscosity analysis of high concentration bovine serum albumin aqueous solutions. *Pharmaceutical Research*, 28(8):1973–83, 2011.

[72] S. Yadav, A. Sreedhara, S. Kanai, J. Liu, S. Lien, H. Lowman, D. Kalonia, and S.J. Shire. Establishing a link between amino acid sequences and self-associating and viscoelastic behavior of two closely related monoclonal antibodies. *Pharmaceutical research*, 28(7):1750–1764, 2011.

[73] B. Connolly, C. Petry, S. Yadav, B. Demeule, N. Ciaccio, J. Moore, S. Shire, and Y. Gokarn. Weak interactions govern the vicosity of concentrated antibdoy solutions: high-throughput analysis using the diffusion interaction parameter. *Biophysical Journal*, 103(1):60–78, 2012.

[74] T.W. Patapoff and O. Esue. Polysorbate 20 prevents the precipitation of a monoclonal antibody during shear. *Pharmaceutical Development and Technology*, 14(6):659–664, 2009.

[75] S. Harding. The intrinsic viscosity of biological macromolecules. Progress in measurement, interpretation and application to structure in dilute solution. *Progress in Biophysical Molecular Biology*, 68(2-3):207–262, 1997.

[76] A. Saluja and D. S. Kalonia. Measurement of fluid viscosity at microliter volumes using quartz impedance analysis. *AAPS PharmSciTech*, 5(3):1–14, 2004.

[77] A. Saluja, A. V. Badkar, D. L. Zeng, S. Nema, and D. S. Kalonia. Ultrasonic storage modulus as a novel parameter for analyzing protein-protein interactions in high protein concentration solutions: Correlation with static and dynamic light scattering measurements. *Biophysical Journal*, 92(1):234–244, 2007.

[78] V. Sharma, A. Jaishankar, Y. Wang, and G. McKinley. Rheology of globular proteins: apparent yield stress, high shear rate viscosity and interfacial viscoelasticity of bovine serum albumin solutions. *Soft Matter*, 7(11):5150–5160, 2011.

[79] C.J. Pipe, T.S. Majmudar, and G.H. McKinley. High shear rate viscometry. *Rheologica Acta*, 47:621–642, 2008.

[80] F. He, G.W. Becker, J.R. Litowski, L. Narhi, D.N. Brems, and V.I. Razinkov. High-throughput dynamic light scattering method for measuring viscosity of concentrated protein solutions. *Analytical Biochemistry*, 399(1):141–143, 2010.

[81] S. Amin, C.A. Rega, and H. Jankevics. Detection of viscoelasticity in aggregation dilute protein solutions through dynamic light scattering-based optical microrheology. *Rheologica Acta*, 51(4):329–342, 2012.

[82] M. Wagner, K. Rieche, A. Blume, and P. Garidel. Viscosity measurements of antibody solutions by photon correlation spectroscopy: an indirect approach - limitations and applicability for high concentration liquid protein solutions. *Pharmaceutical Development and Technology*, 0(0):1–8, 2012.

[83] M. A. H. Capelle and T. Arvinte. High throughput screening of protein formulation stability: practical considerations. *European Journal of Pharmaceutics and Biopharmaceutics*, 65(2):131–148, 2007.

[84] S. Matheus, W. Friess, and H. C. Mahler. FTIR and nDSC as analytical tools for high-concentration protein formulations. *Pharmaceutical Research*, 23(6):1350–1363, 2006.

[85] L. Narhi, J. Schmit, K. Bechtold-Peters, and D. Sharma. Classification of protein aggregates. *Journal of Pharmaceutical Sciences*, 101(2):493–498, 2012.

[86] K. Wilson and J.M. Walker, editors. *Principles and techniques of biochemistry and molecular biology*. Cambridge University Press, 6th edition, 2005.

[87] GE Healthcare, USA. *Affinity Chromatography Manual*.

[88] EMD Millipore, USA. *Tangential flow filtration Manual*.

[89] J.W. Goodwin and R.W. Hughes. *Rheology for Chemists*. RSC Publishing, 2008.

[90] R.G. Larson. *The Structure and Rheology of Complex Fluids*. Oxford University Press, 1st edition, 1999.

[91] F.A. Morrison. *Understanding Rheology*. Oxford University Press, Oxford, 2001.

[92] J. Krägel and S.R. Derkatch. Interfacial shear rheology. *Current Opinion in Colloid & Interface Science*, 15(4):246–255, 2010.

[93] G.G. Fuller and J. Vermant. Complex Fluid-Fluid interfaces: Rheology and Structure. *Annual Review of Chemical and Biomolecular Engineering*, 3:519–543, 2012.

[94] S. Vandebril, A. Franck, G.G. Fuller, P. Moldenaers, and J. Vermant. A double wall-ring geometry for interfacial shear rheometry. *Rheologica Acta*, 49(2):131–144, 2010.

[95] Rheosense, Inc., USA. *mVROC User Manual*.

[96] A. Manz, N. Pamme, and D. Iossifidis. *Bioanalytical Chemistry*. Imperial College Press, London, UK, 1 edition, 2004.

[97] C.N. Pace, F. Vajdos, L. Fee, G. Grimsley, and T. Gray. How to measure and predict the molar absorption coefficient of a protein. *Protein Science*, 4:2411–2423, 1995.

[98] F-X. Schmid. *Biological Macromolecules: UV-visible Spectrophotometry. In: eLS*. John Wiley and Sons Ltd, Chichester, UK, 2001.

[99] M. Dockal, D. C. Carter, and F. Ruker. Conformational transitions of the three recombinant domains of HSA depending on pH. *Journal of Biological Chemistry*, 275(5):3042–3050, 2000.

[100] U.M. Elofsson, P. Dejmek, and M.A. Paulsson. Heat-induced aggregation of β-lactoglobulin studied by dynamic light scattering. *International Diary Journal*, 6:343–357, 1996.

[101] Thermo Scientific, USA. *NanoDrop 2000 User Manual*.

[102] S. Podzimek. *Light scattering, size exclusion chromatography and assymetric flow field fractionation: powerful tools for the characterization of polymers, proteins and nanoparticles*. Wiley and sons, Inc., NJ, USA, 2011.

[103] S.E. Harding and K. Jumel. *Current Protocols in Protein Science*. J. Wiley and Sons, New York, 1st edition, 1998.

[104] U. Nobbmann, M. Connah, B. Fish, P. Varley, C. Gee, S. Mulot, J. Chen, Z. Liang, Y. Lu, F. Sheng, J. Yi, and S.E. Harding. Dynamic light scattering as a relative tool for assessing the molecular integrity and stability of monoclonal antibodies. *Biotechnology and Genetic Engineeering Reviews*, 24:117–128, 2007.

[105] Malvern Instruments, UK. *Malvern Instruments Zetasizer*.

[106] B. Jachimska, M. Wasilewska, and Z. Adamczyk. Characterization of globular protein solution by dynamic light scattering, electrophoretic mobility, and viscosity measurements. *Langmuir*, 24(13):6866–6872, 2008.

[107] H. Bajaj, V. K. Sharma, and D. S. Kalonia. A high-throughput method for detection of protein self-association and second virial coefficient using size-exclusion chromatography through simultaneous measurement of concentration and scattered light intensity. *Pharmaceutical Research*, 24:2071–2083, 2007.

[108] D. Some, E. Hitchner, and J. Ferullo. Characterizing protein-protein interactions via static light scattering: non-specific interactions. *American Biotechnology Laboratory*, 27(2):16–20, 2009.

[109] S. Mori and H.G. Barth. *Size Exclusion Chromatography*. Springer Laboratory, USA, 1999.

[110] Malvern Instruments, UK. *Malvern GPC Manual*.

[111] T. Cosgrove, editor. *Colloid science - Principles, methods and applications*. John Wiley and Sons, Ltd., UK, 1 edition, 2010.

[112] Anton-Paar, Graz, Germany. *Anton-Paar, DMA35N manual*.

[113] P. Gill, T. T. Moghadam, and B. Ranjbar. Differential scanning calorimetry techniques: applications in biology and nanoscience. *Journal of Biomolecular Techniques*, 21:167–193, 2010.

[114] P. J. Haines, M. Reading, and F. W. Wilburn. *Differential thermal analysis and differential scanning calorimetry*, volume 1. Elsevier Science BV, The Netherlands, 1998.

[115] M. Cauchy, S. D'Aoust, B. Dawson, H. Rode, and M.A. Hefford. Thermal stability: a means to assure tertiary structure in therapeutic proteins. *Biologicals*, 30(3):175–85, 2002.

[116] J. Wen, Y. Jiang, and L. Narhi. Applications of DSC for Antibodies and Fc-conjugated proteins. *American Pharmaceutical Review*, 10(6):10–15, 2007.

[117] E. Garber and S.J. Demarest. A broad range of Fab stabilities within a host of therapeutic IgGs. *Biochemical and Biophysical Research Communications*, 355(3):751–757, 2007.

[118] R. Krishnamurthy, M. Sukumar, T.K. Das, and N.A. Lacher. Emerging analytical technologies for biotherapeutics development. *BioProcess International*, pages 32–42, 2008.

[119] Agilent Technologies, USA. *Agilent Protein 230 Kit Guide*.

[120] D. Wu, J. Qin, and B. Lin. Electrophoretic separations on microfluidic chips. *Journal of Chromatography A*, 1184(1-2):542–559, 2008.

[121] S.G. Anema. The use of lab-on-a-chip microfluidic SDS electrophoresis technology for the separation and quantification of milk proteins. *International Dairy Journal*, 19:198–204, 2009.

[122] S. Jeong, S. Biondi, J. Mikkelsen, B. Fathollahi, A. Winoto, M. Spaid, and A. Chow. An automated alternative to SDS-PAGE for protein analysis. *American Biotechnology Laboratory*, 23:8–10, 2005.

[123] O. Salas-Salano, L. Gennaro, and C. Felten. Optimization approaches in the routine analysis of monoclonal antibodies by capillary electrophoresis. *LCGC Europe*, 21(12), 2008.

[124] X.Z. He, A.H. Que, and J.J. Mo. Analysis of charge heterogeneities in mAbs using imaged CE. *Electrophoresis*, 30(5):714–722, 2009.

[125] D.A. Michels, O. Salas-Solano, and C. Felten. Imaged capillary isoelectric focusing for charge-variant analysis of biopharmaceuticals. *BioProcess International*, 9(10):48–54, 2011.

[126] L. Narhi, Y. Jiang, S. Cao, K. Benedek, and D. Shnek. A critical review of analytical methods for subvisible and visible particles. *Current Pharmaceutical Biotechnology*, 10(4):373–381, 2009.

[127] D. Sharma, P. Oma, M.J. Pollo, and M. Sukumar. Quantification and characterisation of subvisible proteinaceous particles in opalescent mAb formulations using micro-flow imaging. *Journal of Pharmaceutical Sciences*, 99(6):2628–2642, 2010.

[128] Afonina N. Awwad M. Bechtold-Peters K. Blue J.T. Chou D. Cromwell M. Krause H-J. Mahler H-C. Meyer B.K. Narhi L. Nesta D.P. Spitznagel T. Singh, S.K. An industry perspective on the monitoring of subvisible particles as a quality attribute for protein therapeutics. *Journal of Pharmaceutical Sciences*, 99(8):3302–3321, 2010.

[129] K. Wuchner, J. Buchler, J. Spycher, P. Dalmonte, and D.B. Volkin. Development of a microflow digital imaging assay to characterize protein particulates during storage of a high concentration IgG1 monoclonal antibody formulation. *Journal of Pharmaceutical Sciences*, 99(8):3343–3361, 2010.

[130] *European Pharmacopoeia*, chapter "Clarity and degree of opalescence of liquids", page 23. 2002.

[131] K. Monkos. On the hydrodynamics and temperature dependence of the solution conformation of human serum albumin from viscometry approach. *Biochimica et Biophysica Acta*, 1700:27–34, 2004.

[132] R. Sudduth. A generalised model to predict the viscosity of solutions with suspended particles. I. *Journal of Applied Polymer Sciences*, 48(1):25–36, 1993.

[133] R. Sudduth. A new method to predict the maximum packing fraction and the viscosity of solutions with a size distribution of suspended particles. II. *Journal of Applied Polymer Sciences*, 48(1):37–55, 1993.

[134] R. Sudduth. A new method to predict the maximum packing fraction and the viscosity of solutions with a size distribution of suspended particles. III. Effects of particle interaction and particle size distribution. *Journal of Applied Polymer Sciences*, 50(1):123–147, 1993.

[135] B. Dames, B.R. Morrison, and N. Willenbacker. (an empirical model predicting the viscosity of highly concentrated, bimodal dispersions with colloidal interactions.

[136] W. Galush, L. Le, and J. Moore. Viscosity behaviour of high-concentration protein mixtures. *Journal of Pharmaceutical Sciences*, 101(3):1012–1020, 2012.

[137] A. Minton. Hard quasispherical particle models for the viscosity of solutions of protein mixtures. *The Journal of Physical Chemistry. B*, 116(31):9310–9315, 2012.

[138] E. Tarelli, A. Mire-Sluis, H.A. Tivnann, B. Bolgiano, D.T. Crane, C. Gee, X. Lemercinier, M.L. Athayde, N. Sutcliffe, P.H. Corran, and B. Rafferty. Recombinant human albumin as a stabilizer for biological materials and for the preparation of international reference reagents. *Biologicals*, 26(4):331–346, 1998.

[139] S. Curry, H. Mandelkow, P. Brick, and N. Franks. Crystal structure of human serum albumin complexed with fatty acid reveals an asymmetric distribution of binding sites. *Nature Structural Biology*, 5(9):827–835, 1998.

[140] E.F. Pettersen, T.D. Goddard, C.C. Huang, G.S. Couch, D.M. Greenblatt, E.C. Meng, and T.E. Ferrin. UCSF Chimera - a visualization system for exploratory research and analysis. *Journal Computer Chemistry*, 25(13):1605–1612, 2004.

[141] M.A. Rixman, D. Dean, C.E. Macias, and C. Ortiz. Nanoscale intermolecular interactions between human serum albumin and alkanethiol self-assembled monolayers. *Langmuir*, 19(15):6202–6218, 2003.

[142] H. Zhao, P.H. Brown, and P. Schuck. On the distribution of protein refractive index increments. *Biophysical Journal*, 100(9):2309–2317, 2011.

[143] A. Jaishankar, V. Sharma, and G. H. McKinley. Interfacial viscoelasticity, yielding and creep ringing of globular protein-surfactant mixtures. *Soft Matter*, 7(17):7623–7634, 2011.

[144] Huai Z.Li. Bubbles in non-Newtonian fluids: formation, interactions and coalescence. *Chemical Engineering Science*, 54(13-14):2247–2254, 1999.

[145] C. Tanford. *Phyical Chemistry of Macromolecules*. John Wiley & sons, Inc., 1st edition, 1961.

[146] P. Clarke and J-L. Brousseau. Advances size exclusion chromatography beneficial to pharmaceutical development. Pharmaceutical Online Magazine. Application note.

[147] J. P. Gabrielson, M.L. Brader, A.H. Pekar, K.B. Mathis, G. Winter, J.F. Carpenter, and T.W. Randolph. Quantitation of aggregate levels in a recombinant humanized monoclonal antibody formulation by size-exclusion chromatography,

assymetrical field flow fractionation, and sedimentation velocity. *Journal of Pharmaceutical Sciences*, 96(2):268–279, 2007.

[148] Arakawa, T. and Ejima, D. and Li, T. and Philo, J.S. The critical role of mobile phase composition in size exclusion chromatography of protein pharmaceuticals. *Journal of Pharmaceutical Sciences*, 99(4):1674–1692, 2010.

[149] S.J. Burton, A.V. Quirk, and P.C. Wood. Refolding human serum albumin at relatively high protein concentration. *European Journal of Biochemistry*, 179:379–387, 1989.

[150] V. Levi and F.L. González Flecha. Reversible fast-dimerization of bovine serum albumin detected by fluorescence resonance energy transfer. *Biochimica et Biophysica Acta*, 1-2(1599):141–148, 2002.

[151] R. Wetzel, J. Becker, J. Behlke, H. Billwitz, S. Böhm, B. Ebert, H. Hamann, J. Krumbiegel, and G. Lassman. Temperature behaviour of human serum albumin. *European Journal of Biochemistry*, 104(2):469–478, 1980.

[152] C. Tanford and J.G. Buzzell. The viscosity of aqueous solutions of bovine serum albumin between pH 4.3 and 10.5. *Journal Physical Chemistry*, 60:225–231, 1956.

[153] A. P. Minton and P. D. Ross. Hard quasispherical model for the viscosity of hemoglobin solutions. *Biochemistry and Biophysical Research Communications*, 76:971, 1977.

[154] J. Lefevre. Viscosity of concentrated protein solutions. *Rheological Acta*, 21(4-5):620–625, 1982.

[155] S.M. Loveday, L.K. Creamer, H. Singh, and M.A. Rao. Phase and rheological behavior of high-concentration colloidal hard-sphere and protein dispersions. *Journal of Food Science*, 72(7):R101–R107, 2007.

[156] W.B. Russel, D.A. Saville, and W.R. Schowalter. *Colloidal Dispersions*. Cambridge University Press, 1st edition, 1989.

[157] J. Richards. Viscosity and the shapes of macromolecules: a physical chemistry experiment using the molecular-level models in the interpretation of macroscopic data obtained from simple measurements. *Journal of Chemical Education*, 70(8):685–689, 1993.

[158] M. Mooney. The viscosity of a concentrated suspension of spherical particles. *Journal of Colloid Science*, 6(2):162–170, 1951.

[159] I.M. Krieger and T.J. Dougherty. A mechanism for non-newtonian flow in suspensions of rigid spheres. *Transactions of the Society of Rheology*, III:137–152, 1959.

[160] G. Brownsey, T. Noel, R. Parker, and S. R. Ring. The glass transition behavior of the globular protein bovine serum albumin. *Biophysical Journal*, 85(6):3942–3950, 2003.

[161] M. Stading and A-M Hermansson. Viscoelastic behaviour of β-lactoglobulin gel structures. *Food Hydrocolloids*, 4(2):121–135, 1990.

[162] H. Inoue and T. Matsumoto. Viscoelastic and SAXS studies of the structural transition in concentrated aqueous colloids of ovalbumin and serum albumins. *Journal of Rheology*, 38(4):973–984, 1994.

[163] Cs. Kotsmar, V. Pradines, V.S. Alahverdjieva, E. Akseneko, V.B. Fainerman, V.I. Kovalchuk, J. Kragel, M.E. Leser, B.A. Noskov, and R. Miller. Thermodynamics, adsorption kinetics and rheology of mixed protein-surfactant interfacial layers. *Advances in Colloid and Interface Science*, 150(1):41–54, 2009.

[164] H.A. Waterman, C. Blom, H.J. Holterman, E.J. Sgravenmade, and J. Mellema. Rheological properties of human saliva. *Archives of Oral Biology*, 33(12):589–596, 1988.

[165] C. Sanchez, D. Renard, P. Robert, C. Schmitt, and J. Lefebvre. Structure and rheological properties of acacia gum dispersions. *Food Hydrocolloids*, 16(3):257–267, 2002.

[166] D.O. Grigoriev, S. Derkatch, J. Kragel, and R. Miller. Relationship between structure and rheological properties of mixed BSA-Tween 80 adsorption layers at the air/water interface. *Food Hydrocolloids*, 21(5-6):823–830, 2007.

[167] S. Roth, B.S. Murray, and E. Dickinson. Interfacial shear rheology of aged and heat-treated β-lactoglobulin films: displacement by nonionic surfactant. *Journal of Agricultural and Food Chemistry*, 48(5):1491–1497, 2000.

[168] J.P. Davis, E.A. Foegeding, and F.K. Hansen. Electrostatic effects on the yield stress of whey protein isolate foams. *Colloids and surfaces*, 34(1):13–23, 2004.

[169] P.R. Majhi, R.R. Ganta, R.P. Vanam, E. Seyrek, K. Giger, and P.L. Dubin. Electrostatically driven protein aggregation: β-lactoflobulin at low ionic strength. *Langmuir*, 22:9150–9159, 2006.

[170] K. Sakurai, M. Oobatake, and Y. Goto. Salt-dependent monomer-dimer equilibrium of bovine β-bactoglobulin at pH 3. *Protein Science*, 10(11):2325–2335, 2001.

[171] S. Uhrinova, M.H. Smith, G.B. Jameson, D. Uhrin, L. Sawyer, and P.N. Barlow. Structural changes accompanying pH-induced dissociation of the β-lactoglobulin dimer. *Biochemistry*, 39(13):3565–3574, 2000.

[172] B.Y. Qin, M.C. Bewley, L.K. Creamer, H.M. Baker, E.N. Baker, and G.B. Jameson. Structural basis of the tanford transition of bovine β-lactoglobulin. *Biochemistry*, 37(40):14014–14023, 1998.

[173] G. Kontopidis, C. Holt, and L. Sawyer. Invited review: *beta*-lactoglobulin: binding properties, structure and function. *Journal Dairy Science*, 87(4):785–796, 2004.

[174] S. Reynaert, C.F. Brooks, Vermant J. Moldenaers, P., and G.G. Fuller. Analysis of the magnetic rod interfacial stress rheometer. *Journal of Rheology*, 52:261–285, 2008.

[175] Suttiprasit, P. and Krisdhasima, V. and McGuire, J. The surface activity of α-lactalbumin, β-lactoglobulin and bovine serum albumin. *Journal of Colloid and Interface Science*, 154(2):316–326, 1992.

[176] P. Gunning, A. Mackie, A. Gunning, N. Woodward, P. Wilde, and V. Morris. Effect of surfactant type on surfactant - protein interactions at the air-water interface. *Biomacromolecules*, 5(3):984–991, 2004.

[177] A. Mackie, A. Gunning, M. Ridout, P. Wilde, and V. Morris. Orogenic displacement in mixed β-lactoglobulin / β-casein films at the air-water interface. *Langmuir*, 17(13):6593–6598, 2001.

[178] R. Wustneck, J. Kragel, R. Miller, Wilde P.J. Fainerman, V.B., D. Sarker, and D. Clark. Dynamic surface tension and adsorption properties of β-casein and β-lactoglobulin . *Food Hydrocolloids*, 10(4):395–405, 1996.

[179] D.A. Edwards, H. Brenner, and D.T. Wasan. *Interfacial transport processes and rheology*. Butterworth-Heinemann, 1991.

[180] R. Piazza and S. Iacopini. Transient clustering in a protein solution. *European Physical Journal E*, 7(1):45–48, 2002.

[181] R. Piazza, S. Iacopini, and M. Galliano. BLGA protein solutions at high ionic strength: Vanishing attractive interactions and "frustrated" aggregation. *Europhysics Letters*, 59(1):149–154, 2002.

[182] J.A. Pathak, R. Sologuren, and R. Narwal. Do clustering monoclonal antibody solutions really have a concentration dependence of viscosity?, 2013. in press.

[183] V. Oganesyan, M. Damschroder, W. Leach, H. Wu, and W.F. Dall'Acqua. Structural characterisation of a mutated, ADCC-enhanced human Fc fragment. *Molecular Immunology*, 45(7):1872–1882, 2008.

[184] R. Cathou, A. Kulczycki, and E. Haber. Structural features of γ-immunoglobulin, antibody, and their fragments. Circular dichroism studies. *Biochemistry*, 7(11):3958–64, 1968.

[185] S. Tetin, F. Prendergast, and S. Venyaminov. Accuracy of protein secondary structure determination from circular dichroism spectra based on immunoglobulin examples. *Analytical Biochemistry*, 321(2):183–187, 2003.

[186] A. Hawe, J.C. Kasper, W. Friess, and W. Jiskoot. Structural properties of monoclonal antibdoy aggregates induced by freeze-thawing and thermal stress. *European Journal of Pharmaceutical Sciences*, 38(2):79–87, 2009.

[187] E. Sahin, W. Weiss IV, A. Kroetsch, K. King, R. Kendall Kessler, T. Das, and C.J. Roberts. Aggregation and pH-Temperature phase behavior for aggregates of an IgG2 antibody. *Journal of Pharmaceutical Sciences*, 101(5):1678–1687, 2012.

[188] K. Forrer, S. Hammer, and B. Helk. Chip-based gel electrophoresis method for the quantification of half-antibody species in IgG4 and their by- and degradation products. *Analytical Biochemistry*, 334(1):81–88, 2004.

[189] H.-C. Mahler, F. Senner, K. Maeder, and R. Mueller. Surface activity of a monoclonal antibody. *Journal of Pharmaceutical Sciences*, 98(12):4525–4533, 2009.

[190] S.R. Croy and G.S. Kwon. Polysorbate 80 and Cremophor EL micelles deaggregate and solubilise Nystatin at the core-corona interface. *Journal of Pharmaceutical Sciences*, 94(11):2345–54, 2005.

[191] JR Bergueiro, M Bao, and JJ Casares. Determination of Hlb of nonionic dispersants by NMR, Part 1. Tween and Span series. *Anales de Quimica*, 74(3):529–530, 1978.

[192] F.O. Ayorinde, S.V. Gelain, J. Jr Johnson, and L.W. Wan. Analysis of some commercial polysorbate formulations using matrix-assisted laser desorption/ionisation time-of-flight mass spectrometry. *Rapid Communications in Mass Spectrometry*, 14(22):2116–2124, 2000.

[193] L. Kreilgaard, LS Jones, TW Randolph, S. Frokjaer, JM Flink, MC Manning, and JF Carpenter. Effect of Tween 20 on freeze-thawing and agitation-induced aggregation of recombinant human factor XIII. *Journal of Pharmaceutical Sciences*, 87(12):1597–1603, 1998.

[194] R. Kishore, A. Pappenberger, I. Dauphin, A. Ross, B. Buergi, A. Staempfli, and H-C. Mahler. Degradation of Polysorbates 20 and 80: Studies on Thermal Autoxidation and Hydrolysis. *Journal of Pharmaceutical Sciences*, 100(2):721–731, 2011.

[195] SS Penfiedl KW Aikens-P Shah DO Patist, A. Bhagwat. On the measurement of critical micelle concentrations of pure and technical-grade nonionic surfactants. *Journal of Pharmaceutical Sciences*, 91:2252–2264, 2002.

[196] R Miller, V.S. Alahverdjieva, and V.B. Fainerman. Thermodynamics and rheology of mixed protein-surfactant adsorption layers. *Soft Matter*, 4(6):1141–1146, 2008.

[197] B.A. Kerwin. Polysorbates 20 and 80 used in the formulation of protein biotherapeutics: structure and degradation pathways. *Journal of Pharmaceutical Sciences*, 97(8):2924–2935, 2007.

[198] E. Ha, W. Wang, and Y.J. Wang. Peroxide formation in polysorbate 80 and protein stability. *Journal of Pharmaceutical Sciences*, 91:2252–2264, 2002.

[199] J.-F. Lutz. Polymerization of oligo(ethylene glycol) (meth)acrylates: toward new generations of smart biocompatible materials. *Macromolecules*, 46(11):3459–3470, 2008.

[200] D.J. Siegwart, J. Kwon Oh, and K. Matyjaszewski. ATRP in the design of functional materials for biomedical applications. *Progress in Polymer Science*, 37(1):18–37, 2012.

[201] H. Lee, J. Pietrasik, S.S. Sheiko, and K. Matyjaszewski. Stimuli-responsive molecular brushes. *Progress in Polymer Science*, 35(1-2):24–44, 2010.

[202] M.M. Ali and H. Stover. Well-defined amphiphilic thermosensitive copolymers based on poly(ethylene glycol monomethacrylate) and methyl methacrylate prepared by ATRP. *Macromolecules*, 37(14):5219–5227, 2004.

[203] J.P. Magnusson, A. Khan, G. Pasparakis, A.O. Saeed, W. Wang, and C. Alexander. Ion-sensitive "Isothermal" responsive polymers prepared in water. *JACS communications*, 130(33):10852–3, 2008.

[204] H. Hussain, K.Y. Mya, and C. He. Self-assembly of brush-like poly[poly(ethylene glycol) methyl ether methacrylate] Synthesized via aqueous Atom Transfer Radical Polymerization. *Langmuir*, 24(34):13279–13286, 2008.

[205] W. Braunecker and K. Matyjaszewski. Controlled/living radical polymerization: Features, developments, and perspectives. *Progress in Polymer Science*, 32(1):93–146, 2007.

[206] Z. Cheng, Kang E.T. Zhu, X., and K.G. Neoh. Brush-type amphiphilic diblock copolymers from living/controlled radical polymerisations and their aggregation behaviour. *Langmuir*, 21(16):7180–7185, 2005.

[207] A. Munoz-Bonilla, A. van Herk, and J.P.A. Heuts. Preparation of hairy particles and antifouling films using brush-type amphiphilic block copolymer surfactants in emulsion polymerisation. *Macromolecules*, 43(6):2721–2731, 2010.

[208] G. Mantovani, F. Lecolley, L. Tao, D. M. Haddleton, J. Clerx, Jjlm Cornelissen, and K. Velonia. Design and synthesis of N-maleimido-functionalized hydrophilic polymers via copper-mediated living radical polymerization: A suitable alternative to PEGylation chemistry. *Journal of the American Chemical Society*, 127(9):2966–2973, 2005.

[209] F. Lecolley, L. Tao, G. Mantovani, I. Durkin, S. Lautru, and D. M. Haddleton. A new approach to bioconjugates for proteins and peptides ("pegylation") utilising living radical polymerisation. *Chemical Communications*, 1(18):2026–2027, 2004.

[210] J. Juarez, P. Taboada, S. Goy-Lopez, A. Cambon, M-B. Madec, S. Yeates, and V. Mosquera. Additional supra-self-assembly of human serum albumin under amyloid-like-forming solution conditions. *Journal of Physical Chemistry B*, 113(36):12391–12399, 2009.

[211] B. Farruggia, F. Rodriguez, R. Rigatuso, G. Fidelio, and G. Pico. The participation of human serum albumin domains in chemical and thermal unfolding. *Journal of Protein Chemistry*, 20(1):81–89, 2001.

[212] A. Tobitani and S.B. Ross-Murphy. Heat-Induced Gelation of Globular Proteins. 1. Model for the effects of time and temperature on the gelation time of BSA gels. *Macromolecules*, 30(17):4845–4854, 1997.

[213] C.R. Becer, S. Hahn, M. Fijten, H. Thijs, R. Hoogenboom, and U. Schubert. Libraries of methacrylic acid and oligo(ethylene glycol) methacrylate copolymers with LCST behavior. *Journal of Polymer Science: Part A: Polymer Chemistry*, 46(21):7138–7147, 2008.

[214] L. Tao, G. Mantovani, F. Lecolley, and D. M. Haddleton. Alpha-aldehyde terminally functional methacrylic polymers from living radical polymerization: Application in protein conjugation "Pegylation". *Journal of the American Chemical Society*, 126(41):13220–13221, 2004.

[215] D.H. Atha and K.C. Ingham. Mechanism of precipitation of proteins by polyethylene glycols. *Journal of Biological Chemistry*, 256(23):12108–12117, 1981.

[216] D. Winzor and P. Wills. Molecular crowding effects of linear polymers in protein solutions. *Biophysical Chemistry*, 119(2):186–195, 2006.

[217] L. Li, A. Kantor, and N.W. Warne. Prediction of relative polypeptide solubility by polyethylene glycol precipitation. Patent, 2007. US 60/801862.

[218] T. Arakawa and Y. Kita. Protection of bovine serum albumin from aggregation by Tween 80. *Journal of Pharmaceutical Sciences*, 89(5):646–652, 2000.

[219] L. G. Presta. Molecular engineering and design of therapeutic antibodies. *Current Opinion in Immunology*, 20(4):460–470, 2008.

[220] J.A.P.P. van Dijk and J.A.M. Smit. Size-exclusion chromatography - multiangle laser light scattering analysis of β-lactoglobulin and bovine serum albumin in

aqueous solution with added salt. *Journal of Chromatography A*, 867(1-2):105–112, 2000.